9-13-2018 1:45 PM

New Algorithms for Locating Faults in Series Capacitive Compensated Transmission Lines

Tirath Bains, *The University of Western Ontario*

Supervisor: Sidhu, Tarlochan S., *The University of Western Ontario*

A thesis submitted in partial fulfillment of the requirements for the Doctor of Philosophy degree in Electrical and Computer Engineering

Abstract

The precise location of the fault in a series capacitive compensated transmission line (SCCTL) plays an integral part in limiting the maintenance time following its tripping due to the occurrence of a permanent fault. Since, an SCCTL acts as a huge corridor of power, its outage will result in huge monetary losses which are directly proportion to the time it remains out of service. In worst case scenario, the tripping of an SCCTL might lead to the cascaded tripping of the parallel transmission lines due to overloading. Therefore, the need for an accurate and robust fault location algorithm for the SCCTLs becomes critical. Consequently, the focus of this thesis is to develop new fault location algorithms for the SCCTLs.

First of all, the concept of fault location in conventional transmission lines and its application to SCCTLs has been explained. The mathematical analysis of impedance-based fault location algorithms for SCCTLs which are the most widely used fault location algorithms for SCCTLs, is performed. The mathematical analysis enables a deeper look into the strengths and deficiencies of the existing algorithms. After the identification of the innate limitations of the existing fault location algorithms, three new impedance-based fault location algorithms have been proposed with the aim of maximum utilization of the available measurements to improve the accuracy of the fault location results in SCCTLs. The proposed impedance-based algorithms are then tested for various fault scenarios using simulations carried out in Matlab, and PSCAD. The comparative analysis of the proposed algorithms with the existing algorithms is also performed.

The interest in traveling wave-based fault location algorithms has been renewed lately due to the availability of commercial relays capable of sampling in the range of 1 MHz. Therefore, the traveling wave theory which forms the basis of traveling wave-based fault location algorithms is discussed. The mathematical analysis of reflection, and transmission of the traveling waves from various points of discontinuity in an SCCTL has been performed which enables the understanding of the shortcomings of the existing fault location algorithms. Thereafter, a new single-ended traveling wave-based fault location algorithm has been proposed in this thesis. The performance of the proposed algorithm has been verified through the simulations carried out in PSCAD.

Keywords: Fault Location, MOV, Series Capacitor, Series Compensated Lines, Transmission Lines, Traveling wave.

Acknowledgments

First of all, I would like to thank my supervisor, Dr. Tarlochan Singh Sidhu for providing pivotal inputs at crucial junctions of my reserach. I would also like to mention Dr. M.R.D Zadeh for introducing me to the the very interesting and fruitful area of power system protection. Special thanks to my labmates Hasan, Rahim, and Hessam for their valuable personal and professional advices.

I would like to acknowledge our industrial partner GE Grid Solutions and NSERC Canada for technical and finacial support for my research. Lastly, I would like to express my deepest gratitude to The University of Western Ontario for providing me with all the resources needed to conduct this research.

Dedication

I dedicate this thesis to my son and daughter Ajeet and Avneet Bains.

Contents

List of Figures

List of Tables

List of Appendices

List of Abbreviations, Symbols, and Nomenclature

ABC: Phase A, Phase B and Phase C Fault

AG: Phase A to Ground Fault

BC: Phase B to Phase C Fault

BCG: Phase B and Phase C to Ground Fault

CVT: Capacitor Voltage Transformer

CT: Current Transformer

DDOCs: Decaying DC Offest Components

DFT: Discrete Fourier Transform

DWT: Discrete Wavelet Transform

EMTDC: Electromagnetic Transients including DC

FACTS: Flexible AC Transmission System

FCDFT: Full-cycle Discrete Fourier Transform

FSC: Fixed Series Capacitor

IED: Intelligent Electronic Devices

MOV: Metal Oxide Varistor

PSCAD: Power Systems Computer-aided Design

SCCTL: Series Capacitive Compensated Transmission Line

SCB: Series Capacitor Bank

SCPU: Series Capacitor Protection Unit

SSFCs: Sub-synchronous Frequency Components

SSR: Sub-synchronous Resonance

TCSC: Thyristor Controlled Series Capacitor

TSSC: Thyristor Switched Series Capacitor

Chapter 1

Introduction

A robust transmission system is the backbone of a power system. Without the means of a secure and dependable transmission system, the power generated at remote generating station cannot be brought to the major urban load centers. With increasing demand of electrical power, the capacity of the transmission system also needs to be increased along with the generation capacity. There are two avenues to increase the capacity of the transmission system: 1-construction of new transmission lines; 2-enhancing the capacity of the existing transmission lines. Since, a transmission line is the biggest component of a power system which spans over hundreds of kilometers, the construction of a new transmission line is very capital cost intensive due to the vast amount of land (right of way) required, material costs and labor costs. The construction of a transmission line is further complicated by the stringent environmental regulations.

The other way to increase the capacity of a transmission system is to enhance the transmission capacity of the existing transmission lines. The transmission capacity of any 3-phase transmission line is given by (1.1) [1],

$$P = 3\frac{|V^S|\,|V^R|}{|X^L|}\sin\delta \tag{1.1}$$

where V^S and V^R are the sending and receiving end phase voltages, respectively. X^L is the reactance of the transmission line, and δ is the power angle. Three avenues could be identified from (1.1) for increasing the power transfer across an existing transmission line:

1. **Increasing voltage level (V^S and V^R)**: In a transmission system as the voltage level is increased the power transfer capacity of the transmission line also rises. The transmission line voltages in North America have reached to 765 kV [1]. Another benefit of higher voltage levels is the transmission losses get reduced. However, the voltage level of any transmission line is designed and set at the time of construction of a transmission line.

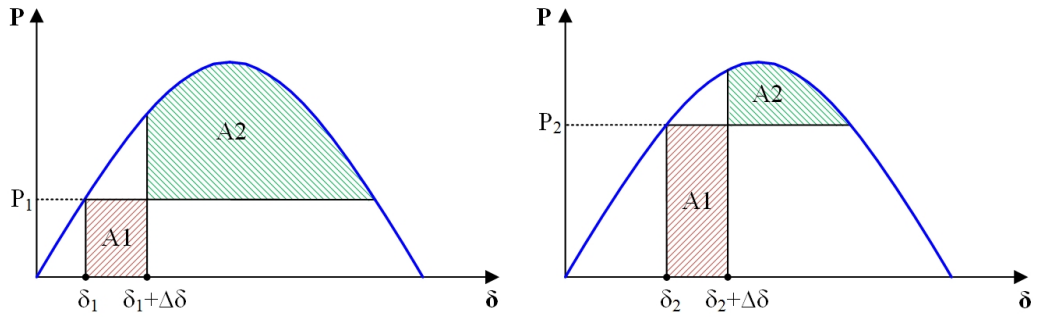

Figure 1.1: Transient stability: (a) Case 1; (b) Case 2.

Once the transmission line is put into service the voltage level of a transmission line could only be increased typically by 5%, increasing the power transmission capacity by 10%. So, for an existing transmission line the power transfer capacity cannot be significantly increased using the voltage levels.

2. **Increasing the power angle** (δ): The power transfer capacity of a transmission line could alternatively be increased by increasing the power angle, i.e., δ. However, as δ increases the incremental change in power transfer capacity keeps becoming smaller as can be observed from (1.2). In other words, same incremental change in δ would have more effect on increasing the power transfer capacity of the line when δ is small.

$$\frac{\partial P}{\partial \delta} = 3\frac{|V^S|\,|V^R|}{|X^L|}\cos\delta \tag{1.2}$$

Another very important aspect of increasing the power transmission capacity through power angle is that as the power angle increases the transient stability of the system gets decreased. Figures 1.1 (a) and (b) show the plots of transmitted electrical power (P) *vs.* power angle (δ), and, the effect of using power angle for increasing power transfer across transmission line on the transient stability of the system. A solid three-phase fault in the transmission line is assumed to occur in the transmission line which produces the shift of $\Delta\delta$ in the power angle when: (a) power angle (δ_1) and power transmission (P_1) are relatively smaller (Case 1); (b) power angle (δ_2) and power transmission (P_2) are relatively large (Case 2).

For a system to be stable during transient state, area A1 should be less or equal to the area A2. In Case 1, area under A2 is quite large in comparison to A1, signifying that the system would recover from the disturbance with a comfortable safety margin. When the power flow is increased to P_2 by increasing power angle to δ_2 (Case 2), the system would keep running in steady state. However, when the same disturbance as in Case 1 is applied

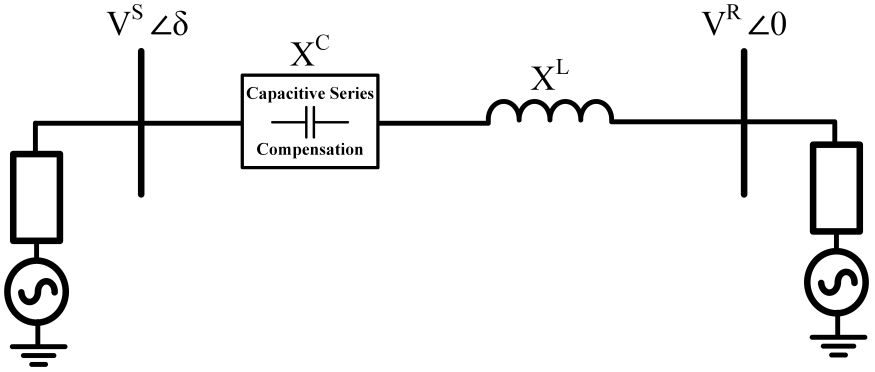

Figure 1.2: Schematic diagram of series compensated transmission line.

to the system, it will not recover as A2<A1. This fact highlights the key point that any considerable increase in power transmission capacity by using power angle would come at the cost of decreasing the transient stability of the system considerably.

3. **Series capacitive compensation (decreasing X^L)**: Another way to increase the power transfer is to decrease the inductive reactance of the transmission line denoted by X^L in Figure (1.1). Inductive reactance of the line can be decreased by putting a capacitive compensation (X^C) in series with the transmission line as shown in Figure 1.2. The series compensation devices could be a Fixed Series Capacitor (FSC), Thyristor Controlled Series Capacitor (TCSC), or a combination of both [1]. FSC as the name suggested has fixed capacitive reactance and is the simplest and least expensive series compensation device. On the other hand, the compensation level of a TCSC can be greatly varied within few milliseconds depending upon the requirements by changing the firing angle of thyristors. A combination of FSC and TCSC can be utilized to obtain inexpensive yet variable series compensation.

   In steady state the power flow across a series compensated transmission line would be given by (1.3) [1].

$$P = 3\frac{|V^S|\,|V^R|}{|X^L - X^C|}\sin\delta \tag{1.3}$$

   where X^C is the steady state capacitive compensation of the compensating device. It should be noted that from here onwards the elaboration of series compensated transmission lines is done using FSC as the standard series compensation device unless mentioned otherwise. The series compensated transmission lines are thus, referred to as Series Capacitive Compensated Transmission Lines (SCCTLs). Figure 1.3 shows the *P-δ* characteristics for a conventional line and a series compensated line with 50% series compensation ($X^C = \frac{X^L}{2}$). It can be seen that for the same power angle (δ) the power

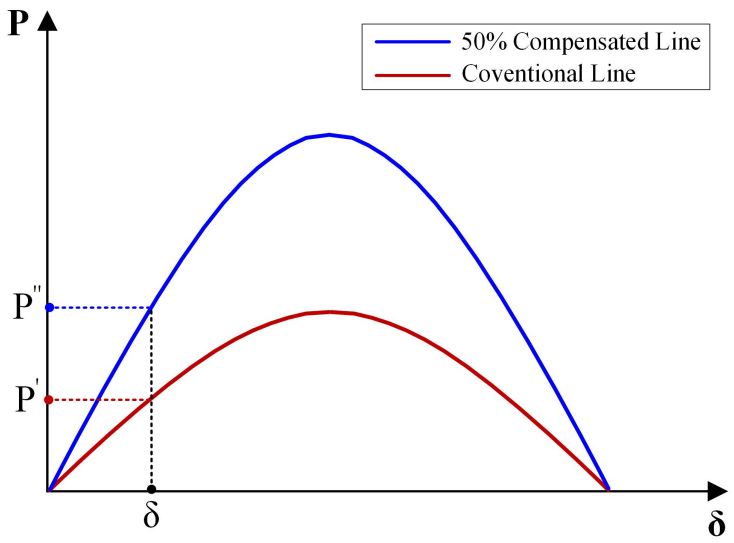

Figure 1.3: Power transfer capacity of a conventional and an SCCTL with 50% series capacitive compensation.

transferred through the SCCTL is double that of the power transferred through the conventional line (i.e., $P'' = 2P'$). Another benefit of the series capacitive compensation of the transmission line is that it increases the steady-state and transient stability of the power system [2].

Consequently, the series compensation has become a very attractive avenue for increasing power transfer capacity of the existing transmission lines [3] [4]. Figure 1.4 shows the Hydro-Quebec 765 kV transmission network [5]. Note the wide usage of series compensation in the network. Another example of wide application of SCCTLs is from [8] which shows the 500 kV Third AC Intertie Project in the Pacific Northwest by Bonneville Power Administration (BPA) and other utilities as shown in Figure 1.5. In Ontario, two SCCTLs have been added to the Hydro One network between Hanmer at Sudbury and Essa at Barrie [2].

1.1 Significance of fault location in transmission lines

The fault is an abnormal operation of the power system which might be caused by natural causes, equipment failure, or operator error [6]. The short-circuit is the most serious type of fault in the electrical power system [7]. The transmission lines are the largest parts of a power system that span across hundreds of kilometers, pass through variety of geographical features, and are exposed to various elements of nature such as wind, rain, snow, lightning etc. As such,

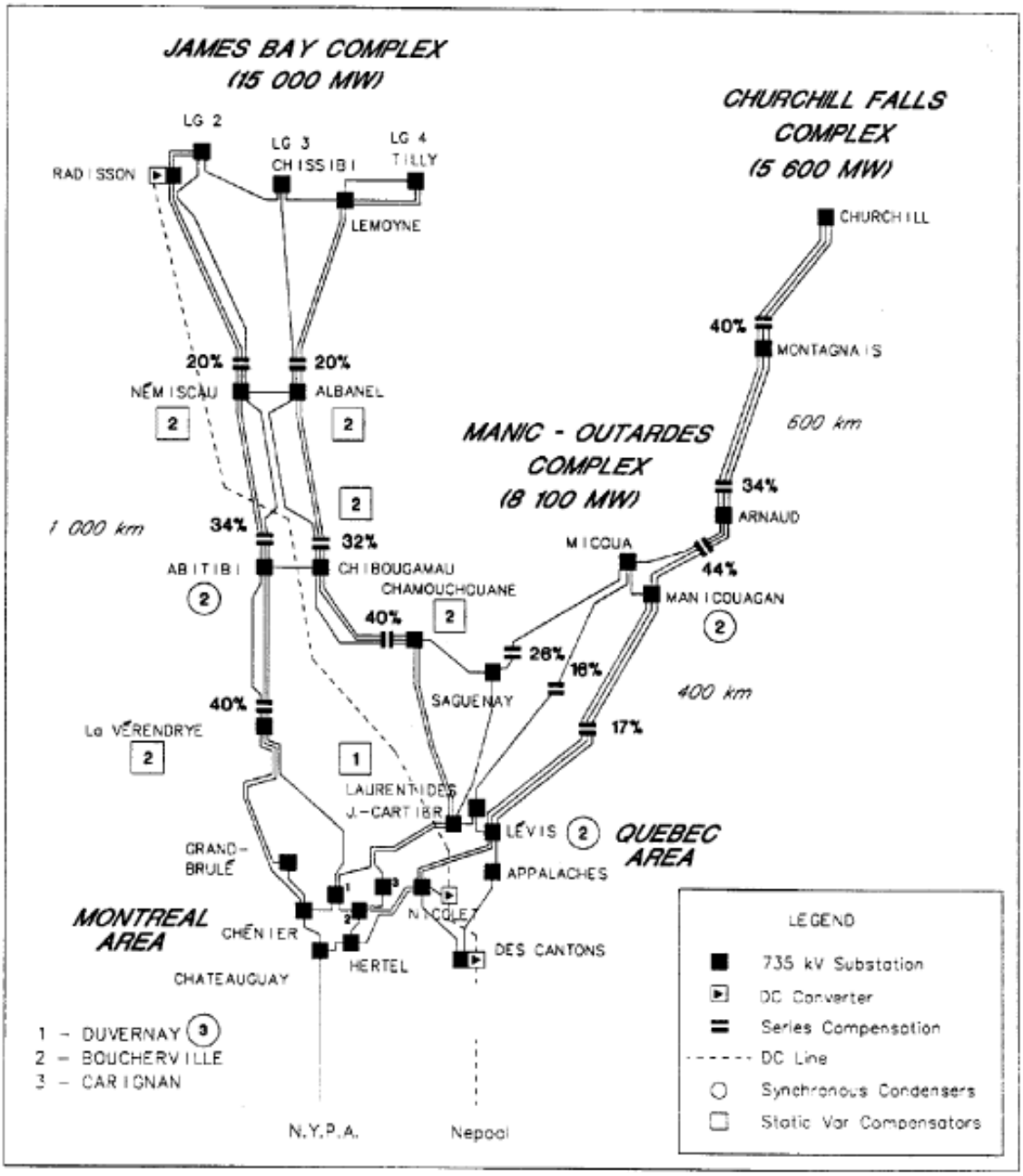

Figure 1.4: Series compensation in 765 kV transmission network of Hydro-Quebec [5].

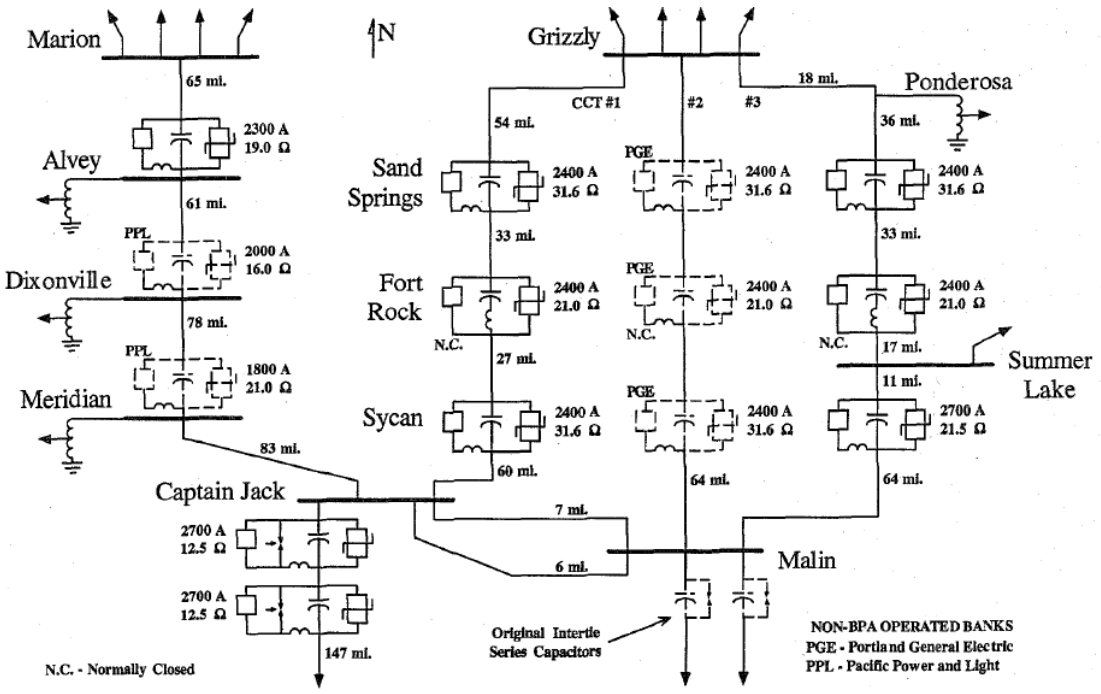

Figure 1.5: Series Capacitors in the Third AC Intertie Project in the Pacific Northwest [8].

the probability of occurrence of a fault and consequent tripping of the faulted transmission lines becomes relatively high. Though the tripping of any transmission line is a very serious event, but due to large amount of power that an SCCTL transfers, the tripping of an SCCTL becomes a very significant event. The tripping of an SCCTL in a best case scenario would result in large monetary losses to the utility, or in a worst case scenario may lead to widespread black-out. The amount of monetary losses due to the tripping of a transmission line are directly proportional to the time that transmission line remains out of service. Moreover, the other transmission lines will now have to carry the extra-load in the absence of the tripped transmission line. In order to minimize the financial losses and to avoid the possible cascaded tripping of parallel transmission lines, it is very important to rapidly locate the fault, complete the required repairs and put the transmission line back in to the service.

Locating the fault in a transmission line through visual inspection is impractical due to the shear length of the SCCTLs. Thus, arises a critical need to have a fault location algorithm for SCCTLs which could pin-point the location of the fault by using the voltage and current measurements. The maintenance crew could then be dispatched directly to that location. The importance of fault location algorithm for transmission lines can be gauged from the fact that a feature called ‘fault locator’ is available in almost all of the commercial protective relays used for the protection of transmission lines.

For a conventional transmission line, a direct relationship can be established between the

measurements (current and voltage) made at the line terminals and the distance of the fault from the transmission line terminals, as the conventional transmission lines have uniform characteristics along their length. Various fault location algorithms for conventional lines could be found in literature [9]-[12]. However, the presence of series capacitor protection system (SCPS) in an SCCTL introduces the non-uniformity to the properties of the SCCTL which makes the process of fault location in SCCTL complicated as discussed in detail in the following section.

1.2 SCPS and fault location in SCCTLs

As we know, the voltage drop across the series capacitor is directly proportional to the current flowing through the transmission line. Under fault conditions, the current flowing through series capacitor becomes excessively large (ranging from 2-10 times of the rated current), which leads to dangerously high voltage drop across the series capacitor which may damage the series capacitor [13]. Therefore, the protection system, i.e, SCPS is integrated to the series capacitor to protect it from the over-voltages resulting from the fault current. The series capacitor along with its protection system has been referred to as Series Capacitor Bank (SCB) in this thesis. The schematic diagram of the most general configuration of SCB is shown in Figure 1.6.

To observe the effect of SCPS operation on the process of fault location it is important to understand its principle. SCPS broadly consists of Metal-oxide Varistor (MOV), bypass gap, bypass switch along with a protection and control system [13], [14]. The functionality of each component of SCPS is as given below.

1. **MOV**: An MOV is a non-linear element which provides immediate over-voltage protection to the SCB. When the voltage across SCB reaches the protection level of MOV, the fault current immediately gets bypassed from series capacitor to MOV. Thus, clamping the voltage across SCB to the protection level of the MOV. The current is re-routed back to the series capacitor only after the voltage has dropped below the protection level of the MOV. This phenomenon could be observed from the waveform shown in Figure 1.7. It can be observed that MOV and series capacitor conduct intermittently in each fundamental cycle after the occurrence of a fault. The period for which an MOV conducts in each cycle depends upon the magnitude of the fault current. Thus, the behavior of parallel combination of an MOV and series capacitor is highly non-linear and fault current dependent. It should be noted that when MOV conducts the fault current it keeps on absorbing the energy, which leads to the rise of temperature of the MOV. So, energy accumulation capacity of an MOV is one of the design criteria that is taken into account while selecting the MOV for an SCB. To protect MOV against overheating or thermal

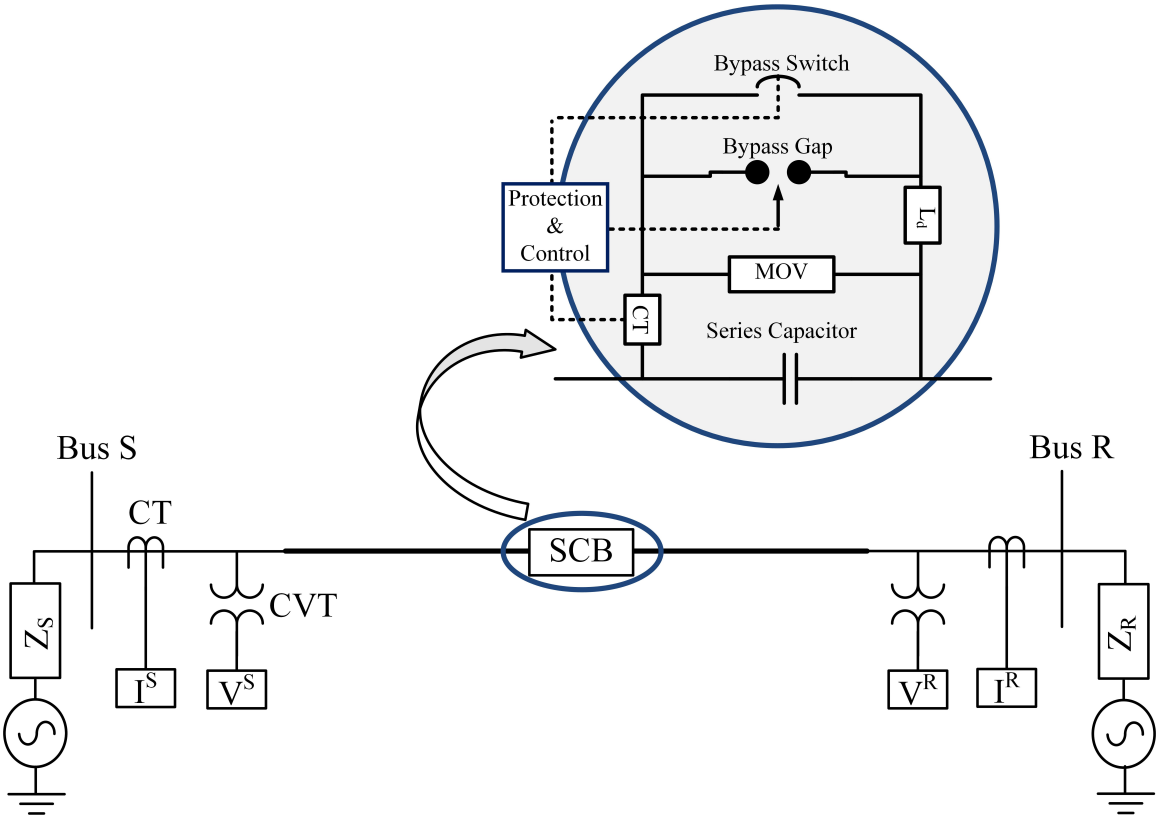

Figure 1.6: Schematic of a series capacitor bank in an SCCTL.

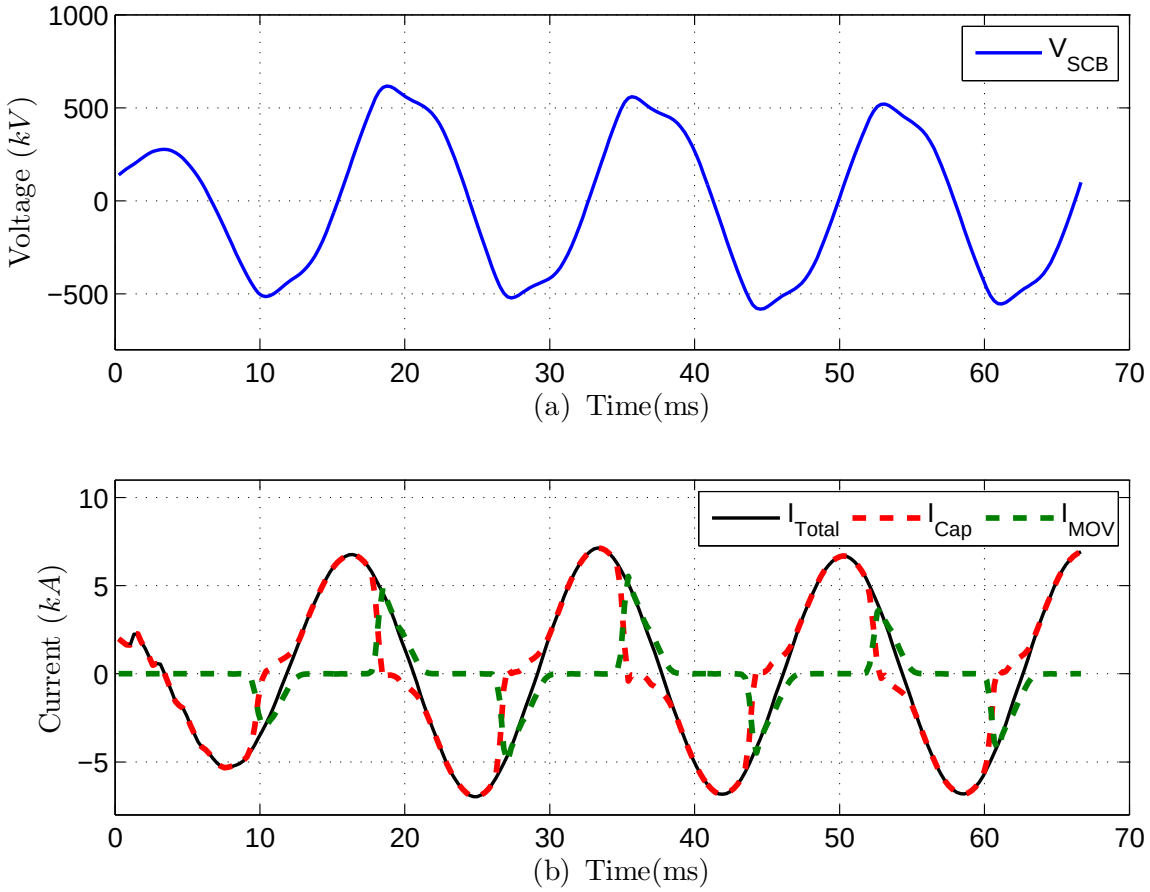

Figure 1.7: Protective action of MOV at fault occurrence: (a) voltage drop across SCB, (b) total current, series capacitor current, MOV current.

rundown due to excessive fault current or due to elongated conduction period, the energy accumulated in an MOV is continuously monitored. The accumulated energy is estimated by measuring the current flowing through MOV branch of the SCB through CT in the MOV branch as shown in Figure 1.6. If the accumulated energy in an MOV reaches its threshold value, the MOV is bypassed by local protection and control system through bypass gap and bypass switch.

2. **Bypass gap**: A bypass gap is incorporated in SCPS to immediately bypass the MOV by striking a spark across its air-gap until the bypass switch has closed its contacts. Bypass gap is triggered: 1-to avoid unnecessary heating of MOV if the fault current is too high and will likely result in MOV reaching its energy accumulation limit [13], [15]; 2-if the heated MOV is re-closed on to a fault [15]. However, with the increase in the energy absorption capacity of MOV and reduction in the closure time of the bypass switch, the newer installation of SCBs are increasingly implemented without using the bypass gap. In this thesis, the configuration of SCB with a bypass gap is called as bypass gap configuration of SCB while the configuration without a bypass gap is called gapless configuration of SCB. The configuration of SCB shown in Figure 1.6 is bypass gap configuration of SCB.

3. **Bypass switch**: Bypass switch protects MOV in gapless configuration, while protects MOV and bypass gap in bypass gap configuration of SCB, respectively; against the elongated conduction period if the protection system of the transmission line fails to operate [13], [14]. In newer installations, bypass switches are replacing the bypass gaps altogether.

It is clear from the above discussion that the behavior of SCPS is highly non-linear and fault current dependent. The non-linearity so introduced hinders the analytical estimation of the voltage drop across an SCB during the fault period which in turn makes the fault location in SCCTLs a cumbersome process. As a matter of fact, the location of SCB relative to the capacitor voltage transformer (CVT) is a determining factor in deciding that if a specialized fault location algorithm for SCCTLs is needed, or a fault location algorithm for conventional lines would suffice. An SCB can be located anywhere in a transmission line, ranging from one of the transmission line ends to the middle of the transmission line. When an SCB is located at a line end and the corresponding CVT is located on the line side of SCB as shown in Figure 1.8 (a), the SCB lies outside the zone between CVTs located at the transmission line ends. The only power system component that lies between the two CVTs is a transmission line which has uniform characteristics along its length. In such cases, the conventional fault

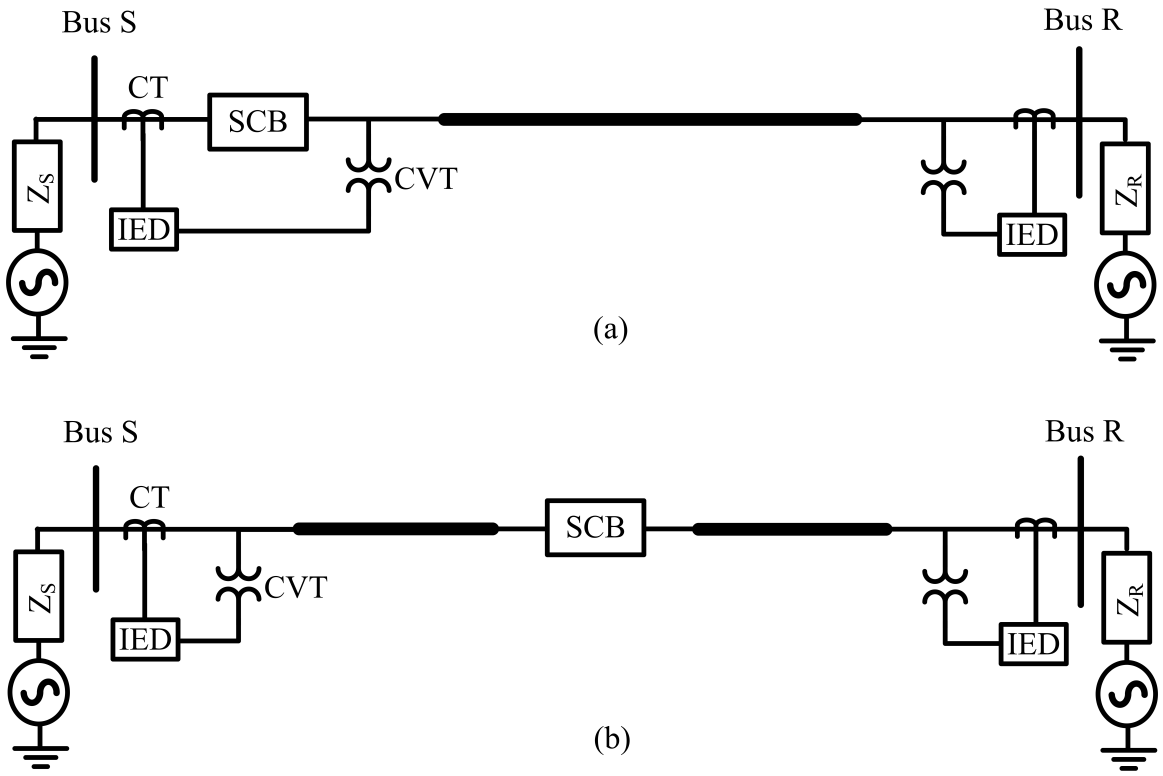

Figure 1.8: Location of SCB with respect to CVTs in an SCCTL with SCB lying: (a) outside the zone between CVTs, (b) inside the zone between CVTs.

location algorithms such as [9]-[12] can be applied to SCCTLs [26]. However, in all other configurations, the SCB will always lie in the zone between two CVTs as shown in Figure 1.8 (b). Now, due to the existence of a non-linear device between the two CVTs, the fault location algorithms for conventional transmission lines cannot be applied to such cases. Therefore, the dedicated fault location algorithms for SCCTLs are needed.

1.3 Existing types of fault location algorithms for SCCTLs

Dierent types of fault location algorithms for SCCTLs have been proposed in the exiting literature which can be classified into three different categories based upon the domain in which the fault location algorithm works:

1. **Instantaneous time-based fault location algorithm:**
   The instantaneous time-based fault location algorithms utilize the instantaneous values of the measured voltage and current signals to solve the differential equations representing transmission line, and compute the location of fault in an SCCTL [16]-[19]. However, the instantaneous time-based algorithms are susceptible to the noise and harmonics present in the measured signals. Moreover, instrument transformers are unable to exactly

replicate the rapidly changing instantaneous measurements required for the implementation of instantaneous time-based fault location algorithms. Consequently, the practical application of such algorithms has been highly limited and not much research has been reported in this area.

2. **Impedance-based fault location algorithm:**
   Impedance-based fault location algorithms use the phasors of the voltage and current signals to obtain the seen impedance of the transmission line from its terminals. The seen impedance of the transmission line is then compared to the impedance of the transmission line to obtain the fault location result. The phasor estimation algorithms like the Discrete Fourier Transform (DFT), and Cosine algorithm attenuate noise significantly and remove the integer harmonics from estimated phasors, thus making impedance-based fault location algorithms immune to the effects of noise and harmonics. Since, the phasors are readily available from the numerical relays present at the line terminals, the impedance-based algorithms can be easily implemented in the protective relays. Additionally, the vast installed base of impedance-based relays in the power system makes the impedance-based algorithms the most widely used fault location algorithms.

3. **Traveling wave-based fault location algorithm:**
   The incidence of fault acts as an application of a step input at the point of fault, which produces a traveling wave which propagates in the transmission line in both directions with speed almost equal to the speed of the light. Since, the traveling wave consists of high frequency components to which series capacitor offers very low impedance, the traveling wave-based fault location algorithms can be applied to SCCTLs. The traveling wave-based fault location algorithms compute the fault location by noting the time difference between two successive traveling waves arriving at the terminal and relating it to the distance covered by the traveling waves in that time period. However, in order to obtain the exact arrival time of the traveling waves, the relays are required to have very high sampling frequency. For example, a relay with 1 MHz frequency would have an accuracy limit of 300 meters. However, 1 MHz is very high sampling frequency with respect to the 'normal' phasor-based digital relays which have sampling frequencies in the range of about 1900-5600 Hz. Consequently, limited application of such algorithms is reported in industry. However, with the advent of relays with very high sampling frequency in last two to three years such as T400L by Schweitzer Engineering Laboratories, the traveling-wave based fault location algorithms are being explored actively.

The fault location algorithms for SCCTLs could also be classified as single-ended fault location algorithm, or double-ended fault location algorithm depending upon the number of terminals

of the transmission line from which the measurements are utilized for the purpose of fault location:

1. **Single-ended fault location algorithm:**
   If the fault location algorithm uses the voltage and current measurements from only one terminal (or local measurements) of the SCCTL, it is called as a single-ended fault location algorithm such as the algorithm given in [20]. The single-ended fault location algorithm of [20] utilizes MOV model for computing the fault location results. The algorithm of [20] has two subroutines, one for each faulted section of the transmission line. Moreover, one of the subroutines is iterative. The correct fault location result is thereafter identified using a special procedure also mentioned in [20]. Due to their dependence on MOV-model and iterative nature, the single-ended fault location algorithms are not usually used for fault location in SCCTLs.

2. **Double-ended fault location algorithm:**
   The double-ended or sometimes called as PMU-based fault location algorithms [22]-[25], utilize measurements from both (local and remote) ends of the transmission lines. The double-ended fault location algorithms are usually based on the fault loop model and do not use the MOV model. Fault loop-based algorithms estimate the fault voltage and fault current in terms of the unknown fault location, and then solve for the fault location under the constraints which vary from one publication to the other. For double-ended fault location algorithms to yield accurate results, it is very important that the measurements from each terminal of an SCCTL correspond to the exact same time instant. Thus, the measurements from each terminal of an SCCTL are required to be synchronized. If the protective devices present at each end of an SCCTL are synchronized using GPS or other means, the measurements are already synchronized. If however the relays are not synchronized, then the measurements from both ends of an SCCTL are needed to be synchronized post-fault as shown in [22]. The double-ended fault location algorithms are widely used for fault location in SCCTLs.

Due to the wide application of phasor-based relays in the field, and the ability of double-ended fault location algorithms to yield fault location results without using MOV-model, the attention is focused on double-ended impedance-based fault location algorithms in this thesis. Also, with the recent advancement in the protective relay technology, the traveling wave-based commercial relays are being introduced which rejuvenated the interest in the traveling-wave based fault location algorithms. Therefore, the traveling-wave based algorithms are also the subject of research in this thesis.

1.4 Challenges and motivations

1.4.1 Impedance-based fault location algorithms

Challenges

As already discussed in Section 1.2, MOVs are present in an SCCTL as part of SCPS. After the occurrence of a fault in an SCCTL the MOV in the faulted phase starts conducting the fault current to limit the over-voltage across the SCB caused by the high fault currents encountered in an SCCTL. However, due to the non-linear behavior of MOV, the impedance of the SCB in the faulted phase cannot be estimated accurately. This is a major hurdle before any impedance-based fault location algorithm for the SCCTLs. The existing impedance-based fault location algorithms have taken one of the two routes to overcome this challenge: 1-use a linearized or an EMTP-derived MOV model as given in [20] and [21]; 2-use fault loop based fault location algorithms such as [22]-[25]. However, each type of fault location algorithms has its strengths and shortcomings which have been explored later in this thesis.

Another challenge that impedance-based fault location algorithms for SCCTLs face is the accuracy of the estimated phasors of the measured voltages and currents. It is due to the fact that SCCTL is essentially an under-damped RLC circuit, and any disturbance such as fault in the SCCTL leads to the injection of sub-synchronous frequency components in addition to the decaying-DC components in the measured signals, which in turn make the estimated phasors oscillatory and imperfect. The oscillatory and imperfect phasors further impact the accuracy of the fault location results. A Prony analysis-based phasor estimation technique has been proposed in [26] which yields consistent estimated phasors. However, it has been shown in [27] that if the fault location results obtained from oscillatory phasors are averaged over the entire period of the fault duration, its accuracy becomes comparable to the Prony analysis-based phasor estimation technique. The details on the aspect of phasor estimation for fault location in SCCTLs could be found in [27], which is also the previous work of the author.

The presence of a parallel transmission line is another factor that has to be taken into account by the impedance-based fault location algorithms for SCCTLs. It can be seen from Figure 1.4 that it is very common for an SCCTL to have parallel transmission lines which could either be a series compensated or a conventional transmission line. If the proposed fault location algorithm for the SCCTLs does not take into account the zero sequence mutual-coupling between the parallel transmission lines, the accuracy of the fault location results obtained will be compromised. Thus, factoring in the presence of parallel transmission lines is very important while proposing a new impedance-based fault location algorithm for SCCTLs.

Motivation

The fact that only the MOV located in the faulted phase conducts the fault current while the series capacitor is exclusively responsible for the conduction of current in non-faulted phase, has not been used in any of the existing impedance-based fault location algorithms. Thus, the voltage drop across SCB in non-faulted phase can be analytically estimated. This extra piece of information can be used toward proposing a new fault location algorithm for SCCTLs.

Another information that is available but has not been utilized by the existing algorithms is the MOV current measurement. It has been mentioned in the Section 1.2 that in order to estimate the accumulated energy in an MOV, the current through MOV is measured in each phase and is used by the protection and control system of the SCB to decide if the MOV needs to be bypassed or not. The total current that flows through an SCB is the summation of the currents flowing through series capacitor, and MOV. The total current that goes into an SCB could be easily estimated using the measurements from transmission line terminals, while MOV current is known from the current measurement at SCB. Therefore, the current flowing through the series capacitor, and hence, the voltage drop across SCB in the faulted phase could be obtained by subtracting MOV-current from the total current flowing through SCB. The usage of MOV current measurement would also result in new fault location algorithms that would not use natural fault loop for the purpose of fault location.

All the existing impedance-based fault location algorithms found in literature are based on the assumption that the series compensation is applied at only one location in an SCCTL. Therefore, at the time of fault there will be one terminal of the SCCTL which would see the fault directly, without SCB being in between the fault and the SCCTL terminal. Thus, the fault voltage equation can be written from this particular end of the SCCTL. However, in practice there are transmission lines in which series compensation is applied at more than one location. None of the existing impedance-based fault algorithms can be applied to such SCCTLs. It is due to the fact that the fault voltage equation cannot be written from any of the SCCTL terminals if the fault lies in the zone between any of the two SCBs. An SCCTL with two SCBs is shown in Figure 1.9 with fault lying in the zone between the two SCBs. Now, the equation for fault voltage cannot be written from any of the terminals of the SCCTL, i.e., Bus S and Bus R, as the unknown voltage drop across SCB1 would be encountered if the attempt is made from Bus S, while the unknown voltage drop across SCB2 would prevent compiling the fault voltage equation from Bus R. Thus, rendering the fault loop-based fault location algorithms useless for the configurations of SCCTLs in which series compensation is applied at multiple locations. Therefore, opportunity arises to present the first ever impedance-based fault location algorithm applicable to SCCTLs with SCBs located at multiple locations in the SCCTL.

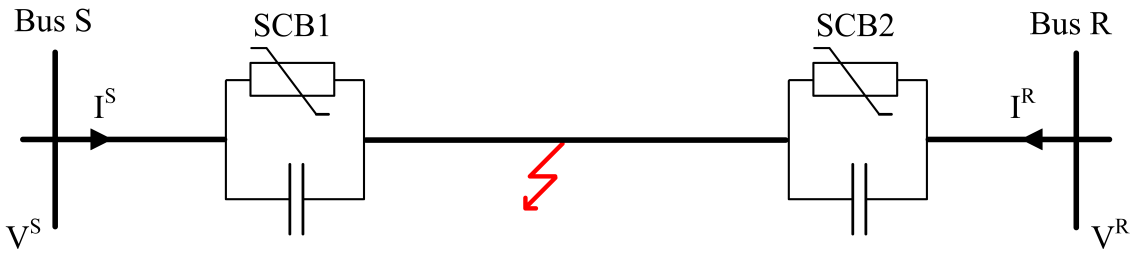

Figure 1.9: Diagram depicting series compensation applied at multiple locations in an SCCTL.

1.4.2 Traveling wave-based fault location algorithms

Challenges

As explained earlier, in order to limit the the uncertainty in the fault location results to 300 meters, the digital relays with sampling frequency close to 1 MHz are required. Though with higher sampling frequencies the the uncertainty in the fault location results, however due to technological limits the usage of1 MHz sampling frequency has been reported in the commercial products. The traveling wave-based fault location algorithms like impedance-based algorithms could be double-ended or single-ended algorithm. For the implementation of double-ended traveling wave-based fault location algorithms, the time instances of the arrival of the first traveling wave at each terminal of the SCCTL are required. In order to obtain accurate results from double-ended traveling wave-based fault location algorithms the measurements from both terminals of the SCCTL have to be synchronized. However, the synchronization of the relays operating at 1 MHz is a very tedious task to accomplish. On the other hand single-ended traveling wave-based fault location algorithms do not require the time synchronization. However, single-ended traveling wave-based fault location algorithms require the time instances of the arrival of the first and second traveling waves arriving at the same terminal of the SCCTL, along with the origination point of the second traveling wave. It is given in [28] that the point of origin of the second traveling wave cannot be determined in all the configurations of the SCCTL, therefore, limiting the applicability of the single-ended traveling wave-based fault location algorithms.

Motivation

The methodology to identify the point of discontinuity in the SCCTL from which the second traveling wave arriving at the terminal of the SCCTL originated, as presented in existing single-ended traveling wave-based fault location algorithms such as [28], [29], [30], and [31] is based on the empirical observations from the EMTP simulations. No mathematical analysis has been

carried out regarding the reflection of the traveling waves in an SCCTL. The mathematical analysis of the phenomenon of reflection and transmission of the traveling waves at various points of discontinuity in an SCCTL would enable the identification of point of discontinuity responsible for the origination of the second traveling wave arriving at a terminal of the SCCTL for all configurations of the SCCTLs.

1.5 Research objectives

1.5.1 Proposition of new impedance-based fault location algorithms for SCCTLs

1. In this thesis, it is aimed to present three new impedance-based fault location algorithms for SCCTLs which are as follows:

   (a) The first impedance-based fault location algorithm would be based on the fact that in the non-faulted phase(s) the current is conducted by the series capacitor only.

   (b) The second impedance-based fault location algorithm would utilize the phasor of the MOV current which is measured at SCB to estimate the energy accumulated in the MOV.

   (c) The third impedance-based fault location algorithm would utilize only magnitude of the phasor of the MOV current.

2. To extend the application of the first proposed algorithm to the SCCTLs with series compensation applied at multiple locations, making it the first and the only impedance-based algorithm to be able to locate faults in SCCTLs with series compensation applied at multiple locations.

3. To present the derivation, advantages, and limitations of the proposed algorithms through detailed mathematical analysis.

4. To study the impact of CT and CVT errors, phasor estimation error, and magnitude of fault resistance on the accuracy of the proposed algorithms using the fault scenarios simulated in PSCAD and Matlab covering various fault locations, fault types, and fault resistance.

1.5.2 Proposition of a new single-ended traveling wave-based fault location algorithm applicable to all configurations of the SCCTL

1. To derive the equations governing the reflection and transmission of the traveling waves from any point of discontinuity in the SCCTL such as fault point, SCB, presence of an inductive source, or another transmission line at the terminals of an SCCTL.

2. To identify the limitations of the single-ended fault location algorithms.

3. To derive and propose a new single-ended traveling wave-based fault location algorithm which does not suffer from the deficiencies of the existing fault location algorithms.

4. To validate the derived mathematical equations and proposed single-ended traveling wave-based fault location algorithm through simulations carried out in PSCAD.

1.6 Contributions

The main contributions of the research presented in this thesis are given as below:

1. The proposition of three new impedance-based fault location algorithms.

   (a) The first algorithm will only utilize the phasors of voltages and currents from both terminals of the SCCTL. The methodology of this algorithm will be applied to SCCTLs with series compensation applied at multiple locations.

   (b) The second algorithm will utilize the phasors of the currents in the MOV branches of the SCB, in addition to the phasors of voltages and currents from both terminals of the SCCTL.

   (c) The third algorithm will utilize the phasor magnitudes of the currents in the MOV branches of the SCB, in addition to the phasors of voltages and currents from both terminals of the SCCTL.

2. Derivation of the equations governing the reflection and transmission of the traveling waves from different points of discontinuity in an SCCTL.

3. The proposition of a new single-ended traveling wave-based fault location algorithm based on the derived equations.

1.7 Thesis outline

This thesis has been organized into eight chapters as described below.

In Chapter 1, an introduction is provided regarding the significance of series compensation of the transmission lines, the technique of fault location in conventional transmission lines as well as SCCTLs, and the types of fault location algorithms. The working of protection system of the series capacitor, and the need for having specialized fault location algorithms for SCCTLs is explained in Chapter 1. The areas in which the research is carried out in this thesis are also identified in Chapter 1.

The existing impedance-based fault location algorithms for SCCTLs are discussed in Chapter 2. It is presented in Chapter 2 that the earlier impedance-based fault location algorithms for SCCTLs attempted to utilize the MOV model. However, the modeling of MOV tends to be imprecise due to the variety of reasons which include highly non-linear nature of the MOV, aging of MOV, ambient temperature, and other environmental conditions. It is presented in Chapter 2 that the focus in later years shifted towards the fault loop-based impedance-based algorithms, which found wide application. It is shown in Chapter 2 through mathematical analysis that all of the impedance-based algorithms that utilize natural fault loop are conceptually equivalent to each other, and entail similar advantage and disadvantages. Chapter 2 shows that under specific fault conditions in an SCCTL, all the fault loop-based impedance-based fault location algorithms will lose accuracy. The findings reported in Chapter 2 are verified through the simulations results which are also incorporated in Chapter 2.

Chapter 3 presents the first impedance-based fault location algorithm which yields accurate results without using the natural fault loop or the model of MOV for single-phase to ground, and double-phase to ground faults which form majority of the faults in a transmission lines (75%-90%) [32]. The proposed algorithm uses synchronized measurements from both ends of the SCCTL. The fault location algorithm presented in Chapter 3 is proposed using the distributed model of the transmission line, which is one of the most accurate models of the transmission line that could be used for analysis in phasor domain. The derivation, advantages, and limitations of the proposed algorithm have been elaborated through mathematical analysis, and simulations carried out in PSCAD, and Matlab.

In Chapter 4, the concept that was derived in Chapter 3 is used to propose a fault location algorithm for the SCCTL with series compensation applied at multiple locations in an SCCTL. The applicability of the proposed algorithm is shown for N number of SCB locations in an SCCTL using the simpler model of the transmission line, i.e., lumped model of transmission line. The usage of lumped model of transmission line avoids the resulting complexity from the application of a detailed transmission line model to $N + 1$ segments of the transmission

line. However, the distributed-model of transmission line is utilized to elaborate the proposed algorithm of Chapter 4 when applied to an SCCTL with SCBs present at two locations. The performance of the proposed method has been tested on variety of metrics through simulations run in PSCAD and Matlab.

Two new impedance-based fault location algorithms for SCCTLs are presented in Chapter 5. The fault location algorithms proposed in Chapter 5 are based on the utilization of the MOV current measured at SCB for the purpose of fault location in the SCCTL. One of the fault location algorithms proposed in Chapter 5 uses the complete phasor of the MOV current while the other algorithm uses only magnitude of the phasor of the MOV current ('second' and 'third' algorithms mentioned in Section 1.5 point 1. (b) and (c), respectively). Both algorithms are derived using the distributed model of the transmission line. The comparative analysis of the results obtained from both algorithms is also performed using the simulations in PSCAD and Matlab.

In Chapter 6 introduction to traveling wave theory, the modeling of transmission line based on traveling wave theory, methodology to detect the arrival of traveling wave, i.e. discrete wavelet transform (DWT), and the working of existing single-ended traveling wave-based fault location algorithms is presented. The factors limiting the application of single-ended traveling wave-based fault location algorithms to SCCTLs have also been identified in Chapter 6. In Chapter 7, the equations for the traveling waves reflected and transmitted from various points of discontinuity in an SCCTL are derived. Thereafter, the applicability of existing single-ended traveling wave-based fault location algorithms to various configurations of the SCCTL is investigated using the derived equations. A new single-ended traveling wave-based fault location algorithm which is applicable to all the configurations of the SCCTL is presented in Chapter 7. The basis of the proposed algorithm is explained analytically using derived expressions, and it is verified using the simulations carried out in PSCAD. The summary, conclusions, and future work for the research carried out in this thesis is given in Chapter 8.

1.8 Summary

In this chapter various avenues of increasing the power transmission capacity of the transmission network have been discussed including the series capacitive compensation of the transmission lines. The importance of fault location algorithms for locating faults in transmission lines has also been highlighted. Thereafter, the need for fault location algorithm designed specifically for SCCTLs is explained along with the various challenges faced by such algorithms. Then the broad classification of the existing fault location algorithms for SCCTLs is presented in this chapter. Thereafter, the area of research i.e., the impedance-based and traveling wave-

based fault location algorithms have been identified. The research opportunities and research objectives in the field associated with the fault location in SCCTL have also been presented in this chapter. Then the outline of the presented thesis is given in this chapter.

Chapter 2

Fundamentals and analysis of Impedance-based algorithms and analysis of existing fault location algorithms

2.1 Introduction

The impedance-based fault location algorithms compute the fault location by comparing the seen impedance at the transmission line terminal to the transmission line impedance. The seen impedance at the terminal of the transmission line is calculated using the phasors of the measured current and voltage. Due to the easy availability of phasors from the numerical relays installed in the field, the impedance-based algorithms are the most widely used fault location algorithms. Moreover, the process of phasor estimation attenuates noise and harmonics present in the measured signals, significantly. Thus, making the fault location results obtained from impedance-based algorithms immune to the adverse effects of noise and harmonics [34]. A brief discussion on the most popular phasor estimation techniques DFT, and the Cosine algorithm has been provided in Appendix A.

In this chapter, Section 2.2 discusses the impedance-based fault location algorithms for conventional lines, and the factors preventing their application to the SCCTLs. The fault location algorithm for SCCTLs that utilize the MOV-model for yielding fault location results are discussed in Section 2.3. A detailed analysis of the fault location algorithms based on natural fault loops is presented in Section 2.4. Key features and limitations of the fault loop-based fault location algorithms have been identified in Sections 2.5 and 2.6, respectively. The discussion of the simulations carried out in PSCAD and Matlab are given in Section 2.7.

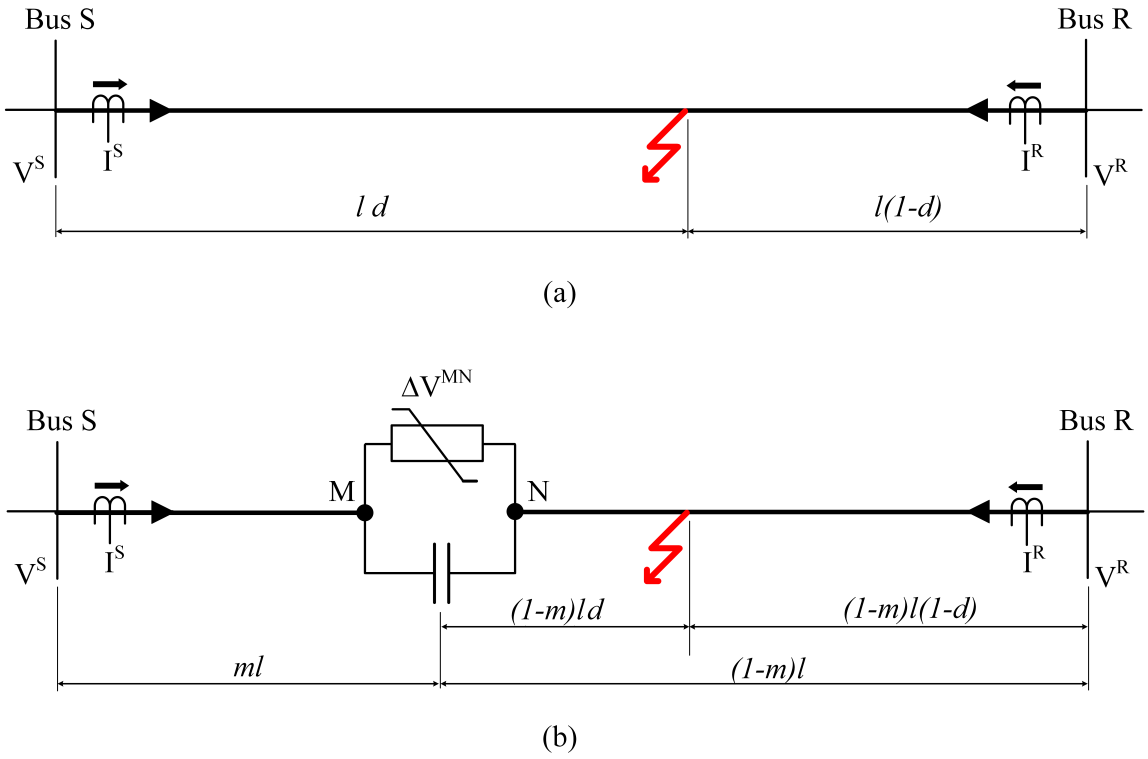

Figure 2.1: Occurrence of a fault in (a) a conventional transmission line, (b) an SCCTL.

2.2 Conventional fault location algorithms and their application to SCCTLs

For the fault scenario in a conventional transmission line as shown in Figure 2.1 (a), the equations for the i^{th} sequence fault voltage (V_i^F) as estimated from Bus S and Bus R could be written as Equations (2.1) and (2.2), respectively.

$$V_i^F = V_i^S \cosh(\gamma_i l d) - Z_{C_i} I_i^S \sinh(\gamma_i l d) \tag{2.1}$$

$$V_i^F = V_i^R \cosh(\gamma_i l(1-d)) - Z_{C_i} I_i^R \sinh(\gamma_i l(1-d)) \tag{2.2}$$

where i attains the value of 0, 1 and 2 for zero, positive, and negative sequence, respectively; V_i^S and I_i^S are the i^{th} sequence sending end voltage and current, respectively; V_i^R and I_i^R are the i^{th} sequence receiving end voltage and current, respectively; Z_{c_i} is the characteristic impedance of the line for i^{th} sequence; γ_i is the propagation constant of the line for i^{th} sequence; l is the length of the transmission line; d is the p.u. distance of the fault from Bus S.

There are two unknowns in Equations (2.1) and (2.2) which are V_i^F and d. By combining Equations (2.1) and (2.2), V_i^F could be eliminated. Thus, yielding the fault location equation

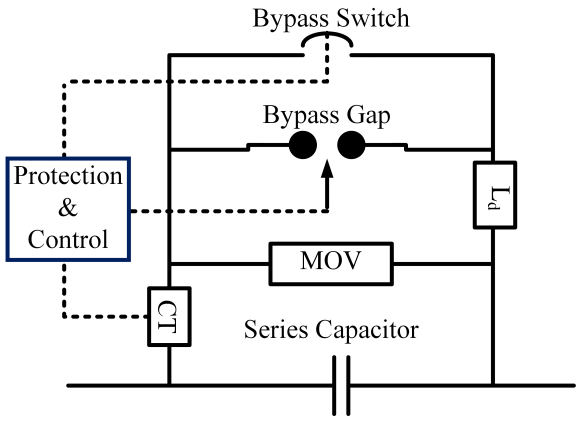

Figure 2.2: SCB: Schematic diagram.

for calculating d as shown in (2.3).

$$d = \frac{1}{\gamma_i l}\tanh^{-1}\left(\frac{V_i^R\cosh(\gamma_i l) - Z_{C_i}I_i^R\sinh(\gamma_i l) - V_i^S}{V_i^R\sinh(\gamma_i l) - Z_{C_i}I_i^R\cosh(\gamma_i l) - Z_{C_i}I_i^S}\right) \tag{2.3}$$

Moving on similar lines the fault location equation for a fault lying in an SCCTL could be written as (2.4) for the fault scenario shown in Figure 2.1 (b).

$$d = \frac{1}{\gamma_i (1-m) l}\tanh^{-1}\left(\frac{V_i^R\cosh((1-m)\gamma_i l) - Z_{C_i}I_i^R\sinh((1-m)\gamma_i l) - V_i^M + \Delta V_i^{MN}}{V_i^R\sinh((1-m)\gamma_i l) - Z_{C_i}I_i^R\cosh((1-m)\gamma_i l) - Z_{C_i}I_i^M}\right) \tag{2.4}$$

where

$$V_i^M = V_i^S\cosh(m\gamma_i l) - I_i^S Z_{C_i}\sinh(m\gamma_i l) \tag{2.5}$$

$$I_i^M = I_i^S\cosh(m\gamma_i l) - \frac{V_i^S}{Z_{C_i}}\sinh(m\gamma_i l) \tag{2.6}$$

V_i^M and I_i^M represent the i^{th} sequence component voltage and current phasors at Node M calculated from Bus S measurements using (2.5) and (2.6), respectively; ΔV_i^{MN} is i^{th} sequence component of the voltage drop across series capacitor bank (SCB) from Node M to Node N; m is the p.u. distance of SCB from Bus S; d is the p.u. distance of the fault as measured from SCB.

Note that d cannot be obtained from (2.4) since the term ΔV_i^{MN} is unknown. The term ΔV_i^{MN} cannot be calculated analytically due to the conduction of the fault current by the metal-oxide varistor (MOV) in the faulted phase which is present as part of the protection system of the SCB as shown in Figure 2.2. An MOV is a non-linear device which starts conducting fault current when the voltage drop across SCB exceeds its threshold value. When MOV conducts,

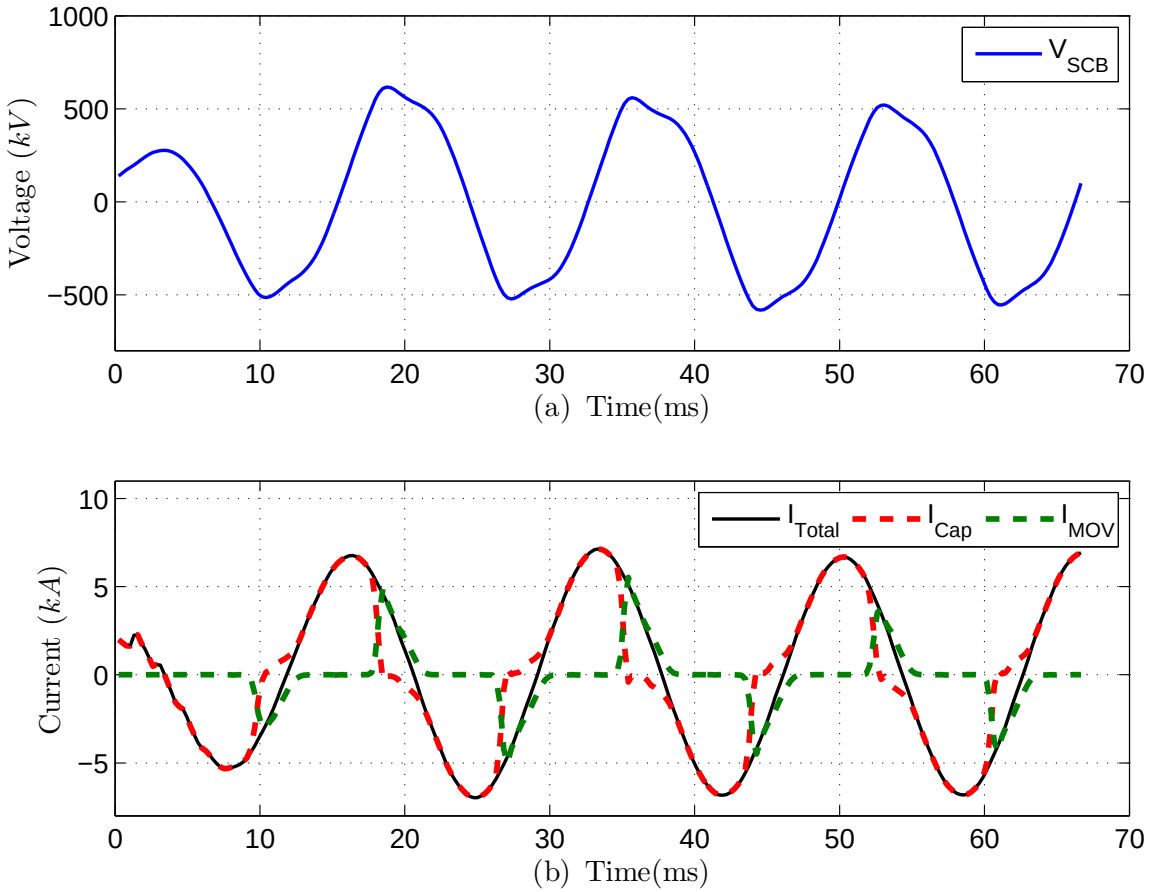

Figure 2.3: Protective action of MOV at fault occurrence: (a) voltage across SCB, (b) current flowing through various series capacitor and MOV in phase A SCB for an AG fault.

the fault current is bypassed from the series capacitor to the MOV as shown in Figure 2.3, therefore, providing the over-voltage protection to series capacitor. However, the action of MOV causes the impedance of SCB in the faulted phase to become non-linear and dependent on the level of fault current, as already discussed in Section 1.2. Hence, the fault location cannot be calculated from Equation (2.4) for an SCCTL. So there arises the need to have fault location algorithms applicable to SCCTL.

However, a significant observation that can be made from Figure 2.3 which is that the total fault current remains sinusoidal while the voltage across SCU though not a perfect sinusoid, still contains great amount of fundamental frequency component. Therefore, it led to the proposition that equivalent impedance for fundamental component can be defined for the parallel combination of series capacitor and MOV [35]. This led to the proposition of the MOV-model based fault location algorithms which aim at providing fault location results by using the equivalent model of the MOV as discussed in the following section.

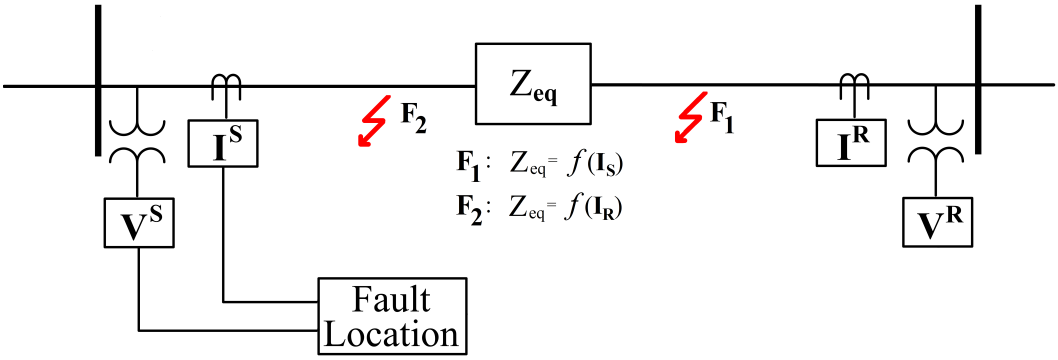

Figure 2.4: Fault Location in SCCTLs: MOV model based.

2.3 MOV-model based fault location algorithms for SCCTLs

An empirical formula for the current dependent equivalent impedance of the parallel combination of series capacitor and MOV has been derived in [35] as represented by (2.7) and (2.8).

$$R^{C'} = X^C \left(0.0745 + 0.49\, e^{-0.243\, I_{pu}} - 35.0\, e^{-5.0\, I_{pu}} - 0.6\, e^{-1.4\, I_{pu}}\right) \tag{2.7}$$

$$X^{C'} = X^C \left(0.1010 - 0.005749\, I_{pu} + 2.088\, e^{-0.8566\, I_{pu}}\right) \tag{2.8}$$

where X^C is the reactance of the series capacitor; $X^{C'}$ and $R^{C'}$ are the equivalent reactance and resistance, respectively, of the parallel combination of MOV and series capacitor; I_{pu} is the per unit current flowing through SCB.

On the similar lines, an attempt has been made in [20] and [21], to predetermine V-I characteristics of MOV for fundamental frequency using ATP-EMTP simulations. It essentially implies the modeling of an MOV as a current dependent impedance which is then used for fault location in SCCTLs using measurements from only one end of the transmission line as shown in Figure 2.4.

However, apart from the challenge of predicting the behavior of MOV for variety of fault scenarios, the algorithms of [20] and [21] are also unable to account for the effects of aging of MOV, ambient temperature and different manufacturer of MOVs on the behavior of MOV. In order to avoid the limitations of using the MOV-model for fault location, the algorithms proposed in [22]-[25] utilized natural fault loops to obtain the fault location results for faults in SCCTLs. As a matter of the fact, most of the commercial relays of today intended for protection of SCCTLs are utilizing the fault loop-based algorithms.

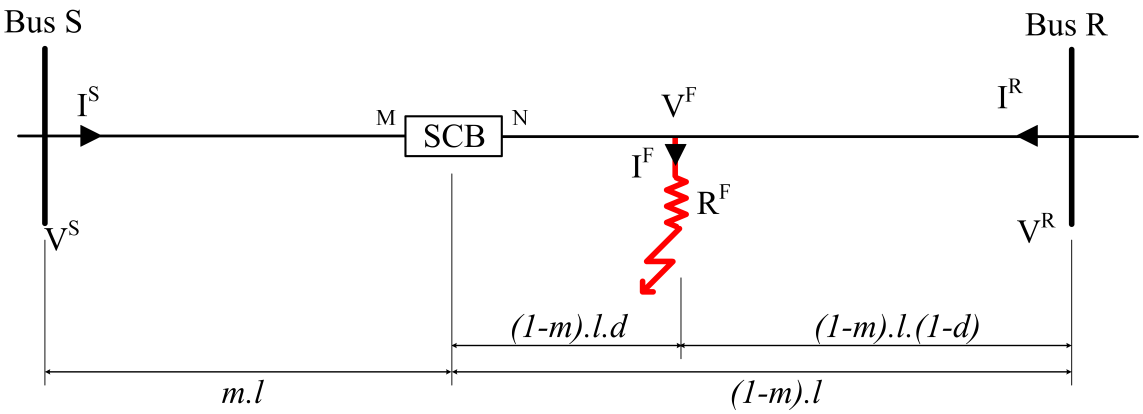

Figure 2.5: Schematic diagram showing the fault scenario in an SCCTL.

2.4 Non-MOV-model or Fault loop-based fault location algorithms for SCCTLs

In fault loop-based fault location algorithms, the equations are written to find the actual phase voltage and current at the fault point in terms of the unknown fault location, instead of computing the fault location from sequence components of voltages and currents [22]. Thereafter, the equations for fault voltage and fault current are solved for the unknown fault location using different constraints mentioned in each publication [22]-[25].

Another point to be noted is that the presence of SCB in an SCCTL divides the transmission line into two sections. For example, in Figure 2.5 SCB divides the transmission line to two sections: section between Bus S and SCB, and section between SCB and Bus R. Any fault occurring in a transmission line could be lying in either of the sections. So, the fault loop-based algorithms use two subroutines for locating the fault with each subroutine yielding one fault location result assuming that fault is lying in 'their' section. The appropriate subroutine is then selected using the procedure given in each publication. It should be noted that the existing fault location algorithms are elaborated using faults lying between SCB and Bus R in this chapter as shown in Figure 2.5. The equations for the faults lying between Bus S and SCB can be derived analogously.

2.4.1 Yu Algorithm

The fault location algorithm of [23] is referred to as "Yu Algorithm" based on the author's name for our reference.

The analytical expressions for obtaining the sequence components of fault voltage and

current in the terms of unknown fault location (d) have been derived in [23] as shown in (2.9) and (2.10), respectively. It can be observed from (2.9) that the expression for the sequence components of fault voltage uses the measured current and voltage only from one end of the transmission line, i.e., Bus R. Equation (2.9) essentially represents the analytical estimation of sequence fault voltage using the distributed transmission line model from measurements at Bus R only. Similarly, the expression for estimating the sequence components of the total fault current is derived as shown in (2.10) using the distributed model of transmission line. It could be observed from (2.10) that the measurements from both ends of the transmission lines, i.e., Bus R, and Bus S, are utilized for estimating sequence components of the total fault.

$$\begin{aligned} V_i^F(d) =& F_V(V_i^R, I_i^R, \gamma_i, Z_{C_i}, d) \\ =& \frac{V_i^R + I_i^R Z_{C_i}}{2} e^{\gamma_i l(1-m)(1-d)} + \frac{V_i^R - I_i^R Z_{C_i}}{2} e^{-\gamma_i l(1-m)(1-d)} \end{aligned} \tag{2.9}$$

$$\begin{aligned} I_i^F(d) =& f_I(V_i^S, I_i^S, V_i^R, I_i^R, \gamma_i, Z_{C_i}, d) \\ =& \frac{1}{Z_{C_i}} \left[\frac{V_i^R + I_i^R Z_{C_i}}{2} e^{\gamma_i l(1-m)(1-d)} - \frac{V_i^R - I_i^R Z_{C_i}}{2} e^{-\gamma_i l(1-m)(1-d)} \right] \\ &+ \frac{1}{Z_{C_i}} \left[\frac{V_i^S + I_i^S Z_{C_i}}{2\, e^{\gamma_i l}} e^{\gamma_i l(1-m)(1-d)} - \frac{V_i^S - I_i^S Z_{C_i}}{2\, e^{\gamma_i l}} e^{-\gamma_i l(1-m)(1-d)} \right] \end{aligned} \tag{2.10}$$

Now the expressions for fault voltage (V^F) and fault current (I^F) are obtained by combining the sequence components of fault voltage and current from (2.9), and (2.10), respectively, as per the type of the fault that has occurred in the SCCTL. The expressions so obtained for V^F and I^F are then solved for d under the assumption that the argument of the current and voltage will be same at the fault point as depicted in (2.11).

$$\angle V^F(d) = \angle I^F(d) \tag{2.11}$$

Since, V^F and I^F can be separated into real and imaginary parts:

$$\begin{aligned} V^F(d) =& \Re\left(V^F(d)\right) + j\, \Im\left(V^F(d)\right) \\ I^F(d) =& \Re\left(I^F(d)\right) + j\, \Im\left(I^F(d)\right) \end{aligned}$$

and the Equation (2.11) could be rewritten as:

$$\begin{aligned} \frac{\Im\left(V^F(d)\right)}{\Re\left(V^F(d)\right)} =& \frac{\Im\left(I^F(d)\right)}{\Re\left(I^F(d)\right)} \\ \implies \Im\left(V^F(d)\right) \times \Re\left(I^F(d)\right) =& \Im\left(I^F(d)\right) \times \Re\left(V^F(d)\right) \end{aligned} \tag{2.12}$$

Now, d could be calculated from the Equation (2.12).

Selection of the subroutine

Two subroutines i.e. Subroutine1 and Subroutine2 of Yu Algorithm are run for any particular fault scenario, therefore, yielding two fault location results for each fault scenario. It necessitates a criterion to select the appropriate subroutine which would yield the actual fault location. In [23], it is claimed that for some of the fault scenarios, the fault location results obtained through the incorrect subroutine will be highly oscillatory and may not converge. For obtaining a definite solution to this problem, it is presented in [23] to calculate the equivalent impedance of the faulted phase SCB by using the fault location results yielded by both subroutines. The equivalent impedance of the faulted phase SCB for Subroutine 1 (Z_{SUB1}) is calculated by estimating the voltage drop across SCB corresponding to fault location result yielded by Subroutine 1 (ΔV_{SUB1}) and dividing it by sending end current (I^S) as shown in (2.13).

$$Z_{\text{SUB1}} = \frac{\Delta V_{\text{SUB1}}}{I^S} \tag{2.13}$$

Similarly, the impedance of the faulted phase SCB for the Subroutine 2 (Z_{SUB2}) is calculated by dividing voltage drop across SCB corresponding to the Subroutine 2 with the receiving end current (I^R).

$$Z_{\text{SUB2}} = \frac{\Delta V_{\text{SUB2}}}{I^R} \tag{2.14}$$

It is claimed in [23] that the resistive part of the impedance yielded by the correct subroutine would be positive while the incorrect subroutine would yield a negative resistive part for the equivalent impedance of the faulted phase SCB. In other words, for the faults lying in the region between SCB and Bus R the following would hold true:

$$\Re\left(Z_{\text{SUB1}}\right) : +ve$$
$$\Re\left(Z_{\text{SUB2}}\right) : -ve$$

while for the faults lying in the region between Bus S and SCB following would hold true:

$$\Re\left(Z_{\text{SUB1}}\right) : -ve$$
$$\Re\left(Z_{\text{SUB2}}\right) : +ve.$$

Table 2.1: Coefficients for finding total fault current for Izykowski Algorithm.

Fault Type	a_1	a_2	a_0
AG	0	3	0
BCG	$\alpha^2 - \alpha$	$\alpha - \alpha^2$	0
BC	0	$\alpha - \alpha^2$	0
ABC	$1 - \alpha^2$	0	0
$\alpha = 1\angle 120^\circ$			

2.4.2 Izykowski Algorithm

Another fault loop-based fault location algorithm for SCCTLs has been presented in [22] which has also been patented in [36]. It has been referred to as "Izykowski Algorithm" using the name of the first author for our reference. In [22] the authors have derived the expressions for analytical estimation of fault current (I^F) and fault voltage (V^F) as the functions of fault location. The analytically obtained expressions are then solved for fault location under the assumption that faults in transmission lines are purely resistive in nature.

Equations (2.15) and (2.16) represent the fault current and voltage, respectively, for the fault lying between SCB and Bus R at per unit distance of d from SCB, as shown in Figure 2.5.

$$I^F(d) = \sum_{i=0}^{2} a_i \frac{I_i^S \cosh(\gamma_i lm) - \frac{V_i^S}{Z_{C_i}} \sinh(\gamma_i lm) + I_i^R \cosh(\gamma_i l(1-m)) - \frac{V_i^R}{Z_{C_i}} \sinh(\gamma_i l(1-m))}{\cosh(\gamma_i l(1-m)d)} \tag{2.15}$$

$$V^F(d) = \sum_{i=0}^{2} af_i \left[V_i^R \cosh(\gamma_i l(1-d)(1-m)) - Z_{C_i} I_i^R \sinh(\gamma_i l(1-d)(1-m)) \right] \tag{2.16}$$

where a_i and af_i are the coefficients for calculating total fault current and fault loop voltage, respectively, and attain different values depending upon the fault type as represented in Tables (2.1) and (2.2).

The expressions so obtained for I^F and V^F in (2.15) and (2.16) are substituted in the fault loop model given in (2.17). The Equation (2.17) is then solved under the constraint that the faults in a transmission lines are always resistive in nature i.e., R^F is a pure real number.

$$V^F(d) - R^F I^F(d) = 0 \tag{2.17}$$

Table 2.2: Coefficients for finding fault loop voltage for Izykowski Algorithm.

Fault Type	af_1	af_2	af_0
AG	1	1	1
BCG	$\alpha^2 - \alpha$	$\alpha - \alpha^2$	0
BC	$\alpha^2 - \alpha$	$\alpha - \alpha^2$	0
ABC	$1 - \alpha^2$	0	0
$\alpha = 1\angle 120°$			

Selection of the subroutine

Now, the other area where the authors have focused their attention is how to identify the faulted section of the line as any fault event can be thought of lying in the region between Bus S and SCB or between SCB and Bus R. It is proposed in [22] that for any particular fault scenario both of the subroutines be run, therefore, yielding two fault location results. In order to find the correct fault location, firstly, the subroutine yielding results lying outside the section range or the negative value of fault location is rejected. Thereafter, the equivalent impedance of the SCB in the faulted phase is calculated using the voltage drop across SCB and the fault current through SCB for both the subroutines. The equivalent impedance of SCB corresponding to the valid subroutine has to be resistive-capacitive in nature due to the presence of MOV and series capacitor in the transmission line. Also, the capacitive part of the SCB impedance in the faulted should be less than or equal to the reactance of the series capacitor at the steady state [22].

2.4.3 Kang Algorithm

A fault loop-based fault location algorithm for double-circuited SCCTLs has been presented in [24]. The expressions for the i^{th} sequence of the fault voltage (V_i^F) and the total fault current (I_i^F) are derived as functions of unknown fault location (d). Thereafter, d is solved using fault location equations which are composed of different combinations of V_i^F and I_i^F depending upon the fault type.

For the faults lying in the section between SCB and Bus R for a single-circuited SCCTL,

the expressions for I_i^F and V_i^F become (2.18) and (2.19):

$$I_i^F = \frac{I_i^S \cosh(\gamma_i lm) - \frac{V_i^S}{Z_{C_i}} \sinh(\gamma_i lm) + I_i^R \cosh(\gamma_i l(1-m)) - \frac{V_i^R}{Z_{C_i}} \sinh(\gamma_i l(1-m))}{\cosh(\gamma_i l(1-m)d)} \tag{2.18}$$

$$V_i^F = V_i^R \cosh(\gamma_i l(1-d)(1-m)) - Z_{C_i} I_i^R \sinh(\gamma_i l(1-d)(1-m)) \tag{2.19}$$

It could be observed that the expressions for V_i^F and I_i^F derived in [24] are identical to the ones derived in [22]. Once the expressions for V_i^F and I_i^F are obtained, fault location equations comprising of different combination of sequence components are solved for d.

- **AG Faults**:
  For AG faults, d is obtained by solving the equation:

$$\Im\left(\frac{V_0^F(d) + V_1^F(d) + V_2^F(d)}{I_1^F(d)}\right) = 0 \tag{2.20}$$

- **BCG Faults**:
  The fault location equation for BCG faults is:

$$\Im\left(\frac{V_0^F(d) - V_1^F(d)}{I_0^F(d)}\right) = 0 \tag{2.21}$$

- **BC Faults**:
  For BC faults, d is obtained by solving the following equation:

$$\Im\left(\frac{V_1^F(d) - V_2^F(d)}{I_1^F(d)}\right) = 0 \tag{2.22}$$

- **ABC Faults**:
  For ABC faults, d is obtained by solving the equation:

$$\Im\left(\frac{V_1^F(d)}{I_1^F(d)}\right) = 0 \tag{2.23}$$

Selection of the subroutine

The authors of [24] have suggested using following metrics for selecting the correct subroutine:

1. The fault location estimate should lie within the assumed range.
2. The fault resistance takes a non-negative value.

3. The equivalent impedances of the series compensation device for all three phases have a non-negative real part and negative imaginary part.

2.4.4 Zhang Algorithm

The analytical expressions for sequence components of fault voltage (V_i^F) and fault current (I_i^F) in terms of d are derived in [25] for double-circuited series compensated line. A "six-sequence component method" is utilized in [25], and a fault location applicable to all fault types is derived and solved for d. It should be noted that for a single-circuited transmission line (which is the case under consideration) the six-sequence component method becomes traditional sequence component method.

For the faults lying in the section between SCB and Bus R for a single-circuited SCCTL, the expressions for I_i^F and V_i^F become (2.24) and (2.25):

$$I_i^F = \frac{I_i^S \cosh(\gamma_i lm) - \frac{V_i^S}{Z_{C_i}} \sinh(\gamma_i lm) + I_i^R \cosh(\gamma_i l(1-m)) - \frac{V_i^R}{Z_{C_i}} \sinh(\gamma_i l(1-m))}{\cosh(\gamma_i l(1-m)d)} \tag{2.24}$$

$$V_i^F = V_i^R \cosh(\gamma_i l(1-d)(1-m)) - Z_{C_i} I_i^R \sinh(\gamma_i l(1-d)(1-m)) \tag{2.25}$$

The fault location equation for Zhang algorithm which would yield d is:

$$\Im\left(\overline{V_A^F(d)} I_A^F(d) + \overline{V_B^F(d)} I_B^F(d) + \overline{V_C^F(d)} I_C^F(d)\right) = 0 \tag{2.26}$$

where, $\overline{V_i^F}$, represents the conjugate of the phasor quantity.

$$\begin{bmatrix} \overline{V_A^F(d)} \\ \overline{V_B^F(d)} \\ \overline{V_C^F(d)} \end{bmatrix} = \begin{bmatrix} 1 & 1 & 1 \\ 1 & \alpha & \alpha^2 \\ 1 & \alpha^2 & \alpha \end{bmatrix} \begin{bmatrix} \overline{V_0^F(d)} \\ \overline{V_1^F(d)} \\ \overline{V_2^F(d)} \end{bmatrix}$$

$$\begin{bmatrix} I_A^F(d) \\ I_B^F(d) \\ I_C^F(d) \end{bmatrix} = \begin{bmatrix} 1 & 1 & 1 \\ 1 & \alpha^2 & \alpha \\ 1 & \alpha & \alpha^2 \end{bmatrix} \begin{bmatrix} I_0^F(d) \\ I_1^F(d) \\ I_2^F(d) \end{bmatrix}$$

Selection of the subroutine

The authors of [25] infer that when one subroutine will have a solution, the other subroutine would have no solution. There is no need to select the appropriate subroutine, since, only one subroutine yields the fault location.

2.5 Key Observation: Equivalence of the fault loop-based fault location algorithms

It could be witnessed from the above discussion that the expressions for V^F and I^F in each algorithm are very similar to each other. It should be noted that all the fault loop-based algorithms discussed above except Yu algorithm, are proposed for double-circuited SCCTLs. The difference in the expressions of each algorithm lies in the fact that how each algorithm 'handles' the mutual zero-sequence coupling between the parallel or double-circuited lines. However, when we are considering a single circuit SCCTL, that difference goes away and we are left with the identical expressions.

In this section, it is shown through brief mathematical analysis that the basic principle of the algorithms presented in [22]-[25] is also equivalent to each other.

- **Yu Algorithm:** In Yu algorithm, after the expressions for V^F and I^F in terms of the unknown d are obtained, they are solved for d using the fact that at the fault point the angle of fault voltage and fault current would be same, i.e.,

$$\angle V^F(d) = \angle I^F(d) \tag{2.27}$$

- **Izykowski Algorithm:** In [22], the expressions for V^F and I^F are substituted in (2.28).

$$V^F(d) - R^F I^F(d) = 0 \tag{2.28}$$

The methodology for solving (2.28) as presented in [22] is to separate it into real and imaginary parts (see (2.29)) and solve for fault resistance (R^F) and fault location (d).

$$\begin{aligned} \Re\left(V^F(d)\right) - R^F \Re\left(I^F(d)\right) = 0 \\ \Im\left(V^F(d)\right) - R^F \Im\left(I^F(d)\right) = 0 \end{aligned} \tag{2.29}$$

The set of equations in (2.29) when rearranged results in (2.30), which shows that the way of solving the Equation (2.28) by separating it into real and imaginary parts essentially makes the fault location algorithm presented in [22], an argument comparison algorithm which compares the arguments of analytically obtained fault voltage (V^F) and

fault current (I^F).

$$\frac{\Im\left(V^F(d)\right)}{\Re\left(V^F(d)\right)} = \frac{\Im\left(I^F(d)\right)}{\Re\left(I^F(d)\right)}$$
$$\implies \tan^{-1}\left(\frac{\Im\left(V^F(d)\right)}{\Re\left(V^F(d)\right)}\right) = \tan^{-1}\left(\frac{\Im\left(I^F(d)\right)}{\Re\left(I^F(d)\right)}\right)$$
$$\implies \angle V^F(d) = \angle I^F(d) \tag{2.30}$$

- **Kang Algorithm:** Following given relations are known facts for their respective fault types:

$$\begin{aligned}
\text{AG Fault:} \quad & V^F = V_0^F + V_1^F + V_2^F \\
& I^F = 3I_1^F \\
\text{BCG Fault:} \quad & V^F = V_0^F - V_1^F \\
& I^F = 3I_0^F \\
\text{BC Fault:} \quad & V^F = \left(\alpha^2 - \alpha\right)\left(V_1^F - V_2^F\right) \\
& I^F = \left(\alpha^2 - \alpha\right) I_1^F \\
\text{ABC Fault:} \quad & V^F = V_1^F \\
& I^F = I_1^F
\end{aligned}$$

When the fault Equations (2.20) to (2.23) are seen in lieu of the above facts one thing becomes clear that the Equations (2.20) to (2.23) depending upon the fault type are different forms of the Equation (2.31).

$$\Im\left(\frac{V^F(d)}{I^F(d)}\right) = 0 \tag{2.31}$$

Now multiplying denominator and numerator in the Equation (2.31) with the conjugate of I^F, i.e., $\overline{I^F}$ we get:

$$\Im\left(\frac{V^F(d)\overline{I^F(d)}}{I^F(d)\overline{I^F(d)}}\right) = 0$$
$$\implies \Im\left(V^F(d)\overline{I^F(d)}\right) = 0$$

Expanding the above equation:

$$\begin{aligned}
&\Im\left(V^F(d)\right)\Re\left(I^F(d)\right) - \Re\left(V^F(d)\right)\Im\left(I^F(d)\right) = 0 \\
&\implies \frac{\Im\left(V^F(d)\right)}{\Re\left(V^F(d)\right)} = \frac{\Im\left(I^F(d)\right)}{\Re\left(I^F(d)\right)} \\
&\implies \tan^{-1}\left(\frac{\Im\left(V^F(d)\right)}{\Re\left(V^F(d)\right)}\right) = \tan^{-1}\left(\frac{\Im\left(I^F(d)\right)}{\Re\left(I^F(d)\right)}\right) \\
&\implies \angle V^F(d) = \angle I^F(d)
\end{aligned} \tag{2.32}$$

Thus, the fault location algorithm presented in [24], i.e., Kang algorithm is based on the argument comparison of the analytically obtained fault voltage and fault current phasors.

- **Zhang Algorithm:** The fault location equation given in [25], i.e., Zhang algorithm is:

$$\Im\left(\overline{V_A^F(d)}I_A^F(d) + \overline{V_B^F(d)}I_B^F(d) + \overline{V_C^F(d)}I_C^F(d)\right) = 0 \tag{2.33}$$

The fault location Equation (2.33) takes following forms for different types of fault.

AG Fault:	$V^F = V_A^F$	$I^F = I_A^F$	$I_B^F = I_C^F = 0$
Fault Location Eq:	$\Im\left(\overline{V^F(d)}I^F(d)\right) = 0$		
BCG Fault:	$V^F = V_B^F = V_C^F$	$I^F = I_B^F + I_C^F$	$I_A^F = 0$
Fault Location Eq:	$\Im\left(\overline{V^F(d)}I^F(d)\right) = 0$		
BC Fault:	$V^F = V_B^F - V_C^F$	$I^F = I_B^F = -I_C^F$	$I_A^F = 0$
Fault Location Eq:	$\Im\left(\overline{V^F(d)}I^F(d)\right) = 0$		
ABC Fault:	$V^F = V_A^F = V_B^F = V_C^F$	$I^F = I_A^F + I_B^F + I_C^F$	
Fault Location Eq:	$\Im\left(\overline{V^F(d)}I^F(d)\right) = 0$		

It is seen from above discussion that for each fault type, the fault location equation becomes:

$$\Im\left(\overline{V^F(d)}I^F(d)\right) = 0$$

Now expanding the above equation:

$$\begin{aligned}
&\Re\left(V^F(d)\right)\Im\left(I^F(d)\right) - \Im\left(V^F(d)\right)\Re\left(I^F(d)\right) = 0 \\
&\implies \frac{\Im\left(V^F(d)\right)}{\Re\left(V^F(d)\right)} = \frac{\Im\left(I^F(d)\right)}{\Re\left(I^F(d)\right)} \\
&\implies \tan^{-1}\left(\frac{\Im\left(V^F(d)\right)}{\Re\left(V^F(d)\right)}\right) = \tan^{-1}\left(\frac{\Im\left(I^F(d)\right)}{\Re\left(I^F(d)\right)}\right) \\
&\implies \angle V^F(d) = \angle I^F(d)
\end{aligned} \tag{2.34}$$

The Equations (2.27), (2.30), (2.32), and (2.34) show that underlying principle of algorithms presented in [22]-[25] is same. The fault location algorithms proposed in [22]-[25] for SC-CTLs, estimate the arguments of fault voltage (V^F) and fault current (I^F) as the function of fault location (d). Thereafter, the value of d for which the arguments of both the analytically estimated quantities (V^F and I^F) match, is considered as fault location result. Therefore, only the algorithm presented in [22] which is one of the most widely cited algorithm is used here-after to elaborate further on the fault loop-based fault location algorithms.

2.6 Limitation of the fault loop-based algorithms for SCCTLs

For the fault scenario shown in Figure 2.5, the expressions for I^F and V^F as per [22] are given in (2.35) and (2.36), respectively.

$$I^F(d) = \sum_{i=0}^{2} a_i \frac{I_i^S \cosh(\gamma_i lm) - \frac{V_i^S}{Z_{C_i}}\sinh(\gamma_i lm) + I_i^R \cosh(\gamma_i l(1-m)) - \frac{V_i^R}{Z_{C_i}}\sinh(\gamma_i l(1-m))}{\cosh(\gamma_i l(1-m)d)} \tag{2.35}$$

$$V^F(d) = \sum_{i=0}^{2} af_i \left[V_i^R \cosh(\gamma_i l(1-d)(1-m)) - Z_{C_i} I_i^R \sinh(\gamma_i l(1-d)(1-m))\right] \tag{2.36}$$

It is worth noting that the only term that contains d in (2.35) is the denominator, which is $\cosh(\gamma_i l(1-m)d)$, where γ_i represents the propagation constant of the line for i^{th} sequence and is a complex number with relatively a large imaginary part as compared to its real part. Therefore, γ_i can be represented as jk_i, where k_i is a real number and $j = \sqrt{-1}$. Consequently,

the denominator of (2.35) becomes:

$$\begin{aligned} D_n &= \cosh(j k_i l(1-m)d) \\ &= \frac{e^{j k_i l(1-m)d} + e^{-j k_i l(1-m)d}}{2} \\ \implies D_n &= \cos(k_i l(1-m)d) \end{aligned} \tag{2.37}$$

which shows that D_n is a real number. As we know that the argument of real number is zero, therefore, $\angle D_n = 0$. The fact that $\angle D_n = 0$ implies that the argument of $I^F(d)$ will be equal to the argument of the numerator of (2.35), which is independent of d. In other words, for any value of d between 0 and 1 'plugged' in (2.35), the argument of $I^F(d)$ would not change and remain constant. It is so because the argument of the $I^F(d)$ will be the argument of the numerator of (2.35). The value of denominator and, consequently, the value of d only acts as a scaling factor for the magnitude of I^F.

So, now only V^F remains a function of d as seen from (2.36). The process of fault location, thus, gets reduced to the following: The Equation (2.36) 'scans' the transmission line from Bus R to SCB and the value of d where the argument of $V^F(d)$ matches the constant argument of I^F is yielded as the location of fault. This process would yield high error in the fault location results if the argument of V^R is very close to the argument of I^F (and consequently, V^F). It is due to the fact that if the argument of V^R and V^F are close then a very narrow band of the argument variation stretches over the section between Bus R and the fault point; and any error in the measurements or phasor estimation will result in an amplified error in the fault location result d. Hence, under some circumstances even Equation (2.36) becomes insensitive to the value of d. This source of error is intrinsic to the fault location algorithms that are based on the comparison of arguments of current and voltage.

2.7 Evaluation of the fault loop-based fault location algorithms

In order to evaluate the performance of the fault loop-based algorithms, a test power system is simulated in PSCAD while fault location algorithm is implemented in Matlab. The Cosine algorithm is the phasor estimation technique utilized for obtaining phasors in the presented analysis to take care of decaying DC.

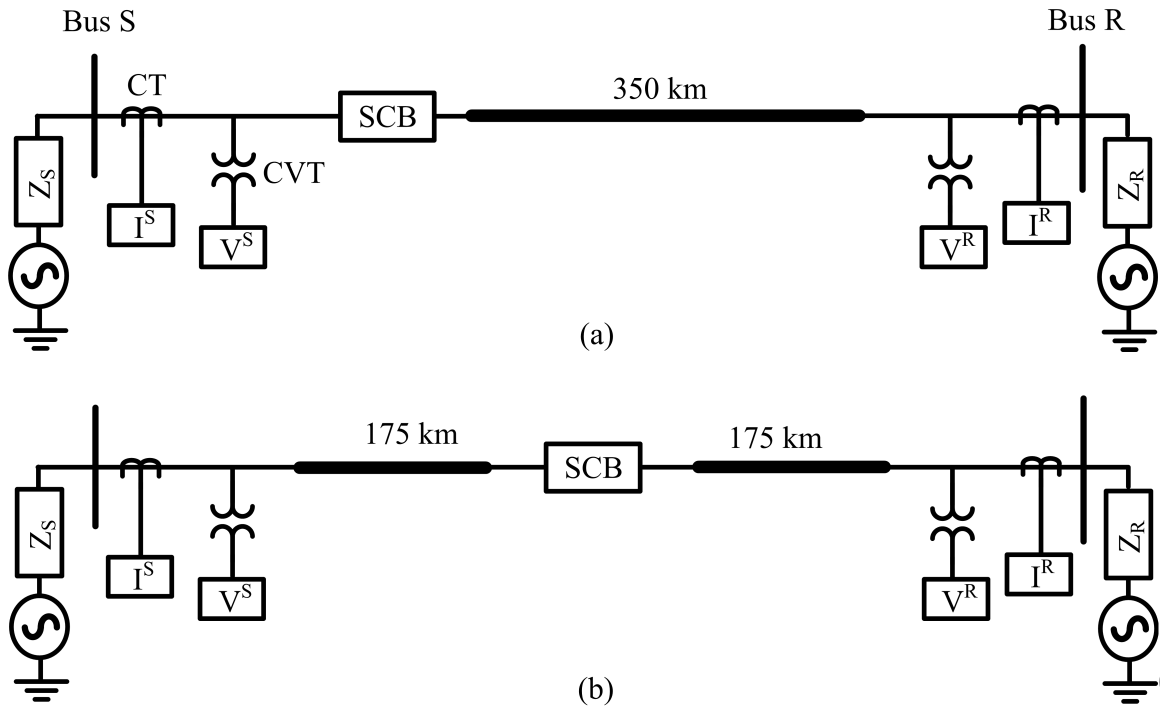

Figure 2.6: Single-line diagram of simulated system in PSCAD; (a) System A, (b) System B.

2.7.1 Test System

A 500 kV, 350 km SCCTL simulated in PSCAD is considered as a test case in this thesis. To simulate the transmission line, a frequency-dependent model of transmission line available in PSCAD is utilized. As shown in Figure 2.6, 70% series compensation which corresponds to an equivalent capacitance of 29.11μF (91.1Ω) is assumed at the sending end of the line for System A and in the middle of the line for System B. The line positive and zero-sequence impedances are $Z_{L1} = (0.0155 + j0.3719)\ \Omega$ per km and $Z_{L0} = (0.3546 + j1.0670)\ \Omega$ per km, respectively. The line positive and zero-sequence admittances are $Y_{L1} = (0 + j4.4099 \times 10^{-6})\ S$ per km, $Y_{L0} = (0 + j2.7844 \times 10^{-6})\ S$ per km, respectively. The positive and zero-sequence impedances for sending end source are $Z_{S1} = (0.5 + j7.5)\ \Omega$ and $Z_{S0} = (1.2 + j12.5)\ \Omega$, respectively. The positive and zero-sequence impedances for receiving end source are $Z_{R1} = (1.2 + j18)\ \Omega$ and $Z_{R0} = (2.6 + j26.5)\ \Omega$, respectively. Load angle is 30° with receiving end source voltage lagging.

Further, current and voltage signals are obtained by using CT and CVT models, respectively, available in PSCAD. A 4^{th} order anti-aliasing filter with a cutoff frequency of 1536 Hz is applied to the output of each instrument transformer, and its output is recorded with the sampling rate of 20 kHz. The recorded signal is then imported to Matlab and downsampled to 3840 Hz. In order to avoid aliasing, the frequencies higher than 1920 Hz need to be sufficiently attenuated before sampling, and that is the reason behind the use of anti-aliasing filter with a

cut-off frequency of 1536 Hz at the output of instrument transformers. The resultant voltage and current signals are then applied to the Cosine algorithm for phasor estimation, the results of which are fed to the fault location algorithm. The fault location algorithm yields a fault location result at every sampled point. However, one value for a fault location result is obtained by averaging fault location results over the entire time period of fault after accounting for Cosine filter response time (=20.83ms). The fault clearance time (total time from fault inception to fault clearance) is considered as 4 cycles of 60Hz.

2.7.2 Simulation results

Most of the algorithms found in literature have been tested on the system when SCB is located in the middle of the transmission line assuming that it is more general configuration of the SCCTLs such as the System B shown in Figure 2.6 (b). However, any fault in System B is located at 50% or greater length of the transmission line from the bus that sees the same fault current as flowing through SCB. For example any fault lying in between SCB and Bus R in System B configuration would lie at least 50% or higher line length away from Bus S which is the bus that sees the same fault current as SCB. In the same way, any fault that lies between Bus S and SCB will lie at least 50% or greater line length away from Bus R which is the bus that sees the same fault current as SCB. Hence, the faults in the range of 0-50% of the line length from the bus which will see the same fault current as SCB, are not possible in System B configuration of an SCCTL. On the other hand, the faults in System A lying between 0-50% of the transmission line length as measured from Bus S will always lie less than 50% of the transmission line length away from the Bus S. Thus, System A offers more varied fault conditions as compared to System B. Moreover, higher amount of transients will be encountered in measured signals in System A as compared to System B due to the proximity of the faults to the source seen through series capacitor, which in turn could affect the accuracy of the fault location results in System A configuration of SCCTL.

Table 2.3 shows the fault location results obtained from Izykowski Algorithm for the various types of solid faults simulated in System A and System B configurations of the SCCTL. It could be observed that the maximum error encountered in System B configuration is 4.71% while it is 24.1% in System A. Also for almost all of the fault scenarios, the error in System B remains below 2% while the numerous fault scenarios in System A lead to an error higher than 2%.

Another observation that could be made from Table 2.3 is that that as the fault moves from 100% towards 50%, the error in fault location results keep on increasing in System A as well as System B. However, as the fault moves from 50% to 0% the error in System A keeps on

Table 2.3: Error (%) in fault location results obtained from Izykowski Algorithm for various solid faults in System A and System B configurations of the SCCTL.

Fault Type	System Type	Actual Fault Location (%)										
		0	10	20	30	40	50	60	70	80	90	100
AG	A	2.53	3.90	5.28	24.1	11.5	5.00	2.71	1.51	0.73	0.29	0.01
	B	0.02	0.19	0.42	0.79	1.25	4.71	2.57	1.46	0.76	0.31	0.01
BCG	A	0.05	0.02	0.03	0.04	6.95	2.43	1.21	0.62	0.30	0.12	0.05
	B	0.04	0.01	0.04	0.09	0.21	2.20	1.14	0.60	0.29	0.12	0.05
BC	A	0.04	0.02	0.02	4.58	1.89	1.04	0.59	0.31	0.15	0.05	0.04
	B	0.04	0.01	0.04	0.09	0.22	2.34	1.18	0.61	0.29	0.12	0.05
ABC	A	0.04	0.04	9.30	2.81	1.53	0.92	0.56	0.31	0.17	0.08	0.05
	B	0.04	0.03	0.05	0.10	0.19	1.95	1.07	0.58	0.30	0.13	0.04

growing until it reaches its maximum for the faults lying around 20%-40%, while in System B, the error keeps on decreasing as the fault location moves from 50% to 0%. The reason behind this divergence in error in fault location results of System A and System B is that due to the location of the SCU in the middle of the SCCTL in System B the faults in 0%-50% range are almost equivalent to the faults lying in 50-100% range. Therefore, the error peaks for the faults lying at 50% line length in System B. While in System A as the fault location moves from 100% towards 0% the severity of fault keeps on increasing until it reaches its maximum for the faults located in the range 20%-40%. As explained earlier, the faults lying in the range 0%-50% in System A are not possible in System B. In the existing fault loop-based algorithms, only System B configuration of the SCCTLs has been studied, thus, the loss of accuracy of fault loop-based algorithms for System A was not discovered. However, as shown in Figure 1.4 most of the transmission lines in Hydro-Quebec system are of System A type. Thus, System A has been selected to elaborate the key points about the performance of the fault loop-based algorithms hereafter.

A total of 176 cases of the fault scenarios covering different fault types, fault resistance, and locations of fault in System A have been generated in PSCAD. The error in the fault location result for each fault scenario has been listed in Table 2.4. It is important to note here that the error in fault location results not higher than 2% is generally accepted limit. However, in Table 2.4 only the fault scenarios for which the fault loop-based algorithm yields higher than 5% error have been highlighted. A 5% error in 350 km transmission line translates into the uncertainty of 17.5 km in location of fault in the transmission line.

It could be noted from Table 2.4 that the error in the fault location results is higher than 2% for almost half of the cases. The number of fault cases in which error is higher than 5% are also significant. Another observation that can be made from Table 2.4 is that that for the

Table 2.4: Error (%) in fault location results obtained from Izykowski Algorithm for different fault scenarios in System A configuration of the SCCTL.

Fault Resist.	Fault Type	Actual Fault Location (%)										
		0	10	20	30	40	50	60	70	80	90	100
0Ω	AG	2.53	3.90	5.28	24.1	11.5	5.00	2.71	1.51	0.73	0.29	0.01
	BCG	0.05	0.02	0.03	0.04	6.95	2.43	1.21	0.62	0.30	0.12	0.05
	BC	0.04	0.02	0.02	4.58	1.89	1.04	0.59	0.31	0.15	0.05	0.04
	ABC	0.04	0.04	9.30	2.81	1.53	0.92	0.56	0.31	0.17	0.08	0.05
10Ω	AG	0.78	3.51	6.85	16.5	24.6	7.26	3.32	1.69	0.81	0.30	0.01
	BCG	2.23	0.13	1.01	2.24	7.18	5.49	1.51	0.66	0.31	0.13	0.03
	BC	1.99	0.76	1.09	3.22	10.3	3.52	1.34	0.62	0.29	0.11	0.04
	ABC	2.40	0.19	1.33	3.19	17.3	3.88	1.45	0.67	0.31	0.12	0.02
50Ω	AG	6.86	3.14	3.52	13.3	25.0	34.5	50.7	28.6	17.0	8.59	4.07
	BCG	8.36	5.81	2.55	1.95	8.29	17.3	29.7	44.3	56.0	40.6	13.1
	BC	4.89	3.83	0.33	5.52	12.4	18.4	38.6	19.0	13.8	8.04	3.36
	ABC	8.12	5.57	1.87	3.09	9.77	18.7	30.0	41.5	47.8	37.5	13.3
100Ω	AG	22.6	18.1	11.4	2.08	12.1	35.4	48.2	34.0	26.5	74.1	36.2
	BCG	22.7	19.3	15.4	11.0	5.93	0.34	8.41	20.8	70.9	36.8	34.3
	BC	14.3	12.1	7.72	0.04	10.6	25.3	45.3	69.7	67.8	72.8	27.2
	ABC	22.2	18.3	13.6	8.34	2.13	5.37	14.8	28.8	72.7	39.3	36.2

low impedance faults (fault resistance of 0Ω and 10Ω) the Izykowski Algorithm suddenly loses the accuracy when the location of the fault in an SCCTL is closer to 40% of the line length as measured from Bus S. For example, for 10Ω AG, BCG, BC, and ABC faults occurring at 40% of the line length as measured from Bus S, the errors in the fault location results are 24.5%, 7.18%, 10.3%, and 17.3%, respectively. As the fault resistance increases, the area in which the Izykowski algorithm loses accuracy also increases, eventually covering the entire transmission line when the fault resistance reaches 100Ω. To understand the reason behind this sudden loss of accuracy of the Izykowski Algorithm it is important to remember the working principle of the fault loop-based algorithms as explained in Section 2.6 which states that the fault loop-based algorithms 'scan' the section of transmission line between Bus R and the fault point using Bus R measurements (see Equation (2.36)), and yield that value of d as fault location for which the argument of fault current and fault voltage become equal. Now for the faults lying at 40% consider the following two factors in lieu of the working principle of the fault loop-based algorithms. Note that Figure 2.7 shows the various phasor quantities and calculated fault location by Izykowski Algorithm for a solid AG fault at 40% line length measured from Bus S.

1. **Condition 1:** When the fault is located close to 40%, the SCB is almost completely compensating for the combined inductance of the source and the faulted transmission line segment (series compensation is effectively reduced from 70% due to MOV conduction). Thus, resulting in a very high and almost resistive fault current contribution from Bus S as compared to the fault current contribution from Bus R. It could be observed from Figure 2.7 (a) that the fault current contribution from Bus S side (I^S) is more than 3 times higher than that from the Bus R (I^R). The fault current from Bus S will now form predominant part of the total fault current at the fault point, and it along with the total fault current will be very close in phase with the Bus S voltage (and consequently with voltage at Bus R which lags Bus S by 30°). Since, the faults are assumed to be purely resistive in nature, therefore, the voltage at the fault point will be very close in phase with the Bus R voltage. This phenomenon could be observed from Figure 2.7 (b) which shows that the phase angles of the Bus S voltage (V^S), Bus R voltage (V^R), total fault current or fault voltage (I^F/V^F) are very close to each other while the argument of Bus R current lies far away. Thus, a very narrow band of argument variation stretches over the section of the transmission line between the fault point and Bus R. In other words, very small error in the estimation of argument of the fault voltage will result in relatively large error in the calculation of d.

2. **Condition 2:** Considerable amount of transients including sub-synchronous frequency

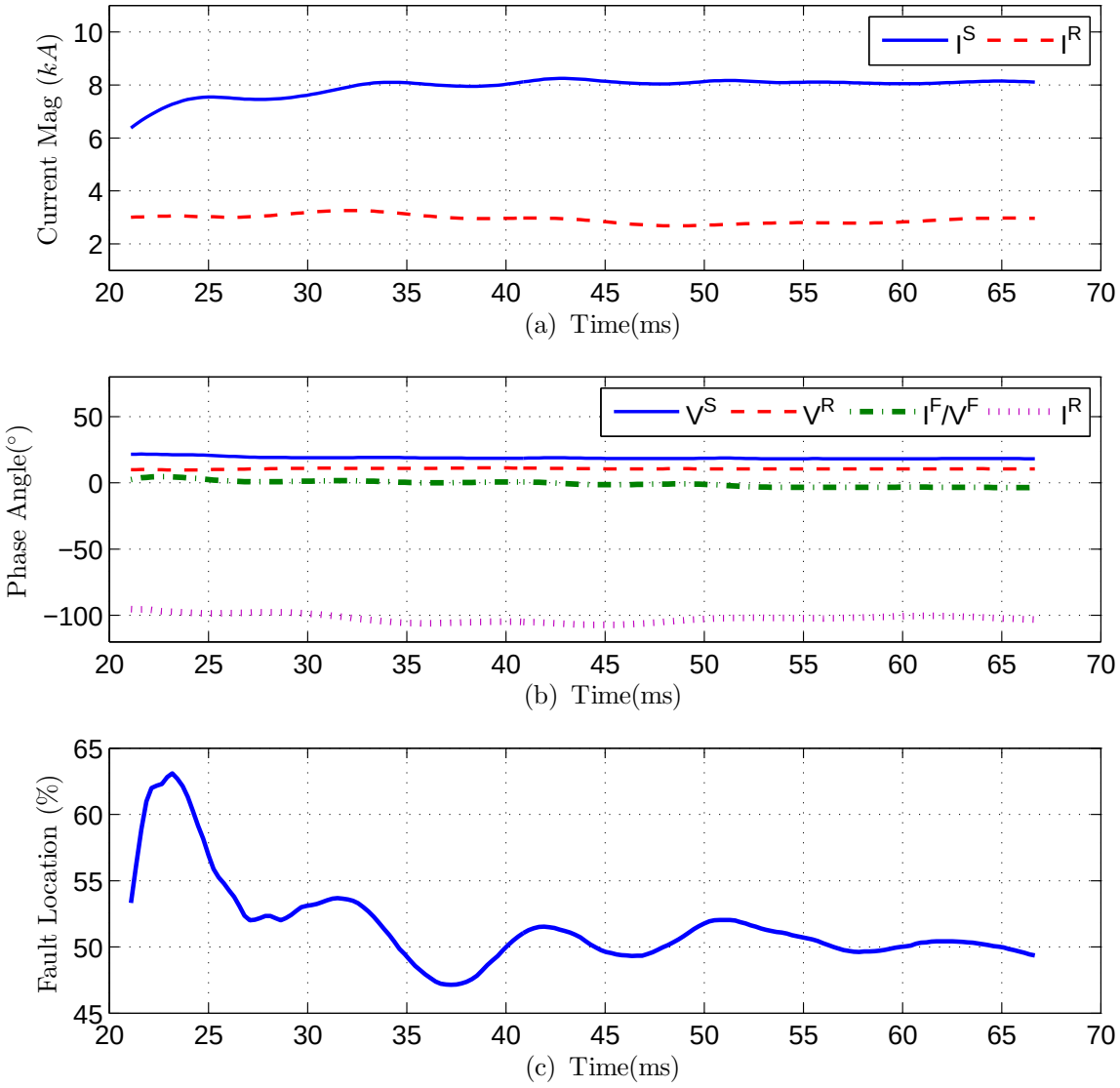

Figure 2.7: The estimated phasors for an AG fault at 40% line length from Bus S: (a) estimated phasor magnitude of fault current at Bus S (I^S) and Bus R (I^R), (b) estimated phasor arguments of Bus S voltage (V^S), Bus R voltage (V^R), fault point current or voltage (I^F/V^F), Bus R current (I^R), (c) calculated fault location.

components (SSFCs) get introduced in the voltage and current signals following the occurrence of fault in an SCCTL, which adversely impact the accuracy of the estimated phasors including the phasor of the total fault current. Therefore, a considerable error will always exist in the argument of the estimated phasor of the total fault current.

Therefore, two factors have combined: 1-a very narrow band of argument variation stretches over the transmission line between fault point and Bus R making the Izykowski Algorithm insensitive to the values of d; 2-there is a considerable error in the estimated argument of the total fault current. Now, the Izykowski Algorithm 'scans' the transmission line from Bus R towards the fault point and 'tries' to find the value of d for which the argument of the fault voltage would become equal to the erroneous argument of the total fault current. Since, the argument of voltage changes very less as the d changes, the error in the argument of the total fault current would result in a large error in d. Figure 2.7 (c) shows the calculated fault location by Izykowski Algorithm fluctuates between 50%-60% range while the fault lies at 40% line length as measured from Bus S. It should be noted that there will always be some error in the argument of the total fault current which means that Condition 2 will always hold true. It is simultaneous occurrence of Condition 1 and Condition 2 that will cause the Izykowski Algorithm to lose accuracy.

As the fault moves away from the 40% towards Bus R, the fault current contribution from Bus R rises and contribution from Bus S is no longer the predominant component of the total fault current. Thus, the argument of the total fault current and the fault voltage will not remain close to that of the Bus R voltage. The Condition 1 is not met, thus, relatively lower error in the fault location results. This phenomenon could be observed from Figure 2.8 which shows various phasor magnitudes and arguments for a solid AG fault at 80% line length as measured from Bus S. It could be seen from Figure 2.8 (a) that the magnitude of Bus S and Bus R fault currents are close to each other, so Bus S fault current would not remain the dominant part. As a result, the arguments of the fault voltage or total fault current would not be close to that of the Bus R voltage as seen from Figure 2.8 (b). The resulting higher accuracy of Izykowski Algorithm in this case could be witnessed from the fact that the calculated fault location remains within the band of 80.5%-81% for a fault at 80% line length from Bus S.

However, when the fault impedance rises, the reduction in the fault current contribution from Bus R is more profound than that from Bus S. It is so because any decrease in fault current level from Bus S will decrease the conduction by MOV, thus, increasing the effective series capacitive compensation which in turn again increases the fault current contribution from Bus S which is also highly resistive in nature. Therefore, for high impedance faults the fault current contribution from Bus S will be predominant part of the total fault current irrespective of the fault location, and also causes the argument of the total fault current to be close to the

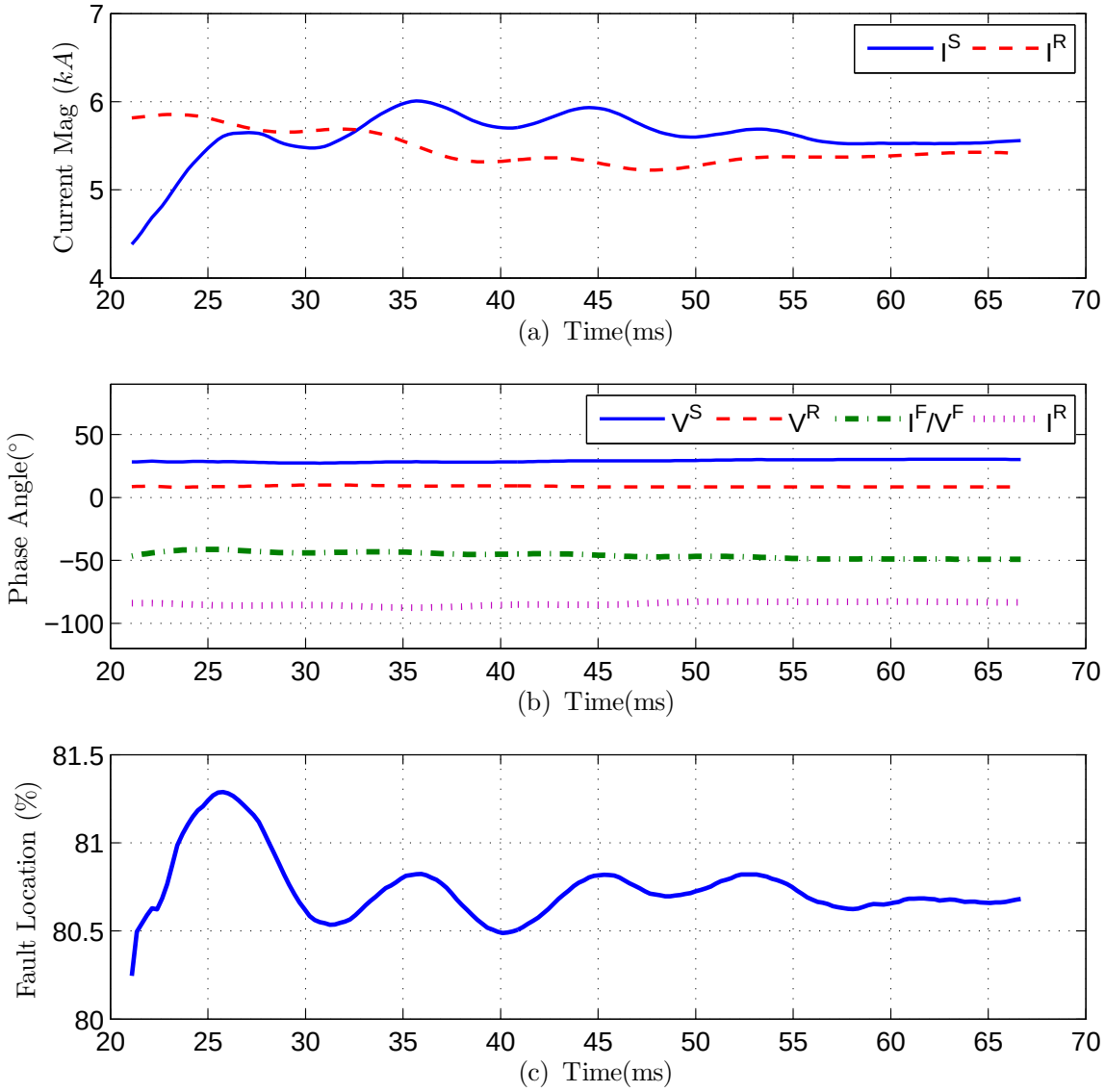

Figure 2.8: The estimated phasors for a solid AG fault at 80% line length from Bus S: (a) Estimated phasor magnitude of fault current at Bus S (I^S) and Bus R (I^R), (b) Estimated phasor arguments of: Bus S voltage (V^S), Bus R voltage (V^R), fault point current or voltage (I^F/V^F), Bus R current (I^R) (c) Calculated fault location.

Bus R voltage. Thereby, satisfying the Condition 1 and causing the Izykowski Algorithm to lose accuracy for all the high impedance faults irrespective of the location of the fault.

2.8 Conclusion

In this chapter, the insufficiency of the conventional impedance-based algorithms for their applicability to SCCTLs has been shown. Thereafter, the two types of fault location algorithms for SCCTLs found in literature, i.e., the MOV-model-based, and fault loop-based impedance-based algorithms have been discussed. It is shown in this chapter through mathematical analysis that the most widely used impedance-based algorithms for SCCTLs, i.e., fault loop-based algorithms are equivalent to each other, and are based on the argument comparison of the fault voltage and fault current for obtaining the fault location results. The simulations covering various fault types, fault resistances, and fault locations have been carried out on two different configurations of SCCTL. It is observed that the configuration of SCCTL when the series capacitor is located at a side of transmission line is more challenging for the fault loop-based algorithms. This configuration of SCCTL has not been evaluated in the previous publications, thus, the existing fault location algorithms stand untested for such configuration of SCCTL. The simulations results have shown that when the series capacitor is present at the side of a transmission line the fault loop-based algorithms lose accuracy for almost all the possible fault locations in an SCCTL for high impedance faults. The reason for the loss of accuracy as identified in this chapter is the limitation of the concept of argument comparison for the purpose of fault location. Since, all the fault loop-based fault location algorithms are based on the argument comparison of the fault voltage and fault current, all the fault loop-based algorithms are prone to yield high errors. Thus, arises a need to have a robust impedance-based algorithm which does not suffer from the innate shortcomings of the fault loop-based algorithms.

Chapter 3

A new impedance-based fault location algorithm for ground faults

3.1 Introduction

As discussed earlier that MOV introduces non-linearity in the voltage drop across SCB, and the existing fault loop-based fault location algorithms avoid using the voltage drop across SCB by using the fault loop-based fault location algorithms. However, the fact that has remained ignored so far is that MOV conducts only in the faulted phase. For healthy phase the series capacitor is responsible for the conduction of the current exclusively. Thus, the voltage drop across SCB in healthy phase could be estimated and used towards proposing a new fault location algorithm. In this chapter, a radically new double-ended fault location algorithm is proposed for single phase to ground and double-phase to ground faults. In the proposed technique, the fault location equations based on each sequence component (positive, negative and zero) are compiled and in each equation the impedance of faulted phase SCB appears as an unknown quantity. Thus, resulting in two unknowns in each equation i.e., fault location and impedance of SCB in the faulted phase. Thereafter, the methodology to remove the unknown impedance of faulted phase SCB from the expressions is presented, which then leads to the fault location results. The advantages of the proposed technique lie in the facts that it overcomes the problem of excessively higher errors observed in fault location results obtained from natural fault loop-based algorithms of [22]-[25], and it is accomplished without using the model of MOV. Another important feature is that the proposed technique unlike the pre-existing algorithms does not require specialized subroutines for determining the faulted segment of the transmission line. The proposed technique is also able to yield accurate fault location results irrespective of the MOV status in the faulted phase, i.e., the fault location can be performed

using the proposed method even if MOV is conducting, idle, or bypassed. In this paper, the measurements from both ends of the transmission line are obtained through synchronized sampling, so no time delay compensation is required. If however, the measurements from both ends are not synchronized, the synchronization techniques such as the ones proposed in [22], [24], [25], and [37] could be used to achieve synchronization before passing on the measurements to the proposed fault location algorithm.

3.2 The proposed technique

Figure 3.1 (a) shows a fault scenario in an SCCTL in which a fault is located in between Bus R and Node N at per unit (p.u.) distance d from SCB. The voltage and current signals are measured at terminals of the SCCTL, i.e., at Bus S and Bus R. From hereafter, the zone between Bus S and Node M is referred to as Zone-SM while that between Node N and Bus R is called as Zone-RN. It should be noted that the proposed fault location algorithm for SCCTLs is derived and elaborated for the faults lying in Zone-RN and it is called as Subroutine-RN in this chapter. For the faults lying in Zone-SM (see Figure 3.1 (b)) i.e., Subroutine-SM, the equations can be obtained analogously.

Now, d could be obtained using i^{th} sequence measurements and parameters of the transmission line from (3.1) [38].

$$d = \frac{1}{\gamma_i (1-m) l} \tanh^{-1}\left(\frac{K_i + \Delta V_i^{MN}}{J_i}\right) \tag{3.1}$$

where

$$\begin{aligned}
J_i &= V_i^R \sinh((1-m)\gamma_i l) - Z_{C_i} I_i^R \cosh((1-m)\gamma_i l) - Z_{C_i} I_i^M \\
K_i &= V_i^R \cosh((1-m)\gamma_i l) - Z_{C_i} I_i^R \sinh((1-m)\gamma_i l) - V_i^M \\
V_i^M &= V_i^S \cosh(m\gamma_i l) - I_i^S Z_{C_i} \sinh(m\gamma_i l) \qquad (3.2) \\
I_i^M &= I_i^S \cosh(m\gamma_i l) - \frac{V_i^S}{Z_{C_i}} \sinh(m\gamma_i l) \qquad (3.3)
\end{aligned}$$

i attains the value of 0, 1 and 2 for depicting zero, positive, and negative sequence components, respectively; V_i^S and I_i^S represent i^{th} sequence component voltage and current phasors at Bus S; V_i^M and I_i^M represent i^{th} sequence component voltage and current phasors at Node M (calculated from Bus R measurements using (3.2) and (3.3), respectively); ΔV_i^{MN} is i^{th} sequence component phasor of voltage drop across SCB from Node M to Node N; Z_{C_i} and γ_i are the i^{th} sequence characteristic impedance and propagation constant of the transmission line, respectively; l is

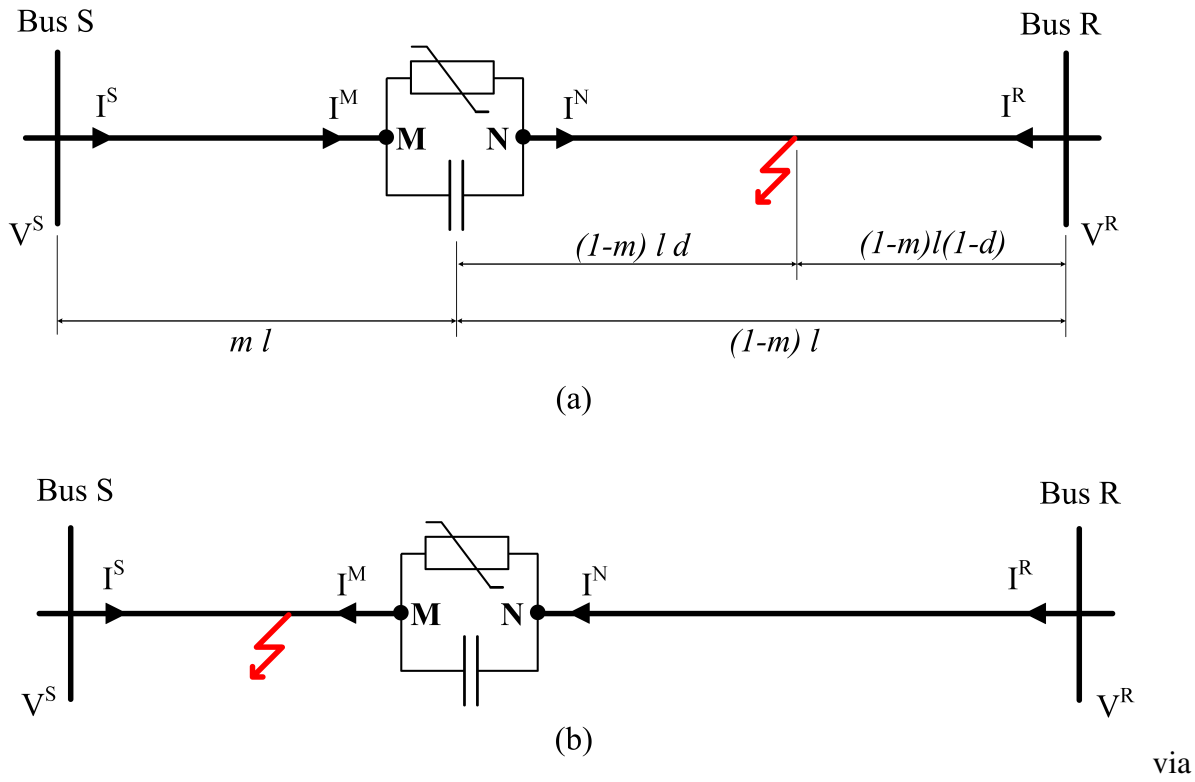

Figure 3.1: Faults in the subsections of the SCCTL: (a) Zone-RN, (b) Zone-SM.

the total length of the transmission line; m is p.u. distance of SCB from Bus S.

In (3.1), ΔV_i^{MN} is another unknown besides d. Now owing to the highly non-linear behavior of MOV, the estimation of ΔV_i^{MN} is not straightforward. In order to overcome this limitation, the fault location equation (3.1) is rearranged to:

$$J_i \tanh((1-m)\,\gamma_i l d) - K_i - \Delta V_i^{MN} = 0$$

Now, multiplying the above expression with a_i and adding each term for all sequence components, (3.4) is obtained.

$$\sum_{i=0}^{2} a_i J_i \tanh((1-m)\,\gamma_i l d) - \sum_{i=0}^{2} a_i K_i - \sum_{i=0}^{2} a_i \Delta V_i^{MN} = 0 \tag{3.4}$$

where a_i is a coefficient for i^{th} sequence component which depending upon the fault type attains different values that are derived later in this chapter. The advantage of using the fault location equation represented in (3.4) is that though ΔV_i^{MN} still remains unknown, but the term $\sum_{i=0}^{2} a_i \Delta V_i^{MN}$ can be estimated as will be shown in this chapter. Thereafter, the fault location

equation (3.4) can be solved for obtaining d.

In order to estimate the term $\sum_{i=0}^{2} a_i \Delta V_i^{MN}$, consider the SCB bank as a series impedance connected in the transmission line. Therefore, the sequence impedance of the SCB bank can be defined using (3.5).

$$[Z_S] = [A]^{-1}[Z_P][A] \tag{3.5}$$

where [A]=$\begin{bmatrix} 1 & 1 & 1 \\ 1 & \alpha^2 & \alpha \\ 1 & \alpha & \alpha^2 \end{bmatrix}$; $\alpha = 1\angle 120^\circ$; $[Z_S]$ is the sequence impedance matrix of SCB bank; $[Z_P]$ is the phase impedance matrix of SCB bank. Equation (3.5) can now be expanded to yield the expressions for sequence impedances of the SCB bank as:

$$\begin{aligned} \left[Z_S\right] &= \frac{1}{3}\begin{bmatrix} 1 & 1 & 1 \\ 1 & \alpha & \alpha^2 \\ 1 & \alpha^2 & \alpha \end{bmatrix}\begin{bmatrix} Z_A & 0 & 0 \\ 0 & Z_B & 0 \\ 0 & 0 & Z_C \end{bmatrix}\begin{bmatrix} 1 & 1 & 1 \\ 1 & \alpha^2 & \alpha \\ 1 & \alpha & \alpha^2 \end{bmatrix} \\ &= \frac{1}{3}\begin{bmatrix} Z_A + Z_B + Z_C & Z_A + \alpha^2 Z_B + \alpha Z_C & Z_A + \alpha Z_B + \alpha^2 Z_C \\ Z_A + \alpha Z_B + \alpha^2 Z_C & Z_A + Z_B + Z_C & Z_A + \alpha^2 Z_B + \alpha Z_C \\ Z_A + \alpha^2 Z_B + \alpha Z_C & Z_A + \alpha Z_B + \alpha^2 Z_C & Z_A + Z_B + Z_C \end{bmatrix} \end{aligned} \tag{3.6}$$

where Z_A, Z_B, Z_C are the impedances of SCBs in phase A, phase B, and phase C, respectively. Now under balanced steady state conditions, only the series capacitors are responsible for the conduction of the current. Therefore, the impedance of SCB in each phase would be identical and equal to the reactance of the series capacitor, i.e., $Z_A = Z_B = Z_C = -jX_C$. The sequence impedance matrix under balanced steady state conditions becomes: $[Z_S]$=$\begin{bmatrix} -jX_c & 0 & 0 \\ 0 & -jX_c & 0 \\ 0 & 0 & -jX_c \end{bmatrix}$

Now, the i^{th}-sequence voltage drop across SCB (ΔV_i^{MN}) could be obtained by multiplying the sequence impedance matrix with the sequence currents flowing through SCB:

$$\left[\Delta V_i^{MN}\right] = \left[Z_S\right]\left[I_i^M\right] \tag{3.7}$$

When a fault occurs in an SCCTL, the MOV located only in the faulted phase conducts. While in the healthy phase, the series capacitor is exclusively responsible for the conduction of current. Therefore, the impedance of the SCB in the healthy phase is equal to the reactance of the series capacitor. On the other hand, the impedance of the SCB in the faulted phase remains unknown. In lieu of the above facts, the expressions for ΔV_i^{MN} obtained from (3.7) would take different forms depending upon the fault type as shown in the following sections.

Since the faulted phases can be arbitrarily labeled as phase A, B, or C; therefore, the proposed technique is elaborated using only phase A to ground (AG), phase B to phase C to ground

(BCG), and phase B to phase C (BC) faults for the single-phase, double-phase to ground, and phase to phase faults, respectively.

3.2.1 Single-phase to ground (AG) faults

For an AG fault, the impedances of SCB in each phase can be represented as: $Z_A = Z^{'}$ (unknown), $Z_B = Z_C = -jX_C$, where X_C denotes the series capacitor reactance. The expression (3.7), thus, gets reduced to:

$$\begin{bmatrix} \Delta V_0^{MN} \\ \Delta V_1^{MN} \\ \Delta V_2^{MN} \end{bmatrix} = \frac{1}{3} \begin{bmatrix} (Z^{'} - 2jX_C) & (Z^{'} + jX_C) & (Z^{'} + jX_C) \\ (Z^{'} + jX_C) & (Z^{'} - 2jX_C) & (Z^{'} + jX_C) \\ (Z^{'} + jX_C) & (Z^{'} + jX_C) & (Z^{'} - 2jX_C) \end{bmatrix} \begin{bmatrix} I_0^M \\ I_1^M \\ I_2^M \end{bmatrix}$$

The simplification of the above matrix yields:

$$\Delta V_0^{MN} = \frac{1}{3}\left[Z^{'}(I_0^M + I_1^M + I_2^M) - jX_C(2I_0^M - I_1^M - I_2^M)\right] \tag{3.8}$$

$$\Delta V_1^{MN} = \frac{1}{3}\left[Z^{'}(I_0^M + I_1^M + I_2^M) - jX_C(2I_1^M - I_2^M - I_0^M)\right] \tag{3.9}$$

$$\Delta V_2^{MN} = \frac{1}{3}\left[Z^{'}(I_0^M + I_1^M + I_2^M) - jX_C(2I_2^M - I_0^M - I_1^M)\right] \tag{3.10}$$

It can be observed that an unknown term $Z^{'}(I_0^M + I_1^M + I_2^M)$ appears in (3.8), (3.9), and (3.10) which prevents the estimation of ΔV_i^{MN}. However, $Z^{'}$ can be eliminated by subtracting (3.9) from (3.8):

$$\Delta V_0^{MN} - \Delta V_1^{MN} = -jX_C(I_0^M - I_1^M) \tag{3.11}$$

The value of the term $\Delta V_0^{MN} - \Delta V_1^{MN}$ as obtained from (3.11), can now be used for fault location in (3.4) with the coefficients a_i as: $a_0 = 1, a_1 = -1, a_2 = 0$. Thus, the fault location equation of (3.4) becomes (3.12):

$$J_0 \tanh(m\gamma_0 ld) - J_1 \tanh(m\gamma_1 ld) - K_0 + K_1 + jX_C(I_0^M - I_1^M) = 0 \tag{3.12}$$

The only unknown in (3.12) is d, which could be solved for by using numerical methods such as Newton-Raphson, to obtain fault location result for an AG fault. It is important to note that similar to (3.12), two more fault location equations can be written which would utilize the information from (3.13) and (3.14), which like (3.11) are also obtained using (3.8), (3.9), and

(3.10).

$$\Delta V_0^{MN} - \Delta V_2^{MN} = -jX_C(I_0^M - I_2^M) \tag{3.13}$$

$$\Delta V_1^{MN} - \Delta V_2^{MN} = -jX_C(I_1^M - I_2^M) \tag{3.14}$$

The fault location equation based on (3.13) could be used an alternative for (3.12), however, the fault location equation compiled based on (3.14) cannot be utilized for fault location as explained below.

It is shown in [22] that:

$$I_i^F = \frac{I_i^{M^S} + I_i^R \cosh\left((1-m)\,\gamma_i l\right) - \frac{V_i^R}{Z_{C_i}} \sinh\left((1-m)\,\gamma_i l\right)}{\cosh\left((1-m)\,\gamma_i l d^{RN}\right)}$$

The denominator of the expression given in [22] is $\cosh(m\gamma_1 l(1-d))$ while in the above expression it is $\cosh\left((1-m)\,\gamma_i l d^{RN}\right)$. The reason for this difference is that d is measured from terminal of the transmission line in [22] while in this chapter d is measured from SCB. Also, the p.u. length of the faulted section in this study is $(1-m)$ (Zone RN) while in [22] the p.u. length of the faulted section is m.

By the definition of J_i from (3.1), the above equation can be written as:

$$I_i^F = \frac{-J_i}{Z_{C_i}\cosh((1-m)\gamma_1 l d)}$$

$$\implies J_i \tanh((1-m)\gamma_1 l d) = -I_i^F Z_{C_i} \sinh((1-m)\gamma_1 l d) \tag{3.15}$$

Now consider the fault location equation based on the positive and negative sequence measurements and parameters of the line:

$$J_1 \tanh((1-m)\,\gamma_1 l d) - J_2 \tanh((1-m)\,\gamma_2 l d) - K_1 + K_2 + jX_C\left(I_1^M - I_2^M\right) = 0 \tag{3.16}$$

Using the expression derived in (3.15), the equation (3.16) can be rewritten as:

$$-I_1^F Z_{C_1} \sinh((1-m)\,\gamma_1 l d) + I_2^F Z_{C_2} \sinh((1-m)\,\gamma_2 l d) - K_1 + K_2 + jX_C\left(I_1^M - I_2^M\right) = 0 \tag{3.17}$$

where, I_1^F, and I_2^F are the positive and negative sequence components of the total fault current, respectively. It is a known fact that the positive and negative sequence parameters of the transmission line are identical, i.e., $Z_{C_1} = Z_{C_2}$ and $\gamma_1 = \gamma_2$. Also, for a single phase to ground fault $I_1^F = I_2^F$ as shown in Figure 3.2(a). In view of the above facts, the expression of (3.17)

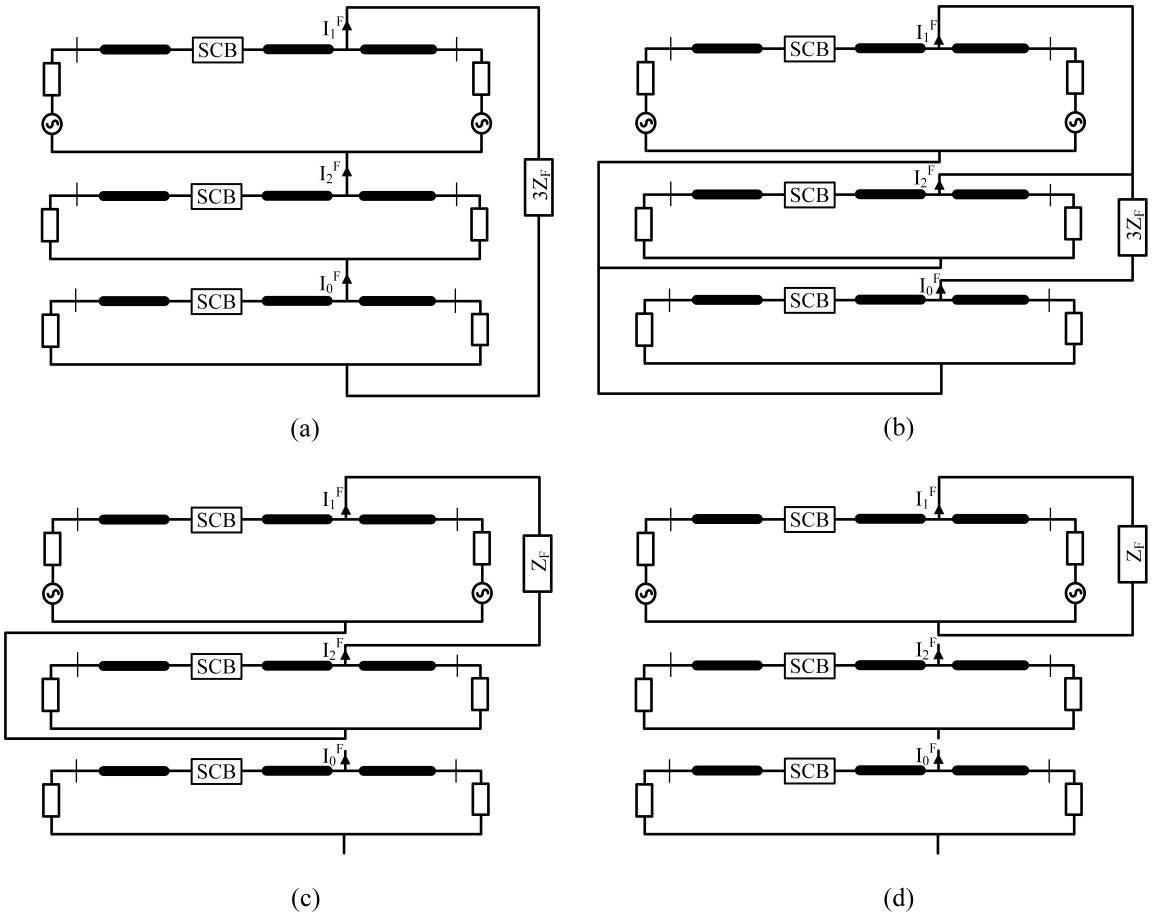

Figure 3.2: Sequence diagram for different faults in an SCCTL: (a) AG Fault, (b) BCG Fault, (c) BC Fault, (d) ABC Fault.

becomes:

$$0 - K_1 + K_2 + jX_C\left(I_1^M - I_2^M\right) = 0 \tag{3.18}$$

It can be seen from (3.18) that the term containing d disappears from the fault location equation. Hence, for a single phase to ground fault, the fault location results have to be obtained from the fault location equations based on 1-positive and zero sequence, or 2-negative and zero sequence measurements and parameters of the transmission line.

3.2.2 Double-phase to ground (BCG) faults

For BCG faults, the impedances of SCB in each phase becomes: $Z_A = -jX_C$, $Z_B = Z_C = Z^{'}$ (unknown) for BCG faults. Therefore, for a BCG fault the expression for ΔV_i^{MN} becomes:

$$\begin{bmatrix} \Delta V_0^{MN} \\ \Delta V_1^{MN} \\ \Delta V_2^{MN} \end{bmatrix} = \frac{1}{3} \begin{bmatrix} (2Z^{'} - jX_C) & -(Z^{'} + jX_C) & -(Z^{'} + jX_C) \\ -(Z^{'} + jX_C) & (2Z^{'} - jX_C) & -(Z^{'} + jX_C) \\ -(Z^{'} + jX_C) & -(Z^{'} + jX_C) & (2Z^{'} - jX_C) \end{bmatrix} \begin{bmatrix} I_0^M \\ I_1^M \\ I_2^M \end{bmatrix}$$

$$\Delta V_0^{MN} = \frac{1}{3}\left[Z^{'}(2I_0^M - I_1^M - I_2^M) - jX_C(I_0^M + I_1^M + I_2^M)\right] \tag{3.19}$$

$$\Delta V_1^{MN} = \frac{1}{3}\left[Z^{'}(2I_1^M - I_2^M - I_0^M) - jX_C(I_0^M + I_1^M + I_2^M)\right] \tag{3.20}$$

$$\Delta V_2^{MN} = \frac{1}{3}\left[Z^{'}(2I_2^M - I_0^M - I_1^M) - jX_C(I_0^M + I_1^M + I_2^M)\right] \tag{3.21}$$

The unknown term $Z^{'}$ appears in (3.19), (3.20) and (3.21) which can be eliminated by adding all the equations:

$$\sum_{i=0}^{2} \Delta V_i^{MN} = -jX_C \sum_{i=0}^{2} I_i^M \tag{3.22}$$

Hence, the fault location equation for BCG fault becomes as shown in (3.23), with $a_0 = 1$, $a_1 = 1$, $a_2 = 1$.

$$\sum_{i=0}^{2} J_i \tanh((1-m)\,\gamma_i ld) - \sum_{i=0}^{2} K_i + jX_C \sum_{i=0}^{2} I_i^M = 0 \tag{3.23}$$

Thus, the value of d can be obtained by solving (3.23) for BCG faults.

3.2.3 Phase to phase (BC) faults

For BC faults, the impedances of SCB in each phase becomes: $Z_A = -jX_C$, $Z_B = Z_C = Z^{'}$ (unknown), as was the case for BCG faults. Thus, the process of obtaining the term $\sum_0^2 a_i \Delta V_i^{MN}$, and fault location d for BC faults remains same as for BCG faults as derived in (3.22) and (3.23), respectively.

However, the equation (3.23) is unable to yield fault location result for BC faults as shown

hereafter. Equation (3.23) can be written as (see Appendix):

$$-\sum_{i=0}^{2} I_i^F Z_{C_i} \sinh((1-m)\,\gamma_i l d) - \sum_{i=0}^{2} K_i + jX_C \sum_{i=0}^{2} I_i^M = 0 \tag{3.24}$$

It can be observed from Figure 3.2(c) that for BC faults, $I_1^F = -I_2^F$, $I_0^F = 0$, and also for a transmission line $Z_{C_1} = Z_{C_2}$, and $\gamma_1 = \gamma_2$. In lieu of these facts, (3.24) becomes (3.25).

$$0 - \sum_{i=0}^{2} K_i + jX_C \sum_{i=0}^{2} I_i^M = 0 \tag{3.25}$$

It can be observed from (3.25) that the term containing d vanishes for BC faults. Thus, implying that the fault location cannot be obtained from (3.23) for BC faults.

3.2.4 Three phase faults

For a three phase fault MOVs located in all three phases would be conducting fault current, which means that the impedances of SCB in each phase will remain unknown $Z_A = Z_B = Z_C = Z^{'}$. Since, three phase faults are symmetrical faults, the negative and zero sequence components of the current through SCB bank will be zero i.e., $I_2^M = 0$, $I_0^M = 0$ as also depicted in Figure 3.2(d). In light of the above facts, the expression for ΔV_i^{MN} becomes:

$$\begin{bmatrix} \Delta V_0^{MN} \\ \Delta V_1^{MN} \\ \Delta V_2^{MN} \end{bmatrix} = \begin{bmatrix} Z^{'} & 0 & 0 \\ 0 & Z^{'} & 0 \\ 0 & 0 & Z^{'} \end{bmatrix} \begin{bmatrix} I_0^M \\ I_1^M \\ I_2^M \end{bmatrix} = \begin{bmatrix} 0 \\ I_1^M Z^{'} \\ 0 \end{bmatrix}$$

$$\implies \Delta V_1^{MN} = I_1^M Z^{'} \tag{3.26}$$

Since, only one equation is available, the unknown term $I_1^M Z^{'}$ cannot be eliminated from (3.26). Thus, preventing the application of the proposed fault location algorithm for three phase faults in transmission line. Table 3.1 lists the values attained by a_i for different types of fault where $\alpha = 1\angle 120°$.

It is worth pointing out that the proposed methodology can be extended for double-circuit line, for which an extra term ($I_0^{RP} Z_{M0}$) corresponding to voltage drop due to zero-sequence mutual coupling between parallel lines would appear in fault location equation, which then

becomes:

$$\sum_{i=0}^{2} a_i J_i \tanh(1 - m\gamma_i ld) - \sum_{i=0}^{2} a_i K_i - \sum_{i=0}^{2} a_i \Delta V_i^{MN} + a_0 I_0^{RP} Z_{M0} = 0$$

where I_0^{RP} is the zero sequence current in the parallel transmission line measured at Bus R; Z_{M0} is the zero sequence mutual impedance between two parallel lines. The values of a_i would remain same for the double-circuit lines as well.

3.3 Equivalence of Subroutines

The fault location equation for the faults lying in Zone-RN (Subroutine-RN) is shown in (3.4). If $m\gamma_i ld^{RN}$ is small then, $\tanh(m\gamma_i ld^{RN}) \approx m\gamma_i ld^{RN}$. Note that superscript RN is added to differentiate the variables of Subroutine-RN from that of Subroutine-SM (SM), which is presented later. In light of the above approximation, the p.u. fault location as calculated by Subroutine-RN (d^{RN}) is obtained from:

$$d^{RN} = \frac{\sum_{i=0}^{2} a_i K_i^{RN} - jX_C \sum_{i=0}^{2} a_i I_i^{M^S}}{(1-m)\, l \sum_{i=0}^{2} a_i \gamma_i J_i^{RN}} \tag{3.27}$$

where

$$\begin{aligned} I_i^{M^S} &= I_i^S \cosh(m\gamma_i l) - \frac{V_i^S}{Z_{C_i}} \sinh(m\gamma_i l) \\ J_i^{RN} &= V_i^R \sinh((1-m)\gamma_i l) - Z_{C_i} I_i^R \cosh((1-m)\gamma_i l) \\ &\quad + V_i^S \sinh(m\gamma_i l) - Z_{C_i} I_i^S \cosh(m\gamma_i l) \\ K_i^{RN} &= V_i^R \cosh((1-m)\gamma_i l) - Z_{C_i} I_i^R \sinh((1-m)\gamma_i l) \\ &\quad - V_i^S \cosh(m\gamma_i l) + Z_{C_i} I_i^S \sinh(m\gamma_i l) \end{aligned} \tag{3.28}$$

Note that J_i^{RN} and K_i^{RN} are obtained when the values of V_i^M and I_i^M from (3.2) and (3.3) are substituted in J_i and K_i of (3.1). The superscript S in $I_i^{M^S}$ represents that $I_i^{M^S}$ is estimated using measurements at Bus S. Once d^{RN} is known, the distance of the fault from Bus S as computed

by Subroutine-RN (D^{RN}) can be estimated as follows:

$$D^{RN} = ml + (1-m)\, ld^{RN}$$
$$D^{RN} = \frac{ml \sum_{i=0}^{2} a_i \gamma_i J_i^{RN} + \sum_{i=0}^{2} a_i K_i^{RN} - jX_C \sum_{i=0}^{2} a_i I_i^{M^S}}{\sum_{i=0}^{2} a_i \gamma_i J_i^{RN}} \tag{3.29}$$

Similar to (3.27), the equation for finding p.u. fault location for the faults in Zone-SM (Subroutine-SM) can be written as (3.30) where d^{SM} is the p.u. fault distance from SCB as yielded by Subroutine-SM.

$$d^{SM} = \frac{\sum_{i=0}^{2} a_i K_i^{SM} - jX_C \sum_{i=0}^{2} a_i I_i^{N^R}}{ml \sum_{i=0}^{2} a_i \gamma_i J_i^{SM}} \tag{3.30}$$

where $I_i^{N^R}$ is the sequence current at Node N estimated from measurements at Bus R.

$$I_i^{N^R} = I_i^R \cosh\left((1-m)\,\gamma_i l\right) - \frac{V_i^R}{Z_{C_i}} \sinh\left((1-m)\,\gamma_i l\right) \tag{3.31}$$
$$J_i^{SM} = V_i^S \sinh(m\gamma_i l) - Z_{C_i} I_i^S \cosh(m\gamma_i l) + V_i^R \sinh((1-m)\gamma_i l) - Z_{C_i} I_i^R \cosh((1-m)\gamma_i l)$$
$$K_i^{SM} = V_i^S \cosh(m\gamma_i l) - Z_{C_i} I_i^S \sinh(m\gamma_i l) - V_i^R \cosh((1-m)\gamma_i l) + Z_{C_i} I_i^R \sinh((1-m)\gamma_i l)$$

The total distance of the fault from Bus S as yielded by Subroutine-SM (D^{SM}) can be estimated as shown below:

$$D^{SM} = ml - mld^{SM}$$
$$D^{SM} = \frac{ml \sum_{i=0}^{2} a_i \gamma_i J_i^{SM} - \sum_{i=0}^{2} a_i K_i^{SM} + jX_C \sum_{i=0}^{2} a_i I_i^{N^R}}{\sum_{i=0}^{2} a_i \gamma_i J_i^{SM}} \tag{3.32}$$

It is worth noting that for any particular fault scenario irrespective of the faulted zone (RN or SM), $J_i^{RN} = J_i^{SM}$ and $K_i^{RN} = -K_i^{SM}$. When the equations of (3.29) and (3.32) are compared in lieu of the above fact, it is observed that (3.29) and (3.32) are identical to each other except for the terms $\sum_{i=0}^{2} a_i I_i^{N^R}$ and $\sum_{i=0}^{2} a_i I_i^{M^S}$. It is important to note that Subroutine-RN estimates the

Table 3.1: Coefficients for obtaining fault location.

Fault Type	a_1	a_2	a_0
AG	-1	0	1
	0	-1	1
BG	$-\alpha^2$	0	1
	0	$-\alpha$	1
CG	$-\alpha$	0	1
	0	$-\alpha^2$	1
BCG	1	1	1
ACG	α^2	α	1
ABG	α	α^2	1

current going through Nodes M and N as $I_i^{M^S}$, using Bus S measurements assuming that fault is lying in Zone-RN. On the other hand Subroutine-SM estimates the current flowing through Nodes N and M as $I_i^{N^R}$, which is estimated from Bus R measurements assuming the fault is in Zone-SM. Now in order to obtain relationship between $I_i^{M^S}$ and $I_i^{N^R}$ consider the expression derived (for faults lying in Zone-RN) in Appendix, i.e.,

$$I_i^F = \frac{I_i^{M^S} + I_i^R \cosh\left((1-m)\,\gamma_i l\right) - \frac{V_i^R}{Z_{C_i}} \sinh\left((1-m)\,\gamma_i l\right)}{\cosh\left((1-m)\,\gamma_i l d^{RN}\right)} \tag{3.33}$$

Since, $(1-m)\,\gamma_i l d^{RN}$ is small, therefore $\cosh((1-m)\,\gamma_i l d^{RN}) \approx 1$. Also using (3.31) the above expression (3.33) can be written as:

$$I_i^F = I_i^{M^S} + I_i^{N^R}$$
$$\implies \sum_{i=0}^{2} a_i I_i^F = \sum_{i=0}^{2} a_i I_i^{M^S} + \sum_{i=0}^{2} a_i I_i^{N^R}$$

It can be observed from Figs. 3.2 (a) and (b) that for the values of a_i in Table 3.1, the term $\sum_{i=0}^{2} a_i I_i^F = 0$, thus, resulting in:

$$\sum_{i=0}^{2} a_i I_i^{M^S} = -\sum_{i=0}^{2} a_i I_i^{N^R} \tag{3.34}$$

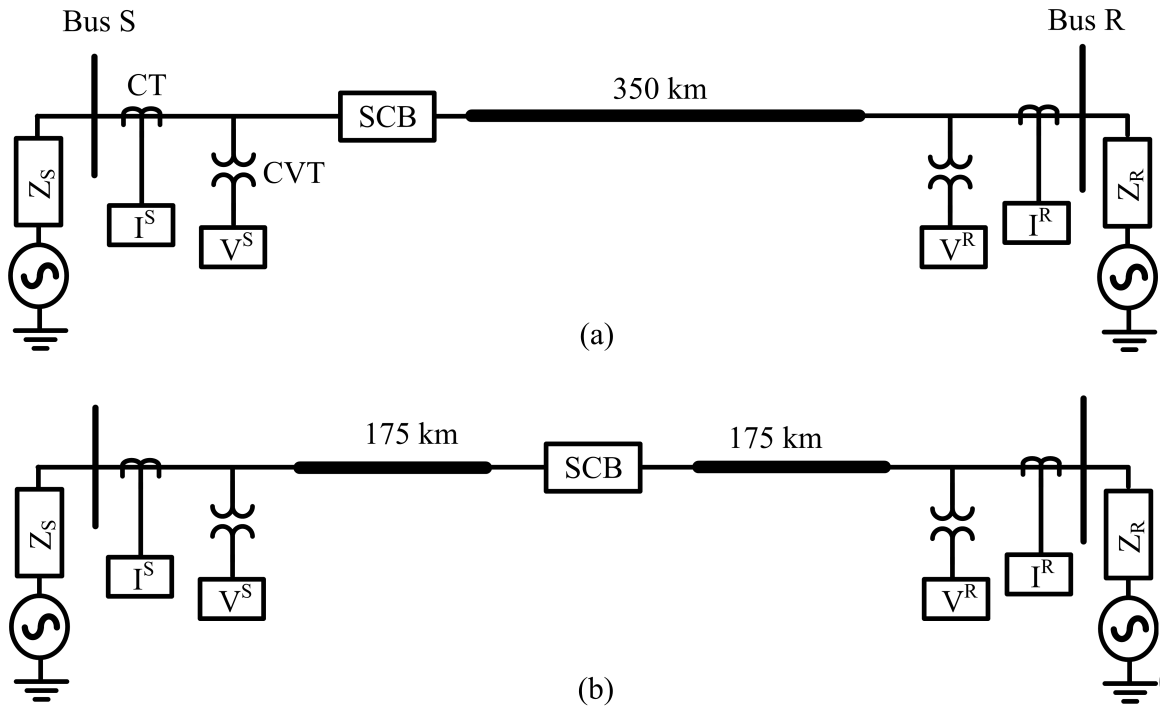

Figure 3.3: Simulated power system in PSCAD: (a) System A, (b) System B.

The significance of the relation derived in (3.34) lies in the fact that the expressions for obtaining total fault distance for both subroutine as given in (3.29) and (3.32), become identical for any specific fault scenario. Similarly, the equivalence of both subroutines can also be shown for faults lying in Zone-SM. Thus, the proposed algorithm eliminates the requirement of special procedure for identifying the faulted section of the line before locating the fault.

3.4 Evaluation and Simulation Results

3.4.1 Test System

For the performance evaluation of the proposed fault location algorithm, a $500kV$ test power system as described in Section 2.7.1 has been simulated in PSCAD while the fault location algorithms have been simulated in Matlab. Two configurations of test power system i.e., System A and System B are simulated. As shown in Figure 3.3, the SCB is located at Bus S and at the midpoint of the transmission line for System A and System B, respectively. The MOV is rated at $273kV$ after considering an overload factor of 1.5. The detailed procedure of sizing the MOV can be found in [39]. The phasors of the measured current and voltage signals are also obtained as per the methodology presented in Section 2.7.1.

3.4.2 Accuracy and the effect of fault resistance

The fault scenarios covering different locations of fault over the full length of the line with different fault resistances are run in PSCAD for both system configurations, i.e., System A and System B. In System A there is wider range of possible locations of fault (0-100%) as compared to System B (50-100%) as all the faults in System B lie at least 50% of the line length away from the bus that sees the same fault current as passing through SCB. Hence, to elaborate the performance of the proposed algorithm System A is utilized, while System B is used to demonstrate the equivalence of the fault location results obtained by both subroutines. The fault location results obtained from the proposed algorithm and the algorithm of [22] are compared to each other for comparative analysis. The proposed algorithm is referred to as Algorithm PM (i.e., Proposed Method) while the algorithm of [22] is called Algorithm EM (i.e, Exiting Method) hereafter. Another point that is worth highlighting here is that the error of 2% and less is acceptable for the fault locators available in the commercial relays [40].

Tables 3.2 and 3.3 show the fault location results for AG and BCG faults in System A (see Figure 3.3 (a)), respectively obtained using Algorithm PM and Algorithm EM. The distance of fault is measured from Bus S as percentage of the total line length. As already shown in Section 3.2.1, Algorithm PM yields the fault location results for AG in two different ways as shown in Table 3.2 with ($a_0 = 1,\ a_1 = -1,\ a_2 = 0$), and ($a_0 = 1,\ a_1 = 0,\ a_2 = -1$). The high accuracy of the Algorithm PM can be witnessed from the fact that error in the results obtained from Algorithm PM remains below 1% for almost all fault scenarios as seen in Tables 3.2 and 3.3. On the other hand the results from Algorithm EM exhibit higher than 2% error for nearly half of the fault scenarios. Furthermore, the highest error in fault location results is 1.45% for Algorithm PM while for Algorithm EM it exceeds 20% for many fault cases.

Another peculiar observation that can be made from Tables 3.2 and 3.3 that when fault resistance is 0 Ω, Algorithm EM loses accuracy when fault is located close to 40%. Figure 3.4 shows the voltage and current waveforms for an AG fault at 40% line length. Note the relative large fault current contribution from Bus S as compared to Bus R contribution (Figure 3.4 (b), and (d)). Also note that it is in phase with Bus S and Bus R voltage (Figure 3.4 (a), (b), and (c)). It so happens that when the fault is located close to 40%, the SCB is almost completely compensating for the inductance of the faulted line segment and source (series compensation is effectively reduced from 70% due to MOV conduction). Thus, resulting in a very high and almost resistive fault current contribution from Bus S as compared to the fault current contribution from Bus R. Note that fault current measured at Bus S is more than double of that measured at Bus R (see Figure 3.5 (b)) and note also that the fault current from Bus S is very close in phase with the voltage at Bus S (see Figure 3.5 (c) and (d)). Now, any

Table 3.2: Error (%) in fault location results for AG faults.

Fault Resistance	Actual Fault Location (%)	Algorithm PM		Algorithm EM
		$a_0=1$ $a_1=-1$ $a_2=0$	$a_0=1$ $a_1=0$ $a_2=-1$	
0Ω	0	0.80	0.52	2.53
	20	0.94	0.87	5.28
	40	0.92	0.79	11.5
	60	0.68	0.55	2.71
	80	0.28	0.19	0.73
	100	0.21	0.24	0.18
10Ω	0	0.76	0.46	0.70
	20	0.89	0.84	6.89
	40	0.92	0.80	24.6
	60	0.69	0.55	3.25
	80	0.30	0.19	0.81
	100	0.11	0.16	0.01
50Ω	0	0.29	0.08	6.88
	20	0.67	0.72	3.52
	40	0.82	0.73	25.0
	60	0.62	0.48	50.7
	80	0.01	0.11	17.0
	100	0.21	0.30	4.07
100Ω	0	0.09	0.27	22.6
	20	0.60	0.70	11.5
	40	0.65	0.59	12.1
	60	0.13	0.01	47.8
	80	0.32	0.49	26.8
	100	0.19	0.33	36.2

Table 3.3: Error (%) in fault location results for BCG faults.

Fault Resistance	Actual Fault Location (%)	Algorithm PM	Algorithm EM
0Ω	0	0.08	0.05
	20	0.99	0.03
	40	0.54	6.95
	60	0.04	1.21
	80	0.47	0.30
	100	0.44	0.05
10Ω	0	0.50	2.23
	20	1.45	1.01
	40	0.78	7.19
	60	0.22	1.51
	80	0.20	0.31
	100	0.23	0.03
50Ω	0	0.53	8.36
	20	0.95	2.55
	40	1.26	8.29
	60	0.82	29.7
	80	0.13	56.0
	100	0.23	13.1
100Ω	0	0.66	22.7
	20	0.38	15.4
	40	0.86	5.93
	60	0.25	8.41
	80	0.46	70.9
	100	0.18	34.3

fault location algorithm that is based on the argument comparison of analytically obtained fault voltage and current (like Algorithm EM) is inherently prone to yield high errors when the fault current contribution from the segment of transmission line containing SCB becomes increasingly higher as compared to the contribution from the other end as seen in Figure 3.5 (e). As the fault resistance increases, the zone in which the Algorithm EM yields excessively high errors keeps getting greater in length eventually covering the whole line when fault resistance increases to 100 Ω. On the other hand, the proposed algorithm i.e., Algorithm PM is immune to such conditions. The waveforms of measured voltages and currents, and the estimated phasors for more fault scenarios are given in Appendix B.

3.4.3 Equivalent subroutine results

The derivation presented in Section 3.3 shows that irrespective of which section of the transmission line does the fault lie, both subroutines of Algorithm PM would yield accurate and almost equal fault location results as long as $\tanh(m\gamma_i ld) \approx m\gamma_i ld$ holds true. In System B shown in Figure 3.3 (b), the fault location results for faults lying in Zone-RN and Zone-SM are yielded by Subroutine-RN and Subroutine-SM respectively for both algorithms. The fault resistance for the fault scenarios shown in Table 3.4 is 0 Ω.

It can be seen from Table 3.4 that for Algorithm EM only one subroutine would yield accurate fault location result (as highlighted) depending upon the faulted section of the transmission line. So a specialized algorithm is needed to select the appropriate subroutine for Algorithm EM as presented in [22]. Even the error in the 'correct' subroutine could be as high as 2%-5% for Algorithm EM. On the other hand, both subroutines of Algorithm PM yield less than 1% error for almost all the fault scenarios, irrespective of which section of the transmission line is faulted. However, it should be noted that for the faults lying at the ends of the transmission line (represented by 0% and 100%), the error in one of the subroutines comes in the vicinity of 1% while the error in the other subroutine remains below 0.5%. For example for AG fault at 100% line length (fault lying close to Bus R), the error yielded by Subroutine-RN (assumes fault lies in Zone-RN) is 0.92% whereas the error in Subroutine-SM (assumes fault lies in Zone-SM) is 0.15%.

Therefore, to minimize the maximum error that can be encountered in Algorithm PM, the 'correct' subroutine should be selected. So when both subroutines point out that fault lies in Zone-RN, the result of Subroutine-RN should take precedence over Subroutine-SM, whereas when the both subroutines indicate Zone-SM as the faulted zone, the results of Subroutine-SM should be treated as more accurate. In light of the above discussion, the selection of the appropriate subroutine for the fault located close to SCB (around 50% line length) becomes

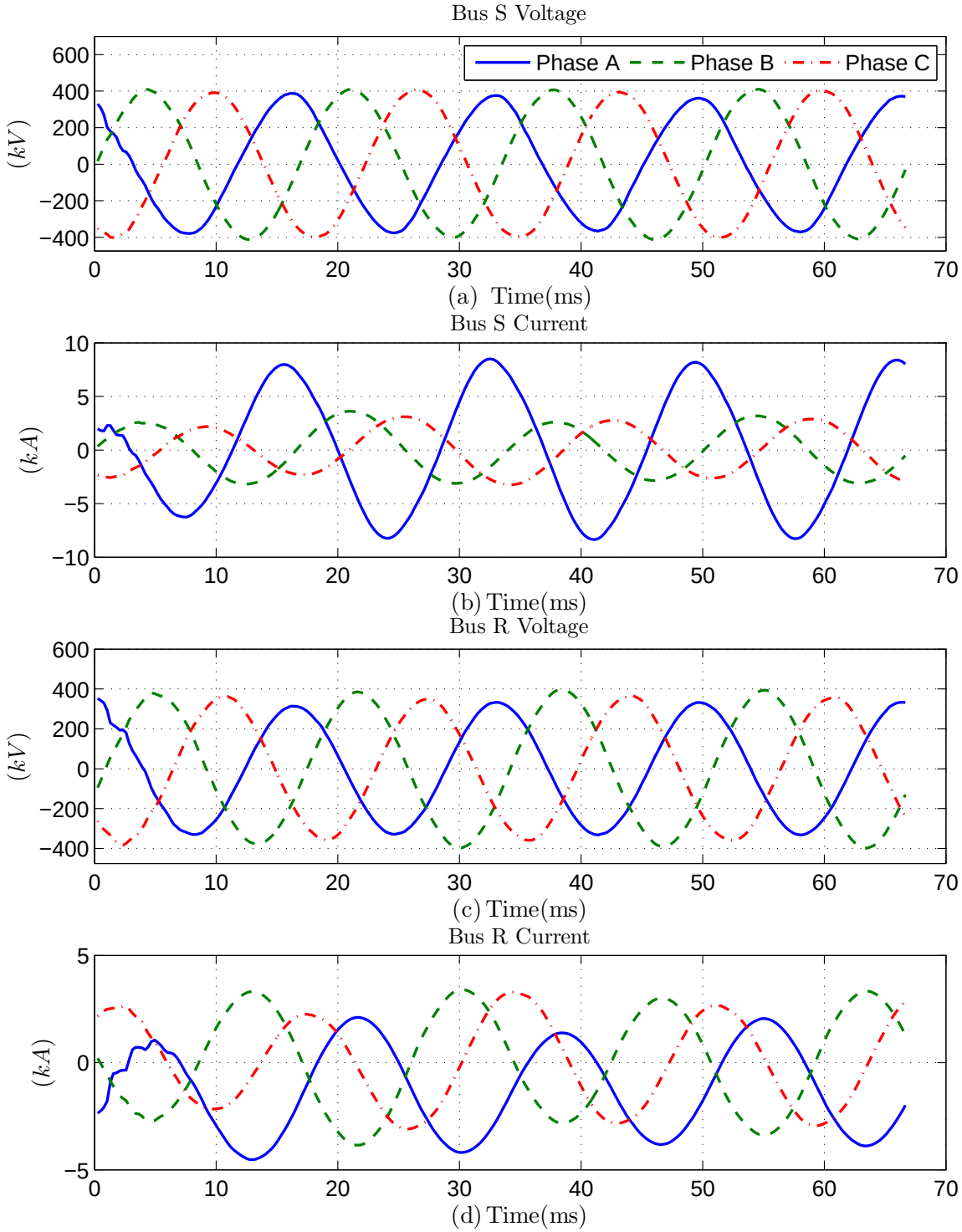

Figure 3.4: Voltage and current waveforms for a solid AG fault at 40% line length from Bus S: (a) Bus S voltage, (b) Bus S current (c) Bus R voltage, (d) Bus R current.

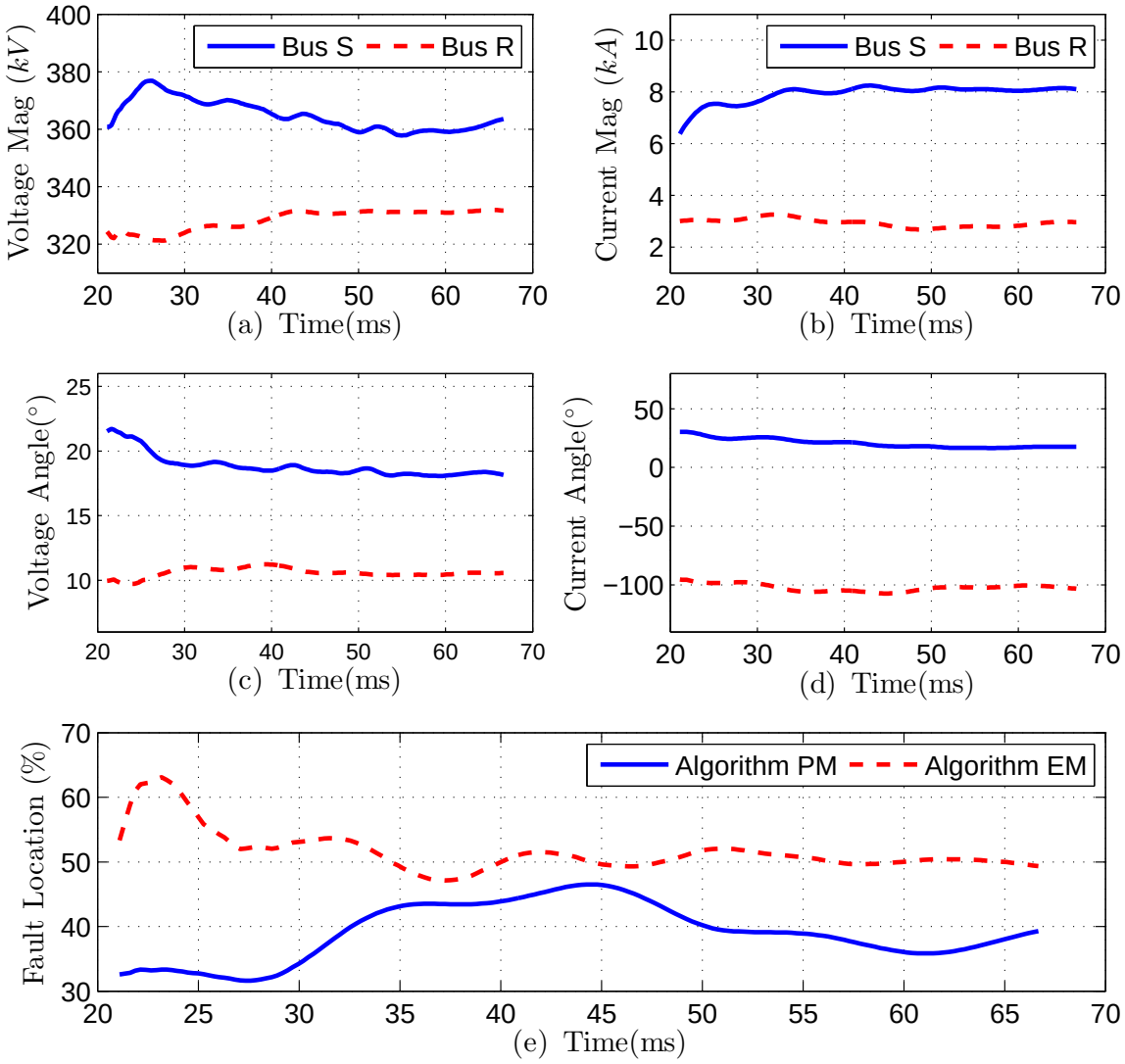

Figure 3.5: (a)-(d): Estimated phasors of phase-A voltage and current signals measured at Bus S and Bus R for a solid AG fault at 40% line length from Bus S; (e) fault location result obtained from Algorithm PM and Algorithm EM.

Table 3.4: Error (%) in fault location results of both subroutines of Algorithm PM and Algorithm EM.

Fault Type	Actual Fault Loc (%)	Algorithm PM		Algorithm EM	
		Sub-RN	Sub-SM	Sub-RN	Sub-SM
AG	0	0.28	1.04	0.02	58.2
	20	0.01	0.31	0.42	50.9
	40	0.57	0.53	1.25	43.5
	50^{-}	0.73	0.73	1.92	39.4
	50^{+}	0.71	0.71	36.4	4.71
	60	0.52	0.57	39.6	2.57
	80	0.06	0.23	43.8	0.76
	100	0.92	0.15	48.6	0.01
BCG	0	0.14	0.91	0.04	70.4
	20	0.51	0.22	0.04	60.1
	40	0.87	0.85	0.21	49.2
	50^{-}	0.86	0.88	0.40	43.9
	50^{+}	0.37	0.39	35.3	2.19
	60	0.05	0.11	38.2	1.41
	80	0.65	0.37	45.1	0.29
	100	1.17	0.41	54.3	0.05

critical as the fault is lying very close to the 'boundary' of each subroutine. In Table 3.4 the fault at 50^{-}% signifies the fault is very close to SCB on Bus S side of SCB, while 50^{+}% means that the fault is close to SCB on the Bus R side of SCB. It can be observed from Table 3.4 that for the faults lying at 50% the error in fault location results yielded by both algorithms is very close to each other, e.g., for BCG fault at 50^{-}% line length the errors in results of Subroutine-RN and Subroutine-SM are 0.86% and 0.88%, respectively. It can thus be inferred that no specialized criteria is required by Algorithm PM for selecting the 'correct' subroutine.

3.4.4 Effect of errors in zero sequence parameters of the transmission line

The error in the fault location results discussed so far has been due to: 1-error that creeps into the phasor estimation due to the high amount of transients present in the measured voltage and current signals; 2-error due to the approximations made during the proposition of the algorithm; 3-due to the modeling of the transmission line. Other sources of error that could impact the accuracy of the fault location results are the error in the estimation of zero sequence transmission line parameters, or, the error originating from the measuring devices, i.e., CT and CVT. In this section the effect of error in transmission line parameters on the accuracy of the

Table 3.5: Effect of error in zero sequence transmission line parameters (%) on the error in fault location results (%) yielded by Algorithm PM for solid faults in the SCCTL.

Fault Location (%)	AG Parameter Error (%)				BCG Parameter Error (%)			
	0%	5%	10%	15%	0%	5%	10%	15%
0	0.80	0.01	0.70	1.29	0.08	0.84	1.49	1.94
20	0.94	0.88	0.84	0.82	0.99	0.28	0.31	0.83
40	0.92	1.04	1.16	1.28	0.54	0.38	0.25	0.14
60	0.68	0.94	1.17	1.37	0.04	0.12	0.27	0.39
80	0.28	0.64	0.94	1.21	0.47	0.11	0.19	0.44
100	0.21	0.18	0.52	0.81	0.44	0.04	0.29	0.59

Table 3.6: Effect of CT and CVT error on the error in fault location results (%) yielded by Algorithm PM for solid faults in the SCCTL.

Fault Location (%)	AG Fault					BCG Fault				
		CT		CVT			CT		CVT	
	0% ∠0°	2% ∠0°	5% ∠3°	2% ∠0°	5% ∠3°	0% ∠0°	2% ∠0°	5% ∠3°	2% ∠0°	5% ∠3°
0	0.80	0.09	1.90	0.77	0.57	0.08	0.39	2.04	0.12	0.28
20	0.94	1.73	1.47	0.95	0.92	0.99	1.60	0.04	0.98	0.87
40	0.92	1.78	0.95	0.92	0.90	0.54	1.23	0.56	0.53	0.49
60	0.68	1.45	0.22	0.68	0.70	0.04	0.49	1.48	0.03	0.01
80	0.28	0.82	0.27	0.29	0.33	0.47	0.17	1.75	0.46	0.40
100	0.21	0.07	0.20	0.21	0.21	0.44	0.30	0.73	0.44	0.44

proposed algorithm is investigated.

The zero-sequence parameters of a transmission line depends upon the resistivity of the ground, which in turn is highly dependent upon the environmental conditions such as precipitation, soil moisture etc. On the other hand the positive sequence parameters of the transmission line depend upon the geometrical arrangement of the conductors, physical characteristics, etc which practically remain constant and does not change with change in environmental conditions. Thus, there always remains some ambiguity in the accuracy of the estimated zero-sequence parameters of the transmission line. Thus, the effect of error in zero-sequence parameters of the transmission lines on the performance of the proposed algorithm has been evaluated in this section.

In order to observe the effects of imperfect estimation of zero sequence parameters of the transmission line on the accuracy of Algorithm PM, various amounts of errors are added to the zero sequence parameters of the transmission line. Thereafter, the results of Algorithm PM are observed in lieu of the amount of error added to the transmission line parameters for solid AG and BCG faults in the SCCTL (see Table 3.5). It could be observed from Table 3.5 that when there is no error in the zero sequence parameters of the transmission line the error in fault location results remain below 1% for all locations of the fault. When the error in zero sequence parameters is gradually increased to 15%, the error of more than 1% is yielded by Algorithm PM in 4 out of 6 fault scenarios for AG faults. On the other hand the error in fault location results yielded by Algorithm PM for BCG faults the error remains below 1% for most of the fault scenarios irrespective of the error in the zero sequence parameters of the transmission line. The highest error of 1.94% for BCG faults is seen when the error in zero sequence parameters is 15% and the fault located at 0% line length. It could be seen from Table 3.5 that the error for all the fault scenarios remains below 2% which is the industrially accepted limit of the error in fault locators of the commercial relays.

Thus, the proposed algorithm maintains its accuracy even with significant error in the zero-sequence parameters of the transmission lines. The effect of error in zero sequence parameters of the transmission line on the performance of Algorithm PM could further be minimized by using the algorithms for estimating the zero sequence transmission line parameters such as the one proposed in [41].

3.4.5 Sensitivity to CT and CVT errors

The instrument transformers (CT and CVT) are unable to perfectly replicate the primary side signals after the occurrence of the fault. As a result, the estimated phasors for current and voltage signals become imperfect. In order to emulate the effect of CT and CVT errors on the

Algorithm PM, deliberate errors are added to the magnitude (2%, 5%) and phase angle (0°, 3°) of the faulted phase current and voltage phasors. Table 3.6 shows the fault location results results yielded by Algorithm PM for solid AG and BCG faults after various amounts of error are added to the voltage and current signals of the faulted phase. It could be observed from Table 3.6 that the addition of error in faulted phase current produces higher error in the fault location results as compared to the case when the error is added to the voltage. For example, the maximum error in fault location results for AG and BCG faults are 1.90% and 2.04%, respectively and in both cases the error of $5\%\angle 3°$ is added to the CT measurements. On the other hand the fault location error remains below 1% for all the fault scenarios of AG and BCG faults irrespective of the error in the CT or CVT measurements. Therefore, it could be concluded that error in CT measurements impacts the accuracy of Algorithm PM relatively more than the error in CVT measurements. However, the error in fault location results remain below 2% even with addition of considerable error of $5\%\angle 3°$ in CT and CVT measurements, thus, highlighting the robustness of the Algorithm PM with respect to the error in CT and CVT measurements.

3.4.6 Need to reduce computational burden for practical implementation

The Algorithm PM has been proposed using distributed model of the transmission line which results in the exponential functions appearing in the fault location equation. As can be observed from equation (3.4), the unknown fault location d appears as an exponential. The solution to such equations would have to found using numerical methods, which are very time consuming. For example, for the sampling rate of 64 samples per fundamental cycle, and total four cycles of fault time period, we have 256 samples. After ignoring the first 80 samples due to transient time period the Cosine filter, it took MATLAB about 30 seconds for yielding fault location results for remaining 176 samples. Such type of computing power is not available in the numerical relays, thus, arises need to reduce the computational burden of the proposed algorithm. The usage of the simpler model of the transmission line would reduce the computational burden but will also impact the accuracy of the fault location results. Therefore, a very careful approach would be needed to simplify the transmission line models for decreasing the computational burden, and at the same time to limit the degradation in the accuracy of the Algorithm PM.

3.5 Conclusion

A new fault location algorithm is presented in this chapter for single-phase to ground and double-phase to ground faults in SCCTLs. The proposed algorithm provides accurate fault lo-

cation results while avoiding simultaneously, the modeling of MOV and the use of natural fault loop. It has also been shown that proposed algorithm does not lose accuracy for specific fault scenarios for which fault loop-based fault location algorithms would yield high errors. The equivalence of the fault location results from both subroutines regardless of the faulted section of the transmission line is mathematically proved as well as using simulations. Additionally, it has been demonstrated that the maximum error in the proposed algorithm can further be reduced by selecting the corresponding subroutine to the faulted section of the transmission line. Another salient feature of the proposed technique is that for the selection of appropriate subroutine no specialized procedure is needed. The performance and the features of the proposed algorithm have been verified through simulations in PSCAD and MATLAB. The future avenues for research in the this field could focus into the effects of non-ideal transposition of the transmission line, error in estimation of transmission line parameters, error in phasor estimation on the performance of the proposed fault location algorithm.

Chapter 4

Impedance-based fault location algorithm for ground faults in SCCTLs compensated with multiple series capacitor banks

4.1 Introduction

As shown in Section 2.4, the fault loop-based impedance-based fault location algorithms like [22]-[25] estimate the fault voltage as function of the unknown fault location (d) using measurements from that end of the transmission line which does not see SCB between itself and the fault. For example, for the fault scenario shown in Figure 4.1 the fault voltage function ($V^F(d)$) is not written using Bus S measurements as the SCB falls in between Bus S and the fault point, and the impedance of SCB is unknown. Therefore, the fault voltage function will be compiled using the measurements of Bus R. Thereafter, the $V^F(d)$ is solved for d under the condition that at the fault point the arguments of fault voltage and the fault current will be same, i.e.,

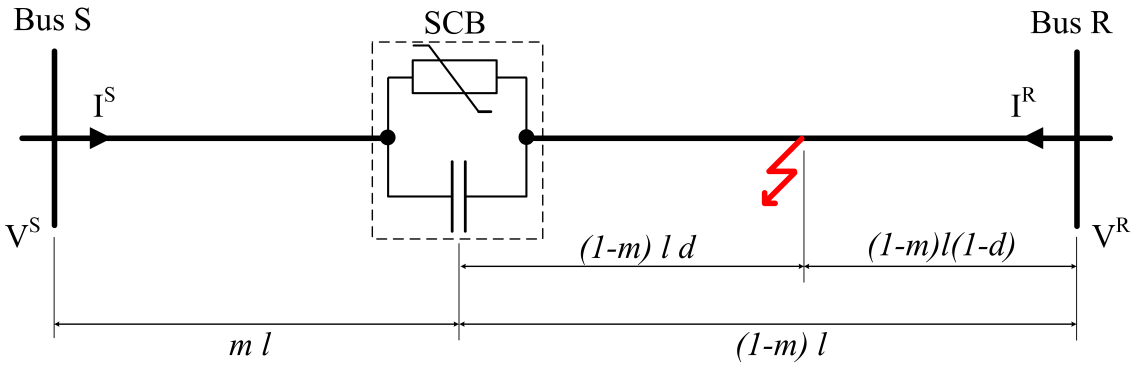

Figure 4.1: Diagram depicting a fault in an SCCTL located between SCB and Bus R.

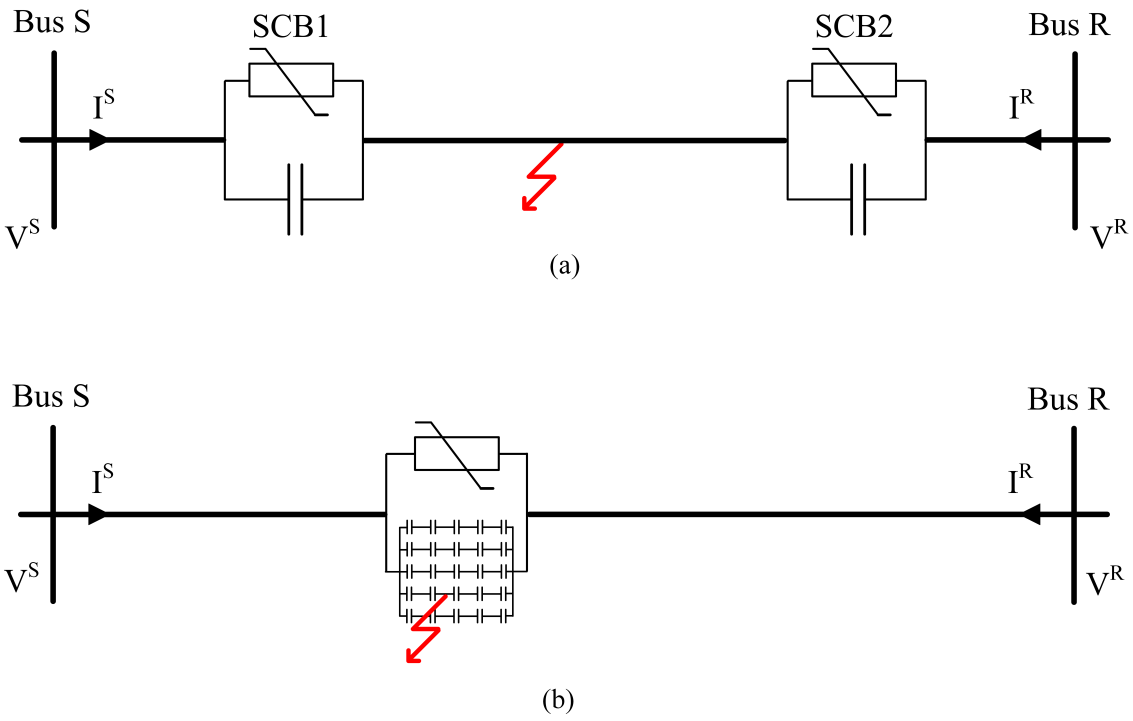

Figure 4.2: Non-applicability of fault loop-based fault location algorithms: (a) series compensation applied at multiple locations, (b) the fault lies in the SCB

$\angle V^F(d) = \angle I^F$. Apart from the shortcomings of fault loop-based algorithms as listed in Section 2.6, the fault loop-based fault location algorithms are inapplicable if: 1-series compensation is applied at more than one location in an SCCTL, and the fault is lying in between the two SCBs as shown in Figure 4.2 (a); 2-the fault lies in the SCB, even if there is only one SCB in an SCCTL as shown in Figure 4.2 (b). It is worth noting here that SCB rather than consisting of only one series capacitor is a combination of multiple capacitors connected in parallel and series (see Figure 4.2 (b)). For both fault scenarios shown in Figure 4.2 (a) and (b), the MOVs will be present on both sides of the fault, preventing the derivation of the fault voltage function, $V^F(d)$ from either terminal of the SCCTL. Therefore, the application of the fault loop-based algorithms to both fault scenarios shown in Figure 4.2 (a) and (b), will yield erroneous fault location results. Thus, no impedance-based fault location algorithm exists that is applicable to the SCCTLs with multiple series compensating devices, and to the faults occurring in the SCBs. In this chapter, it is shown that the fault location algorithm proposed in Chapter 3 for ground faults could be modified and applied to the SCCTLs with SCBs located at multiple locations, and to the faults occurring in SCB.

The proposed algorithm is firstly presented for N-number of series compensating devices using lumped element model of transmission line in Section 4.2. Thereafter, the application

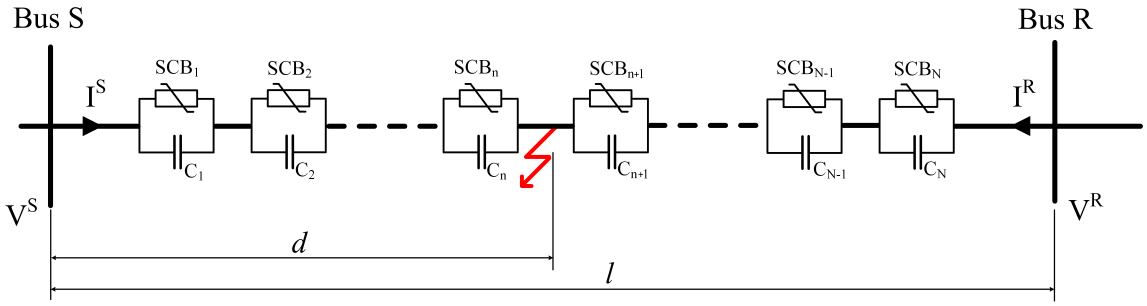

Figure 4.3: Fault scenario in an SCCTL compensated with N number of SCBs.

of the proposed algorithm to the double-circuited transmission lines is presented in Section 4.3. In Section 4.4 the algorithm is presented using more accurate model of transmission line, i.e., distributed model of transmission line for two SCBs in an SCCTL. The simulation results showing the performance of the proposed fault location algorithm are given in Section 4.5.

4.2 The Proposed Algorithm

Consider a transmission line of total length l units, compensated with the total number of N SCBs as shown in Figure 4.3. Let the fault be located at distance d units from Bus S, and lying between the n^{th} and $(n+1)^{th}$ SCB as counted from Bus S. Now, the equations for the i^{th} sequence of the fault voltage, i.e., V_i^F could be written from Bus S and Bus R as given in (4.1) and (4.2), respectively.

$$V_i^F = V_i^S - I_i^S z_i d - \sum_{k=1}^{n} \Delta V_{i,k} \tag{4.1}$$

$$V_i^F = V_i^R - I_i^R z_i (l-d) - \sum_{k=n+1}^{N} \Delta V_{i,k} \tag{4.2}$$

Equating (4.1) and (4.2) we obtain:

$$V_i^S - V_i^R - I_i^S z_i d + I_i^R z_i (l-d) - \sum_{k=1}^{n} \Delta V_{i,k} + \sum_{k=n+1}^{N} \Delta V_{i,k} = 0 \tag{4.3}$$

$$\implies d = \frac{V_i^S - V_i^R + I_i^R z_i l - \sum_{k=1}^{n} \Delta V_{i,k} + \sum_{k=n+1}^{N} \Delta V_{i,k}}{\left(I_i^S + I_i^R\right) z_i} \tag{4.4}$$

where i attains the values of 0, 1 and 2 for representing zero, positive, and negative sequence components, respectively; V_i^S and I_i^S represent i^{th} sequence component voltage and current

Table 4.1: Coefficients for obtaining fault location.

Fault Type	a_1	a_2	a_0
AG	-1	0	1
	0	-1	1
BG	$-\alpha^2$	0	1
	0	$-\alpha$	1
CG	$-\alpha$	0	1
	0	$-\alpha^2$	1
BCG	1	1	1
ACG	α^2	α	1
ABG	α	α^2	1

phasors at Bus S; V_i^R and I_i^R represent i^{th} sequence component voltage and current phasors at Bus R. $\Delta V_{i,k}$ is i^{th} sequence component phasor of voltage drop across k^{th} SCB as counted from Bus S; z_i is the i^{th} sequence impedance of the transmission line per unit distance; l is the total length of the transmission line.

In the fault location equation (4.4), there are two unknowns: firstly, the voltage drop across k^{th} SCU bank, i.e., $\Delta V_{i,k}$ is unknown; secondly, the number n which is the number of SCUs lying between Bus S and fault point is also unknown, thus, preventing the estimation of d.

It is shown in Chapter 3 that though the term $\Delta V_{i,k}$ would remain unknown, however, the term $\sum_{i=0}^{2} a_i \Delta V_{i,k}$ could be estimated for the values of a_i listed in Table 4.1. Now, in order to utilize the term $\sum_{i=0}^{2} a_i \Delta V_{i,k}$, the fault location equation (4.4) needs to be modified. It is done by multiplying (4.3) with the constant a_i, through out and adding each term for all the sequence components. As a result, the Equation (4.5) will be obtained.

$$\sum_{i=0}^{2} a_i \left(V_i^S - V_i^R - I_i^S z_i d + I_i^R z_i (l-d)\right) - \sum_{k=1}^{n}\sum_{i=0}^{2} a_i \Delta V_{i,k} + \sum_{k=n+1}^{N}\sum_{i=0}^{2} a_i \Delta V_{i,k} = 0$$

$$\implies d = \frac{\sum_{i=0}^{2} a_i \left(V_i^S - V_i^R + I_i^R z_i l\right) - \sum_{k=1}^{n}\sum_{i=0}^{2} a_i \Delta V_{i,k} + \sum_{k=n+1}^{N}\sum_{i=0}^{2} a_i \Delta V_{i,k}}{\sum_{i=0}^{2} a_i z_i \left(I_i^S + I_i^R\right)} \tag{4.5}$$

Now, the term $\sum_{i=0}^{2} a_i \Delta V_{i,k}$ could be evaluated as per the methodology presented in the previous

chapter, but n still remains unknown. The method to eliminate n from Equation (4.5) for various types of fault is presented in the following sections. Since the faulted phases can arbitrarily be labeled as phase A, B, or C, therefore, the proposed algorithm is explained using only phase A to ground (AG), phase B to phase C to ground (BCG), and phase B to phase C (BC) faults for the single-phase, double-phase to ground, and phase to phase faults, respectively.

4.2.1 Single-phase to ground (AG) faults

It can be observed from Table 4.1 that for an AG fault, two sets of a_i could be used. The derivation of the fault location presented in this section is based on $a_0 = 1$, $a_1 = -1$, $a_2 = 0$. For the other set of values of a_i, the fault location equation can be derived analogously.

As per the Equation (3.11), derived in Section 3.2.1, following expression could be obtained for the k^{th} SCU for an AG fault:

$$\sum_{i=0}^{2} a_i \Delta V_{i,k} = \Delta V_{0,k} - \Delta V_{1,k} = -jX_{C_k}\left(I_{0,k} - I_{1,k}\right)$$

$$\implies \sum_{k=1}^{n}\sum_{i=0}^{2} a_i \Delta V_{i,k} = -j\sum_{k=1}^{n} X_{C_k}\left(I_{0,k} - I_{1,k}\right) \tag{4.6}$$

where $a_0 = 1$, $a_1 = -1$, $a_2 = 0$; X_{C_k} denotes reactance of the series capacitor in the k^{th} SCB; $I_{0,k}$ and $I_{1,k}$ are the zero and positive sequence currents flowing through the k^{th} SCB.

For all the SCBs lying between the Bus S and the fault point, the current flowing through each SCB will be same and equal to I_i^S, i.e., for $k \in [0, n]$, $I_{i,k} = I_i^S$. Thus, the Equation (4.6) becomes:

$$\sum_{k=1}^{n}\sum_{i=0}^{2} a_i \Delta V_{i,k} = -j\left(I_0^S - I_1^S\right)\sum_{k=1}^{n} X_{C_k} \tag{4.7}$$

Similarly, for the SCBs lying between SCB and Bus R, the term $\sum_{k=n+1}^{N}\sum_{i=0}^{2} a_i \Delta V_{i,k}$ could be estimated from Equation (4.8).

$$\sum_{k=n+1}^{N}\sum_{i=0}^{2} a_i \Delta V_{i,k} = -j\left(I_0^R - I_1^R\right)\sum_{k=n+1}^{N} X_{C_k} \tag{4.8}$$

Substituting the values of a_i i.e. $a_0 = 1$, $a_1 = -1$, $a_2 = 0$, and Equations (4.7), and (4.8) in

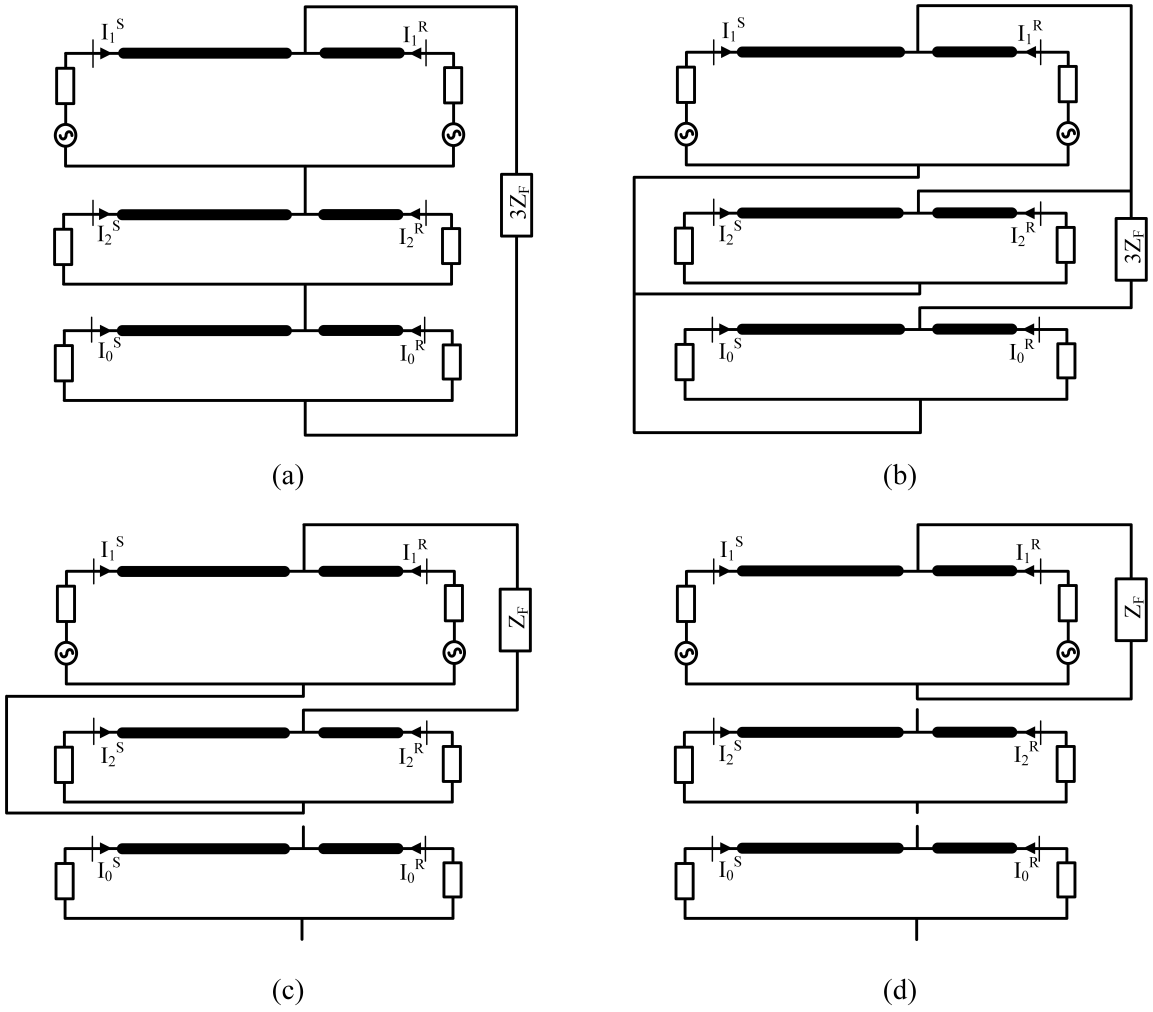

Figure 4.4: Sequence diagram for different faults in an SCCTL: (a) AG Fault, (b) BCG Fault, (c) BC Fault, (d) ABC Fault.

Equation (4.5) the following is obtained:

$$d = \frac{\left(\left(V_0^S - V_1^S\right) - \left(V_0^R - V_1^R\right) + \left(I_0^R z_0 - I_1^R z_1\right) l\right) + j\left(I_0^S - I_1^S\right) \sum_{k=1}^{n} X_{C_k} - j\left(I_0^R - I_1^R\right) \sum_{k=n+1}^{N} X_{C_k}}{z_0\left(I_0^S + I_0^R\right) - z_1\left(I_1^S + I_1^R\right)} \tag{4.9}$$

Tt can be observed from Figure 4.4 (a) that (4.10) holds true for an AG fault.

$$I_0^S + I_0^R = I_1^S + I_1^R \tag{4.10}$$

$$\implies I_0^S - I_1^S = -\left(I_0^R - I_1^R\right) \tag{4.11}$$

Substituting (4.11) in (4.9):

$$d = \frac{\left(\left(V_0^S - V_1^S\right) - \left(V_0^R - V_1^R\right) + \left(I_0^R z_0 - I_1^R z_1\right) l\right) - j\left(I_0^R - I_1^R\right)\left(\sum_{k=1}^{n} X_{C_k} + \sum_{k=n+1}^{N} X_{C_k}\right)}{z_0\left(I_0^S + I_0^R\right) - z_1\left(I_1^S + I_1^R\right)}$$

$$\implies d = \frac{\left(\left(V_0^S - V_1^S\right) - \left(V_0^R - V_1^R\right) + \left(I_0^R z_0 - I_1^R z_1\right) l\right) - j\left(I_0^R - I_1^R\right) \sum_{k=1}^{N} X_{C_k}}{z_0\left(I_0^S + I_0^R\right) - z_1\left(I_1^S + I_1^R\right)} \tag{4.12}$$

All the terms on the R.H.S of the Equation (4.12) are known, thus, d could be obtained from (4.12) for an AG fault.

Similarly, fault location equation utilizing negative sequence measurements and parameters could be obtained as (4.13) with $a_0 = 1$, $a_1 = 0$, $a_2 = -1$.

$$d = \frac{\left(\left(V_0^S - V_2^S\right) - \left(V_0^R - V_2^R\right) + \left(I_0^R z_0 - I_2^R z_2\right) l\right) + j\left(I_0^S - I_2^S\right) \sum_{k=1}^{N} X_{C_k}}{z_0\left(I_0^S + I_0^R\right) - z_2\left(I_2^S + I_2^R\right)} \tag{4.13}$$

Therefore, the fault location result for an AG fault could be calculated from two different Equations (4.12) and (4.13). A question might arise that why not derive the fault location equation which utilizes the positive and negative sequence component measurements and parameters, i.e, $a_0 = 0$, $a_1 = 1$, $a_2 = -1$. However, the denominator of such a equation will become zero because of the fact that for a transmission line the positive sequence impedance is equal to its negative sequence impedance, i.e., $z_1 = z_2$. Thus, the value of d would become indeterminate.

4.2.2 Double-phase to ground (BCG) faults

The values of a_i for a BCG fault are $a_0 = 1$, $a_1 = 1$, $a_2 = 1$, as can be observed from the Table 4.1. Thus, the Equation (4.5) for a BCG fault becomes (4.14).

$$\implies d = \frac{\sum_{i=0}^{2}\left(V_i^S - V_i^R + I_i^R z_i l\right) - \sum_{k=1}^{n}\sum_{i=0}^{2}\Delta V_{i,k} + \sum_{k=n+1}^{N}\sum_{i=0}^{2}\Delta V_{i,k}}{\sum_{i=0}^{2} z_i\left(I_i^S + I_i^R\right)} \tag{4.14}$$

Using the relation derived in Equation (3.22) in Section 3.2.2, following expression could be derived for the k^{th} SCB.

$$\begin{aligned}\sum_{i=0}^{2}\Delta V_{i,k} &= -jX_{C_k}\sum_{i=0}^{2} I_{i,k} \\ \implies \sum_{k=1}^{n}\sum_{i=0}^{2}\Delta V_{i,k} &= -j\sum_{k=1}^{n}\left(X_{C_k}\sum_{i=0}^{2} I_{i,k}\right)\end{aligned} \tag{4.15}$$

For all the SCBs lying between Bus S and the fault point, the current flowing through each SCB will be equal to the I_i^S, i.e., for $k \in [0, n]$, $I_{i,k} = I_i^S$. Since the current is equal for all the SCBs, the term $\sum_{i=0}^{2} I_{i,k}$ could be taken out of the summation and replaced with the term $\sum_{i=0}^{2} I_i^S$ in (4.15), thus yielding the Equation (4.16).

$$\sum_{k=1}^{n}\sum_{i=0}^{2}\Delta V_{i,k} = -j\sum_{i=0}^{2} I_i^S \sum_{k=1}^{n} X_{C_k} \tag{4.16}$$

For the SCBs lying between fault point and Bus R, the current through each SCB will be I_i^R, i.e., for $k \in [n+1, N]$, $I_{i,k} = I_i^R$. The Equation (4.17) could be derived analogous to (4.16).

$$\sum_{k=n+1}^{N}\sum_{i=0}^{2}\Delta V_{i,k} = -j\sum_{i=0}^{2} I_i^R \sum_{k=n+1}^{N} X_{C_k} \tag{4.17}$$

Substituting the values of the terms $\sum_{k=1}^{n}\sum_{i=0}^{2}\Delta V_{i,k}$, and $\sum_{k=n+1}^{N}\sum_{i=0}^{2}\Delta V_{i,k}$ from Equations (4.16) and (4.17) in (4.14), the following expression is obtained:

$$d = \frac{\sum_{i=0}^{2}\left(V_i^S - V_i^R + I_i^R z_i l\right) + j\sum_{i=0}^{2} I_i^S \sum_{k=1}^{n} X_{C_k} - j\sum_{i=0}^{2} I_i^R \sum_{k=n+1}^{N} X_{C_k}}{\sum_{i=0}^{2} z_i\left(I_i^S + I_i^R\right)} \tag{4.18}$$

The only unknown in the Equation (4.18) is n. Considering the Figure 4.4 (b), it can be seen that:

$$\begin{aligned} I_0^S + I_0^R + I_1^S + I_1^R + I_2^S + I_2^R &= 0 \\ \implies I_0^S + I_1^S + I_2^S &= -\left(I_0^R + I_1^R + I_2^R\right) \\ \implies \sum_{i=0}^{2} I_i^S &= -\sum_{i=0}^{2} I_i^R \end{aligned} \tag{4.19}$$

Substituting (4.19) in (4.18), the Equation (4.20) is obtained. Since all the terms on the R.H.S of (4.20) are known, d could be calculated from (4.20) for BCG faults.

$$d = \frac{\sum_{i=0}^{2}\left(V_i^S - V_i^R + I_i^R z_i l\right) - j\sum_{i=0}^{2} I_i^R \sum_{k=1}^{N} X_{C_k}}{\sum_{i=0}^{2} z_i\left(I_i^S + I_i^R\right)} \tag{4.20}$$

4.2.3 Phase to phase (BC) faults

Though not listed in Table 4.1, the set of values of a_i for BC faults remain same as that for the BCG faults. Therefore, the fault location equation for BC faults will remain same as that for BCG Faults, i.e., Equation (4.20).

However, the zero sequence circuit does not see the fault as shown in Figure 4.4 (c), which implies that $I_0^S + I_0^R = 0$. As a result, the denominator (D_r) of the Equation (4.20) is reduced to 0 as shown through the following analysis.

$$\begin{aligned} D_r &= z_0\left(\underbrace{I_0^S + I_0^R}_{=0}\right) + z_1\left(I_1^S + I_1^R\right) + z_2\left(I_2^S + I_2^R\right) \\ \implies D_r &= z_1\left(I_1^S + I_1^R\right) + z_2\left(I_2^S + I_2^R\right) \end{aligned} \tag{4.21}$$

For a transmission line, the positive and negative impedance are identical, i.e., $z_o = z_1$. Also for a BC fault the $\left(I_1^S + I_1^R\right) = -\left(I_2^S + I_2^R\right)$, as evident from Figure 4.4 (c). In lieu of these facts the Equation (4.21), becomes (4.22).

$$D_r = 0 \tag{4.22}$$

Since, the denominator of the Equation (4.20) becomes 0 for a BC fault, the value of d cannot be determined from (4.20) for a BC fault. Thus, the proposed method cannot be applied to BC faults.

4.2.4 Three phase faults

For a three phase fault, no combination of values of a_i could be derived which would make the term $\sum_{i=0}^{2} a_i \Delta V_{i,k}$ independent of the unknown impedance of MOV as shown in Section 3.2.4. Thus, preventing the estimation of d using the proposed algorithm for a three phase fault.

4.2.5 The general equation

The general form of fault location equation for locating ground faults in an SCCTL with series compensation applied at multiple locations, will be as given in (4.23) with values of a_i given in Table 4.1.

$$d = \frac{\sum_{i=0}^{2} a_i \left(V_i^S - V_i^R + I_i^R z_i l \right) + j \sum_{i=0}^{2} a_i I_i^S \sum_{k=1}^{N} X_{C_k}}{\sum_{i=0}^{2} a_i z_i \left(I_i^S + I_i^R \right)} \tag{4.23}$$

One of the peculiar advantage of the proposed algorithm is that it directly yields d, without depending upon the number of SCBs lying on either side of the fault as it is independent of n.

4.3 Application to double-circuited transmission lines

In case of the double-circuited transmission lines, the effect of zero sequence mutual coupling has to be considered. The equations for zero sequence component of the voltage at fault point from both ends of the transmission line considering zero sequence mutual coupling could be written as:

$$V_0^F = V_0^S - I_0^S z_0 d - \sum_{k=1}^{n} \Delta V_{0,k} - I_0^{SP} z_{m_0} d \tag{4.24}$$

$$V_0^F = V_0^R - I_0^R z_0 (l - d) - \sum_{k=n+1}^{N} \Delta V_{0,k} - I_0^{RP} z_{m_0} (l - d) \tag{4.25}$$

where I_0^{SP} and I_0^{RP} are the zero sequence currents in the parallel transmission line measured at Bus S and Bus R, respectively; z_{m_0} is the zero sequence mutual impedance per unit length between two parallel lines.

Equating (4.24) and (4.25):

$$V_0^S - V_0^R - I_0^S z_0 d + I_0^R z_0 (l-d) - \sum_{k=1}^{n} \Delta V_{0,k} + \sum_{k=n+1}^{N} \Delta V_{0,k} - I_0^{SP} z_{m_0} d + I_0^{RP} z_{m_0} (l-d) = 0 \quad (4.26)$$

Since the fault does not lie in the parallel transmission line, therefore $I_0^{RP} = -I_0^{SP}$. The Equation (4.26) becomes:

$$V_0^S - V_0^R - I_0^S z_0 d + I_0^R z_0 (l-d) - \sum_{k=1}^{n} \Delta V_{0,k} + \sum_{k=n+1}^{N} \Delta V_{0,k} - I_0^{SP} z_{m_0} l = 0 \quad (4.27)$$

Since the mutual coupling phenomenon is observed only in zero sequence network, the equations for positive and negative sequence components remain unchanged. As a result, the fault location equation becomes as (4.28) considering the effect of zero sequence mutual coupling.

$$d = \frac{\sum_{i=0}^{2} a_i \left(V_i^S - V_i^R + I_i^R z_i l \right) - \sum_{k=1}^{n} \sum_{i=0}^{2} a_i \Delta V_{i,k} + \sum_{k=n+1}^{N} \sum_{i=0}^{2} a_i \Delta V_{i,k} - a_0 I_0^{SP} z_{m_0} l}{\sum_{i=0}^{2} a_i z_i \left(I_i^S + I_i^R \right)} \quad (4.28)$$

It is to be noted that values of a_i remain same as given in Table 4.1.

4.4 Implementation of the proposed algorithm on distributed model of transmission line

So far, the lumped model of the transmission line has been utilized to elaborate the proposed fault location algorithm. The usage of lumped model the transmission line offered the simplicity in elaborating the principle of the fault location algorithm, at the expense of accuracy of the algorithm. As a matter of fact, the elimination of the unknown variable n that appears in the Equations (4.9) and (4.18) could only be eliminated from the subsequent equations due to the usage of lumped model of the transmission line. Now, the implementation of the proposed fault location algorithm using distributed model of the transmission line would be presented, in order to increase the accuracy of the fault location results. However, the complexity of the equations will increase with the usage of distributed model of the transmission line.

Figure 4.5 shows a fault located between the two SCBs at p.u. distance d as measured from SCB1. The voltage and current are measured at Bus S and Bus R, respectively. The expression for d could be derived in terms of i^{th} sequence voltages and currents at Nodes M and Q as

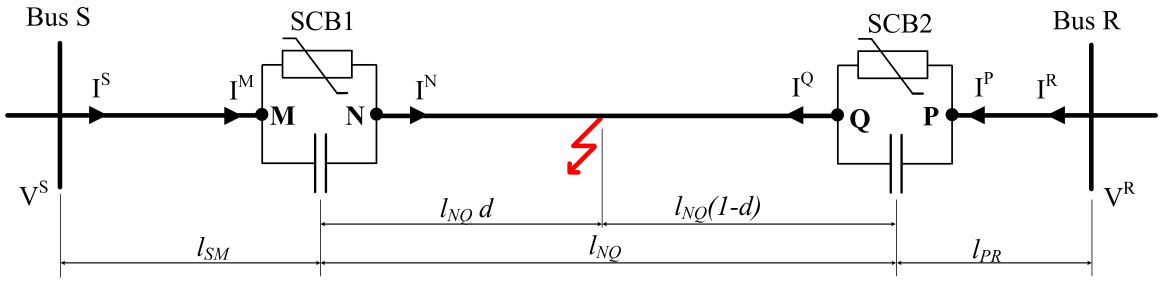

Figure 4.5: Fault located between two SCBs in an SCCTL containing two SCBs.

(4.29).

$$d = \frac{1}{(\gamma_i l_{NQ})} \tanh^{-1}\left(\frac{V_i^Q \cosh(\gamma_i l_{NQ}) - Z_{C_i} I_i^Q \sinh(\gamma_i l_{NQ}) - V_i^N}{V_i^Q \sinh(\gamma_i l_{NQ}) - Z_{C_i} I_i^Q \cosh(\gamma_i l_{NQ}) - Z_{C_i} I_i^N}\right) \tag{4.29}$$

where i attains the value of 0, 1 and 2 for depicting zero, positive, and negative sequence components, respectively; V_i^Q and I_i^Q represent i^{th} sequence component voltage and current phasors at Node Q; V_i^N and I_i^N represent i^{th} sequence component voltage and current phasors at Node N; Z_{C_i} and γ_i are the i^{th} sequence characteristic impedance and propagation constant of the transmission line, respectively; l_{NQ} is the length of the transmission line between Node N and Node Q;

Now, the voltages and currents at Nodes N and Q will have to be estimated using the measurements at Bus S and Bus R, respectively as shown in (4.30)-(4.33).

$$V_i^N = V_i^S \cosh(\gamma_i l_{SM}) - I_i^S Z_{C_i} \sinh(\gamma_i l_{SM}) - \Delta V_i^{MN} \tag{4.30}$$

$$I_i^N = I_i^M = I_i^S \cosh(\gamma_i l_{SM}) - \frac{V_i^S}{Z_{C_i}} \sinh(\gamma_i l_{SM}) \tag{4.31}$$

$$V_i^Q = V_i^R \cosh(\gamma_i l_{RP}) - I_i^R Z_{C_i} \sinh(\gamma_i l_{RP}) - \Delta V_i^{PQ} \tag{4.32}$$

$$I_i^Q = I_i^P = I_i^R \cosh(\gamma_i l_{RP}) - \frac{V_i^R}{Z_{C_i}} \sinh(\gamma_i l_{RP}) \tag{4.33}$$

where V_i^S and I_i^S represent i^{th} sequence component voltage and current phasors at Bus S; V_i^R and I_i^R represent i^{th} sequence component voltage and current phasors at Bus R; ΔV_i^{MN} and ΔV_i^{PQ} represent the i^{th} sequence voltage drop across SCB1 and SCB2, respectively; l_{SM} is the distance between Bus S and Node M; l_{RP} is the distance between Bus R and Node P.

Substituting the Equations (4.30)-(4.33) in (4.29), the Equation (4.34) is obtained.

$$d = \frac{1}{(\gamma_i l_{NQ})} \tanh^{-1}\left(\frac{K_i + \Delta V_i^{MN} - \Delta V_i^{PQ} \cosh(\gamma_i l_{NQ})}{J_i - \Delta V_i^{PQ} \sinh(\gamma_i l_{NQ})}\right) \tag{4.34}$$

where,

$$J_i = V_i^R \sinh\left(\gamma_i \left(l_{RP} + l_{NQ}\right)\right) - Z_{C_i} I_i^R \cosh\left(\gamma_i \left(l_{RP} + l_{NQ}\right)\right) + V_i^S \sinh\left(\gamma_i l_{SM}\right) - Z_{C_i} I_i^S \cosh\left(\gamma_i l_{SM}\right)$$
$$K_i = V_i^R \cosh\left(\gamma_i \left(l_{RP} + l_{NQ}\right)\right) - Z_{C_i} I_i^R \sinh\left(\gamma_i \left(l_{RP} + l_{NQ}\right)\right) - V_i^S \cosh\left(\gamma_i l_{SM}\right) + Z_{C_i} I_i^S \sinh\left(\gamma_i l_{SM}\right)$$

In Equation (4.34), the terms ΔV_i^{MN}, $\Delta V_i^{PQ} \cosh\left(\gamma_i l_{NQ}\right)$, and $\Delta V_i^{PQ} \sinh\left(\gamma_i l_{NQ}\right)$ are unknown. It is shown in Chapter 3 that though the i^{th} sequence voltage drop across any SCB, i.e., ΔV_i cannot be estimated individually, but the composite sum $(\sum_{i=0}^{2} a_i \Delta V_i)$ could be estimated for the values of a_i given in Table 4.1. Accordingly, the Equation (4.34) is rearranged to obtain (4.35).

$$\sum_{i=0}^{2} a_i J_i \tanh\left((\gamma_i l_{NQ})d\right) - \underbrace{\sum_{i=0}^{2} a_i \Delta V_i^{PQ} \sinh\left(\gamma_i l_{NQ}\right) \tanh\left(\gamma_i l_{NQ} d\right)}_{I}$$
$$- \sum_{i=0}^{2} a_i K_i - \underbrace{\sum_{i=0}^{2} a_i \Delta V_i^{MN}}_{II} + \underbrace{\sum_{i=0}^{2} a_i \Delta V_i^{PQ} \cosh\left(\gamma_i l_{NQ}\right)}_{III} = 0 \qquad (4.35)$$

Focusing our attention on the terms I and III in (4.35), it could be seen that though the term $\sum_{i=0}^{2} a_i \Delta V_i^{PQ}$ could be estimated, but the composite terms $\sum_{i=0}^{2} a_i \Delta V_i^{PQ} \sinh\left(\gamma_i l_{NQ}\right) \tanh\left(\gamma_i l_{NQ} d\right)$ and $\sum_{i=0}^{2} a_i \Delta V_i^{PQ} \cosh\left(\gamma_i l_{NQ}\right)$ cannot be estimated with the available measurements. Therefore, approximations are needed for the terms I and III, while term II could be evaluated as it is. It should be noted that the approximations to the terms I and III might affect the accuracy. It might seem that the implementation of the proposed algorithm using the distributed model of the transmission line is a self-defeating purpose, however, the simulation results show that even with the approximations, the results obtained from distributed model based implementation of the proposed algorithm are considerably more accurate than those obtained from the lumped model of the transmission line.

In term I, the factor $\sinh\left(\gamma_i l_{NQ}\right) \tanh\left(\gamma_i l_{NQ} d\right)$ could be taken out of the summation only if the propagation constant γ_i is same for all the sequences, i.e., $\gamma_1 = \gamma_2 = \gamma_0$. However, for a transmission $\gamma_1 = \gamma_2$, but $\gamma_0 \neq \gamma_1$ and $\gamma_0 \neq \gamma_2$. Therefore, γ_i is replaced with $\left(\frac{\gamma_0+\gamma_1}{2}\right)$ in term I. Now the term $\sinh\left(\left(\frac{\gamma_0+\gamma_1}{2}\right) l_{NQ}\right) \tanh\left(\left(\frac{\gamma_0+\gamma_1}{2}\right) l_{NQ} d\right)$ becomes common for all the sequences and can be taken out of the summation, as shown in (4.36).

$$\sum_{i=0}^{2} a_i \Delta V_i^{PQ} \sinh\left(\gamma_i l_{NQ}\right) \tanh\left(\gamma_i l_{NQ} d\right) \approx \left[\sinh\left(\left(\frac{\gamma_0 + \gamma_1}{2}\right) l_{NQ}\right) \tanh\left(\left(\frac{\gamma_0 + \gamma_1}{2}\right) l_{NQ} d\right)\right] \sum_{i=0}^{2} a_i \Delta V_i^{PQ} \qquad (4.36)$$

Moving on a similar lines, the term III is estimated as shown in (4.37).

$$\sum_{i=0}^{2} a_i \Delta V_i^{PQ} \cosh(\gamma_i l_{NQ}) \approx \left[\cosh\left(\left(\frac{\gamma_0+\gamma_1}{2}\right) l_{NQ}\right)\right] \sum_{i=0}^{2} a_i \Delta V_i^{PQ} \tag{4.37}$$

Substituting Equations (4.36) and (4.37) in (4.35), the Equation (4.38) is obtained. Now, all the variables in (4.38) are known except d, which can be obtained by solving (4.38).

$$\sum_{i=0}^{2} a_i J_i \tanh((\gamma_i l_{NQ})d) - G \sum_{i=0}^{2} a_i \Delta V_i^{PQ} - \sum_{i=0}^{2} a_i K_i - \sum_{i=0}^{2} a_i \Delta V_i^{MN} = 0 \tag{4.38}$$

where,

$$G = \sinh\left(\left(\frac{\gamma_0+\gamma_1}{2}\right) l_{NQ}\right) \tanh\left(\left(\frac{\gamma_0+\gamma_1}{2}\right) l_{NQ} d\right) - \cosh\left(\left(\frac{\gamma_0+\gamma_1}{2}\right) l_{NQ}\right)$$

$$\sum_{i=0}^{2} a_i \Delta V_i^{PQ} = -jX_{C_2} \sum_{i=0}^{2} I_i^P = -jX_{C_2} \sum_{i=0}^{2} \left(I_i^R \cosh(\gamma_i l_{RP}) - \frac{V_i^R}{Z_{C_i}} \sinh(\gamma_i l_{RP})\right)$$

$$\sum_{i=0}^{2} a_i \Delta V_i^{MN} = -jX_{C_1} \sum_{i=0}^{2} I_i^M = -jX_{C_1} \sum_{i=0}^{2} \left(I_i^S \cosh(\gamma_i l_{SM}) - \frac{V_i^S}{Z_{C_i}} \sinh(\gamma_i l_{SM})\right)$$

It is worth noting that the fault location equation (4.38) is derived for the fault lying between SCB1 and SCB2 in the SCCTL. Similarly, the fault location equations for the faults lying in the sections between 1-Bus S and SCB1, 2-SCB2 and Bus R could be derived. This might lead to a question that why three different fault location equations are needed for locating faults in different regions of SCCTL when the distributed model is utilized, while only one fault location equation i.e., (4.23) was derived irrespective of the faulted region when utilizing the lumped model. The answer lies in the fact that due to the simplicity of the lumped model of transmission line, the fault location equation for each section of the transmission line became identical to each other. The fault location equations based on distributed model for different sections of the SCCTL are also similar to each other. As a matter of fact, one fault location equation is sufficient to locate the fault in all sections of the transmission line. This phenomenon has also been illustrated through the simulation results presented in Section 4.5.

4.5 Evaluation of the proposed algorithm

A $500kV$, 350km long SCCTL with series compensation applied at two locations has been simulated in PSCAD. The transmission line and source parameters are as per given in Table 4.2. In System A configuration of the SCCTLs, a series compensation equivalent of 35%

Table 4.2: System Parameters.

Source Impedance		
	Positive Seq.	Zero Seq.
Sending End (Ω)	1.6 + j18.5	2.8 + j32.4
Receiving End (Ω)	1.2 + j13.8	2.1 + j24.5
Transmission Line		
	Positive Seq.	Zero Seq.
Impedance (Ω/km)	0.0155 + j0.3719	0.3546 + j1.0670
Admittance (S/km)	j4.4099×10^{-6}	j2.7844×10^{-6}

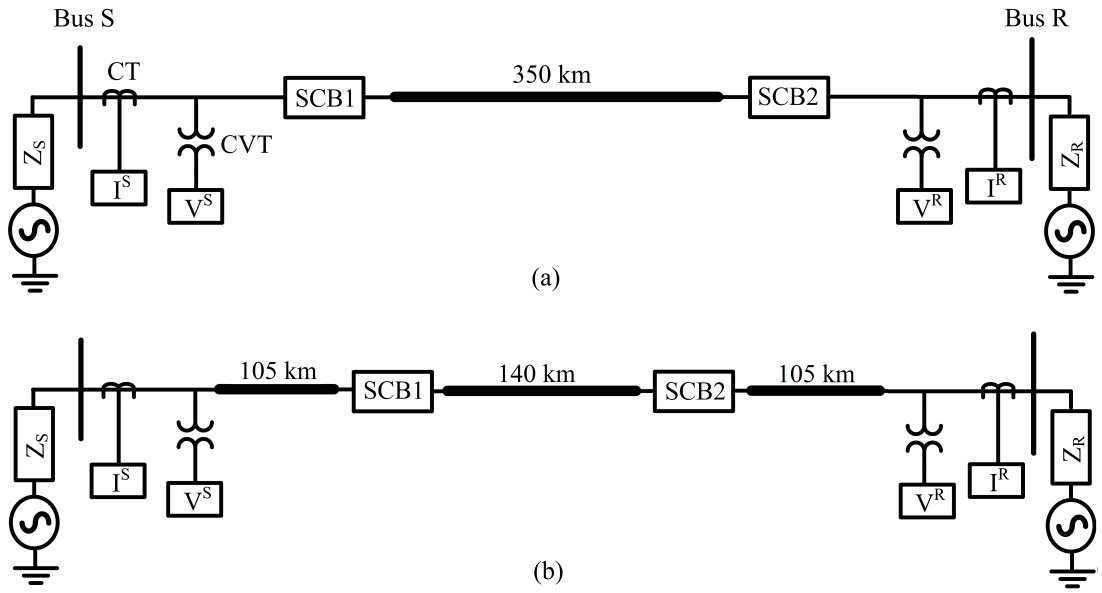

Figure 4.6: Presence of two SCBs in an SCCTL: (a) System A, (b) System B.

($C = 58.22\mu F$) is present at each terminal, while in System B, two SCBs equivalent to 35% series compensation each are present at 30% and 70% of line length as measured from Bus S of the SCCTL. The schematic diagrams showing System A and B configurations of the SCCTL are shown in Figure 4.6 (a) and (b), respectively. The System A offers wider variations in the location of fault while System B is utilized to elaborate the fact that one subroutine is sufficient to locate the fault in the three subsections of the SCCTL which are: 1-Bus S-SCB1; 2-SCB1-SCB2; 3-SCB2-Bus R. The load angle across the length of the SCCTL is 30° with Bus S voltage leading Bus R voltage.

The CT and CVT models available in PSCAD have been utilized to measure the current and voltage signals. The output of CTs and CVTs is passed through a 4^{th} order filter called anti-aliasing filter, and is then recorded with the sampling frequency of 20kHz. The recorded voltage and current signals are imported into Matlab, where they are resampled at 3840Hz. Thereafter, the resampled current and voltage signals are passed onto the phasor estimation algorithm, i.e., the Cosine algorithm. The estimated phasors are then applied to the proposed fault location algorithm to obtain the fault location results. The total time period from the inception of the fault to the opening of the transmission line circuit breakers is assumed to be 4 cycles of the fundamental frequency. The final fault location result is obtained by averaging the fault location results over the entire duration of the fault after discarding the $1\frac{1}{4}$ cycle worth of results which correspond to the transient time period of the Cosine filter.

4.5.1 Relative accuracy of the proposed algorithm using lumped and distributed model of transmission lines

The total number of 88 cases covering AG and BCG faults for different locations of fault and fault resistances have been simulated in PSCAD in System A configuration of the SCCTL. Table 4.3 shows the error in fault location results for each of the 88 cases. It could be observed from Table 4.3 that the proposed algorithm using distributed model consistently yields the error below 2% except for 5 fault cases. The highest error encountered in the fault location results obtained from distributed model of the proposed algorithm is 2.96% for a 100Ω BCG fault located at Bus S. On the other hand, the proposed algorithm using lumped model yields the error greater than 2% for 45 cases out of the total 88 cases. In particular, the errors yielded by the proposed algorithm using lumped model become increasingly excessive for the high impedance faults lying in the region of 60%-100% of the transmission line length as measured from the Bus S. The highest errors encountered for AG and BCG faults in the results obtained from the proposed algorithm using lumped model are 9.68%, and 9.97%, respectively. On the other hand, the highest errors for AG and BCG faults obtained from proposed algorithm based

Table 4.3: Error (%) in fault location results obtained from the proposed algorithm using lumped and distributed model of transmission line for different fault scenarios in System A configuration of the SCCTL.

Fault Type	Fault Location(%)	Lumped				Distributed			
		0Ω	10Ω	50Ω	100Ω	0Ω	10Ω	50Ω	100Ω
AG	0	0.81	0.14	2.28	2.39	0.58	0.73	2.15	2.89
	10	2.04	1.74	0.90	1.11	0.64	0.68	0.13	0.82
	20	2.31	2.12	1.77	2.22	0.50	0.55	0.22	0.66
	30	1.85	1.69	1.46	1.97	0.40	0.48	0.27	0.58
	40	0.91	0.80	0.58	0.81	0.35	0.37	0.17	0.45
	50	0.23	0.33	0.71	1.22	0.32	0.28	0.13	0.10
	60	1.27	1.66	2.47	3.54	0.07	0.34	0.41	0.62
	70	1.95	2.35	4.00	5.73	0.45	0.25	0.46	0.91
	80	2.43	2.88	4.99	7.63	0.79	0.66	0.26	1.03
	90	2.36	2.92	5.26	8.94	1.01	0.93	0.14	0.89
	100	1.40	2.20	4.89	9.68	1.07	1.04	0.51	0.60
BCG	0	1.04	0.41	2.34	2.23	1.40	0.70	2.37	2.96
	10	2.61	2.53	1.19	1.47	1.47	1.53	0.76	0.77
	20	2.67	2.69	2.02	2.56	1.55	1.53	1.11	0.38
	30	1.77	1.59	1.51	2.08	1.65	1.81	1.16	0.13
	40	1.16	0.06	0.31	0.91	0.63	2.09	1.01	0.18
	50	0.17	0.46	1.22	1.19	0.27	0.38	0.80	0.19
	60	1.06	1.39	2.97	3.81	0.94	0.69	0.69	0.75
	70	2.63	2.81	4.77	6.22	0.92	0.91	0.77	1.06
	80	3.48	3.69	5.54	8.24	1.00	1.17	0.07	1.22
	90	3.23	3.89	5.72	9.51	1.30	1.25	0.50	1.11
	100	1.68	2.70	5.26	9.97	1.28	1.21	0.51	0.80

on distributed model of the transmission line are 2.89%, and 2.96%, respectively.

It is worth noting that the acceptable limit for the error in the fault location results is 2% or below in the commercially available numerical relays [40]. In order to achieve the performance closer to this benchmark, the proposed algorithm needs to be implemented using distributed model of the transmission line. Therefore, all the fault location results presented hereafter have been obtained from the proposed algorithm based on the distributed model of the transmission line.

Table 4.4: Error (%) in fault location results obtained from the proposed algorithm using distributed model of transmission line for different fault scenarios in System B configuration of the SCCTL.

Fault	AG Faults				BCG Faults			
Location(%)	0Ω	10Ω	50Ω	100Ω	0Ω	10Ω	50Ω	100Ω
0	1.22	1.24	1.03	0.84	0.97	1.21	1.03	0.80
10	1.20	1.33	1.24	1.11	0.49	0.46	1.38	1.16
20	0.91	1.13	1.35	1.42	0.10	0.36	1.73	1.61
30^-	0.49	0.75	1.34	1.61	0.62	0.77	1.96	2.01
30^+	0.47	0.55	0.47	0.17	1.64	2.08	1.55	0.39
40	0.41	0.41	0.32	0.27	0.55	2.09	1.28	0.20
50	0.41	0.37	0.19	0.15	0.23	0.40	0.97	0.26
60	0.13	0.42	0.47	0.59	0.82	0.52	0.76	0.71
70^-	0.22	0.01	0.62	0.92	0.87	0.81	0.93	1.05
70^+	0.46	0.52	0.39	0.35	0.33	0.27	1.24	0.17
80	0.12	0.18	0.07	0.59	0.76	0.18	0.60	0.49
90	0.29	0.19	0.45	0.52	1.11	0.56	0.17	0.51
100	0.73	0.58	0.71	0.34	1.18	0.80	0.70	0.34

4.5.2 Sufficiency of one subroutine for fault location throughout SCCTL

In System B configuration of the SCCTL, a fault may lie between any section of the SCCTL which are: 1-Bus S-SCB1, 2-SCB1-SCB2, 3-SCB2-Bus R. Table 4.4 shows the error (%) in the fault location results for different locations of AG and BCG faults in System B configuration as measured from Bus S, and for different fault resistances. However, the point worth noting here is that the fault location results shown in Table 4.4 are yielded by only one subroutine, which assumes that the fault is lying in the section of the SCCTL between SCB1 and SCB2. Total of 104 cases of the fault scenarios were simulated in PSCAD. The signs '-' and '+' in super scripts for the faults at 30% and 70% denote the faults lying on the left and right side, respectively of the SCB1 and SCB2.

It could be seen from Table 4.4 that except for 3 cases, the error in the fault location results for all other cases is below 2%. As a matter of fact, for majority of the cases the error is blow 1.5%. The 3 fault scenarios for which the error is higher than 2% are 100Ω BCG fault at 30^-%, 10Ω BCG fault at 30^+%, and 10Ω BCG fault at 40%,with errors are 2.01%, 2.08%, and 2.09%, respectively. However, the only fault scenario with error higher than 2% that lies outside the zone of the used subroutine is the BCG fault at 30^-% with fault resistance 100Ω with error of 2.01%, which exceeds the commercial acceptable limit of 2% by a negligible amount. Thus, underscoring the fact that only one subroutine of the proposed algorithm is sufficient to locate

Table 4.5: Effect of errors in zero sequence parameters of the transmission line on the fault location results yielded by the proposed algorithm for solid AG and BCG faults in the SCCTL.

		AG Faults				BCG Faults			
	Fault Location (%)	Parameter Error (%)				Parameter Error (%)			
		0%	5%	10%	15%	0%	5%	10%	15%
Error in Zero Seq.	0	0.83	0.41	0.05	0.05	1.40	0.88	0.44	0.06
	20	0.50	0.29	0.12	0.12	1.55	1.20	0.90	0.65
	40	0.35	0.26	0.18	0.18	0.63	0.42	0.23	0.05
	60	0.07	0.02	0.13	0.13	0.94	0.95	0.99	1.03
	80	0.79	0.78	0.78	0.78	1.00	0.85	0.75	0.68
	100	1.07	0.76	0.49	0.49	1.28	0.88	0.55	0.27

the faults in the SCCTL, irrespective of the faulted section of the SCCTL.

4.5.3 Effect of errors in zero sequence parameters of the transmission line

In order to observe the effects of imperfect estimation of zero sequence parameters of the transmission line on the accuracy of the proposed algorithm, the deliberate errors of 5%, 10%, and 15% are introduced in zero sequence parameters of the transmission line, and the variation in the fault location results is noted as shown in Table 4.5. The maximum error noted for AG faults is 1.07% when the fault is located at 100% line length, while for BCG faults the maximum error of 1.55% is observed when the fault is located at 20% line length. Out of the total 48 cases, the error higher than 1% is observed in only 7 cases. The most significant point to note here is that the errors in all cases is below the industrially accepted limit of 2% [40].

Another metric to observe the immunity of the proposed algorithm to the error in zero sequence parameters of the transmission line is the variation in the error in fault location results as the error in zero sequence transmission line parameters changes. For example, for the case of AG fault at 100% line length, when the error in the zero sequence parameters is increased from 0% to 15% the error in fault location results decreases from 1.07% to 0.49%. The significance of this observation lies in the fact that with over the course of change in error from 0% to 15%, the variation in the fault location result has only been 0.58% between 1.07% to 0.49%. Similarly, for an AG fault at 60% line length, the maximum variation in the fault location results is 0.11% between 0.02% and 0.13% as the error in transmission line parameters changed from 0% to 15%. From the above discussion, it could be concluded that the proposed algorithm is relatively immune to the error in the zero sequence parameters of the transmission line.

Table 4.6: Effect of CT and CVT error on the error in fault location results (%) yielded by the proposed algorithm for solid faults in the SCCTL.

Fault Type	Fault Location (%)	Error in Fault Location with zero in CT\CVT error (%)	CT Error (%)				CVT Error (%)			
			Bus S		Bus R		Bus S		Bus R	
			2% ∠0°	5% ∠3°	2% ∠0°	5% ∠3°	2% ∠0°	5% ∠3°	2% ∠0°	5% ∠3°
AG	0%	0.83	0.81	0.80	0.83	0.24	0.83	0.83	0.83	0.80
	20%	0.50	0.85	1.09	0.41	0.83	0.50	0.50	0.50	0.46
	40%	0.35	0.90	1.04	0.06	1.39	0.35	0.35	0.35	0.34
	60%	0.07	0.56	0.59	0.36	1.41	0.07	0.07	0.08	0.09
	80%	0.79	0.42	0.19	1.07	1.52	0.79	0.79	0.79	0.76
	100%	1.07	0.85	0.47	1.05	1.04	1.07	1.07	1.08	1.07
BCG	0%	1.40	1.37	1.33	1.42	0.82	1.40	1.40	1.39	1.35
	20%	1.55	1.88	2.06	1.47	0.02	1.55	1.55	1.54	1.47
	40%	0.63	1.17	1.30	0.32	1.22	0.63	0.63	0.63	0.60
	60%	0.94	0.36	0.43	1.30	2.36	0.94	0.94	0.94	0.91
	80%	1.00	0.51	0.73	1.24	1.75	1.00	1.00	0.99	0.93
	100%	1.28	1.05	0.96	1.26	1.23	1.28	1.28	1.29	1.27

4.5.4 Sensitivity to CT and CVT errors

Another potential source of error that might affect the performance of the proposed algorithm is the error in signal measurements, i.e., CT and CVT error. The magnetizing current, leakage reactance and relay burden are some of the factors that limit the accuracy of the instrument transformers. The occurrence of a fault introduces considerable amount of transients into the current and voltage signals. As a result the instrument transformers are unable to faithfully replicate the primary side measurements at the secondary side especially under fault conditions.

In order to observe the effect of errors emanating from CT and CVT, two sets of deliberate error have been added to the estimated current and voltage phasors of the faulted phases. The two sets of the errors that have been used in this section are: 1- 2% error in phasor magnitude and no error in phase angle; 2- 5% error in phasor magnitude, and 3° error in phase angle. Each set of error is applied separately to Bus S and Bus R current and voltage phasors, which are then passed onto the proposed fault location algorithm. The fault location results for each scenario has been listed in Table 4.6.

It could be observed that addition of error in CT measurements affects the fault location results relatively more than the errors in CVT measurements. For example, for an AG fault at 40% line length the error in fault location result without any CT\CVT error is 0.35%. When an error of 2%∠0° is added to CT measurement at Bus S and Bus R the errors in fault location

result become 0.90% and 0.06%, respectively. When an error of 5%∠3° is introduced to Bus S and Bus R CT measurements, it produces the errors of 1.04% and 1.39%, respectively. However, when the same errors are added to the CVT measurements to either Bus S or Bus R, the error in fault location results remains at 0.35% or very close to it (=0.34%). This trend also holds for all other fault scenarios including BCG faults. The highest variation in fault location error for CVT error is noted for a BCG fault at 80% line length where the error of 5%∠3° produces an error of 0.93% in the fault location results while the error in fault location result is 1.00% when there is no CT and CVT error. In all of the the scenarios shown in Table 4.6, there is only one fault scenario for which the error in the fault location result is higher than 2% which is a BCG fault at 60% line length with 5%∠3° error in the CT measurement at Bus R.

From above discussion, it could be concluded that the proposed algorithm is highly immune to CVT errors that could be encountered in the faulted phase. On the other hand, the effect of CT error on the proposed algorithm is noticeable, however, the proposed algorithm is able to maintain adequate accuracy even under considerable error in CT measurement.

4.6 Conclusion

The impedance-based fault location algorithm proposed in this chapter is the first and only one of its kind that yields correct results for ground faults in the SCCTLs in which series compensation is applied at more than one location in an SCCTL. A general case of the proposed algorithm with N SCB locations in an SCCTL has been derived using lumped model of the transmission line. Thereafter, the proposed algorithm has been presented for two SCBs in an SCCTL using more accurate distributed model of the transmission line. Thereafter, the proposed algorithm has been evaluated for its performance on various metrics such as equivalence of the subroutines, the effect of errors in zero-sequence transmission line parameters, CT and CVT measurements on the fault location results yielded by the proposed algorithm through simulations carried out in PSCAD and Matlab.

Chapter 5

New MOV current measurement enabled impedance-based fault location algorithms

5.1 Introduction

As already discussed in previous chapters, the MOV located in the faulted phase conducts the fault current to protect SCB from the over-voltage caused by the fault current. During the process of fault current conduction, MOV in the faulted phase starts accumulating energy which results in the heating of the MOV. As an example, consider the Figure 5.1 which shows the MOV accumulated energy and the MOV current. Note that the accumulated energy in an MOV increases (see 5.1(a)) with each period of current conduction by the MOV (see 5.1(b)), leading to abrupt heating of MOV. This process lasts till the fault is cleared by the opening of the breakers located at the ends of the transmission line which is about 60-100 ms. Any meaningful dissipation of energy from MOV cannot be achieved irrespective of the cooling mechanism employed in such a rapid process.

Therefore, the energy accumulated in MOV needs to be estimated to avoid the runaway heating of MOV. The estimation of the energy accumulated in an MOV is accomplished by measuring the current flowing through it [14] as shown in Figure 5.2. Note the presence of CT to measure the current flowing through the MOV. It may seem from Figure 5.2 that the current going through bypass switch and bypass gap will also be measured by the CT. However, the bypass gap and bypass switch only conduct in case of MOV failure or the transmission line protection failure. For 'normal' fault conditions, MOV alone provides over-voltage protection to the series capacitor. The estimation of the amount of energy accumulated in an MOV using the current flowing through it is accomplished using one of various ways listed in [14].

From the prospective of fault location, the most important point to be noted from above dis-

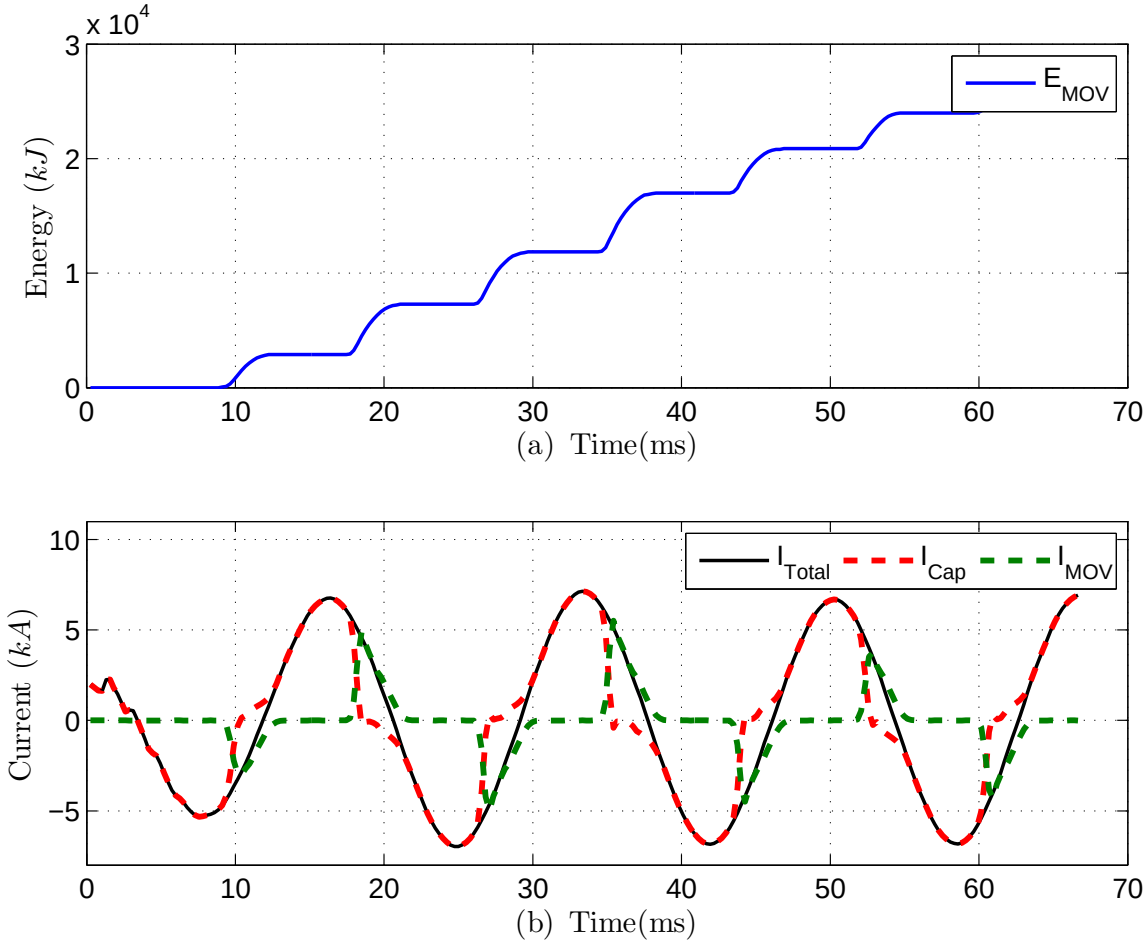

Figure 5.1: Heating of MOV due to fault current conduction: (a) accumulated energy in phase-A MOV, (b) current flowing through various elements of SCB in phase A for an AG fault.

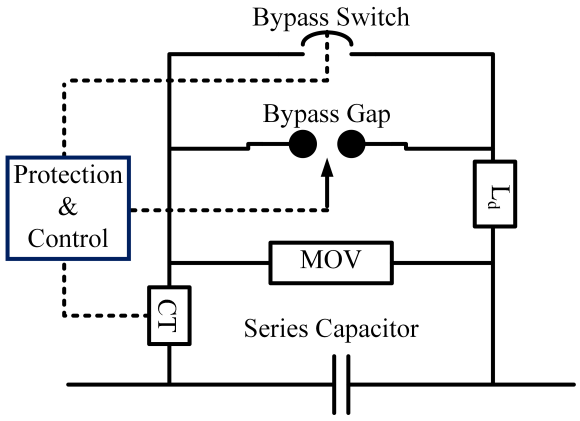

Figure 5.2: Series capacitor bank with current transformer in the MOV branch.

cussion is that the current flowing through MOV is measured. The measured MOV current can be used to propose new fault location algorithms which would only utilize positive sequence measurements and parameters of transmission line.

In this chapter, two new fault location algorithms are proposed which utilize the MOV current measurement from the SCB bus in addition to the SCCTL terminal measurements. The first fault location technique assumes that complete phasor information (magnitude and phase angle) is available from the CT located in MOV branch. The second fault location algorithm presented in this chapter is based on the scenario when only magnitude part of the phasor of the MOV current is known. It is important to note here that for the calculation of the MOV accumulated energy only the magnitude is needed. Therefore, in scenarios when phase angle of the current phasor of MOV current is not available, the second fault location algorithm would be applied. The fault location algorithm utilizing complete phasor is referred to Algorithm CP while the algorithm based only on magnitude of phasor is called Algorithm MP.

Firstly, Algorithm CP is presented in Section 5.2. Thereafter, Algorithm MP is presented in Section 5.3. The evaluation of the proposed algorithms through simulations carried out is presented in Section 5.4. The conclusion of the chapter is presented in 5.5.

5.2 Algorithm CP

As shown in Figure 5.3, the presence of the SCB in an SCCTL divides the transmission line in two sections: 1-section between Bus R and SCB; 2-section between SCB and Bus S. Any particular fault could lie in any of the two sections. Therefore, two subroutines are run simultaneously for each fault scenario with each subroutine dedicated to locate the fault in 'their' section. It would yield us two fault location results, one from each subroutine. The correct subroutine is then identified using the methodology presented in Section 5.2.3. As an example, for the system shown in Figure 5.3 (a), Subroutine 1 is used for locating faults lying between SCB and Bus R while Subroutine 2 is used to locate the fault between Bus S and SCB (Figure 5.3 (b)).

5.2.1 Subroutine 1

Consider an SCCTL with total length of l units, with SCB located at the p.u. distance of m from Bus S. Assume a fault lying at p.u. distance d from the SCB in the section between SCB ,and Bus R, as shown in Figure 5.3 (a). Note that the polarities of CTs have also been marked in Figure 5.3. The expression for the i^{th} sequence component of the fault voltage (V_i^F) could be

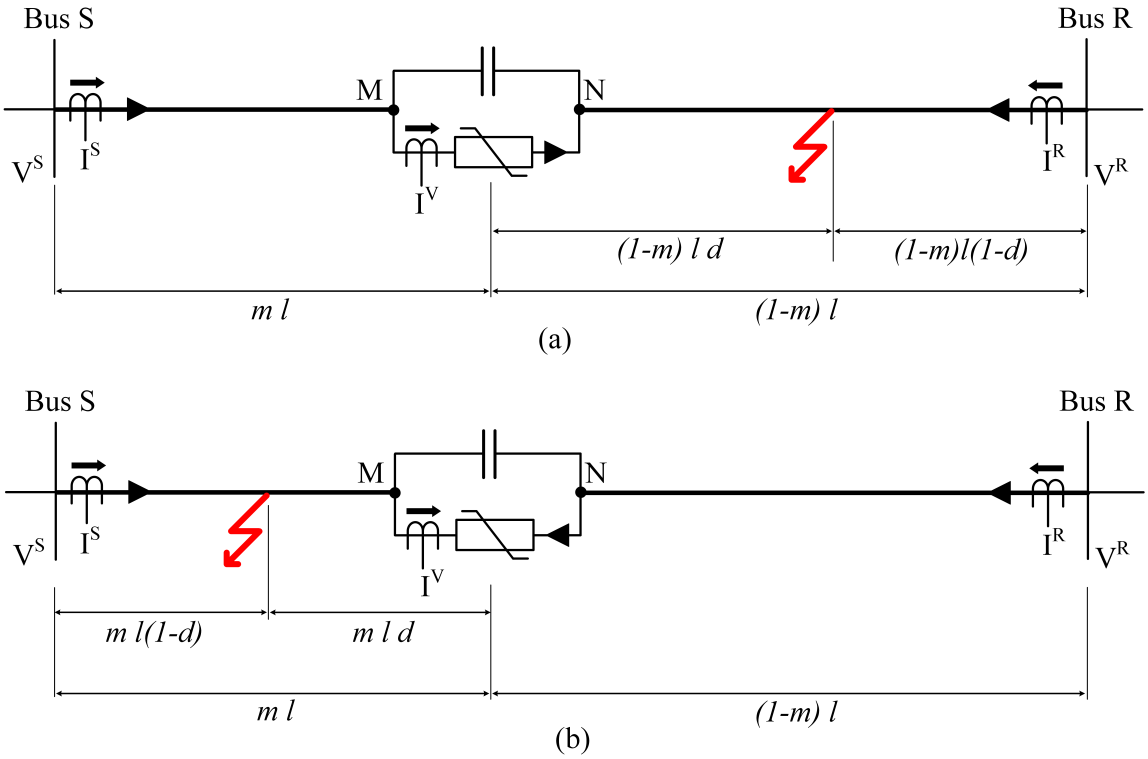

Figure 5.3: Faults in an SCCTL in between: (a) SCB and Bus R, (b) Bus S and SCB.

written as (5.1), using the voltage and currents at Node M.

$$V_i^F = \left(V_i^M - \Delta V_i^{MN}\right)\cosh\left((1-m)\,\gamma_i l d\right) - Z_{c_i} I_i^M \sinh\left((1-m)\,\gamma_i l d\right) \tag{5.1}$$

where i attains the value of 0, 1 and 2 for depicting zero, positive, and negative sequence components, respectively; V_i^M and I_i^M represent i^{th} sequence component voltage and current phasors at Node M as calculated from Bus S measurements using (5.2) and (5.3), respectively; ΔV_i^{MN} is the i^{th} sequence voltage drop across the SCB as measured from Node M to Node N; Z_{c_i} and γ_i are the i^{th} sequence characteristic impedance and propagation constant of the transmission line, respectively; l is the total length of the transmission line; m is p.u. distance of SCB from Bus S.

$$V_i^M = V_i^S \cosh\left(m\gamma_i l\right) - Z_{c_i} I_i^S \sinh\left(m\gamma_i l\right) \tag{5.2}$$

$$I_i^M = I_i^S \cosh\left(m\gamma_i l\right) - \frac{V_i^S}{Z_{c_i}} \sinh\left(m\gamma_i l\right) \tag{5.3}$$

Similarly, the expression for V_i^F as written from Bus R will be:

$$V_i^F = V_i^R \cosh\left((1-m)\,\gamma_i l\,(1-d)\right) - Z_{c_i} I_i^R \sinh\left((1-m)\,\gamma_i l\,(1-d)\right) \tag{5.4}$$

where V_i^R and I_i^R represent i^{th} sequence component voltage and current phasors at Bus R.

Equating (5.1) and (5.4) we get:

$$d = \frac{1}{\gamma_i\,(1-m)\,l} \tanh^{-1}\left(\frac{V_i^R \cosh((1-m)\,\gamma_i l) - Z_{c_i} I_i^R \sinh((1-m)\,\gamma_i l) - V_i^M + \Delta V_i^{MN}}{V_i^R \sinh((1-m)\,\gamma_i l) - Z_{c_i} I_i^R \cosh((1-m)\,\gamma_i l) - Z_{c_i} I_i^M}\right) \tag{5.5}$$

Now each term in (5.5) is known except ΔV_i^{MN}. The term ΔV_i^{MN} could be estimated using the current measurement in MOV branch, i.e., I^V. It can be observed from Figure 5.3 (a) that the voltage drop across SCBs of phase A, B, and C can be obtained by using (5.6)-(5.8), respectively.

$$\Delta V_A^{MN} = -j\left(I_A^M - I_A^V\right) X_c \tag{5.6}$$

$$\Delta V_B^{MN} = -j\left(I_B^M - I_B^V\right) X_c \tag{5.7}$$

$$\Delta V_C^{MN} = -j\left(I_C^M - I_C^V\right) X_c \tag{5.8}$$

where ΔV_A^{MN}, ΔV_B^{MN}, ΔV_C^{MN} are the voltage drops across SCB in phase A, B, and C; respectively. I_A^M, I_B^M, I_C^M are the currents entering SCBs in phase A, B, and C; respectively. I_A^V, I_B^V, and I_C^V represent the measured current by MOV CT's of phase A, B, and C; respectively. X_c is the reactance of the series capacitor in each phase.

Now, the sequence component of the voltage drop across SCB could be obtained from:

$$\begin{bmatrix} \Delta V_0^{MN} \\ \Delta V_1^{MN} \\ \Delta V_2^{MN} \end{bmatrix} = \frac{1}{3} \begin{bmatrix} 1 & 1 & 1 \\ 1 & \alpha & \alpha^2 \\ 1 & \alpha^2 & \alpha \end{bmatrix} \begin{bmatrix} \Delta V_A^{MN} \\ \Delta V_B^{MN} \\ \Delta V_C^{MN} \end{bmatrix} \tag{5.9}$$

where $\alpha = 1\angle 120^\circ$.

Substituting the values of ΔV_A^{MN}, ΔV_B^{MN}, ΔV_C^{MN} from (5.6)-(5.8) in (5.9):

$$\begin{bmatrix} \Delta V_0^{MN} \\ \Delta V_1^{MN} \\ \Delta V_2^{MN} \end{bmatrix} = \frac{1}{3} \begin{bmatrix} 1 & 1 & 1 \\ 1 & \alpha & \alpha^2 \\ 1 & \alpha^2 & \alpha \end{bmatrix} \begin{bmatrix} -j\left(I_A^M - I_A^V\right) X_c \\ -j\left(I_B^M - I_B^V\right) X_c \\ -j\left(I_C^M - I_C^V\right) X_c \end{bmatrix}$$

By performing the multiplication operation of the matrices in the above expression and utilizing

the identity: $1 + \alpha + \alpha^2 = 0$, following expressions will be obtained:

$$\Delta V_0^{MN} = -j\left(I_0^M - I_0^V\right)X_c \tag{5.10}$$

$$\Delta V_1^{MN} = -j\left(I_1^M - I_1^V\right)X_c \tag{5.11}$$

$$\Delta V_2^{MN} = -j\left(I_2^M - I_2^V\right)X_c \tag{5.12}$$

The expressions listed in (5.10)-(5.12) can be summarized as (5.13) in more generalized form:

$$\Delta V_i^{MN} = -j\left(I_i^M - I_i^V\right)X_c \tag{5.13}$$

Substituting the value of ΔV_i^{MN} from (5.13) in (5.5), the Equation (5.14) is obtained. It could be noted that all the variables on R.H.S. of (5.14) are known, thus, d could be calculated from (5.14).

$$d = \frac{1}{\gamma_i\,(1-m)\,l}\tanh^{-1}\left(\frac{V_i^R\cosh((1-m)\,\gamma_i l) - Z_{c_i}I_i^R\sinh((1-m)\,\gamma_i l) - V_i^M - j\left(I_i^M - I_i^V\right)X_c}{V_i^R\sinh((1-m)\,\gamma_i l) - Z_{c_i}I_i^R\cosh((1-m)\,\gamma_i l) - Z_{c_i}I_i^M}\right) \tag{5.14}$$

The total distance of the fault from Bus S could now be calculated from (5.15) where value of d is obtained from (5.14).

$$D_{S1} = ml + (1-m)ld \tag{5.15}$$

5.2.2 Subroutine 2

For the faults lying at p.u. distance d from SCB in the section between Bus S and SCB as shown in Figure 5.3 (b), the equation for obtaining d could be written as:

$$d = \frac{1}{\gamma_i ml}\tanh^{-1}\left(\frac{V_i^S\cosh(m\gamma_i l) - Z_{c_i}I_i^S\sinh(m\gamma_i l) - V_i^N + \Delta V_i^{NM}}{V_i^S\sinh(m\gamma_i l) - Z_{c_i}I_i^S\cosh(m\gamma_i l) - Z_{c_i}I_i^N}\right) \tag{5.16}$$

where V_i^N and I_i^N represent i^{th} sequence component voltage and current phasors at Node N as calculated from Bus R measurements using (5.17) and (5.18), respectively; ΔV_i^{NM} is the i^{th} sequence voltage drop across the SCB as measured from Node N to Node M.

$$V_i^N = V_i^R\cosh\left((1-m)\,\gamma_i l\right) - Z_{c_i}I_i^R\sinh\left((1-m)\,\gamma_i l\right) \tag{5.17}$$

$$I_i^N = I_i^R\cosh\left((1-m)\,\gamma_i l\right) - \frac{V_i^R}{Z_{c_i}}\sinh\left((1-m)\,\gamma_i l\right) \tag{5.18}$$

The only term that is unknown in (5.16) is ΔV_i^{NM} which can be estimated using the measured current I^V, flowing through the MOV branch of the SCB. The voltage drops across Node N to Node M in phases A, B, and C could be obtained from (5.19)-(5.21), respectively.

$$\Delta V_A^{NM} = -j\left(I_A^N + I_A^V\right) X_c \tag{5.19}$$

$$\Delta V_B^{NM} = -j\left(I_B^N + I_B^V\right) X_c \tag{5.20}$$

$$\Delta V_C^{NM} = -j\left(I_C^N + I_C^V\right) X_c \tag{5.21}$$

where ΔV_A^{NM}, ΔV_B^{NM}, ΔV_C^{NM} are the voltage drops across SCB in phase A, B, and C as measured from Node N to Node M; respectively. I_A^N, I_B^N, I_C^N are the currents entering SCBs in phase A, B, and C at Node N; respectively. It is worth noting that the sign of I^V for Subroutine 2 is opposite to that of Subroutine 1, it is due to the polarity of CT of MOV being opposite to that of I^V for Subroutine 2 while for Subroutine 1 the polarity of I^V and MOV CT was same.

The sequence components of the voltage drop across Nodes M to N could be obtained from the following equation:

$$\begin{bmatrix} \Delta V_0^{NM} \\ \Delta V_1^{NM} \\ \Delta V_2^{NM} \end{bmatrix} = \frac{1}{3} \begin{bmatrix} 1 & 1 & 1 \\ 1 & \alpha & \alpha^2 \\ 1 & \alpha^2 & \alpha \end{bmatrix} \begin{bmatrix} \Delta V_A^{NM} \\ \Delta V_B^{NM} \\ \Delta V_C^{NM} \end{bmatrix} \tag{5.22}$$

Combining Equations (5.19)-(5.21), and (5.22) we obtain following equations:

$$\Delta V_0^{NM} = -j\left(I_0^M + I_0^V\right) X_c \tag{5.23}$$

$$\Delta V_1^{NM} = -j\left(I_1^M + I_1^V\right) X_c \tag{5.24}$$

$$\Delta V_2^{NM} = -j\left(I_2^M + I_2^V\right) X_c \tag{5.25}$$

Equations (5.23) to (5.25) in a generalized way could be written as:

$$\Delta V_i^{NM} = -j\left(I_i^M + I_i^V\right) X_c \tag{5.26}$$

which could be utilized in (5.16) to yield (5.27). Since, all the variables on R.H.S. of (5.16) are known, d could be obtained from (5.27).

$$d = \frac{1}{\gamma_i m l} \tanh^{-1}\left(\frac{V_i^S \cosh(m\gamma_i l) - Z_{c_i} I_i^S \sinh(m\gamma_i l) - V_i^N - j\left(I_i^M + I_i^V\right) X_c}{V_i^S \sinh(m\gamma_i l) - Z_{c_i} I_i^S \cosh(m\gamma_i l) - Z_{c_i} I_i^N}\right) \tag{5.27}$$

The total distance of the fault from Bus could now be obtained from the Equation (5.28), where

value of d is used from (5.27).

$$D_{S2} = ml - mld \tag{5.28}$$

It should be noted that though the fault location Equations (5.14) and (5.27) could be compiled using any of positive, negative or zero sequence parameters and measurements, exclusively. However, only the positive sequence based fault location equations will be used to calculate fault location results. It is due to the fact that positive sequence currents are present in all of the fault types, and the estimated positive sequence parameters of the transmission lines are relatively more accurate as compared to zero sequence parameters. Thus, the performance evaluation of Algorithm CP will be performed on positive sequence based fault location equations.

5.2.3 Selection of Subroutine

For any fault scenario, each subroutine of the Algorithm CP would yield a fault location result, and only one of the two fault location results would be accurate. Therefore, a procedure is needed to select the 'correct' subroutine. One seemingly intuitive solution to this challenge would be comparing the MOV current (I^V) of the faulted phase with the current of the corresponding phase at each terminal of the transmission line, i.e., I^S and I^R. If I^V is close to I^S, then the fault must lie between SCB and Bus R, and Subroutine1 would be correct. On the other hand, if I^V is closer to I^R, then the fault would lie in between Bus S and SCB, and Subroutine2 would yield correct fault location. However, this scheme would fail for the fault scenarios where fault current is too small to force the conduction by MOV in the faulted phase. This would be particularly true for the high impedance faults occurring far from the SCB. Moreover, I^V would be available in its phasor form, and due to the intermittent nature of I^V, its phasor would be highly oscillatory in nature as compared to I^S and I^R. Therefore, comparison of I^V to I^S and I^R for selecting the appropriate subroutine might not yield the correct results.

Therefore, the methodology for selecting the appropriate subroutine as presented in [22] would be utilized for identifying the correct subroutine of Algorithm CP. As per the methodology of [22], the impedance of the SCB in a faulted phase is calculated using the fault location results of Subroutine 1 and Subroutine 2 as denoted by Z_{SUB1}^{SCB} and Z_{SUB2}^{SCB}, respectively. If the real part of either Z_{SUB1}^{SCB}, or Z_{SUB2}^{SCB} is negative, then the fault location result of the corresponding subroutine is rejected. If however, the real of both SCB impedances is positive then the imaginary part of the the SCB impedances is observed. The imaginary part of the correct subroutine would be negative, and its magnitude will be less than the reactance of the series capacitor.

5.3 Algorithm MP

As already mentioned that in order to avoid the overheating of MOV, the energy accumulated in the MOV is estimated by measuring the current passing through it. For the estimation of the accumulated energy, only the magnitude of the current passing through MOV is required. Thus, the situation may arise that only the magnitude of the MOV current phasor is available for the purpose of fault location. The fault location algorithm that will be presented in this section, estimates the location of a fault in an SCCTL using the magnitude of MOV current only, and has been referred to as Algorithm MP in this thesis.

It is a known fact that SCB consists of a parallel combination of an MOV, and a series capacitor. The MOV acts as a resistive element while conducting the fault current. Thus, the SCB could be seen as a parallel combination of a series capacitor of known capacitance and unknown resistance (of MOV) in the faulted phase. Though, this assumption is not completely accurate as the series capacitor and MOV conduct alternatively during each fundamental cycle of the fault current as could be observed from Figure 5.1 (b). Therefore, the SCB acts as: 1-a pure capacitance when series capacitor is conducting the fault current; 2-a pure resistance for the time period MOV is conducting fault current. Now, to extrapolate above fact into assumption that the resulting combination will be a parallel combination of known capacitance and an unknown resistance is not entirely accurate, it nevertheless gives us a useful information that could be used towards fault location in an SCCTL.

As in the case of Algorithm CP, the Algorithm MP would need two subroutines with Subroutine1 for the faults lying between SCB and Bus R, and Subroutine2 for the faults lying in the region between Bus S and SCB. Thereafter, the correct subroutine would be selected using specialized procedure to obtain the location of the fault in the SCCTL.

5.3.1 Subroutine1

Consider a fault scenario in an SCCTL with fault lying at p.u. distance of d from SCB between SCB and Bus R as shown in Figure 5.4 (a). The length of the transmission line is l units with SCB located at the p.u. distance of m from Bus S. The following relations would hold true with reference to Figure 5.4 (a):

$$\begin{aligned} I_p^M &= I_p^C + I_p^V \\ \implies I_p^C &= I_p^M - I_p^V \end{aligned} \tag{5.29}$$

where p represents phase A, B, and C. I_p^M represents the p^{th} phase current at Node M; I_p^C and I_p^V are the p^{th} phase currents passing through series capacitor and MOV, respectively.

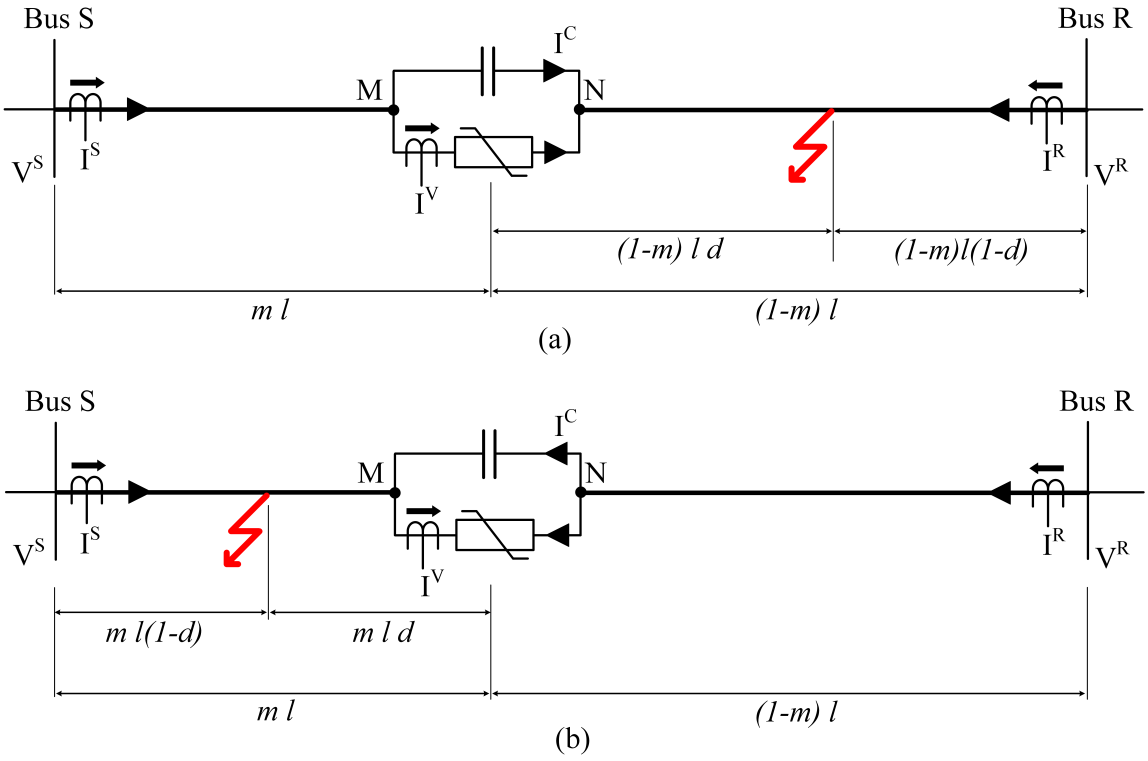

Figure 5.4: Faults in an SCCTL in between, (a) SCB and Bus R, (b) Bus S and SCB.

The Equation (5.29) could be written as (5.30) by resolving the MOV current phasor I_p^V into its magnitude and argument.

$$I_p^C = I_p^M - |I_p^V| e^{j\theta^{I_p^V}} \tag{5.30}$$

I_p^M is calculated from Bus S measurements using Equation (5.3); $|I_p^V|$ is known from the MOV current measurement. The only unknown that prevents the estimation of I_p^C from (5.30) is $\theta^{I_p^V}$. It is a known fact that for an RC parallel combination the Capacitor current will lead the current in resistive branch by 90°. The phasor representation of the currents I_p^C, I_p^M, and I_p^V would be as given in Figure 5.5. From Figure 5.5, it can be observed that:

$$\theta^{I_p^V} = \theta^{I_p^M} - \cos^{-1}\left(\frac{|I_p^V|}{|I_p^M|}\right)$$

Substituting value of $\theta^{I_p^V}$ in (5.30), the Equation (5.31) is obtained which yields the value of I_p^C.

$$I_p^C = I_p^M - |I_p^V| e^{j\left(\theta^{I_p^M} - \cos^{-1}\left(\frac{|I_p^V|}{|I_p^M|}\right)\right)} \tag{5.31}$$

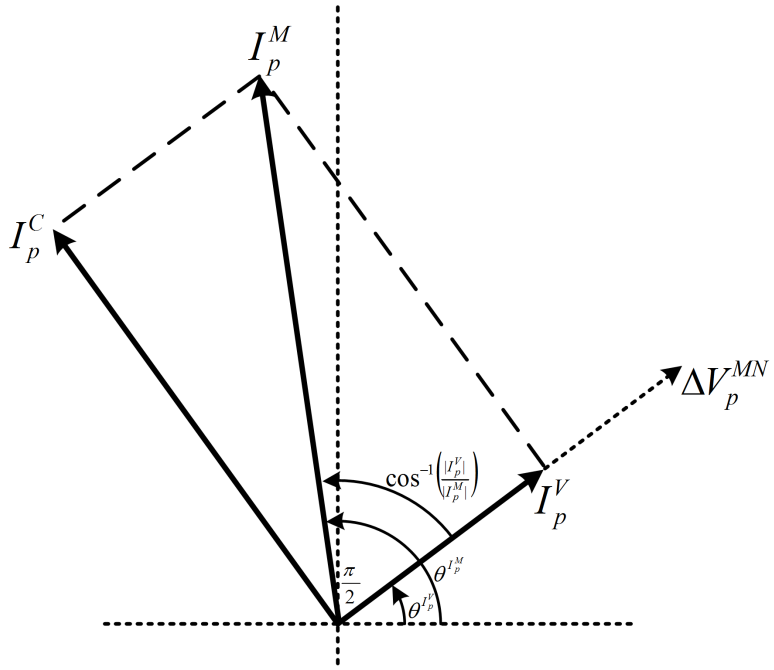

Figure 5.5: Phasor diagram depicting various currents in an SCB with respect to the voltage drop across SCB for Subroutine1.

Consequently, the voltage drop across SCB in p^{th} phase, i.e., ΔV_p^{MN} could be obtained from the following equation:

$$\Delta V_p^{MN} = -jX_C I_p^C = -jX_C \left(I_p^M - |I_p^V| e^{j\left(\theta^{I_p^M} - \cos^{-1}\left(\frac{|I_p^V|}{|I_p^M|}\right)\right)} \right) \tag{5.32}$$

The sequence component of the voltage drop across SCB could be obtained from (5.33).

$$\begin{bmatrix} \Delta V_0^{MN} \\ \Delta V_1^{MN} \\ \Delta V_2^{MN} \end{bmatrix} = \frac{1}{3} \begin{bmatrix} 1 & 1 & 1 \\ 1 & \alpha & \alpha^2 \\ 1 & \alpha^2 & \alpha \end{bmatrix} \begin{bmatrix} -jX_C \left(I_A^M - |I_A^V| e^{j\left(\theta^{I_A^M} - \cos^{-1}\left(\frac{|I_A^V|}{|I_A^M|}\right)\right)} \right) \\ -jX_C \left(I_B^M - |I_B^V| e^{j\left(\theta^{I_B^M} - \cos^{-1}\left(\frac{|I_B^V|}{|I_B^M|}\right)\right)} \right) \\ -jX_C \left(I_C^M - |I_C^V| e^{j\left(\theta^{I_C^M} - \cos^{-1}\left(\frac{|I_C^V|}{|I_C^M|}\right)\right)} \right) \end{bmatrix} \tag{5.33}$$

Now, d would be obtained from the Equation (5.34) for the Subroutine1, where value of ΔV_i^{MN} is obtained from (5.33).

$$d = \frac{1}{\gamma_i (1-m) l} \tanh^{-1} \left(\frac{V_i^R \cosh((1-m)\gamma_i l) - Z_{c_i} I_i^R \sinh((1-m)\gamma_i l) - V_i^M + \Delta V_i^{MN}}{V_i^R \sinh((1-m)\gamma_i l) - Z_{c_i} I_i^R \cosh((1-m)\gamma_i l) - Z_{c_i} I_i^M} \right) \tag{5.34}$$

The total distance of the fault from the Bus S by Subroutine1 (D_{S1}) will be given by Equation (5.35).

$$D_{S1} = ml + (1 - m)ld \tag{5.35}$$

5.3.2 Subroutine2

For Subroutine2, consider the fault lying between Bus S and SCB at p.u. distance of d units from SCB as shown in Figure 5.4 (b). Noting the polarity of the MOV CT and the current direction in the MOV for faults lying between Bus S and SCB, the following expressions would hold true at Node N:

$$\begin{aligned} I_p^N &= I_p^C - I_p^V \\ \implies I_p^C &= I_p^N + I_p^V \end{aligned} \tag{5.36}$$

where I_p^N represents the p^{th} phase current at Node N. I_p^N is estimated from Bus R measurements using Equation (5.18), and converting sequence currents to phase currents. The magnitude of I_p^V is also known from the SCB measurements. The Equation (5.36) could be written as (5.37) where the only unknown quantity is $\theta^{I_p^V}$, which prevents the estimation of the I_p^C and consequently, the voltage drop across SCB ΔV_p^{NM}.

$$I_p^C = I_p^N + |I_p^V| e^{j\theta^{I_p^V}} \tag{5.37}$$

For the faults lying between Bus S and SCB, and the direction of currents as shown in Figure 5.4 (b), the phasor diagram for currents in SCB could be drawn as shown in Figure 5.6. Now referring to the Figure 5.6, the following relationship could be derived.

$$\theta^{I_p^V} = \theta^{I_p^N} + \pi - \cos^{-1}\left(\frac{|I_p^V|}{|I_p^N|}\right)$$

Substituting the value of $\theta^{I_p^V}$ in (5.37):

$$\begin{aligned} I_p^C &= I_p^N + |I_p^V| e^{j\theta^{I_p^N} + \pi - \cos^{-1}\left(\frac{|I_p^V|}{|I_p^N|}\right)} \\ &= I_p^N - |I_p^V| e^{j\theta^{I_p^N} - \cos^{-1}\left(\frac{|I_p^V|}{|I_p^N|}\right)} \qquad \left(\because e^{j\pi} = -1\right) \\ \implies \Delta V_p^{NM} &= -jX_C I_p^C = -jX_C \left(I_p^N - |I_p^V| e^{j\theta^{I_p^N} - \cos^{-1}\left(\frac{|I_p^V|}{|I_p^N|}\right)}\right) \end{aligned} \tag{5.38}$$

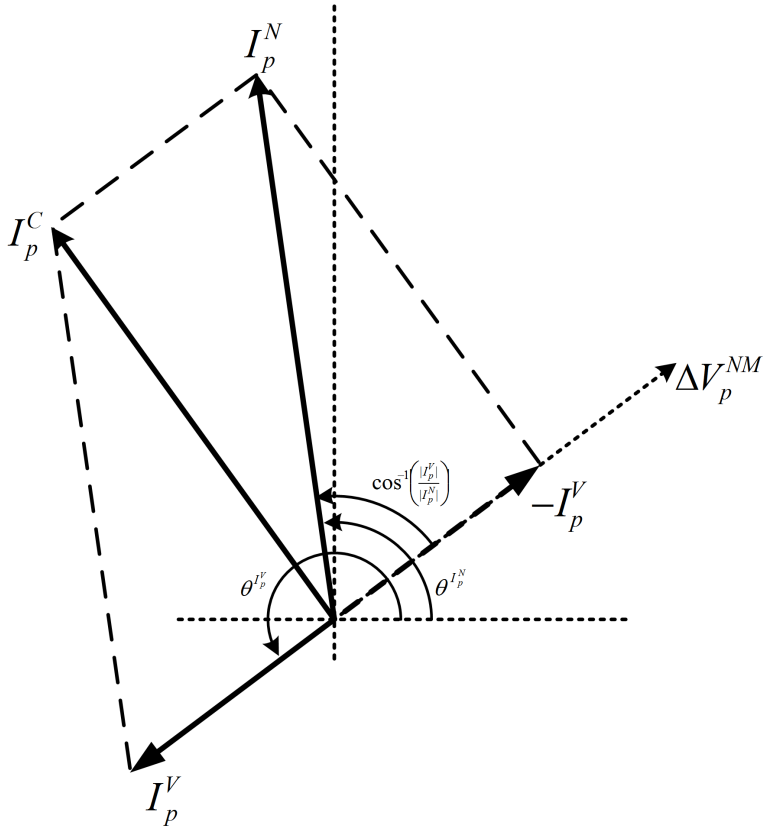

Figure 5.6: Phasor diagram depicting various currents in SCB with respect to the voltage drop across SCB for Subroutine2.

where V_p^{NM} is the voltage drop across Node N to Node M in p^{th} phase.

Accordingly, the sequence component of the voltage drop, i.e., V_i^{NM} could be obtained from:

$$\begin{bmatrix} \Delta V_0^{NM} \\ \Delta V_1^{NM} \\ \Delta V_2^{NM} \end{bmatrix} = \frac{1}{3}\begin{bmatrix} 1 & 1 & 1 \\ 1 & \alpha & \alpha^2 \\ 1 & \alpha^2 & \alpha \end{bmatrix} \begin{bmatrix} -jX_C\left(I_A^N - |I_A^V|e^{j\left(\theta^{I_A^N} - \cos^{-1}\left(\frac{|I_A^V|}{|I_A^N|}\right)\right)}\right) \\ -jX_C\left(I_B^N - |I_B^V|e^{j\left(\theta^{I_B^N} - \cos^{-1}\left(\frac{|I_B^V|}{|I_B^N|}\right)\right)}\right) \\ -jX_C\left(I_C^N - |I_C^V|e^{j\left(\theta^{I_C^N} - \cos^{-1}\left(\frac{|I_C^V|}{|I_C^N|}\right)\right)}\right) \end{bmatrix} \tag{5.39}$$

Now d would be obtained from the Equation (5.40) for the Subroutine2, where value of ΔV_i^{NM} is obtained from (5.39).

$$d = \frac{1}{\gamma_i ml}\tanh^{-1}\left(\frac{V_i^S\cosh(m\gamma_i l) - Z_{c_i}I_i^S\sinh(m\gamma_i l) - V_i^N + \Delta V_i^{NM}}{V_i^S\sinh(m\gamma_i l) - Z_{c_i}I_i^S\cosh(m\gamma_i l) - Z_{c_i}I_i^N}\right) \tag{5.40}$$

The total distance of the fault from the Bus S by Subroutine1 (D_{S1}) will be given by Equation (5.41).

$$D_{S2} = ml - mld \tag{5.41}$$

Similar to the Algorithm CP, the performance evaluation of Algorithm MP will be performed on positive sequence based fault location equations only.

5.3.3 Selection of Subroutine

The correct subroutine for Algorithm MP is selected following the same procedure as performed for the Algorithm CP as detailed in Section 5.2.3.

5.4 Evaluation of the proposed algorithms

5.4.1 Test System

The System A and System B configurations of the power system described in Section 2.7.1 have been utilized in this chapter to validate the performance of the Algorithm CP and Algorithm MP. The schematic diagrams of System A ,and System B configurations are shown in Figure 5.7 (a), and (b), respectively. The configuration of System A offers wider variety of the fault scenarios to test the performance of the proposed fault location algorithms while System B is used to show the need for different subroutines for locating faults in different sections of the

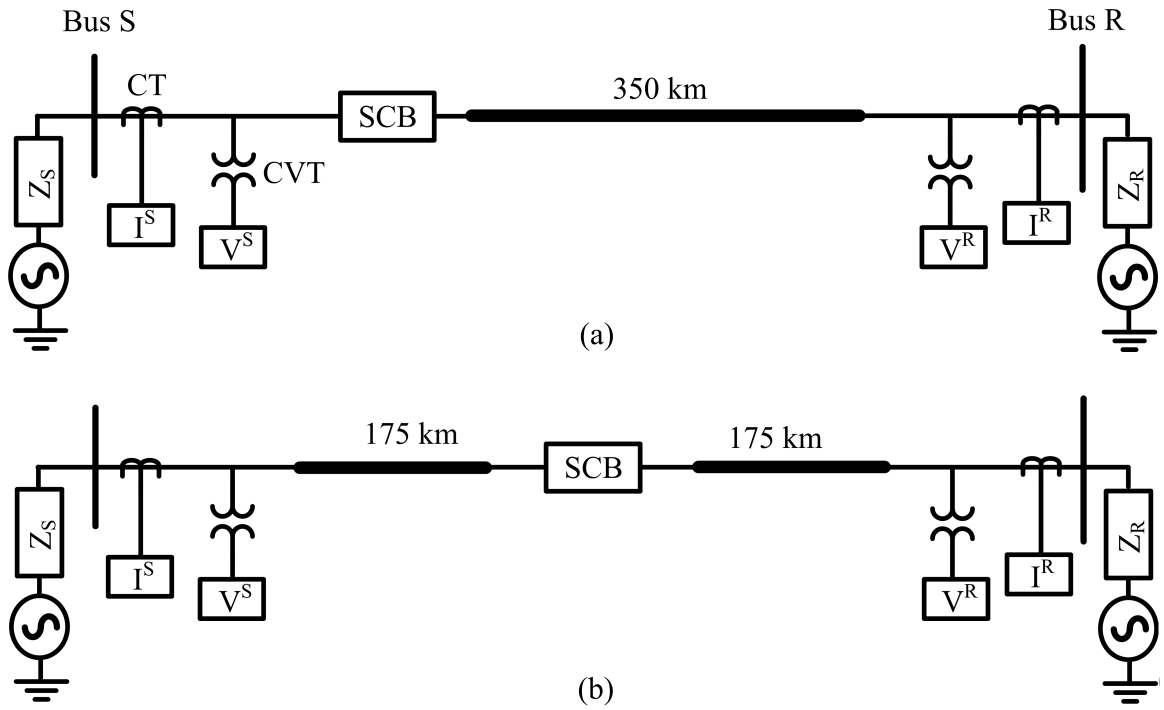

Figure 5.7: Single-line diagram of simulated system in PSCAD; (a) System A, (b) System B.

SCCTL. The MOV current measurement at the SCB is the only additional measurement that has been added to the power system of Section 2.7.1.

5.4.2 Accuracy and the effect of fault resistance on the Algorithm CP and Algorithm MP

The Table 5.1 shows the error in fault location results yielded by Algorithm CP and Algorithm MP for different fault types, fault resistances and fault locations. The fault location is measured as percentage of the total line length as measured from Bus S. It could be observed from Table 5.1 that for lower fault resistances (0Ω and 10Ω), the error yielded by the Algorithm CP remains below 2% for all types of faults and locations of the fault. The highest errors yielded by Algorithm CP for each type of low resistive faults are 1.48% for 10Ω AG fault at 80% line length, 1.84% for 0Ω BCG fault at 0% line length, 1.57% for 10Ω BC fault at 20% line length, 1.77 % for 0Ω ABC fault at 0% line length. For fault resistance 50Ω, the errors yielded by Algorithm CP are relatively higher than those for the low impedance fault, still the errors are below 2% level for all the fault scenarios except one which is the error of 2.89% for fault at 80% line length. However, as the fault resistance reaches 100Ω the errors yielded by Algorithm CP exceed 2% level for multiple fault scenarios. The error as high as 4.26% is observed for a 100Ω AG fault at 80% line length. The reason for this increase in error yielded

Table 5.1: Error (%) in the fault location results yielded by Algorithm CP and Algorithm MP.

Fault Resistance	Actual Fault Location (%)	AG Fault		BCG Fault		BC Fault		ABC Fault	
		CP	MP	CP	MP	CP	MP	CP	MP
0Ω	0	1.11	2.17	1.84	3.18	0.83	3.59	1.77	3.00
	20	0.23	7.93	0.37	8.10	0.86	9.87	0.28	6.66
	40	0.28	4.59	0.44	4.37	0.54	4.28	0.16	4.17
	60	0.79	1.35	0.80	1.97	1.02	1.42	0.37	2.35
	80	1.48	1.00	1.07	0.01	1.44	0.71	0.53	0.74
	100	1.43	1.37	1.08	0.90	1.16	1.05	0.65	0.39
10Ω	0	0.97	1.68	1.52	2.22	1.52	3.29	1.58	2.04
	20	0.56	8.91	1.01	10.1	1.57	11.4	0.94	9.39
	40	0.24	4.85	0.15	5.61	0.36	5.11	0.08	5.35
	60	0.80	1.36	0.65	2.57	0.93	1.82	0.27	2.86
	80	1.45	0.98	0.93	0.35	1.35	0.45	0.47	0.97
	100	1.19	1.15	0.96	0.74	1.14	0.96	0.59	0.29
50Ω	0	0.91	1.52	1.24	1.84	1.75	2.94	1.44	1.83
	20	0.92	6.30	1.10	6.51	2.12	9.08	1.73	6.80
	40	0.20	3.50	0.32	5.07	0.59	6.94	0.95	5.94
	60	1.47	0.30	0.62	1.78	0.43	2.82	0.12	2.84
	80	2.89	2.84	1.75	1.27	1.18	0.15	0.81	0.12
	100	1.91	1.92	1.85	1.85	1.34	1.27	1.62	1.62
100Ω	0	0.01	0.25	0.42	0.71	1.72	2.64	0.71	0.84
	20	0.22	1.49	0.05	1.89	1.70	5.69	0.95	2.66
	40	1.90	0.87	1.27	0.37	0.93	5.20	0.18	1.94
	60	4.22	4.15	2.88	2.41	0.48	1.60	1.31	0.70
	80	4.26	4.26	3.66	3.66	1.99	1.58	2.83	2.82
	100	2.64	2.65	2.22	2.22	2.01	2.01	1.90	1.91

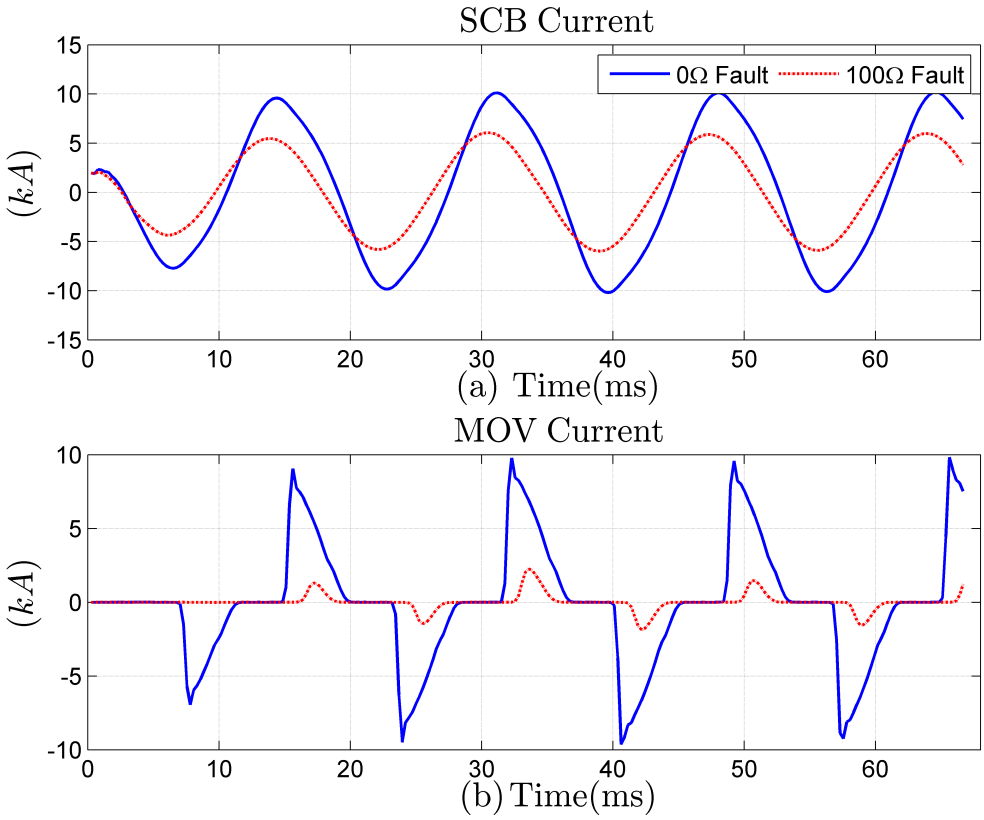

Figure 5.8: The current flowing through SCB and MOV for 0Ω and 100Ω AG faults at 20% line length: (a) total phase A current flowing through SCB, (b) current flowing through MOV of phase A.

by Algorithm CP with increasing fault resistance is similar to the loss of accuracy of distance relay for the high impedance fault which is due to the fact that with increase in fault resistance the fault current decreases which makes the fault location algorithm relatively insensitive to the location of the fault.

The Algorithm MP on the other hand yields the error higher than 2% for almost half of the fault scenarios irrespective of the fault resistance. However, the error is extraordinarily high for the low resistive faults lying at 20% line length. For example, the errors for AG, BCG, BC, and ABC faults at 20% line length are 7.93%, 8.10%, 9.87%, and 6.66%, respectively. The error then gradually decreases as the fault moves away from Bus S. Also, as the fault resistance increases the error for the faults located at 20% line length also decreases. The relatively high errors from Algorithm MP for the low impedance faults lying in the range of 20-40% line length is due to the high MOV activity for the faults lying in that range. Since, the proposition of Algorithm MP is based on the assumption that the MOV and series capacitor form a parallel combination during fault period, which as mentioned in Section 5.3, is not completely

accurate as the series capacitor and MOV conduct alternatively during each fundamental cycle of the fault current. The underlying assumption becomes erroneous whenever MOV conducts for considerable part of the fundamental cycle. As the fault moves away from 40% line length towards Bus R, or as the fault resistance becomes higher the conduction through MOV decreases which in turn improves the accuracy of the Algorithm MP as the assumption becomes true again. Figure 5.8 shows the effect of fault resistance on the current flowing through phase A SCB, and MOV for 0Ω and 100Ω AG faults at 20% line length. It could be seen from Figure 5.8 (a) that the total fault current flowing through phase A SCB for 100Ω AG fault is considerably less as compared to 0Ω AG fault. As a result, the MOV conducts for very less time in the case of 100Ω AG fault as compared to the case of 0Ω AG fault as evident from Figure 5.8 (b). The magnitude of MOV current for 100Ω fault is very small as compared to that for 0Ω fault. Thus, the higher activity in phase-A MOV for 0Ω AG fault translates into relatively higher error in the fault location result. The waveforms of MOV current and the total current flowing through SCB in all three phases for all the simulated fault scenarios are shown in Appendix D. As could be observed from Appendix D, the fault scenarios for which MOV conducts for longer time period within a fundamental cycle are the ones for which Algorithm MP yields significant error.

Another peculiar observation that could be made from Table 5.1 is that for the high impedance faults lying close to the Bus R, i.e., 100% line length, the errors yielded by Algorithm CP and Algorithm MP become almost identical. This is due to the fact that the fault current flowing through SCB for the high impedance faults located close to Bus R is not high enough for MOV to start conduction. Therefore, the series capacitor is exclusively responsible for the conduction of the fault current, consequently, the voltage drop across SCB as calculated by both algorithms is equivalent. Hence, the identical fault location error is yielded by both algorithms for the high impedance faults lying close to the Bus R.

5.4.3 Relative accuracy of the Algorithm CP, Algorithm MP, Algorithm PM and Algorithm EM

The fault loop based fault location algorithms for SCCTLs have been discussed in Chapter 2, while a new fault location algorithm for ground faults has been proposed in Chapter 3. Two new fault location algorithms which use the MOV current measurement have been proposed in this chapter. In this section, the accuracy of all the proposed impedance-based fault locations and the existing fault loop based fault location algorithms is compared to each other for different scenarios in System A configuration of the SCCTL.

The fault location algorithm of Chapter 3 is denoted by Algorithm PM while the existing

Table 5.2: Comparison of the accuracy of the different fault location algorithms.

Fault Type	Fault Location(%)	Fault Resistance: 0Ω				Fault Resistance: 100Ω			
		CP	MP	PM	EM	CP	MP	PM	EM
AG	0	1.11	2.17	0.27	0.59	0.01	0.25	0.01	24.08
	20	0.23	7.93	0.52	3.62	0.23	1.49	0.11	12.95
	40	0.28	4.59	0.61	12.73	1.90	0.88	0.22	10.27
	60	0.79	1.36	0.59	3.54	4.23	4.15	0.58	51.05
	80	1.48	1.01	0.41	1.18	4.26	4.27	0.80	29.40
	100	1.43	1.37	0.04	0.04	2.65	2.65	0.43	34.80
BCG	0	1.85	3.19	0.56	1.96	0.42	0.71	0.56	24.19
	20	0.37	8.10	0.25	1.64	0.06	1.90	0.42	16.72
	40	0.44	4.37	0.09	8.11	1.28	0.37	0.20	7.17
	60	0.80	1.98	0.14	2.05	2.88	2.42	0.56	7.02
	80	1.07	0.01	0.31	0.73	3.67	3.66	0.92	66.51
	100	1.08	0.91	0.26	0.05	2.22	2.23	0.47	36.78
BC	0	0.83	3.60	–	1.96	1.73	2.64	–	15.97
	20	0.87	9.88	–	1.64	1.70	5.70	–	9.20
	40	0.54	4.28	–	10.17	0.93	5.20	–	8.91
	60	1.03	1.42	–	2.08	0.49	1.61	–	43.05
	80	1.44	0.72	–	0.73	1.99	1.59	–	70.39
	100	1.17	1.05	–	0.05	2.01	2.01	–	26.21
ABC	0	1.77	3.01	–	1.97	0.72	0.85	–	23.68
	20	0.28	6.67	–	1.66	0.95	2.66	–	14.97
	40	0.16	4.17	–	5.85	0.18	1.95	–	3.46
	60	0.37	2.36	–	1.96	1.31	0.71	–	13.29
	80	0.53	0.74	–	0.74	2.84	2.82	–	68.50
	100	0.66	0.40	–	0.04	1.91	1.91	–	36.78

algorithm fault loop based algorithms are denoted by Algorithm EM in Table 5.2. The Table 5.2 shows the fault location results obtained from each type of fault location algorithm for solid and 100Ω faults. Since the Algorithm PM proposed in Chapter 3 provides fault location results for only ground faults in SCCTLs, the column for fault location results for BC and ABC by Algorithm PM remain blank. The errors over 2% in the fault location results have been highlighted in Table 5.2.

For solid faults the Algorithm CP and Algorithm PM yield error below 2% for all the fault scenarios. In particular, the error yielded by Algorithm PM remains below 1%. The maximum error in the fault location results obtained from Algorithm CP in case of solid faults is 1.85% for BCG fault at 0% line length while the maximum error yielded by Algorithm PM is 0.61% for an AG fault at 40% line length. On the other hand the Algorithm MP and Algorithm EM

yield error in excess of 2% for almost half of the solid fault scenarios. Another significant point to be noted is that an excessively large error are seen in case of Algorithm MP when the fault lies close to of 20% of the line length, while in the case of Algorithm EM the largest errors are observed when the fault is close to 40% of the transmission line length. For example, for faults at 20% line length the errors yielded by Algorithm MP for AG, BCG, BC, and ABC faults are 7.93%, 8.10%, 9.88%, and 6.67% respectively. The error yielded by Algorithm EM for faults lying at 40% line length the errors are 12.7%, 8.11%, 10.17%, and 5.85% for AG, BCG, BC, and ABC faults, respectively. The maximum MOV activity for the fault lying at 20% line length as explained in the Section 5.4.2 is the reason for high error in Algorithm CP. On the other hand the reason for high error yielded by Algorithm EM for the faults lying at 40% line length is the 'closeness' of the argument of the total fault current to the argument of Bus R as explained in detail in Section 2.7.2.

As the fault resistance reaches 100Ω the error yielded by Algorithm PM still remains below 1% with maximum error of 0.92% for BCG fault at 80% line length. The Algorithm EM on the other hand loses accuracy for virtually all of the fault scenarios with errors in excess of 10% seen for almost all the fault scenarios. The performance of Algorithm CP and Algorithm MP becomes almost equivalent to each other for AG and BCG faults with the fault resistance of 100Ω as the MOV activity has decreased drastically due to lower fault current. However, for the BC and ABC faults close to 20% line length where the fault current through SCB is relatively higher even with the fault resistance of 100Ω, the Algorithm MP still yields relatively higher errors as compared to Algorithm CP. For example, for 100Ω BC fault at 20% line length the errors yielded by Algorithm CP and Algorithm MP are 1.70% and 5.70%, respectively.

Thus, it could be concluded that Algorithm PM yields the most accurate fault location results, followed by Algorithm CP. Though it is worth noting that Algorithm CP is applicable to all types of faults while Algorithm PM is only applicable to the ground faults. The Algorithm MP and Algorithm EM are susceptible to higher errors. However, it is worth noting that accuracy of Algorithm MP improves with increase in fault resistance while the accuracy of Algorithm EM decays with increase in fault resistance.

5.4.4 Effect of errors in zero sequence parameters of the transmission line

It has already been mentioned that the fault location equations used by both algorithms, i.e., Algorithm CP and Algorithm MP utilize only positive sequence parameters of the transmission line. Therefore, the Algorithm CP and Algorithm MP would remain unaffected by the amount of error in the zero sequence parameters of the transmission line. In order to elaborate this

Table 5.3: Effect of errors in zero sequence parameters of the transmission line on the error in fault location results (%) yielded by the Algorithm CP and Algorithm MP.

Algorithm CP												
Fault Loc. (%)	AG Faults			BCG Faults			BC Faults			ABC Faults		
	Parameter Error			Parameter Error			Parameter Error			Parameter Error		
	0%	10%	15%	0%	10%	15%	0%	10%	15%	0%	10%	15%
0	1.11	1.11	1.11	1.85	1.85	1.85	0.83	0.83	0.83	1.77	1.77	1.77
20	0.23	0.23	0.23	0.37	0.37	0.37	0.87	0.87	0.87	0.28	0.28	0.28
40	0.28	0.28	0.28	0.44	0.44	0.44	0.54	0.54	0.54	0.16	0.16	0.16
60	0.79	0.79	0.79	0.80	0.80	0.80	1.03	1.03	1.03	0.37	0.37	0.37
80	1.48	1.48	1.48	1.07	1.07	1.07	1.44	1.44	1.44	0.53	0.53	0.53
100	1.43	1.43	1.43	1.08	1.08	1.08	1.17	1.17	1.17	0.66	0.66	0.66

Algorithm MP												
Fault Loc. (%)	AG Faults			BCG Faults			BC Faults			ABC Faults		
	Parameter Error			Parameter Error			Parameter Error			Parameter Error		
	0%	10%	15%	0%	10%	15%	0%	10%	15%	0%	10%	15%
0	2.17	2.17	2.17	3.19	3.19	3.19	3.60	3.60	3.60	3.01	3.01	3.01
20	7.93	7.93	7.93	8.10	8.10	8.10	9.88	9.88	9.88	6.67	6.67	6.67
40	4.59	4.59	4.59	4.37	4.37	4.37	4.28	4.28	4.28	4.17	4.17	4.17
60	1.36	1.36	1.36	1.98	1.98	1.98	1.42	1.42	1.42	2.36	2.36	2.36
80	1.01	1.01	1.01	0.01	0.01	0.01	0.72	0.72	0.72	0.74	0.74	0.74
100	1.37	1.37	1.37	0.91	0.91	0.91	1.05	1.05	1.05	0.40	0.40	0.40

point, the deliberate errors of 10% and 15% are added to the zero sequence parameters of the transmission lines, and the fault location results are calculated for the solid faults occurring in the SCCTL. The fault location results so obtained are given in Table 5.3.

It could be seen from Table 5.3 irrespective of the error in the zero sequence parameters of the transmission line, the error in fault location results obtained from Algorithm CP and Algorithm MP remains constant. For example, a the errors in fault location results yielded by Algorithm CP and Algorithm MP for an AG fault at 60% line length are 0.79%, and 1.36%, respectively and remain constant for 0%, 10%, and 15% errors in the zero sequence parameters of the transmission line. Thus, it could be concluded that the Algorithm CP and Algorithm MP are immune to the errors in the zero sequence parameters of the transmission line.

5.4.5 Sensitivity to CT and CVT errors

In this section, the effect of CT and CVT errors on the performance of the proposed fault location algorithms, Algorithm CP and Algorithm MP has been investigated using the System

A configuration of the SCCTL. A deliberate errors of 5% in phasor magnitude, and 3° in phasor angle are applied to the estimated current and voltage phasors of the faulted phases, separately. There are three points for current measurement in the test power system which are Bus S, Bus R, and SCB (MOV) while voltage measurement is done at two points Bus S and Bus R. Therefore, the error of 5%∠3° is added to current measurements at Bus S, Bus R, and MOV, while for voltage measurements the error 5%∠3° is added to the Bus and Bus R. The fault location results obtained from Algorithm CP, and Algorithm MP after the addition of error at different measurement points are given in Table 5.4.

It could be seen from Table 5.4 that the widest fluctuation in fault location error due to addition of error in CT measurements is observed for the faults lying close to Bus S and when the error lies in CT located at Bus S. For example, for a solid AG faults at 0% line length the fault location error yielded by Algorithm CP without any CT\CVT error is 1.11%. However, when the error of 5%∠3° is added to CT measurement at Bus S, the error in fault location result becomes 4.74%. In the same way, the fault location result error yielded by Algorithm MP for the same fault scenario without any CT\CVT error is 2.17%. However, with the addition of error 5%∠3° to the current measurement at Bus S the fault location errors yielded by Algorithm MP becomes 6.03%, thus highlighting the higher effect of error in Bus S CT on the accuracy of Algorithm MP. Similar observations are made from BCG, BC, and ABC faults lying at 0% line length regarding the relatively higher influence of error in CT located at Bus S on the fluctuation of the fault location results yielded by Algorithm CP and Algorithm MP. As the faults move away from the Bus S the effect of CT error on the fault location results decreases. This observation is evident from the fact that the fault location error yielded by both algorithms fluctuates in a band smaller than 1% for all the faults lying at 100% line length.

However, the introduction of error to the CTs located at Bus R and MOV does not lead to wider variations in the fault location errors yielded by Algorithms CP and Algorithm MP. As an example when the error 5%∠3° is added to the CTs located at Bus R and MOV for a solid AG fault at 0% line length, the errors in fault location results become 1.93% and 1.40%, respectively while the error in fault location results without any CT\CVT is 1.11%. The widest variation in the fault location results yielded by Algorithm CP and caused by the error in CT located at Bus R is found for a solid BC fault at 0% line length when the fault location error changes from 0.83% with no CT\CVT error to 2.68% with introduction of error at Bus R CT. Moving on similar lines it could be seen that the error in CTs located at Bus R and MOV bank does impact the output of the fault location location algorithms, however, the effect is relatively smaller as compared to that of the error in CT located at Bus S, especially for the fault located at 0% line length.

The effect of CVT error on the fault location results obtained from both algorithms is also

Table 5.4: Effect of CT and CVT error on the error in fault location results (%) yielded by the Algorithm CP and Algorithm MP for solid faults in the SCCTL.

Algorithm CP							
Fault Type	Fault Location (%)	Error in Fault Location without error in CT\CVT	Error in CT			Error in CVT	
			Bus S	Bus R	MOV	Bus S	Bus R
AG	0	1.11	4.74	1.93	1.40	2.31	1.01
	40	0.28	1.94	1.82	0.90	1.49	1.10
	60	0.79	0.13	1.35	1.05	0.67	0.31
	100	1.43	1.92	1.31	1.44	0.79	1.42
BCG	0	1.85	5.49	2.65	2.08	1.53	1.63
	40	0.44	1.49	1.43	1.55	1.34	0.56
	60	0.80	0.26	1.01	1.50	0.65	0.54
	100	1.08	1.59	0.98	1.16	0.53	1.08
BC	0	0.83	4.28	2.68	1.58	4.43	1.26
	40	0.54	1.50	1.75	1.68	1.70	0.73
	60	1.03	0.45	1.38	1.81	0.88	0.70
	100	1.17	1.72	1.08	1.30	0.47	1.31
ABC	0	1.77	5.73	2.39	1.99	1.78	1.39
	40	0.16	1.66	0.93	1.38	0.87	0.63
	60	0.37	0.12	0.45	1.12	0.20	0.20
	100	0.66	1.17	0.57	0.72	0.15	0.66

Algorithm MP							
Fault Type	Fault Location (%)	Error in Fault Location without error in CT\CVT	Error in CT			Error in CVT	
			Bus S	Bus R	MOV	Bus S	Bus R
AG	0	2.17	6.03	2.99	2.18	1.26	2.07
	40	4.59	7.58	3.06	3.04	3.37	5.98
	60	1.36	2.47	0.73	0.62	1.46	1.84
	100	1.37	1.84	1.26	1.41	0.74	1.37
BCG	0	3.19	7.01	4.01	3.18	0.19	2.98
	40	4.37	7.30	3.26	2.24	3.45	5.38
	60	1.98	3.14	1.58	0.78	2.10	2.24
	100	0.91	1.36	0.84	1.01	0.35	0.91
BC	0	3.60	7.61	5.37	3.80	1.66	4.02
	40	4.28	7.21	2.98	2.18	3.10	5.56
	60	1.42	2.56	0.89	0.22	1.54	1.76
	100	1.05	1.56	1.01	1.19	0.35	1.20
ABC	0	3.01	7.12	3.64	3.01	0.54	2.63
	40	4.17	6.99	3.23	1.98	3.44	4.96
	60	2.36	3.52	2.07	1.08	2.51	2.54
	100	0.40	0.82	0.35	0.51	0.11	0.40

higher for when the error is applied to CVT located at Bus S and the fault lies close to Bus S. For example, the fault location error yielded by Algorithm CP changes from 0.83% when there is no error in the measurements to 4.43% when the error 5%∠3° is added to the CVT measurements at Bus S for a solid BC fault at 0% line length. For the same fault scenario, the error yielded by Algorithm MP change from 3.60% when there is no measurement error to 1.66% when the error of 5%∠3° is added to Bus S CVT measurements. Another example depicting the same phenomenon is the solid BCG fault at 0% line length when the fault location error yielded by Algorithm MP changes from 3.19% to 0.19% when error of 5%∠3° is added to CVT measurement at Bus S. Similar to the case of CT error, the effect of CVT error at Bus S on the performance of both fault location algorithms lessens as the fault moves closer to Bus R.

On the other hand, the effect of error in CVT located at Bus R on the performance of both algorithms is relatively lower when compared to the effect of Bus S CVT error. It is evident from the fact that when the error is added to CVT at Bus R the observed changes in fault location error are less than 1% for all the fault scenarios. For example, for a solid BC fault at 0% line length the error yielded by Algorithm CP changes from 0.83% when there is no CT\CVT error to 1.26% when the error 5%∠3° is added to the Bus R CVT. Similar, observation regarding the effect of Bus R CVT error on the output of Algorithm CP, and Algorithm MP could be made from all other fault scenarios shown in Table 5.4.

Thus, it could be concluded from the above discussion that when SCB is present at Bus S terminal of the transmission line then the Algorithm CP and Algorithm MP become susceptible to error in Bus S measurements, particularly for the faults lying closer to Bus S.

5.4.6 Selection of subroutines

If the SCB is located anywhere in the SCCTL apart from its terminals, the dedicated subroutines are needed to locate the fault in each section of the SCCTL. For example, in System B configuration as shown in Figure 5.7 (b), one subroutine would assume the fault to be located between Bus S and SCB and will yield a fault location result. Similarly, the other subroutine will yield a fault location result assuming the fault is located between SCB and Bus R. Thus, arises the need to select the 'correct' subroutine and to discard the 'wrong' subroutine.

The different fault scenarios are simulated in System B configuration, with faults between 0-50^{-}% line length as measured from Bus S lying between Bus S and SCB, while faults between 50^{+}-100% line length as measured from Bus S lying between SCB and Bus R. The Tables 5.5, and 5.6 show the fault location results obtained from both subroutines of Algorithm CP, and Algorithm MP, respectively. The real and imaginary parts of impedance of the SCB

Table 5.5: The selection of subroutine for Algorithm CP

Fault Type	Actual Fault Location (%)	Subroutine1 Estimated Fault Loc. (%)	Subroutine1 $\Re(Z_{SCB})$ (Ω)	Subroutine1 $\Im(Z_{SCB})$ (Ω)	Subroutine2 Estimated Fault Loc. (%)	Subroutine2 $\Re(Z_{SCB})$ (Ω)	Subroutine2 $\Im(Z_{SCB})$ (Ω)
AG	0	70.51	-45.7	-155.6	1.45	14.7	-83.0
	20	91.36	-88.0	-170.4	21.05	17.1	-84.9
	40	108.60	-153.7	-217.6	40.05	22.2	-85.8
	50^-	116.89	17.5	-283.8	49.06	2.93	-86.0
	50^+	49.71	27.2	-73.5	17.99	180.6	-226.5
	60	59.48	24.6	-78.9	8.99	118.4	-239.2
	80	78.98	18.4	-87.5	9.68	18.8	-217.7
	100	98.93	14.7	-90.5	29.89	-25.9	-169.5
BCG	0	70.1	-58.4	-85.7	1.11	22.4	-93.5
	20	90.01	-64.9	-93.7	20.71	27.4	-87.3
	40	108.31	-83.3	-117.6	39.78	31.1	-77.3
	50^-	117.17	-88.3	-137.1	49.38	32.1	-72.0
	50^+	49.44	31.9	-60.6	18.23	11.2	-233.8
	60	59.30	31.2	-65.1	9.15	-22.3	-202.9
	80	79.09	28.7	-74.6	9.79	-50.7	-144.7
	100	99.14	25.0	-85.6	30.11	-62.7	-106.6
BC	0	70.13	-6.87	-90.7	1.09	13.5	-99.4
	20	89.74	-19.5	-95.7	20.44	24.9	-92.2
	40	107.99	-29.3	-121.7	39.44	30.7	-79.6
	50^-	116.90	-25.6	-143.1	49.09	32.1	-72.8
	50^+	49.33	31.9	-58.3	18.33	88.8	-208.2
	60	59.14	31.3	-62.7	9.30	39.9	-186.5
	80	78.81	29.2	-71.5	9.52	-3.84	-135.9
	100	98.86	25.6	-80.7	29.82	-8.98	-102.0
ABC	0	69.72	-10.2	-92.0	0.70	27.4	-86.4
	20	89.58	-26.2	-103.6	20.28	32.1	-77.5
	40	108.16	-40.1	-136.9	39.63	33.9	-66.6
	50^-	117.16	-40.6	-164.7	49.38	34.0	-60.9
	50^+	49.76	32.9	-56.9	17.94	55.5	-172.8
	60	59.67	32.1	-62.9	8.80	25.3	-156.4
	80	79.55	28.7	-74.9	10.25	-3.92	-121.8
	100	99.49	22.4	-86.5	30.48	-7.64	-98.03

Table 5.6: The selection of subroutine for Algorithm MP.

Fault Type	Actual Fault Location (%)	Subroutine1 Error Fault Loc. (%)	Subroutine1 $\Re(Z_{SCB})$ (Ω)	Subroutine1 $\Im(Z_{SCB})$ (Ω)	Subroutine2 Error Fault Loc. (%)	Subroutine2 $\Re(Z_{SCB})$ (Ω)	Subroutine2 $\Im(Z_{SCB})$ (Ω)
AG	0	70.57	-45.8	-155.8	1.40	15.1	-83.6
	20	90.55	-86.3	-167.7	21.75	17.4	-86.1
	40	102.15	-133.2	-181.2	38.56	22.0	-90.7
	50^-	104.01	15.8	-242.9	46.49	2.2	-79.2
	50^+	53.60	22.4	-79.9	9.02	133.6	-209.2
	60	62.13	20.7	-83.5	4.08	98.1	-225.6
	80	79.78	16.4	-89.3	12.55	13.9	-208.2
	100	99.06	13.8	-91.2	31.07	-26.0	-166.4
BCG	0	69.66	-58.0	-85.0	0.68	20.7	-96.8
	20	84.61	-61.5	-82.5	18.78	24.3	-93.4
	40	89.83	-77.7	-68.0	36.06	26.6	-84.7
	50^-	79.04	-89.6	-25.2	44.90	27.2	-79.4
	50^+	53.42	28.4	-64.4	25.43	-93.1	-129.9
	60	62.36	27.9	-68.3	11.74	-55.5	-150.7
	80	80.41	26.3	-76.2	19.17	-54.4	-124.3
	100	99.39	23.7	-85.9	33.01	-61.3	-101.9
BC	0	70.61	-6.9	-91.4	0.56	14.0	-103.7
	20	85.78	-19.7	-87.2	18.32	23.8	-99.5
	40	89.97	-39.9	-72.1	35.61	28.1	-88.5
	50^-	78.60	-65.9	-29.4	44.62	29.1	-81.7
	50^+	53.24	30.1	-63.5	38.87	-144.8	-103.4
	60	61.98	29.6	-66.7	23.85	-58.0	-111.4
	80	79.83	28.1	-73.4	21.68	-19.0	-109.4
	100	99.03	25.1	-81.3	34.43	-10.3	-94.2
ABC	0	68.55	-10.1	-90.2	0.23	27.6	-89.9
	20	82.30	-26.0	-87.1	18.34	31.5	-83.7
	40	88.45	-47.6	-75.1	36.04	32.5	-74.6
	50^-	86.58	-64.9	-54.5	45.14	32.4	-69.3
	50^+	53.41	30.4	-61.9	31.42	-75.3	-83.4
	60	62.58	29.6	-67.2	13.67	-19.5	-112.0
	80	81.01	26.6	-77.8	20.20	-13.1	-103.1
	100	99.86	21.1	-88.0	33.64	-8.4	-93.1

in the faulted phase, as calculated using fault location results of both subroutines of Algorithm CP, and Algorithm MP, are also given in the Tables 5.5, and 5.6. For AG faults, the impedance of phase A SCB is given while for BCG, BC, and ABC faults the impedance of phase B SCB is given.

To find the correct subroutine, first of all the real part of the SCB impedance is observed. The subroutine whose SCB impedance has negative real part is immediately discarded and the result of subroutine whose SCB impedance has positive real part is regarded as the correct fault location result. For example, it could be seen from Table 5.5 that for an AG fault at 40% line length Subroutine1 of Algorithm CP yields the fault location result as 91.36% while Subroutine2 of Algorithm CP yields the fault location result as 21.05%. The real part of the impedance of the faulted phase SCB calculated by Subroutine1 is -88.0Ω while that calculated by Subroutine2 is 17.1Ω. Therefore, the result of Subroutine2, i.e., 21.05% is selected as the correct fault location result.

In case the real part of the impedances of the faulted phase SCB calculated by both subroutines is positive, then the imaginary part of the SCB impedances has to be observed. The imaginary part of the correct subroutine would be negative, and its magnitude will be less than or equal to the reactance of the series capacitor. One such example is the BCG fault at 50^{+}% of the line length where Subroutine1 of Algorithm CP yields the result as 49.44% with real part of SCU impedance as 31.9Ω, while Subroutine2 of Algorithm CP yields the result as 18.23% with real part of SCB impedance as 11.2Ω. Looking at imaginary parts of SCB impedances it could be observed that the imaginary part of SCB impedance yielded by Subroutine1 is -60.6Ω which is negative, and its magnitude is less than 91Ω, while that yielded by Subroutine2 is -233.8Ω which is negative, but its magnitude is quite large as compared to 91Ω. Therefore, the result of Subroutine1 of Algorithm CP, i.e., 49.44% is regarded as correct fault location result.

The correct subroutine for Algorithm CP, and Algorithm MP for all other fault scenario could be identified by using the above shown procedure. The correct subroutines of Algorithm CP and Algorithm MP have been highlighted in Tables 5.5 and 5.6, respectively.

5.5 Conclusion

In this chapter, two new faults location algorithms have been presented which utilize the MOV current measurement from SCB. The first proposed fault location algorithm utilizes the complete phasor, i.e., phasor magnitude and phase angle of the measured MOV current for the purpose of fault location. The second proposed fault location algorithm uses only phasor magnitude of the measured MOV current. Both of the proposed fault location algorithms are independent of the zero sequence parameters of the transmission line. As the presence of SCB

in an SCCTL splits the transmission line into two sections, both of the proposed fault location algorithms need a dedicated subroutine for locating the fault in each section of the transmission line. The process for identifying the correct subroutine which is based on the proposition of [22], is presented in the chapter. The simulations carried out in PSCAD and Matlab have been utilized to verify the performance of the proposed fault location algorithms on various metrics such as the effect of error in CT\CVT measurements, error in zero sequence parameters of the transmission line on the performance of the proposed algorithms. The accuracy of the proposed algorithms has been compared to that of the algorithm proposed in Chapter 3, and the fault loop-based fault location algorithm of [22]. The criteria for selecting the correct subroutine has been elaborated through simulations.

Chapter 6

Fundamentals: Traveling wave-based fault location algorithms

6.1 Introduction

The occurrence of fault in a transmission line acts as an application of a step voltage at the point of fault. This sudden application of step voltage produces the traveling waves which start traveling from the fault point towards each end of the transmission line. As a matter of fact, the traveling wave is the mechanism through which any 'incident' gets 'communicated' through the transmission system. For example, assume that a fault occurs at distance d kilometers away from one of the terminals of the transmission line at time $t = 0\,\text{s}$, where s denotes second. Let the propagation speed of traveling wave in the transmission line be u kilometers per second. The traveling wave generated at fault point would reach that particular end of the transmission line at $t = \frac{d}{u}\,\text{s}$. For the time period between $t = 0\,\text{s}$ to $t = \frac{d}{u}\,\text{s}$, the source at the terminal remains 'oblivious' to the fact that a fault has occurred in the transmission line and keeps supplying the steady state current to the transmission line. At the time $t = \frac{d}{u}\,\text{s}$ the traveling wave arrives at the source, and then source 'reacts' to the fault by making the changes to the voltage and current at its terminal.

A key inference that could be drawn from the above discussion is that if time taken by the traveling wave to arrive at a terminal of the transmission line from the fault point is known then the distance of the fault could be easily calculated. This is what forms the basis of the traveling wave-based fault location algorithms. It led to the advent of traveling wave-based fault location algorithms. The application of the concept of traveling waves for the distance protection of transmission lines was first proposed in [29] in 1983. Thereafter, numerous fault location algorithms for conventional as well as series capacitor compensated transmission lines have

been proposed (SCCTLs) [28], [30], [31]. However, the practical application of the traveling wave-based fault location algorithms did not happen until about late 2015, when Schweitzer Engineering Laboratories introduced SEL-T400L. This delay between the proposition and implementation of the traveling wave-based fault location algorithms is due to the fact that the traveling waves travel at the speeds which are close to the speed of light, and to obtain an acceptable accuracy of the fault location results a very high sampling frequency is required. Higher the sampling frequency, higher will be the accuracy of the the fault location results. However, the technological barriers have limited the sampling frequency to 1 MHz in commercial products as reported for SEL-T400L. The sampling frequency of 1 MHz will reduce the uncertainty in the fault location results to 300 meters. However, most of the numerical relays used in the power systems have sampling frequency below 5 kHz. With the introduction of high sampling frequency relay like SEL-T400L, the interest in traveling wave-based fault location algorithms has re-emerged.

In this chapter, the fundamental concepts forming the basis of the traveling wave-based fault location algorithms for SCCTLs such as the modeling of transmission lines for traveling wave, detection of a traveling wave, types of traveling wave-based fault location algorithms etc. are discussed. The Section 6.2 presents the background to the theory of traveling waves and modeling of transmission line, while Section 6.3 presents the introduction of wavelet transformation which is used for the detection of traveling waves in the measured signals. The two types of existing traveling wave-based fault location algorithms, i.e., single-ended, and double-ended fault location algorithms are explained in Section 6.4.

6.2 Modeling of the transmission line

The transmission line is usually considered as an inductive component when modeling a power system, and it holds true for the relatively slower events in the power systems with the time period of few tens of milliseconds. However, when analyzing the traveling waves in a transmission line which travel at the speed close to that of light, the steady state models of transmission line cannot reflect the behavior of the transmission line properly. Highly detailed and accurate models of the transmission line have been proposed in literature [43]. However, Bergeron model, which assumes that the line is lossless is relatively simpler to analyze, and could be used for studying the first few traveling waves following a fault in a transmission line. In the following section, the equations representing traveling waves in a transmission line are derived which further lead to the proposition of Bergeron model of the transmission line.

Figure 6.1 shows an infinitesimally small section of a lossless transmission line of length dx located at the distance of x units from the Bus S. In Figure 6.1, k represents α, β, or γ modes;

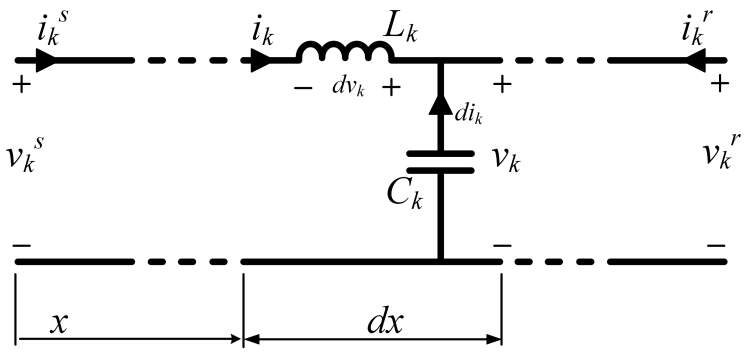

Figure 6.1: Representation of a lossless line using a series of lumped elements.

v_k and i_k represent the k^{th} mode instantaneous voltage and current, respectively at point x units away from Bus S; L_k and C_k represent the k^{th} mode inductance per unit length, and capacitance per unit length of the transmission line, respectively.

In Figure 6.1, the voltage drop across the infinitesimally small section is given by:

$$\partial v_k = -L_k \partial x \, \frac{\partial i_k}{\partial t}$$

Rearranging the above equation we get equation (6.1).

$$\frac{\partial v_k}{\partial x} = -L_k \frac{\partial i_k}{\partial t} \tag{6.1}$$

Similar equation could be written for the current flowing through the infinitesimally small section:

$$\begin{aligned} \partial i_k &= -C_k \partial x \, \frac{\partial v_k}{\partial t} \\ \implies \frac{\partial i_k}{\partial x} &= -C_k \frac{\partial v_k}{\partial t} \end{aligned} \tag{6.2}$$

The equations (6.1) and (6.2) are mutually coupled and are famously known as 'Telegrapher's Equations'. By combining both equations the term i_k could be eliminated, resulting in:

$$\begin{aligned} \frac{\partial^2 v_k}{\partial t^2} &= \frac{1}{L_k C_k} \frac{\partial^2 v_k}{\partial x^2} \\ \implies \frac{\partial^2 v_k}{\partial t^2} - \frac{1}{L_k C_k} \frac{\partial^2 v_k}{\partial x^2} &= 0 \end{aligned} \tag{6.3}$$

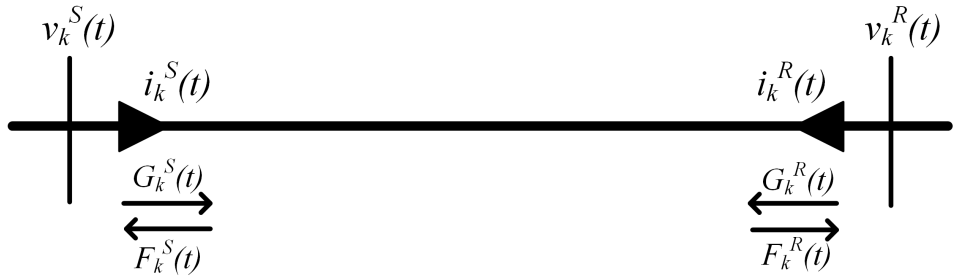

Figure 6.2: Voltage and current in a transmission line along with the traveling waves.

The general solution for equation (6.3) is

$$v_k(x,t) = G_k\left(x - \frac{t}{\sqrt{L_k C_k}}\right) + F_k\left(x + \frac{t}{\sqrt{L_k C_k}}\right) \tag{6.4}$$

In equation (6.4), the term $G_k\left(x - \frac{t}{\sqrt{L_k C_k}}\right)$ represents the wave traveling in forward direction while the term $F_k\left(x + \frac{t}{\sqrt{L_k C_k}}\right)$ denotes the wave traveling in the backward direction. By substituting (6.4) in (6.2), the wave equation for the k^{th} mode current could be obtained as:

$$i_k(x,t) = \frac{1}{Z_{ck}} G_k\left(x - \frac{t}{\sqrt{L_k C_k}}\right) - \frac{1}{Z_{ck}} F_k\left(x + \frac{t}{\sqrt{L_k C_k}}\right) \tag{6.5}$$

where $Z_{ck} = \sqrt{\frac{L_k}{C_k}}$ represents the k^{th} mode characteristic impedance of the transmission line. A well-known fact that voltage at any point in the transmission line is the summation of the forward and backward traveling waves while current is equal to the difference of the forward and backward traveling waves divided by the characteristic impedance of the transmission line, could be verified from (6.4) and (6.5), respectively.

It can also be derived from (6.4) and (6.5) that:

$$G_k\left(x - \frac{t}{\sqrt{L_k C_k}}\right) = \frac{v_k(x,t) + i_k(x,t) Z_{ck}}{2} \tag{6.6}$$

$$F_k\left(x + \frac{t}{\sqrt{L_k C_k}}\right) = \frac{v_k(x,t) - i_k(x,t) Z_{ck}}{2} \tag{6.7}$$

Now let us focus our attention at Bus R of the transmission line as shown in Figure 6.2. At Bus R, the following equations would hold true with reference to the equations derived in (6.4)

and (6.5):

$$G_k^R(t) + F_k^R(t) = v_k^R(t)$$
$$G_k^R(t) - F_k^R(t) = Z_{ck} i_k^R(t)$$

where G_k^R and F_k^R are k^{th}-mode forward and backward propagating waves at Bus R, respectively; i_k^R and v_k^R are the k^{th}-mode current and voltage at Bus R, respectively.

If the time taken by a traveling wave to traverse whole of the transmission line is τ time units, then the backward propagating wave present at Bus R ($F^R(t)$) was present at Bus S τ time units ago, as forward traveling wave ($G_k^S(t-\tau)$). Therefore, the above equations become:

$$G_k^R(t) + G_k^S(t-\tau) = v_k^R(t) \tag{6.8}$$
$$G_k^R(t) - G_k^S(t-\tau) = Z_{ck} i_k^R(t) \tag{6.9}$$

Subtracting (6.9) from (6.8) we obtain:

$$2G_k^S(t-\tau) = v_k^R(t) - Z_{ck} i_k^R(t)$$
$$\implies \frac{2G_k^S(t-\tau)}{Z_{ck}} = \frac{v_k^R(t)}{Z_{ck}} - i_k^R(t) \tag{6.10}$$

Moving on similar lines, an equation for the Bus S could be derived as:

$$\frac{2G_k^R(t-\tau)}{Z_{ck}} = \frac{v_k^S(t)}{Z_{ck}} - i_k^S(t) \tag{6.11}$$

The equivalent model of a transmission line that describes the model derived in equations (6.10) and (6.11) is shown in Figure 6.3, which is known as Bergeron model of transmission line.

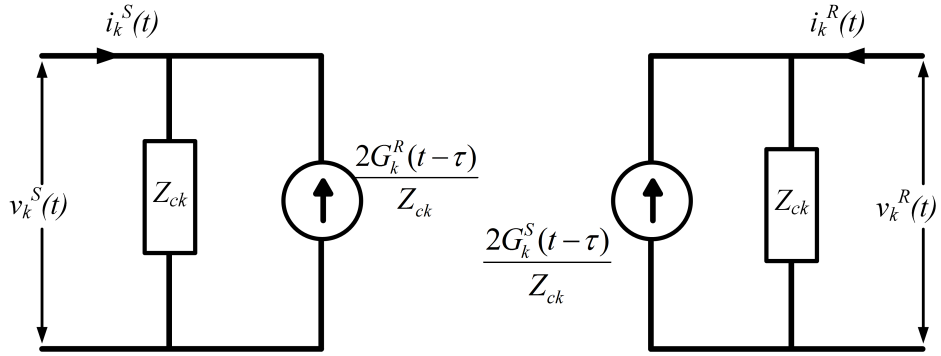

Figure 6.3: The Bergeron model of transmission line.

6.3 Wavelet transform

For the application of the traveling wave-based fault location algorithms, the arrival of a traveling wave at the terminal of the transmission line needs to be detected. The arrival of a traveling wave at transmission line terminals manifests itself as a sudden change in voltage and current signals. The two types of measured signals, i.e., voltage, and current are available for sensing the arrival of the traveling wave. However, the voltage transformers being highly inductive in nature, offer high impedance to high frequency components (like traveling wave) of the measured voltage. On the other hand, the current transformers are able to reproduce the high frequency components at their secondary side with relatively smaller attenuation. Therefore, the current signal is often used to detect the arrival of a traveling wave by the fault location algorithms found in literature.

After the selection of the type of signal, i.e., current signal, the next factor that needs to be considered is the selection of an appropriate signal processing technique. The Fourier transform depicted mathematically by (6.12), is an excellent tool for analyzing stationary signals. However, the kernel $e^{-j\omega t}$ in (6.12) keeps oscillating till infinite time, therefore, any local information or change with respect to time cannot be sensed using Fourier transform [42].

$$\mathscr{F}\{f(t)\} = \int_{-\infty}^{\infty} f(t)\, e^{-j\omega t} \tag{6.12}$$

This shortcoming of Fourier transform could be overcome by using short-time Fourier transform (STFT) which gives both frequency and time information. The trade-off between the frequency and time information obtained depends on the size of window used for implement-

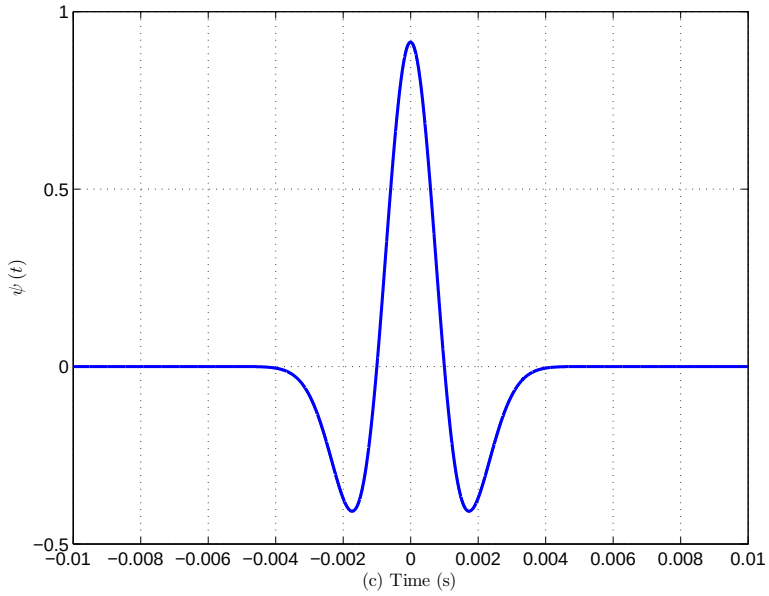

Figure 6.4: Mexican-hat wavelet.

ing STFT. However, another type of signal processing technique which has been widely used in the existing fault location algorithms and is better suited to detect the traveling waves is Wavelet transform originally proposed in [44].

A wavelet is an oscillating function localized in time with its mean equal to zero. For example, a wavelet called Mexican-hat wavelet as shown in Figure 6.4 is obtained from the expression given in (6.13) with $\sigma = 0.001$. It is so called due to its shape resembling a Mexican hat. Note that the waveform is localized between the time interval of -0.004s to 0.004s.

$$\psi(t) = \frac{2}{\sqrt{3\sigma}\pi^{\frac{1}{4}}}\left(1 - \left(\frac{t}{\sigma}\right)^2\right)e^{-\frac{t^2}{2\sigma^2}} \tag{6.13}$$

The integral form of continuous wavelet transformation of function f is given in (6.14):

$$W_\psi[f](a,b) = \int_{-\infty}^{\infty} f(t)\ \frac{1}{\sqrt{|a|}}\overline{\psi}\left(\frac{t-b}{a}\right)dt \tag{6.14}$$

where $\psi(t)$ is the mother wavelet function; $\overline{\psi}(t)$ represents the conjugate of $\psi(t)$. a is the scaling factor while b is the translation factor where $a, b \in \mathbb{R}$ and $a \neq 0$. The factor $\frac{1}{\sqrt{|a|}}$ is used for energy normalization across the different scales.

As the scaling factor a changes, the width of wavelet also changes as shown in Figure 6.5. For $a < 1$ the width of the resulting wavelet is the 'compressed version' of the mother wavelet (corresponding to higher frequencies). Also the resulting wavelet becomes highly localized in time. For example, in Figure 6.5 (a) when the value of a is 0.5, it is compressed as compared

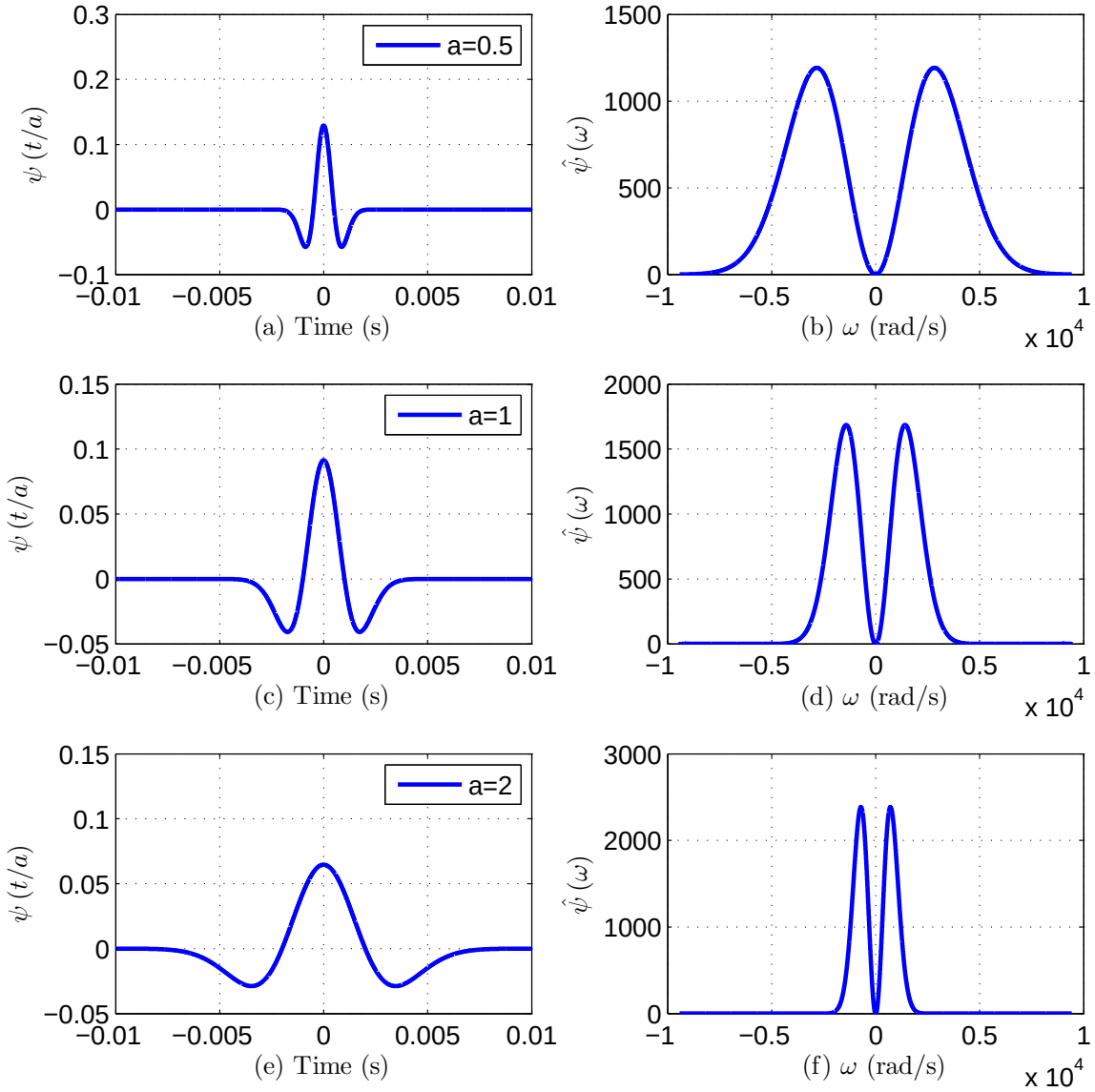

Figure 6.5: Time dilation of Mexican-hat wavelet and corresponding Fourier transform for different values of a: (a) and (b) with $a < 1$ ($a = 0.5$), (c) and (d) with $a = 1$, (e) and (f) with $a > 1$ ($a = 2$).

to the wavelet with $a = 1$ or $a = 2$ as shown in Figures 6.5 (c) and (e), respectively. For $a > 1$ the width of the wavelet increases (corresponding to lower frequencies). Also, the Fourier transform of the wavelets show that for lower value of a the wavelet becomes more sensitive to the higher frequencies as compared to the wavelets with the higher value of a (see Figures (b), (d), and (f)). Depending upon the requirement a signal can be analyzed at different resolutions by varying the value of a. Generally, the wavelet with smaller scaling factor are ideal for detecting the traveling wave in the measured signal. The translation factor b is utilized to move the wavelet window across the signal to be analyzed.

Most of the modern power system protective relays and fault locators utilize sampled signals, therefore, it requires us to utilize the Discrete Wavelet Transform (DWT). DWT could be obtained from its continuous counterpart by discretizing a and b. The variables a and b are discretized by substituting $a = a_0^m$, and $b = nb_0a_0^m$ where $a_0(> 1)$ and $b_0(> 0)$ are fixed real values, while m and n are integers [42]. Also, the time variable t has been replaced with the sample number, k.

$$\psi_{m,n}(k) = \frac{1}{\sqrt{a_0^m}}\psi\left(\frac{k - nb_0a_0^m}{a_0^m}\right) \tag{6.15}$$

The values of $a_0 = 2$, and $b_0 = 1$ are commonly used as they result in a binary dilation of 2^m and a dyadic translation of $n2^m$ [42]. Thus, the most common expression that is used for finding DWT becomes:

$$W_\psi[f](m,n) = \sum_k f(k)\frac{1}{\sqrt{2^m}}\overline{\psi}\left(\frac{k - n2^m}{2^m}\right) \tag{6.16}$$

6.3.1 An Example: Singularity detection through DWT

Figure 6.6 shows the DWT of a 60 Hz signal with noise level of 3%. It can be seen from Figure 6.6 (a) that abrupt changes occur in 60 Hz sinusoid at around the time instances of 16 ms, 32 ms, and 54 ms. Correspondingly, a spike is observed in the DWT of the 60 Hz signal whenever the singularity is encountered as can be seen from Figure 6.6 (b). The wavelet function *Symlet-4* is used for carrying out the transformation. Thus, DWT could be utilized to detect the arrival of the traveling waves from the signals measured at the transmission line terminals.

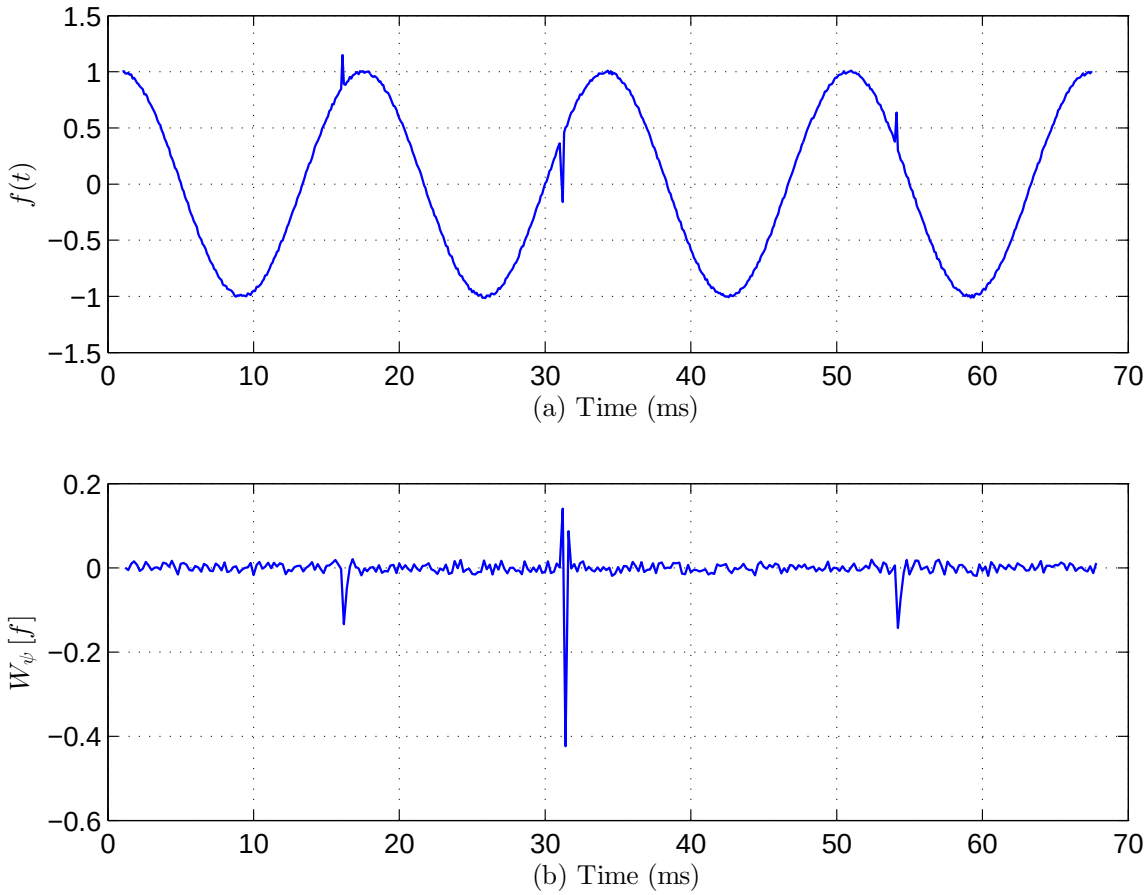

Figure 6.6: Singularity detection through DWT: (a) abrupt changes occurring in 60 Hz sinusoidal signal with noise level of 3%; (b) DWT of the waveform of (a).

6.4 Existing traveling wave-based fault location algorithms

The modeling of the transmission line for traveling wave, and the signal processing for detecting the traveling waves have been discussed so far. Now, let us focus our attention on the fault location algorithms for SCCTLs based on the traveling wave theory. The traveling wave-based fault location algorithms relate the time of arrival of a traveling wave at a terminal of the transmission line to the distance of the fault from that terminal of the transmission line. The traveling wave-based fault location algorithms for SCCTLs could be broadly categorized as: 1-single-ended traveling wave-based fault location algorithms; 2-double-ended traveling wave-based fault location algorithms. Single-ended fault location algorithms utilize the measurements from only one terminal of the transmission line while double-ended fault location algorithms utilize the measurements from both terminals of the transmission line.

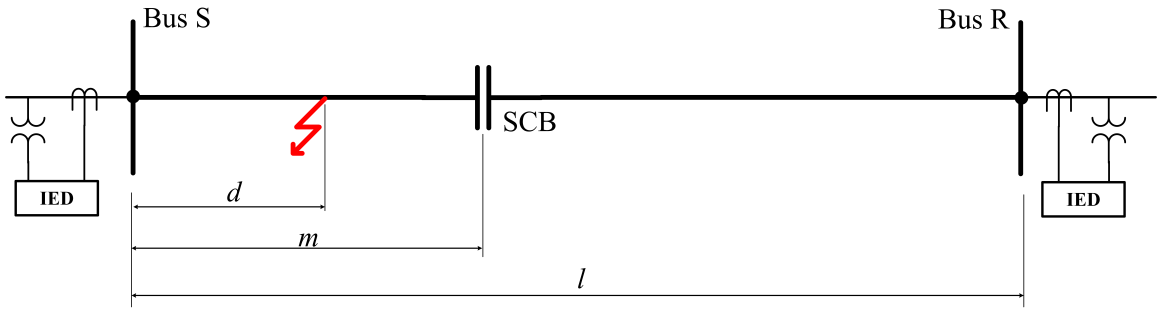

Figure 6.7: Diagram of an SCCTL with fault lying between Bus S and SCB.

6.4.1 Double-ended traveling wave-based fault location algorithms

The double-ended fault location algorithms utilize the time instance of arrival of the first traveling wave at each terminal of the transmission line. Consider the fault scenario depicted in Figure 6.7 where a fault is located at an unknown distance d units from the Bus S. The SCB is located m units away from Bus S. The total length of the transmission line is l units. The occurrence of the fault in a transmission line produces traveling waves at the fault point which propagate towards both ends of the transmission line. Now the time taken by the traveling wave to reach Bus S from the fault point will be $t_S = \frac{d}{u_k}$, where u_k is the speed of the k^{th} mode traveling wave. Similarly, the time taken by the traveling wave to reach Bus R will be $t_R = \frac{l-d}{u_k}$. Now it should be noted that a part of the traveling wave which is moving towards Bus R might get reflected from SCB which lies in the way, however, the time of arrival of the traveling wave at Bus R remains unaffected by the presence of SCB in the way.

Now subtracting t_R from t_S we obtain (6.17).

$$\begin{aligned} \Delta t = t_S - t_R &= \frac{2d - l}{u_k} \\ \implies d &= \frac{l + u_k \Delta t}{2} \end{aligned} \tag{6.17}$$

The fault location result d could thus be obtained from (6.17). It should be noted that if the traveling wave reaches Bus S before Bus R, then Δt is negative, and fault will lie between 0 units to $\frac{l}{2}$ units as measured from Bus S. On the other hand, if traveling wave reaches Bus R before Bus S then Δt is positive, and fault will lie between $\frac{l}{2}$ units to l units as measured from Bus S. If both reach at the exact same time interval then Δt will be zero and the fault lies exactly at the mid point of the transmission line. For the external faults Δt will either be $\frac{l}{u_k}$ or $-\frac{l}{u_k}$. Therefore, for the external faults, the double-ended algorithm would yield 0 units or l units as the fault location result, which would be discarded if the relay has picked up the fault as an external fault.

It could be seen that the underlying principle of double-ended fault location algorithms is straight forward. However, the accuracy of time synchronization between the measurements from both terminals of the transmission line becomes a critical factor governing the accuracy of the fault location algorithm. As an example, consider a scenario with fault located exactly in the middle of the transmission line. The Δt is supposed to be zero in this case. If however the measurements from each end of the transmission line are not perfectly synchronized Δt would attain some finite value which would introduce an error in the fault location result yielded by double-ended fault location algorithm. Since, the traveling waves travel at the speeds close to that of the light, the synchronization error of $1\mu s$ would incur an error of 300 meters in the fault location results. The single-ended fault location algorithms on the other hand do not require synchronization of the measurements, which makes the usage of single-ended traveling wave-based algorithms an attractive avenue of locating faults in an SCCTL.

6.4.2 Single-ended traveling wave-based fault location algorithms

Single-ended traveling wave-based fault location algorithms as the name suggests utilize the measured signals (usually current) from only one end of the transmission line. A single-ended traveling wave-based fault location algorithm estimates the distance of the fault by using the time difference between the arrival of the first two traveling waves arriving at that terminal of the transmission line where the fault locator is located. Apart from the time difference between first two successive traveling-waves, a single-ended fault location algorithm also needs the information regarding the point from where the second traveling got reflected before arriving at the terminal of the SCCTL.

It is a known fact that any traveling wave would keep propagating in the transmission line till it encounters any point of discontinuity, which could be the fault point, terminal of the transmission line, series capacitor etc. in a faulted SCCTL. At the point of discontinuity the incident traveling wave splits into two parts, one which gets reflected in the reverse direction and the other which gets transmitted from that point onwards in the direction of the incident wave. Thus, the second traveling wave that would arrive at Bus S could be a wave reflected from any of the above mentioned points of discontinuity. The question might arise: “Why the point of reflection of the second traveling wave is needed?”.

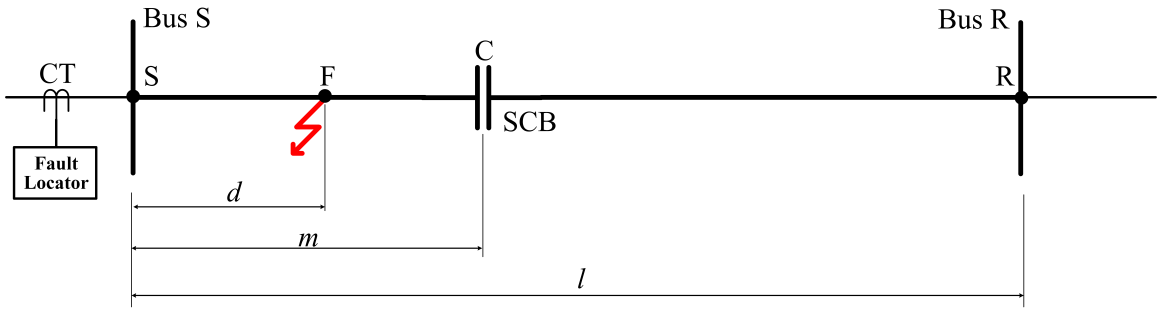

Figure 6.8: Schematic diagram showing a fault in an SCCTL between Bus S and SCB.

To elaborate this point, let us consider the fault scenario shown in Figure 6.8 where a fault is located between Bus S, and SCB at a distance of d units away from Bus S in an SCCTL of length l. The SCB is located at distance of m units from Bus S. The fault locator is located at Bus S. As there would be multiple traveling waves traveling along the entire span of the SCCTL, the methodology used to label the traveling waves should be noted before proceeding further. The traveling wave is denoted by the symbol G followed by letters in subscript and superscript. The letter k in subscript denotes the mode of the wave, i.e., α, β, or γ. The first letter in the superscript represents the point of origin of the wave, the last letter identifies the final detection point, while all the letters in between represent the points where the wave got reflected. The superscript letters 'F', 'S', 'R', and 'C' represent fault point, Bus S, Bus R, and point of SCB coupling, respectively. As an example, a wave named G_{α}^{FRS} would represent an α-mode traveling wave which originated at fault point, traveled towards Bus R, gets reflected from Bus R, and then gets detected at Bus S.

After the occurrence of the fault in an SCCTL, the first traveling wave that would arrive at Bus S will be G_k^{FS}. The distance covered by G_k^{FS} will be d units, as shown in Figure 6.8. The second traveling wave arriving at the Bus S could be reflected from any one of the multiple possibilities. Various types of traveling waves that could arrive at Bus S as second traveling wave are given as follows:

1. G_k^{FSFS}: If the second traveling wave arriving at Bus S is G_k^{FSFS}, then the distance traveled by this wave would be $3d$ units. Assuming that the time difference between the successive waves is Δt, the distance of fault from Bus S (d) would be calculated as follows:

$$\begin{aligned} \Delta t &= \frac{3d}{u_k} - \frac{d}{u_k} \\ \implies d &= \frac{u_k \Delta t}{2} \end{aligned} \tag{6.18}$$

2. G_k^{FCS}: Let the second wave that arrives at Bus be G_k^{FCS}. The distance covered by wave

G_k^{FCS} will be $2m - d$ units. If the time difference between the arrival of the first and second wave is Δt then the d could be found as per:

$$\Delta t = \frac{2m - d}{u_k} - \frac{d}{u_k}$$
$$\implies d = m - \frac{u_k \Delta t}{2} \tag{6.19}$$

3. G_k^{FRS}: Though for the fault scenario shown in Figure 6.8, the traveling wave G_k^{FCS} would always reach Bus S before G_k^{FRS}, however, for the faults lying close to Bus R (not shown in Figure 6.8), the second wave that arrives at Bus S will be G_k^{FRS}. Since, the location of fault is unknown before the fault locator yields the result, the arrival of G_k^{FRS} as second traveling wave at Bus S is a possibility. The distance covered by G_k^{FRS} will be $2l - d$ units $(=l - d + l)$. If the time difference between the arrival of these waves is Δt then following equation would hold true:

$$\Delta t = \frac{2l - d}{u_k} - \frac{d}{u_k}$$
$$\implies d = l - \frac{u_k \Delta t}{2} \tag{6.20}$$

From above discussion it can be seen that depending upon which type of traveling wave arrives at Bus S after G_k^{FS}, only one of the fault location equations given in (6.18) - (6.20) would be 'correct'. Therefore, the single-ended traveling wave-based fault location algorithms for SCCTLs would require some form of mechanism to find the point of discontinuity in the SCCTL from which the second traveling wave arriving at the fault locator got reflected. Different publications have tried to overcome this challenge in different ways.

The authors of [30] have proposed to put the fault locator at the SCB bus, and to integrate directionality into the fault locator using incremental changes in voltage and current measurements. Due to the location of the fault locator at SCB, the traveling wave reflected from SCB will not be detected by the fault locator. For the fault lying in the section between SCB and Bus R, the directional element of the fault locator will reject all the waves that get reflected from Bus S and then reach the fault locator. Therefore, the fault locator will only accept that traveling wave which either has been reflected from fault point, or from Bus R. In order to decide the point of reflection between Bus R, and fault point, the authors of [30] have proposed to use the polarity of the second traveling wave with respect to the first traveling wave to arrive

at fault locator. However, this scheme of fault location would fail when the terminal that is closer to the fault (Bus R in this case) has a group of other transmission lines connected to it as shown later in the next chapter. Similar conclusion could be arrived at for the faults lying in the section between Bus S and SCB.

Though, the algorithm proposed in [31] is for non-compensated transmission lines, however, the observations of [31] have been considered. The authors of [31] have claimed that for ungrounded faults, the remote end of the transmission line do not cause significant reflection of the traveling waves. Therefore, the traveling waves detected at local terminal will be the traveling waves that were reflected from the fault point. For the grounded faults, the authors of [31] claim that for the faults lying between 0-50% of the line length as measured from Bus S the ground mode traveling waves arriving at Bus S would have significant peaks while for the faults between 50-100% the ground mode traveling waves reaching Bus S will show no significant peaks. Thus, if the significant peaks are observed in ground mode traveling waves then the second wave to arrive at Bus S was reflected from the fault point. On the other hand, if no significant peaks are observed in ground mode traveling waves then the second wave to arrive at Bus S will be the one reflected from remote terminal, i.e., Bus R. However, this methodology would not have high reliability for the faults lying in the region around 50% line length as measured from Bus S as the change in the peaks of the ground mode traveling waves will change gradually as fault moves from first half to the second half of the transmission line.

A distance protection scheme is presented in [29] which works on the principle of estimating the distance of fault from the given terminal of the transmission line. The authors of [29] have also used the polarity of the reflected wave to determine whether it got reflected from remote bus or from fault point. However, the proposed technique is only presented for only one configuration of the transmission line in which only an inductive source is present at each terminal of the transmission line. As a matter of fact when an inductive source is present at one terminal while a group of transmission lines is present at the other terminal, the proposed protection scheme of [29] would fail as shown later.

In [28] it is presented that the series capacitor would not reflect any traveling wave rather it acts as short circuit for the traveling waves. Thus, there are only two types of points of discontinuity in the SCCTL from where the second traveling wave arriving at Bus S would have been reflected, which are fault point and the remote bus. The authors of [28] also proposed to use the polarity of the second traveling wave arriving at the fault locator to determine whether it was reflected from the fault point, or from the remote terminal of the transmission line. Three configurations of SCCTLs as shown in Figure 6.9 have been studied in [28], and the polarity of the second wave with respect to the first wave in each configuration has been utilized to identify the second traveling wave as follows:

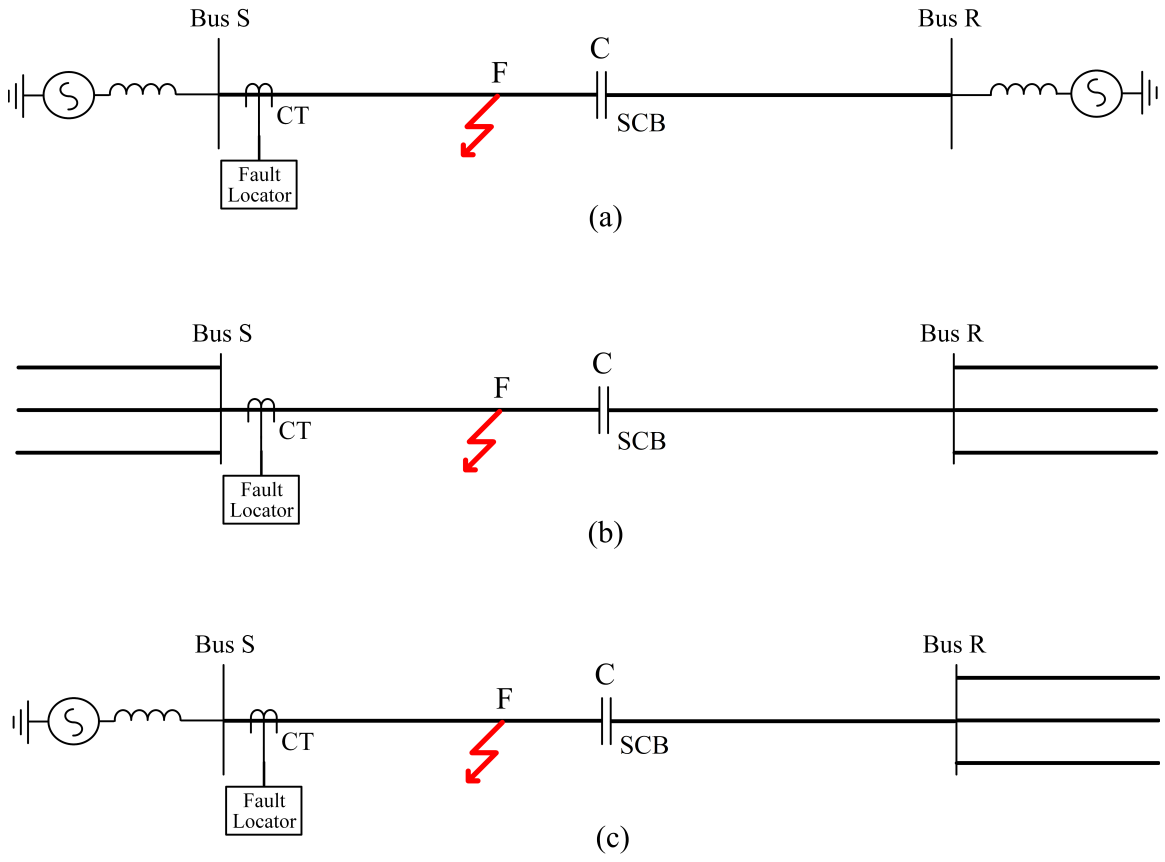

Figure 6.9: Schematic diagram showing various configurations of SCCTL studied in [28]: (a) Configuration1, (b) Configuration2, and (c) Configuration3.

1. In Configuration1, an inductive source is present at each end of a transmission line as shown in Figure 6.9 (a). In this configuration if the polarity of the second traveling wave arriving at Bus S (fault locator) is same as that of the first traveling wave, then the second traveling wave was reflected from the remote end of the SCCTL, i.e., Bus R. If however the polarity of the second traveling wave is opposite to that of the first one then the second traveling wave was reflected from the fault point.

2. In Configuration2 as shown in Figure 6.9 (b), a group of transmission lines is present at each end of the SCCTL. In this configuration if the polarity of first traveling wave is same as that of second traveling wave, it implies that the second traveling wave was reflected from the fault point. In case the polarities of first two traveling waves are opposite to each other then the second traveling was reflected from Bus R.

3. In Configuration3, a source is present at Bus S while at Bus R the SCCTL is connected to other transmission lines as shown in Figure 6.9 (c). Authors contend that the polarity of the waves reflected from fault point and the Bus R will have the same polarity among themselves, and, thus, cannot be distinguished from each other by comparing their polarities to the polarity of the first traveling wave to arrive at Bus S. Therefore, the algorithm of [28] is not applicable to Configuration3 of the SCCTL.

It is worth noting that the recognition of the second traveling wave using polarity of the traveling wave as proposed in [30], [31], [29], and [28] are all based on the observation of the EMTD simulations. No mathematical analysis regarding the effect of a certain type of discontinuity on the polarity of the reflected wave has been presented. Also, most of the publications have focused on only one configuration of the transmission line in which an inductive source is present at each terminal of the transmission line which in fact is very rare configuration. The only publication to consider the other configurations of SCCTL is [28]. The effect of the fault resistance, the level of series compensation, the type of electrical component connected at terminal of the transmission line on the reflected traveling wave has not been studied in the existing publications. Thus, there arises a need to conduct a detailed mathematical analysis of the traveling wave-based fault location algorithms.

6.5 Conclusion

In this chapter, an introduction to the application of the traveling wave theory to the process of fault location has been presented. The most popular technique for detection of the traveling waves, i.e., DWT has also been explained in this chapter. Thereafter, the concepts underlying

the double-ended, and single-ended traveling wave-based fault location algorithms have been explained. The key challenge facing the single-ended fault location algorithms is identified, which is identification of the point of discontinuity in the SCCTL from which the second traveling wave to arrive at fault locator is reflected. Thereafter, different methodologies to identify the reflection point of the second traveling wave, as employed by the different publications have been investigated. It is found that the existing publications are based on the empirical observations from EMTP simulations of the traveling waves. Moreover, the existing solutions have been proposed for a specific configuration of a transmission line. The need to have a detailed mathematical analysis of the single-ended algorithm has been identified, which could open further avenues for the improvement to the existing algorithm or for the proposition of new fault location algorithms based on traveling wave theory.

Chapter 7

A new traveling wave-based single-ended fault location algorithm

7.1 Introduction

It was stated in the previous chapter that the single-ended traveling wave algorithms do not require synchronization of the measurements from both ends of the SCCTL, which is a significant advantage over the double ended fault location algorithms. The single-ended algorithms yield fault location results by noting the time difference between the first and second traveling waves arriving at the fault locator. However, as explained in detail in Section 6.4.2, the single-ended algorithms also need to identify the point of discontinuity in the SCCTL from where the second traveling wave to arrive at fault locator was reflected. The path taken by the authors of the existing single-ended algorithms like [28], [29], and [30] is to compare the polarity of the second traveling wave to arrive at the fault locator to the polarity of the first traveling wave. It is postulated in [29], and [30] that the polarity of the second traveling wave to arrive at fault locator will be opposite to that of the first traveling wave if the second traveling wave was reflected from the fault point. On the other hand, the polarity of the second and the first wave will be same if the second traveling wave was reflected from the remote terminal of the SCCTL. However, the only configuration of SCCTL studied in [29], and [30] is the one in which only an inductive source is present at both ends of the SCCTL, which as we know is a very rare configuration of the SCCTL. In [28], three configurations of the SCCTL are studied: in Configuration1, only an inductive source is present at each end; in Configuration2, a group of transmission lines is present at each end; Configuration3 has an inductive source on the one end and a group of transmission lines on the other. It is mentioned in [28] that the fault could be located for the Configuration1 and Configuration2 by comparing the polarity of the first and

second traveling wave to arrive at fault locator. However, this methodology cannot be applied to Configuration 3 [28].

It is aimed in this chapter to mathematically analyze the phenomenon of the reflection of traveling waves from different types of discontinuities in the SCCTL and to identify the configurations of the SCCTL to which the single-ended traveling wave-based fault location algorithms in their current form remain inapplicable. After the identification of the cause of inapplicability of the single-ended traveling wave-based algorithms to specific configurations of the SCCTL, it is aimed to develop a new single-ended traveling wave-based fault location algorithm which is applicable to all the configurations of SCCTL.

Firstly, the mathematical expressions for the traveling waves reflected from different point of discontinuities are derived in Section 7.2. Thereafter, different configurations of the SCCTL are investigated for the applicability of the single-ended fault location algorithm in Section 7.3 in lieu of the presented mathematical analysis. The simulated test power system is described in Section 7.4. The proposed single-ended traveling wave-based algorithm which is applicable to all configurations of the SCCTLs is given in Section 7.5 along with simulated results. More simulation results for the proposed algorithm are given in Appendix D. The conclusion of the chapter is given in Section 7.6.

7.2 Mathematical analysis of the reflected traveling waves

The various points of discontinuity in an SCCTL are: SCB, transmission line terminals, and fault point. In this section, the analytical expressions are derived for the reflected traveling wave when a incident wave hits each type of discontinuity. The incident wave used for the analysis is the step function traveling wave, which is due to the fact that occurrence of the fault is analogous to the application of a step voltage at the fault point.

7.2.1 Series capacitor bank

The equivalent model of an SCCTL is shown in Figure 7.1, where Z_{ck} is the characteristic impedance of the transmission line. G_k^{SC} represents the wave traveling from Bus S to SCB, while G_k^{CS} represents the wave traveling from SCB towards Bus S. Similarly, G_k^{RC} represents the wave traveling from Bus R to SCB, while G_k^{CR} represents the wave traveling from SCB to Bus R. C_o denotes the capacitance of the series capacitor. The presence of Z_{ck} on both sides of capacitor represents the presence of transmission line on both sides of the SCB. v_k^{CS} and i_k^{CS} represent k^{th} mode voltage and current at Bus S side of SCB, respectively; v_k^{CR} and i_k^{CR} represent k^{th} mode voltage and current at Bus R side of SCB, respectively. τ^{CS} and τ^{CR} represent the time

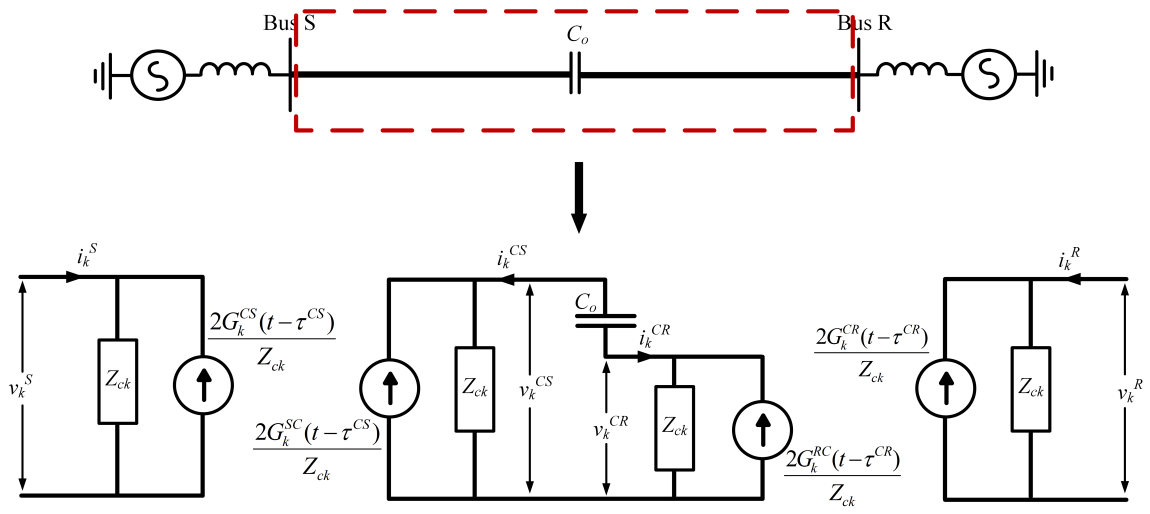

Figure 7.1: Equivalent model of SCCTL for traveling wave analysis.

taken by the traveling wave to travel between SCB to Bus S, and SCB to Bus R, respectively.

It should be noted that the sources at both ends of the SCCTL are not shown. For the sake of simplicity of the analysis, the initial value of all the traveling waves in the transmission line are assumed to be zero. However, for a general case the existing values of the traveling waves can be superimposed on the values of the traveling waves found out through the presented analysis without affecting the accuracy of the analysis.

Now question may arise that why MOV has not been included in the model. Actually, MOV starts conducting only when the voltage across series capacitor has reached the protective threshold value of the MOV which usually does not occurs during first few traveling wave reflections in the transmission line. Since, the time period of our interest for fault location only stretches to the first two traveling waves reaching the fault locator, the MOV is considered as non-conducting for the analysis carried out and not included in the modeling.

Let us assume that a step voltage in k^{th}-mode, v_k^S is applied to the transmission line at Bus S. Since the initial value of G_k^{CS} is zero, the value of G_k^{SC} which gets generated at Bus S will be given by:

$$G_k^{SC} = \frac{v_k^S + i_k^S Z_{ck}}{2} = \frac{v_k^S + \frac{v_k^S}{Z_{ck}} Z_{ck}}{2} = v_k^S \tag{7.1}$$

After the time τ^{CS} units has elapsed, the traveling wave G_k^{SC} generated at Bus S would reach SCB. The arrival of the wave G_k^{SC} at SCB is equivalent of applying a step change of $\frac{2v_k^S}{Z_{ck}}$ to the current source on Bus S side of SCB. Now the value of G_k^{RC} is zero because no voltage was applied to Bus R. Now assuming the instance of arrival of G_k^{SC} at SCB as $t = 0$ units, the

expressions for i_k^{CS} and i_k^{CR} can now be obtained as per the integral equation (7.2).

$$i_k^{CS}(t) = -i_k^{CR}(t) = -\frac{2v_k^S}{2Z_{ck} + \frac{1}{C_o}\int dt} \tag{7.2}$$

The solution of the integral equation (7.2) can be obtained by taking its Laplace transform. Since the applied voltage v_k^S is a step voltage, its Laplace transform becomes $\frac{v_k^S}{s}$. Hence, the Laplace transform of the equation (7.2) becomes (7.3).

$$i_k^{CS}(s) = -i_k^{CR}(s) = -\frac{v_k^S}{Z_{ck}\left(s + \frac{1}{2Z_{ck}C_o}\right)} \tag{7.3}$$

Now taking the Laplace inverse of (7.3), the expression for the currents i_k^{CS} and i_k^{CR} are obtained as (7.4).

$$i_k^{CS}(t) = -i_k^{CR}(t) = -\frac{v_k^S}{Z_{ck}} e^{-\frac{t}{2Z_{ck}C_o}} \tag{7.4}$$

Following similar steps the voltage v_k^{CS} could be obtained as shown in (7.5).

$$v_k^{CS}(t) = v_k^S\left(2 - e^{-\frac{t}{2Z_{ck}C_o}}\right) \tag{7.5}$$

The voltage v_k^{CR} can be obtained as per (7.6) using the value of i_k^{CR} from (7.4).

$$v_k^{CR}(t) = i_k^{CR}(t)\, Z_{ck} = v_k^S e^{-\frac{t}{2Z_{ck}C_o}} \tag{7.6}$$

Now all the currents and voltages shown in Figure 7.1 are known, the reflected traveling wave from the series capacitor towards Bus S (G_k^{CS}), and the transmitted traveling wave from series capacitor towards Bus R (G_k^{CR}) could be obtained as:

$$G_k^{CS}(t) = \frac{v_k^{CS} + i_k^{CS} Z_{ck}}{2} = v_k^S\left(1 - e^{-\frac{t}{2Z_{ck}C_o}}\right) \tag{7.7}$$

$$G_k^{CR}(t) = \frac{v_k^{CR} + i_k^{CR} Z_{ck}}{2} = v_k^S e^{-\frac{t}{2Z_{ck}C_o}}. \tag{7.8}$$

It can be observed from (7.7) that the reflected traveling wave G_k^{CS} is a bounded exponential with the time constant of $2Z_{ck}C_o$. The value of G_k^{CS} rises from $G_k^{CS} = 0$ at $t = 0$, to reach its final value of $G_k^{CS} = v_k^S$ as t approaches infinity. On the other hand, the traveling wave G_k^{CR} as given by (7.8) is a decaying exponential with the time constant of $2Z_{ck}C_o$. The wave G_k^{CR} decays from $G_k^{CR} = v_k^S$ at $t = 0$ to $G_k^{CR} = 0$ as time t tends to infinity. It is evident that for the

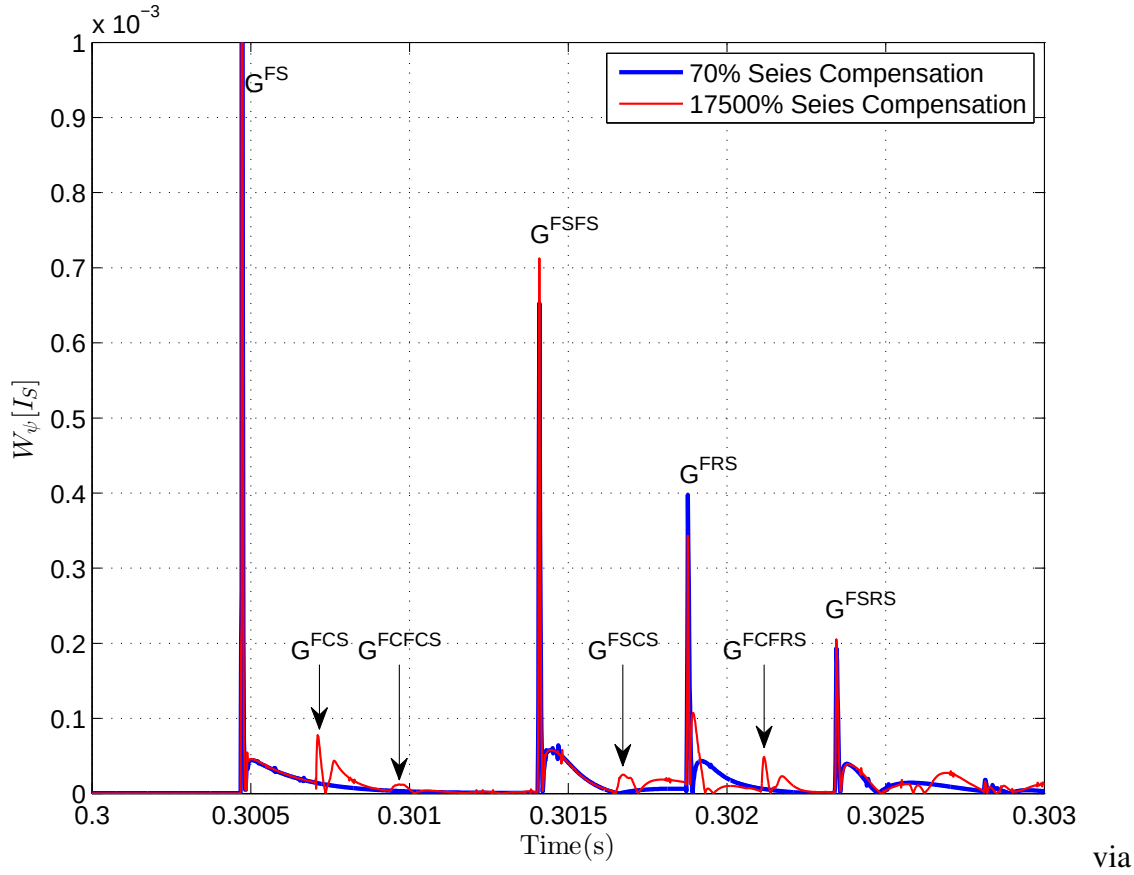

Figure 7.2: Arrival of traveling waves at Bus S after a 50Ω three phase fault at 40% transmission line length from Bus S.

G_k^{CS} to be detected from voltage and current measurements, it has to produce sharp change in v_k and i_k. For this to occur, the term $e^{-\frac{t}{2Z_{ck}C_o}}$ has to decay rapidly.

For the power system described in Section 2.7.1 of Chapter 2, the α-mode time constant $2Z_{c\alpha}C_o$ of the traveling wave G_k^{CS} with $Z_{c\alpha} = 290\Omega$ and $C_o = 29.11\mu F$ becomes $0.0168838s$. In comparison, the total time taken for α-mode traveling wave to traverse the whole 350 km line is $\tau = 0.0011681s$. Thus, it can be observed that the term $e^{-\frac{t}{2Z_{ck}C_o}}$ is a very slowly decaying exponential. In other words, v_k and i_k would change by only 6.67% till the next wave (reflected from Bus R) reaches Bus S in $0.0011681s$. Now, detecting a traveling wave with such a slowly changing wavefront would be a major challenging through any type of signal processing including DWT. In order to make the term $e^{-\frac{t}{2Z_{ck}C_o}}$ decay faster and to make it 'detectable', the value of C_o needs to be unrealistically small. As a matter of fact, the detection of traveling wave reflected from SCB for all practical implementations of series capacitive compensation is very unlikely.

Figure 7.2 shows the various traveling waves detected at Bus S following a single-phase to ground fault at 40% transmission line length from Bus S for two series compensation levels: 70% and 17500%. Though the series capacitive compensation level of 17500% (C_o = $0.116\mu F$) is unrealistic, this extraordinary high level of compensation is selected to exaggerate the amount of traveling waves getting reflected from the series capacitor. In this way, we obtain the point in time when a traveling wave reflected from series capacitor would reach Bus S for the 70% compensation level which otherwise could not be identified as shown through mathematical analysis. Any traveling wave reflected from SCB has letter 'C' in the superscript. It could be observed from Figure 7.2 that any traveling wave reflected even once from SCB during its trajectory, cannot be detected for 70% series compensation. In conclusion, it could be inferred that series capacitor could be regarded as 'non-existent' or as a 'short-circuit' for the purpose of fault location through traveling waves. It essentially implies that the traveling wave-based fault location algorithms for conventional lines and SCCTLs could be applied interchangeably. Thus, the claim made by authors of [28] that SCB does not reflect the traveling waves will hold true for all the practical series compensation levels.

7.2.2 Fault point

Fault in a transmission line could be a: 1-single-phase fault, 2-double-phase to ground fault, 3-phase to phase fault, 4-three phase fault. Since any phase could be arbitrarily labeled as phase A, B, or C, the analysis presented in this chapter is for: phase A to ground fault, phase B to phase C to ground fault, phase B to phase C fault, and ABC fault. The traveling wave fault location algorithms are implemented in $\alpha\beta\gamma$ domain while the faults occur in phase domain. Therefore, drawing of equivalent diagram of a fault in an SCCTL is not as straightforward as for the case of series capacitor. Thus, faults need to be analyzed in $\alpha\beta\gamma$ domain to find the expressions for reflected wave from the faulted point.

The matrix for transforming phase domain quantities to $\alpha\beta\gamma$ domain quantities is given in (7.9), while the matrix used for converting $\alpha\beta\gamma$ domain quantities to phase domain quantities is given in (7.10).

$$\begin{bmatrix} i_A \\ i_B \\ i_C \end{bmatrix} = \begin{bmatrix} 1 & 0 & 1 \\ -\frac{1}{2} & \frac{\sqrt{3}}{2} & 1 \\ -\frac{1}{2} & -\frac{\sqrt{3}}{2} & 1 \end{bmatrix} \begin{bmatrix} i_\alpha \\ i_\beta \\ i_\gamma \end{bmatrix} \tag{7.9}$$

$$\begin{bmatrix} i_\alpha \\ i_\beta \\ i_\gamma \end{bmatrix} = \frac{2}{3} \begin{bmatrix} 1 & -\frac{1}{2} & -\frac{1}{2} \\ 0 & \frac{\sqrt{3}}{2} & -\frac{\sqrt{3}}{2} \\ \frac{1}{2} & \frac{1}{2} & \frac{1}{2} \end{bmatrix} \begin{bmatrix} i_A \\ i_B \\ i_C \end{bmatrix} \tag{7.10}$$

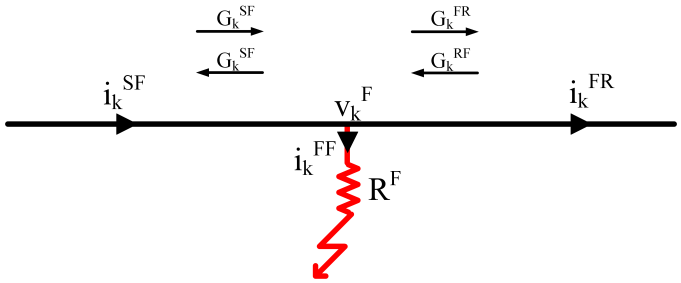

Figure 7.3: Vicinity of the fault point in a transmission line

Now, suppose a step voltage is applied to Bus S of SCCTL and the resulting traveling wave G_k^{SF} is traveling towards the fault point from Bus S side. After reaching the fault point G_k^{SF} splits into two parts: G_k^{FS} which gets reflected back towards Bus S; and G_k^{FR} which gets transmitted from fault point towards Bus R. As only Bus S is energized, the wave traveling from Bus R to the fault point is zero, i.e.,

$$G_k^{RF} = 0. \tag{7.11}$$

The wave G_k^{RF} will only attain a value after the wave G_k^{FR} has reached Bus R and consequently, reflected from Bus R. The only known traveling wave is G_k^{SF}, the traveling waves G_k^{FS} and G_k^{FR} will attain different values depending on the fault type as discussed below.

AG fault

At the fault point following relations would hold true for an AG fault:

$$v_A^F = i_A^{FF} R^F \tag{7.12}$$

$$i_B^{FF} = i_C^{FF} = 0 \tag{7.13}$$

where v_A^F represents the phase A voltage at the fault point; i_A^{FF}, i_B^{FF}, and i_C^{FF} represent the currents in phase A, B, and C respectively which flow into the fault; and R^F is the fault resistance.

The $\alpha\beta\gamma$ domain equivalent of the expression (7.12) becomes:

$$v_\alpha^F + v_\gamma^F = \left(i_\alpha^{FF} + i_\gamma^{FF}\right) R^F \tag{7.14}$$

It can be observed from Figure 7.3 that $i_k^{FF} = i_k^{SF} - i_k^{FR}$, where i_k^{SF} is the incoming k^{th}-mode from Bus S at the fault point; while i_k^{FR} is the k^{th}-mode current leaving the fault point towards

Bus R. The expression (7.14) now becomes:

$$v_\alpha^F + v_\gamma^F = \left(i_\alpha^{SF} + i_\gamma^{SF} - i_\alpha^{FR} - i_\gamma^{FR}\right) R^F \tag{7.15}$$

It is a known fact that the k^{th} mode voltage at any point in a transmission line is the summation of the forward and backward traveling waves at that point, while the current is given by the difference of the forward and backward traveling waves divided by the characteristic impedance of the transmission line. Therefore, the traveling wave equivalent of the expression (7.15) becomes:

$$G_\alpha^{SF} + G_\alpha^{FS} + G_\gamma^{SF} + G_\gamma^{FS} = \left(\frac{G_\alpha^{SF}}{Z_{c\alpha}} - \frac{G_\alpha^{FS}}{Z_{c\alpha}} + \frac{G_\gamma^{SF}}{Z_{c\gamma}} - \frac{G_\gamma^{FS}}{Z_{c\gamma}} - \frac{G_\alpha^{FR}}{Z_{c\alpha}} + \frac{G_\alpha^{RF}}{Z_{c\alpha}} - \frac{G_\gamma^{FR}}{Z_{c\gamma}} + \frac{G_\gamma^{RF}}{Z_{c\gamma}}\right) R^F \tag{7.16}$$

Another point to be noted here is that the k^{th} mode voltage at the fault point will be the summation of traveling waves in the segment between Bus S and fault, as well as the segment between fault and Bus R, i.e,

$$\begin{aligned} v_k^F =& G_k^{FR} + G_k^{RF} = G_k^{SF} + G_k^{FS} \\ \implies & G_k^{FR} = G_k^{SF} + G_k^{FS} \qquad (\because G_k^{RF} = 0) \end{aligned} \tag{7.17}$$

Now substituting (7.17) in (7.16), we get:

$$G_\alpha^{SF} + G_\alpha^{FS} + G_\gamma^{SF} + G_\gamma^{FS} = -2\left(\frac{G_\alpha^{FS}}{Z_{c\alpha}} + \frac{G_\gamma^{FS}}{Z_{c\gamma}}\right) R^F \tag{7.18}$$

In the expression (7.18), there are two unknowns: G_α^{FS} and G_γ^{FS}. Thus, one more equation is needed to solve for G_α^{FS} and G_γ^{FS}, which is obtained by simplifying the equation (7.13) in $\alpha\beta\gamma$ domain:

$$\begin{aligned} & i_B^{FF} = i_C^{FF} = 0 \\ \implies & -\frac{1}{2} i_\alpha^{FF} + \frac{\sqrt{3}}{2} i_\beta^{FF} + i_\gamma^{FF} = -\frac{1}{2} i_\alpha^{FF} - \frac{\sqrt{3}}{2} i_\beta^{FF} + i_\gamma^{FF} = 0 \\ & \implies i_\beta^{FF} = 0 \qquad (7.19) \\ & \& \quad i_\alpha^{FF} = 2 i_\gamma^{FF} \qquad (7.20) \end{aligned}$$

The expression (7.20) could be written as:

$$\implies i_{\alpha}^{SF} - i_{\alpha}^{FR} = 2\left(i_{\gamma}^{SF} - i_{\gamma}^{FR}\right)$$

The traveling wave equivalent of the above expression becomes:

$$\frac{G_{\alpha}^{SF}}{Z_{c\alpha}} - \frac{G_{\alpha}^{FS}}{Z_{c\alpha}} - \frac{G_{\alpha}^{FR}}{Z_{c\alpha}} = 2\left(\frac{G_{\gamma}^{SF}}{Z_{c\gamma}} - \frac{G_{\gamma}^{FS}}{Z_{c\gamma}} - \frac{G_{\gamma}^{FR}}{Z_{c\gamma}}\right). \tag{7.21}$$

Substituting the value of G_k^{FR} from (7.17) in (7.21), and simplifying we get:

$$\frac{G_{\alpha}^{FS}}{Z_{c\alpha}} = 2\left(\frac{G_{\gamma}^{FS}}{Z_{c\gamma}}\right). \tag{7.22}$$

Solving equations (7.18) and (7.22) the expressions for the waves reflected back from fault point, i.e., G_{α}^{FS}, and G_{γ}^{FS} are obtained as given in (7.23) and (7.24), respectively.

$$G_{\alpha}^{FS} = -2\left[\frac{G_{\alpha}^{SF} + G_{\gamma}^{SF}}{2 + \frac{Z_{c\gamma}}{Z_{c\alpha}} + 6\frac{R^F}{Z_{c\alpha}}}\right] \tag{7.23}$$

$$G_{\gamma}^{FS} = -\left[\frac{G_{\alpha}^{SF} + G_{\gamma}^{SF}}{1 + 2\frac{Z_{c\alpha}}{Z_{c\gamma}} + 6\frac{R^F}{Z_{c\gamma}}}\right] \tag{7.24}$$

The expressions for the transmitted waves from fault point onwards towards Bus R, i.e., G_{α}^{FR}, and G_{γ}^{FR} for an AG fault are given in (7.25) and (7.26):

$$G_{\alpha}^{FR} = G_{\alpha}^{SF} + G_{\alpha}^{FS} = \left[\frac{\frac{Z_{c\gamma}}{Z_{c\alpha}}G_{\alpha}^{SF} + 6\frac{R^F}{Z_{c\alpha}}G_{\alpha}^{SF} - 2G_{\gamma}^{SF}}{2 + \frac{Z_{c\gamma}}{Z_{c\alpha}} + 6\frac{R^F}{Z_{c\alpha}}}\right] \tag{7.25}$$

$$G_{\gamma}^{FR} = G_{\gamma}^{SF} + G_{\gamma}^{FS} = \left[\frac{2\frac{Z_{c\alpha}}{Z_{c\gamma}}G_{\gamma}^{SF} + 6\frac{R^F}{Z_{c\gamma}}G_{\gamma}^{SF} - G_{\alpha}^{SF}}{1 + 2\frac{Z_{c\alpha}}{Z_{c\gamma}} + 6\frac{R^F}{Z_{c\gamma}}}\right] \tag{7.26}$$

Therefore, it can be observed from equations (7.23)-(7.26) that the reflected waves, will have opposite polarities to the incident waves while the transmitted waves will have same polarities as that of the incident traveling waves. It may occur to the reader here that what if the traveling waves G_{α}^{SF}, and G_{γ}^{SF} are of mutually opposite polarities, it might make the polarity of the reflected waves same as that of the incident wave. However, it must be remembered that for an AG fault G_{α}^{SF}, and G_{γ}^{SF} will have the same polarities.

In β-mode, the fault current is zero for an AG fault as derived in the expression (7.19).

$$\begin{aligned} & i_\beta^{FF} = 0 \\ \implies & i_\beta^{SF} = i_\beta^{FR} \\ \implies & \frac{G_\beta^{SF}}{Z_{c\beta}} - \frac{G_\beta^{FS}}{Z_{c\beta}} = \frac{G_\beta^{FR}}{Z_{c\beta}} - \frac{G_\beta^{RF}}{Z_{c\beta}} \\ \implies & \frac{G_\beta^{SF}}{Z_{c\beta}} - \frac{G_\beta^{FS}}{Z_{c\beta}} = \frac{G_\beta^{FR}}{Z_{c\beta}} \qquad (\because G_k^{RF} = 0) \end{aligned} \tag{7.27}$$

It also known from (7.17) that:

$$G_\beta^{FR} = G_\beta^{SF} + G_\beta^{FS} \tag{7.28}$$

From equations (7.27) and (7.28) it can be concluded that:

$$\begin{aligned} & G_\beta^{FS} = 0 \\ \implies & G_\beta^{FR} = G_\beta^{SF} \end{aligned} \tag{7.29}$$

It can be observed from (7.29) that the incident wave in β-mode G_β^{SF} is transmitted as is towards Bus R as G_β^{FR}, and no reflection of traveling wave takes place.

BCG fault

For a BCG fault, the following equations would hold true:

$$v_B^F + v_C^F = \left(i_B^{FF} + i_C^{FF}\right) R^F \tag{7.30}$$

$$i_A^{FF} = 0 \tag{7.31}$$

In $\alpha\beta\gamma$ domain, the expression (7.30) could be written as:

$$\begin{aligned} -v_\alpha^F + 2v_\gamma^F &= \left(-i_\alpha^{FF} + 2i_\gamma^{FF}\right) R^F \\ -v_\alpha^F + 2v_\gamma^F &= \left(-i_\alpha^{SF} + i_\alpha^{FR} + 2i_\gamma^{SF} - 2i_\gamma^{FR}\right) R^F \end{aligned} \tag{7.32}$$

Writing the above expression in traveling wave form (7.33) is obtained.

$$-G_\alpha^{SF} - G_\alpha^{FS} + 2G_\gamma^{SF} + 2G_\gamma^{FS} = \left(-\frac{G_\alpha^{SF}}{Z_{c\alpha}} + \frac{G_\alpha^{FS}}{Z_{c\alpha}} + \frac{G_\alpha^{FR}}{Z_{c\alpha}} - \frac{G_\alpha^{RF}}{Z_{c\alpha}} + 2\frac{G_\gamma^{SF}}{Z_{c\gamma}} - 2\frac{G_\gamma^{FS}}{Z_{c\gamma}} - 2\frac{G_\gamma^{FR}}{Z_{c\gamma}} + 2\frac{G_\gamma^{RF}}{Z_{c\gamma}}\right) R^F \tag{7.33}$$

Since, k^{th}-mode voltage will be equal as seen from both sides of transmission line, therefore, $v_k^F = G_k^{FR} + G_k^{RF} = G_k^{SF} + G_k^{FS}$. With $G_k^{RF} = 0$, the relation becomes $G_k^{FR} = G_k^{SF} + G_k^{FS}$. Now substituting the value of G_k^{FR} in (7.33), the following expression is obtained.

$$-G_\alpha^{SF} - G_\alpha^{FS} + 2G_\gamma^{SF} + 2G_\gamma^{FS} = 2\left(\frac{G_\alpha^{FS}}{Z_{c\alpha}} + 2\frac{G_\gamma^{FS}}{Z_{c\gamma}}\right)R^F \tag{7.34}$$

Consider the expression (7.31), and transforming it into $\alpha\beta\gamma$-domain, the equation (7.35) is obtained.

$$\begin{aligned} & i_A^{FF} = 0 \\ \implies & i_\alpha^{FF} + i_\gamma^{FF} = 0 \\ \implies & i_\alpha^{SF} - i_\alpha^{FR} = -i_\gamma^{SF} + i_\gamma^{FR} \end{aligned} \tag{7.35}$$

Substituting traveling waves in (7.35), following is obtained:

$$\frac{G_\alpha^{SF}}{Z_{c\alpha}} - \frac{G_\alpha^{FS}}{Z_{c\alpha}} - \frac{G_\alpha^{FR}}{Z_{c\alpha}} + \frac{G_\alpha^{RF}}{Z_{c\alpha}} = -\frac{G_\gamma^{SF}}{Z_{c\gamma}} + \frac{G_\gamma^{FS}}{Z_{c\gamma}} + \frac{G_\gamma^{FR}}{Z_{c\gamma}} - \frac{G_\gamma^{RF}}{Z_{c\gamma}} \tag{7.36}$$

Now substituting $G_k^{FR} = G_k^{SF} + G_k^{FS}$ and $G_k^{RF} = 0$ in (7.36):

$$\begin{aligned} \frac{G_\alpha^{SF}}{Z_{c\alpha}} - \frac{G_\alpha^{FS}}{Z_{c\alpha}} - \frac{G_\alpha^{SF}}{Z_{c\alpha}} - \frac{G_\alpha^{FS}}{Z_{c\alpha}} &= -\frac{G_\gamma^{SF}}{Z_{c\gamma}} + \frac{G_\gamma^{FS}}{Z_{c\gamma}} + \frac{G_\gamma^{FS}}{Z_{c\gamma}} \\ \frac{G_\alpha^{FS}}{Z_{c\gamma}} &= -\frac{G_\gamma^{FS}}{Z_{c\gamma}} \end{aligned} \tag{7.37}$$

Solving (7.34) and (7.37) for G_α^{FS} and G_γ^{FS}, the following expressions are obtained:

$$G_\alpha^{FS} = -\left[\frac{G_\alpha^{SF} - 2G_\gamma^{SF}}{1 + 2\frac{Z_{c\gamma}}{Z_{c\alpha}} + 6\frac{R^F}{Z_{c\alpha}}}\right] \tag{7.38}$$

$$G_\gamma^{FS} = -\left[\frac{2G_\gamma^{SF} - G_\alpha^{SF}}{2 + \frac{Z_{c\alpha}}{Z_{c\gamma}} + 6\frac{R^F}{Z_{c\gamma}}}\right] \tag{7.39}$$

The expression for the traveling waves transmitted from fault point towards Bus R, i.e., G_{α}^{FR} and G_{γ}^{FR} for a BCG faults are given by:

$$G_{\alpha}^{FR} = G_{\alpha}^{SF} + G_{\alpha}^{FS} = \left[\frac{2\frac{Z_{c\gamma}}{Z_{c\alpha}} G_{\alpha}^{SF} + 6\frac{R^F}{Z_{c\alpha}} G_{\alpha}^{SF} + 2G_{\gamma}^{SF}}{1 + 2\frac{Z_{c\gamma}}{Z_{c\alpha}} + 6\frac{R^F}{Z_{c\alpha}}} \right] \tag{7.40}$$

$$G_{\gamma}^{FR} = G_{\gamma}^{SF} + G_{\gamma}^{FS} = \left[\frac{\frac{Z_{c\alpha}}{Z_{c\gamma}} G_{\gamma}^{SF} + 6\frac{R^F}{Z_{c\gamma}} G_{\gamma}^{SF} + G_{\alpha}^{SF}}{2 + \frac{Z_{c\alpha}}{Z_{c\gamma}} + 6\frac{R^F}{Z_{c\gamma}}} \right] \tag{7.41}$$

It should be noted here that that for a BCG fault, the polarities of the waves G_{α}^{SF} and G_{γ}^{SF} will be opposite to each other while their magnitudes will be equal. Therefore, the reflected waves G_{α}^{FS} and G_{γ}^{FS} will have opposite signs as compared to G_{α}^{SF} and G_{γ}^{SF}, respectively. On the other hand, the transmitted waves G_{α}^{FR} and G_{γ}^{FR} will have same polarity as G_{α}^{SF} and G_{γ}^{SF}, respectively.

For β-mode traveling waves in a BCG fault, following relation would hold true:

$$v_B^F - v_C^F = \left(i_B^{FF} - i_C^{FF} \right) R^F.$$

Above expression is converted to $\alpha\beta\gamma$-domain and simplified. The expressions for the reflected (G_{β}^{FS}) and transmitted traveling waves (G_{β}^{FR}) in β-mode for BCG faults are obtained as shown in (7.42) and (7.43)

$$\begin{aligned} v_{\beta}^F &= i_{\beta}^{FF} R^F \\ \implies v_{\beta}^F &= \left(i_{\beta}^{SF} - i_{\beta}^{FR} \right) R^F \\ \implies G_{\beta}^{SF} + G_{\beta}^{FS} &= \left(\frac{G_{\beta}^{SF}}{Z_{c\beta}} - \frac{G_{\beta}^{FS}}{Z_{c\beta}} - \frac{G_{\beta}^{FR}}{Z_{c\beta}} + \frac{G_{\beta}^{RF}}{Z_{c\beta}} \right) R^F \end{aligned}$$

Since, $G_k^{FR} = G_k^{SF} + G_k^{FS}$ and $G_k^{RF} = 0$, therefore, the above expression becomes:

$$\begin{aligned} G_{\beta}^{SF} + G_{\beta}^{FS} &= -2\frac{G_{\beta}^{FS}}{Z_{c\beta}} R^F \\ \implies G_{\beta}^{FS} &= -\frac{G_{\beta}^{SF}}{1 + 2\frac{R^F}{Z_{c\beta}}} \end{aligned} \tag{7.42}$$

The transmitted traveling wave from fault point towards Bus R is obtained as:

$$G_{\beta}^{FR} = G_{\beta}^{SF} + G_{\beta}^{FS} = \frac{G_{\beta}^{SF}}{1 + \frac{Z_{c\beta}}{2R^F}} \tag{7.43}$$

It can be seen from (7.42) and (7.43) that in β mode as well the reflected traveling wave will have the opposite polarity to the incident wave while the transmitted traveling wave will have the same polarity as that of the incident wave.

7.2.3 BC faults

For a BC fault, following relations would hold true:

$$i_B^{FF} = -i_C^{FF} \tag{7.44}$$

$$i_A^{FF} = 0 \tag{7.45}$$

$$v_B^F - v_C^F = i_B^{FF} R^F \tag{7.46}$$

Transforming the expression (7.44) to $\alpha\beta\gamma$ domain, equation (7.47) is obtained.

$$\begin{aligned} i_B^{FF} &= -\, i_C^{FF} \\ \implies -\frac{1}{2} i_\alpha^{FF} + \frac{\sqrt{3}}{2} i_\beta^{FF} + i_\gamma^{FF} &= \frac{1}{2} i_\alpha^{FF} + \frac{\sqrt{3}}{2} i_\beta^{FF} - i_\gamma^{FF} \\ \implies i_\alpha^{FF} &= 2 i_\gamma^{FF} \end{aligned} \tag{7.47}$$

Similarly, using (7.45) the expression (7.48) could be obtained.

$$\begin{aligned} i_A^{FF} &= 0 \\ \implies i_\alpha^{FF} + i_\gamma^{FF} &= 0 \\ \implies i_\alpha^{FF} &= -\, i_\gamma^{FF} \end{aligned} \tag{7.48}$$

From (7.47), and (7.48), it can be observed that:

$$i_\alpha^{FF} = 0 \tag{7.49}$$

$$i_\gamma^{FF} = 0. \tag{7.50}$$

The expression (7.49) is then converted to its traveling waves equivalent as shown in (7.51).

$$\begin{aligned} & i_\alpha^{FF} = 0 \\ \implies & i_\alpha^{SF} = i_\alpha^{FR} \\ \implies & \frac{G_\alpha^{SF}}{Z_{c\alpha}} - \frac{G_\alpha^{FS}}{Z_{c\alpha}} = \frac{G_\alpha^{FR}}{Z_{c\alpha}} - \frac{G_\alpha^{RF}}{Z_{c\alpha}} \\ \implies & \frac{G_\alpha^{SF}}{Z_{c\alpha}} - \frac{G_\alpha^{FS}}{Z_{c\alpha}} = \frac{G_\alpha^{FR}}{Z_{c\alpha}} \qquad (\because G_k^{RF} = 0) \end{aligned} \tag{7.51}$$

Since the α-mode voltage is same as seen from both sides of the fault, therefore following would hold true.

$$\begin{aligned} G_\alpha^{FR} + G_\alpha^{RF} =& G_\beta^{SF} + G_\beta^{FS} \\ \implies G_\alpha^{FR} =& G_\beta^{SF} + G_\beta^{FS} \qquad (\because G_k^{RF} = 0) \end{aligned} \tag{7.52}$$

From equations (7.51) and (7.52) it can be concluded that:

$$G_\alpha^{FS} = 0 \tag{7.53}$$

$$G_\alpha^{FR} = G_\alpha^{SF} \tag{7.54}$$

Similarly, it can be shown that:

$$G_\gamma^{FS} = 0 \tag{7.55}$$

$$G_\gamma^{FR} = G_\gamma^{SF} \tag{7.56}$$

Thus, α-mode and γ-mode traveling waves do not see a BC fault, and are transmitted as it is towards the Bus R as shown by the equations (7.54) and (7.56). No reflection of α-mode and γ-mode traveling waves takes place at fault point for a BC fault as shown by the equations (7.53) and (7.55).

Now, consider the expression (7.46):

$$\begin{aligned} & v_B^F - v_C^F = i_B^{FF} R^F \\ \implies & -\frac{1}{2}v_\alpha^F + \frac{\sqrt{3}}{2}v_\beta^F + v_\gamma^F + \frac{1}{2}v_\alpha^F + \frac{\sqrt{3}}{2}v_\beta^F - v_\gamma^F = \left(-\frac{1}{2}i_\alpha^{FF} + \frac{\sqrt{3}}{2}i_\beta^{FF} + i_\gamma^{FF}\right)R^F \\ \implies & \sqrt{3}v_\beta^F = \left(-\frac{1}{2}i_\alpha^{FF} + \frac{\sqrt{3}}{2}i_\beta^{FF} + i_\gamma^{FF}\right)R^F \end{aligned} \tag{7.57}$$

It is already shown in (7.49) and (7.50) that $i_\alpha^{FF} = 0$, and $i_\gamma^{FF} = 0$, therefore, the expression

(7.57) becomes:

$$v_\beta^F = -\frac{1}{2} i_\beta^{FF} R^F \tag{7.58}$$

The traveling wave equivalent of the above expression becomes:

$$G_\beta^{SF} + G_\beta^{FS} = \frac{1}{2}\left(\frac{G_\beta^{SF}}{Z_{c\beta}} - \frac{G_\beta^{FS}}{Z_{c\beta}} - \frac{G_\beta^{FR}}{Z_{c\beta}} + \frac{G_\beta^{RF}}{Z_{c\beta}}\right) R^F$$

Since, $G_k^{FR} = G_k^{SF} + G_k^{FS}$ and $G_k^{RF} = 0$, therefore the above expression becomes:

$$\begin{aligned} G_\beta^{SF} + G_\beta^{FS} &= -\frac{G_\beta^{FS}}{Z_{c\beta}} R^F \\ \implies G_\beta^{FS} &= -\frac{G_\beta^{SF}}{1 + \frac{R^F}{Z_{c\beta}}} \end{aligned} \tag{7.59}$$

The β-domain traveling wave reflected from fault point (G_β^{FS}) for a BC fault is given by equation (7.59). The β-domain traveling wave transmitted from fault point towards Bus R (G_β^{FR}) for a BC fault is given in (7.60).

$$G_\beta^{FR} = G_\beta^{SF} + G_\beta^{FS} = \frac{G_\beta^{SF}}{1 + \frac{Z_{c\beta}}{R^F}} \tag{7.60}$$

It is observed from (7.59) and (7.60) that the polarity of the reflected wave is opposite to that of the incident wave, while the polarity of the transmitted wave is same as the polarity of the incident wave.

7.2.4 ABC faults

For an ABC fault following equations hold true:

$$v_A^F = i_A^{FF} R^F \tag{7.61}$$

$$v_B^F = i_B^{FF} R^F \tag{7.62}$$

$$v_C^F = i_C^{FF} R^F \tag{7.63}$$

The expressions given (7.64)-(7.66) could be derived from (7.61)-(7.63).

$$v_\alpha^F = i_\alpha^{FF} R^F \tag{7.64}$$

$$v_\beta^F = i_\beta^{FF} R^F \tag{7.65}$$

$$v_\gamma^F = i_\gamma^{FF} R^F \tag{7.66}$$

Now transforming the equation (7.64) into its traveling wave equivalent we obtain:

$$\begin{aligned} v_\alpha^F &= \left(i_\alpha^{SF} - i_\alpha^{FR}\right) R^F \\ \implies G_\alpha^{SF} + G_\alpha^{FS} &= \left(\frac{G_\alpha^{SF}}{Z_{c\alpha}} - \frac{G_\alpha^{FS}}{Z_{c\alpha}} - \frac{G_\alpha^{FR}}{Z_{c\alpha}} + \frac{G_\alpha^{RF}}{Z_{c\alpha}}\right) R^F \end{aligned} \tag{7.67}$$

It is a known fact that $G_\alpha^{FR} + G_\alpha^{RF} = G_\alpha^{SF} + G_\alpha^{FS}$, and $G_\alpha^{RF} = 0$. Substituting these relations in (7.67), the α-mode traveling wave reflected from fault point to Bus S for an ABC fault is obtained as shown in (7.68).

$$\begin{aligned} G_\alpha^{SF} + G_\alpha^{FS} &= -2\frac{G_\alpha^{FS}}{Z_{c\alpha}} R^F \\ \implies G_\alpha^{FS} &= -\frac{G_\alpha^{SF}}{1 + 2\frac{R^F}{Z_{c\alpha}}} \end{aligned} \tag{7.68}$$

The transmitted α-mode traveling wave from fault point towards Bus R for an ABC fault is obtained as given in (7.69) using the value of G_α^{FS} from (7.68).

$$G_\alpha^{FR} = G_\alpha^{SF} + G_\alpha^{FS} = \frac{G_\alpha^{SF}}{1 + \frac{Z_{c\alpha}}{2R^F}} \tag{7.69}$$

Moving on the similar lines, the expressions for β-mode and γ-mode traveling waves reflected and transmitted from the fault point for an ABC fault could be obtained as shown in equations

(7.70)-(7.73).

$$G_{\beta}^{FS} = -\frac{G_{\beta}^{SF}}{1 + 2\frac{R^F}{Z_{c\beta}}} \tag{7.70}$$

$$G_{\beta}^{FR} = \frac{G_{\beta}^{SF}}{1 + \frac{Z_{c\beta}}{2R^F}} \tag{7.71}$$

$$G_{\gamma}^{FS} = -\frac{G_{\gamma}^{SF}}{1 + 2\frac{R^F}{Z_{c\gamma}}} \tag{7.72}$$

$$G_{\gamma}^{FR} = \frac{G_{\gamma}^{SF}}{1 + \frac{Z_{c\gamma}}{2R^F}} \tag{7.73}$$

It is evident from equations (7.68)-(7.73) that the polarity of the reflected waves is opposite to that of the incident waves while the transmitted waves have same polarity as that of the incident waves.

It can thus be concluded from the above discussion that the polarity of the reflected wave from the fault point will be opposite to that of the incident wave, while the transmitted wave retains the polarity of the incident wave. This fact holds true irrespective of the fault type.

7.2.5 Line terminal

At the terminal of a transmission line, one of the two types of electrical components would exist: 1-a group of other transmission lines; 2-an inductive source such as generator, transformer. The expressions for the reflected waves have been derived for each case as follows:

1. **Presence of only a source at the transmission line terminal:** Figure 7.4 (a) shows the configuration of Bus R, and its equivalent circuit diagram when only an inductive source is present at Bus R terminal of the transmission line. It can be seen from the Figure 7.4 (a) that the equivalent diagram consists of inductance as well as resistance, therefore, the analysis has to be carried out in Laplace domain and then converted into time domain.

   Assume that the traveling wave G_k^{SR} is comprised of a step voltage v_k^F in k^{th}-mode, i.e., $G_k^{SR} = v_k^F$, and is incident on Bus R. Also, let the sinusoidal voltage of the source connected at the Bus R be $v_k^T \cos(\omega t + \phi)$, where v_k^T and ω are the magnitude and angular frequency of the inductive source. Z_{ck} is the k^{th} mode characteristic impedance of the transmission line, while L_o represents the inductance of the source. Now the terminal

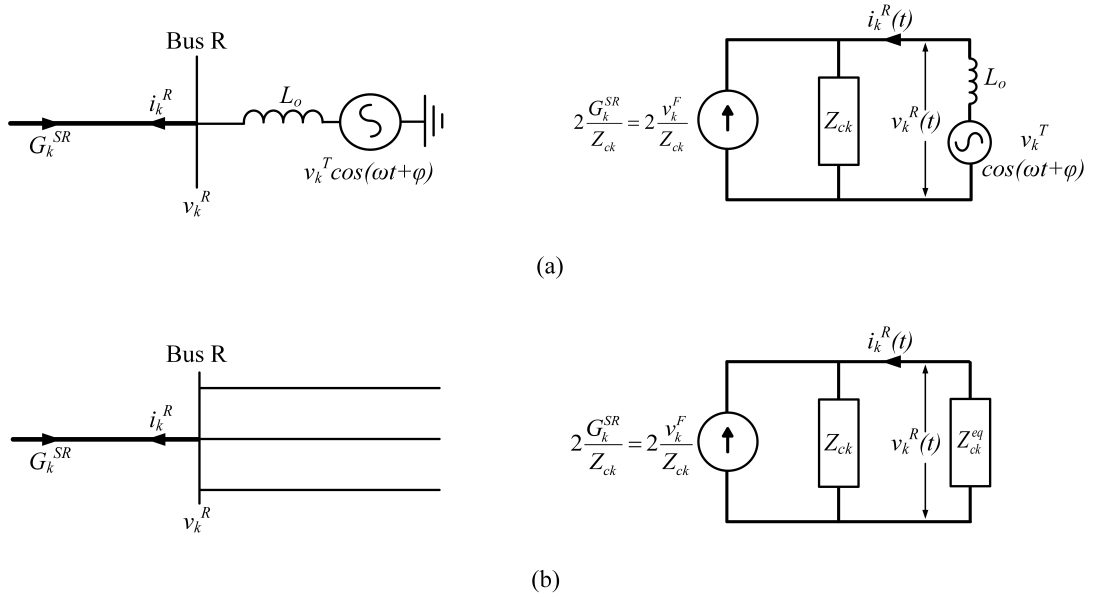

Figure 7.4: Schematic diagram showing various types of components connected at Bus R terminal of the SCCTL: (a) an inductive source, (b) other transmission lines.

current in Laplace domain $i_k^R(s)$ will be given by:

$$i_k^R(s) = -\frac{2v_k^F}{s\left(Z_{ck} + L_o s\right)} + \frac{v_k^T \cos\left(\phi\right) s}{\left(s^2 + \omega^2\right)\left(Z_{ck} + L_o s\right)} - \frac{v_k^T \sin\left(\phi\right) s}{\left(s^2 + \omega^2\right)\left(Z_{ck} + L_o s\right)} \tag{7.74}$$

Taking the Laplace inverse of the above expression, i_k^R in time domain is obtained as:

$$\begin{aligned} i_k^R(t) &= -\frac{2v_k^F}{Z_{ck}}\left(1 - e^{-\frac{Z_{ck}}{L_o}t}\right) + \frac{v_k^T}{\sqrt{Z_{ck}^2 + \omega^2 L_o^2}}\cos\left(\omega t + \widetilde{\phi}\right) - \frac{v_k^T \cos\widetilde{\phi}}{\sqrt{Z_{ck}^2 + \omega^2 L_o^2}} e^{-\frac{Z_{ck}}{L_o}t} \\ &= -\frac{2v_k^F}{Z_{ck}} + \frac{v_k^T}{\sqrt{Z_{ck}^2 + \omega^2 L_o^2}}\cos\left(\omega t + \widetilde{\phi}\right) - \left(\frac{v_k^T \cos\widetilde{\phi}}{\sqrt{Z_{ck}^2 + \omega^2 L_o^2}} - \frac{2v_k^F}{Z_{ck}}\right) e^{-\frac{Z_{ck}}{L_o}t} \end{aligned} \tag{7.75}$$

where

$$\widetilde{\phi} = \tan^{-1}\left(\frac{Z_{ck}\sin\phi - \omega L_o \cos\phi}{Z_{ck}\cos\phi + \omega L_o \sin\phi}\right)$$

Similarly, v_k^R in time domain is obtained as:

$$v_k^R(t) = 2v_k^F e^{-\frac{Z_{ck}}{L_o}t} + \frac{v_k^T Z_{ck}}{\sqrt{Z_{ck}^2 + \omega^2 L_o^2}}\cos\left(\omega t + \widetilde{\phi}\right) - \frac{v_k^T Z_{ck}\cos\widetilde{\phi}}{\sqrt{Z_{ck}^2 + \omega^2 L_o^2}}e^{-\frac{Z_{ck}}{L_o}t} \tag{7.76}$$

It can be seen from the expressions (7.75), and (7.76) that at $t = 0$: $i_k^R(0) = 0$, while $v_k^R(0) = 2v_k^F$; which is typical of an open circuited transmission line. This observed phenomenon is due to the presence of source inductance, which does not let the current through it change abruptly, thus, acting as an open circuit at $t = 0$. Now, the traveling wave originating at Bus R which travels towards Bus S, i.e., G_k^{RS} will be given by (7.77).

$$\begin{aligned} G_k^{RS}(t) =& \frac{v_k^R(t) + i_k^R(t)Z_{ck}}{2} \\ =& v_k^F\left(2e^{-\frac{Z_{ck}}{L_o}t} - 1\right) + \frac{v_k^T Z_{ck}}{\sqrt{Z_{ck}^2 + \omega^2 L_o^2}}\cos\left(\omega t + \widetilde{\phi}\right) - \frac{v_k^T Z_{ck}\cos\widetilde{\phi}}{\sqrt{Z_{ck}^2 + \omega^2 L_o^2}}e^{-\frac{Z_{ck}}{L_o}t} \\ =& \left(\frac{v_k^T Z_{ck}}{\sqrt{Z_{ck}^2 + \omega^2 L_o^2}}\cos\left(\omega t + \widetilde{\phi}\right) - v_k^F\right) - \left(\frac{v_k^T Z_{ck}\cos\widetilde{\phi}}{\sqrt{Z_{ck}^2 + \omega^2 L_o^2}} - 2v_k^F\right)e^{-\frac{Z_{ck}}{L_o}t} \end{aligned} \tag{7.77}$$

Additional point that could be noted here is that the polarity of a traveling wave is decided by the sign of the edge of traveling wave, i.e., the value of G_k^{RS} at $t = 0$. Since, $G_k^{RS}(0) = v_k^F$, therefore, G_k^{RS} will have the same polarity as that of the incident traveling wave G_k^{SR}.

2. **Presence of other transmission lines at the transmission line terminal:** The Figure 7.4 (b) shows the configuration of Bus R and its equivalent circuit digram with Bus R connected to a group of n transmission lines. Z_{ck} is the k^{th} mode characteristic impedance of the transmission line; Z_{ck}^{eq} represents the equivalent k^{th}-mode characteristic impedance of N-transmission lines connected in parallel ($\frac{1}{Z_{ck}^{eq}} = \frac{1}{Z_{ck1}} + \frac{1}{Z_{ck2}} + \cdots + \frac{1}{Z_{ckn}} + \cdots + \frac{1}{Z_{ckN}}$). v_k^R and i_k^R represent the k^{th}-mode voltage and current at Bus R.

   Let us assume that a traveling wave G_k^{SR} traveling from Bus S towards Bus R and comprised of a step voltage v_k^F in k^{th}-mode is incident on Bus R, i.e., $G_k^{SR} = v_k^F$. i_k^R and v_k^R would then be as per the expressions (7.78) and (7.79).

$$i_k^R = -\frac{2v_k^F}{Z_{ck}^{eq} + Z_{ck}} \tag{7.78}$$

$$v_k^R = 2v_k^F\frac{Z_{ck}^{eq}}{Z_{ck}^{eq} + Z_{ck}} \tag{7.79}$$

The traveling wave that gets produced at Bus R and travels towards Bus S, i.e., G_k^{RS} will be given by:

$$G_k^{RS} = \frac{v_k^R + i_k^R Z_{ck}}{2} = v_k^F \frac{Z_{ck}^{eq} - Z_{ck}}{Z_{ck}^{eq} + Z_{ck}} \tag{7.80}$$

Since the Z_{ck}^{eq} is the characteristic impedance of the parallel combination of the transmission lines, therefore $Z_{ck}^{eq} < Z_{ck}$. Thus, the polarity of the G_k^{RS} will be opposite to that of G_k^{SR} when a terminal of a transmission line is connected to a group of other transmission lines. However, in an unlikely configuration when there is only one transmission line connected at Bus R and its characteristic impedance is larger than Z_{ck}, the polarity of reflected wave will become same as that of incident wave.

Now, the transmitted wave in n^{th} transmission line connected at Bus R G_{kn}^{RT} will be given by:

$$G_{kn}^{RT} = \frac{v_{kn}^R + i_{kn}^R Z_{ckn}}{2}$$

Since all the transmission lines are in parallel, therefore, $v_{kn}^R = v_k^R = 2v_k^F \frac{Z_{ck}^{eq}}{Z_{ck}^{eq}+Z_{ck}}$. Also, $i_{kn}^R = \frac{v_{kn}^R}{Z_{ckn}} = 2v_k^F \frac{Z_{ck}^{eq}}{(Z_{ck}^{eq}+Z_{ck})Z_{ckn}}$. Substituting, the values of v_{kn}^R and i_{kn}^R in the above equation it becomes (7.81).

$$G_{kn}^{RT} = 2v_k^F \frac{Z_{ck}^{eq}}{Z_{ck}^{eq} + Z_{ck}} \tag{7.81}$$

It can be seen from (7.81) that the polarity of the transmitted traveling wave along n^{th} transmission line will be same as that of the incident traveling wave when a group of N-transmission lines is connected at Bus R.

The polarities of the reflected and transmitted waves with respect to the polarity of the incident wave from various points of discontinuity in a transmission line as derived in the section above are summarized in Table 7.1. The polarity of the incident wave is assumed positive for all the cases. It should be noted that the transmitted wave when only an inductive source is present at a transmission line terminal is 'not available (NA)' as there exists no medium of transmission beyond the inductive source.

Table 7.1: Relative polarities of the reflected and transmitted traveling waves from various points of discontinuity in a transmission line

Type of Discontinuity	Component Connected	Polarity		
		Incident Wave	Reflected Wave	Transmitted Wave
Fault Point	Fault Resistance	+	−	+
Terminal	Inductive Source	+	+	NA
	Other Transmission Lines	+	−	+

7.3 Applicability of the single-ended algorithms to various configurations of SCCTL

In order to locate a fault in an SCCTL using the measurements from only one terminal of the transmission line, it is imperative to know the origin of the second traveling wave to arrive at that terminal of the transmission line as shown in Section 6.4.2. For example, for the application of single-ended fault location at Bus S, it needs to be identified that the second traveling wave to arrive at Bus S is G_k^{FSFS} or G_k^{FRS}. If the second traveling wave arriving at fault locator is G_k^{FSFS} then the fault location (d) is measured using equation (6.18). If on the other hand the second traveling wave to arrive at fault locator is G_k^{FRS}, then d is obtained through equation (6.20). Similar approach would be needed at Bus R as well to distinguish between G_k^{FRFR} and G_k^{FSR} for the purpose of fault location. It is also worth noting that series capacitor can be regarded as a short circuit for traveling waves as shown in Section 7.2.1, therefore, the traveling waves reflected from SCB could be ignored without affecting the accuracy of the fault location.

A methodology has been proposed in [28] which identifies the second traveling wave to arrive at the transmission line terminal by comparing the polarity of the second traveling wave to that of the first traveling wave to arrive at the same terminal. For instance, at Bus S the algorithm of [28] would compare the polarity of the second wave to that of G_k^{FS}, and consequently identify the second wave as G_k^{FSFS} or as G_k^{FRS}. In this section, the methodology of [28] is examined in lieu of the Table 7.1 for various configurations of an SCCTL as shown in Figure 7.5 (a)-(c). The limitations of the methodology presented in [28] are identified, and thereafter, a solution is proposed to overcome those challenges based on the mathematical expressions derived in Section 7.2. It should be noted that the traveling waves produced by the occurrence of the fault, i.e., G_k^{FS} and G_k^{FR} have been assumed to have '+' polarity.

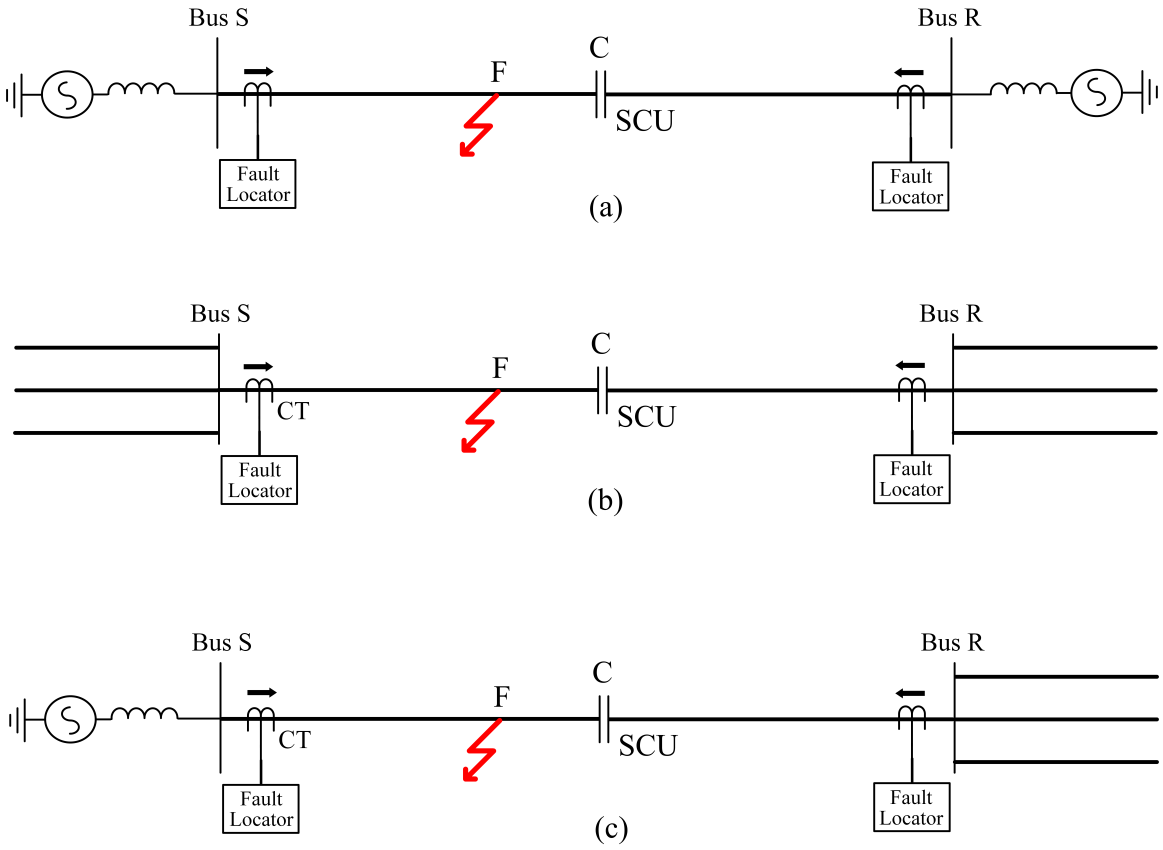

Figure 7.5: Schematic diagram showing various configurations of an SCCTL: (a) Configuration A, (b) Configuration B, (c) Configuration C.

1. **Configuration A**: In Configuration A, an inductive source is present at each end of an SCCTL as shown in Figure 7.5 (a). The trajectories and polarities of the traveling waves G_k^{FSFS}, and G_k^{FRS} in Configuration A of an SCCTL are discussed as below:

   (a) $\boldsymbol{G_k^{FSFS}}$ and $\boldsymbol{G_k^{FSR}}$

      i. **Fault point**: The traveling wave G_k^{FS} gets generated at fault point with polarity '+'. G_k^{FS} starts traveling from the fault point towards Bus S.

      ii. **Bus S**: G_k^{FS} arrives at Bus S with polarity '+'; the inductive source reflects part of the wave G_k^{FS} towards fault point with the same polarity as G_k^{FS} i.e., '+'.

      iii. **Fault point**: The reflected wave from Bus S arrives at fault point where it splits into two parts, G_k^{FSFS} which gets reflected towards Bus S with polarity '–', and G_k^{FSR} which is transmitted towards Bus R with polarity '+'.

      iv. A. **Bus S**: The traveling wave G_k^{FSFS} arrives at Bus S with polarity '–'.

      B. **Bus R**: The traveling wave G_k^{FSR} arrives at Bus R with polarity '+'.

   (b) $\boldsymbol{G_k^{FRS}}$ and $\boldsymbol{G_k^{FRFR}}$

      i. **Fault point**: The traveling waves G_k^{FR} is generated at fault point with polarity '+' G_k^{FR} starts traveling towards Bus R.

      ii. **Bus R**: G_k^{FR} arrives at Bus R with polarity '+'; the inductive source reflects a part of the wave G_k^{FR} towards fault point with the same polarity as G_k^{FR} i.e., '+'.

      iii. **Fault point**: The reflected wave from Bus R arrives at fault point where it splits into two parts, G_k^{FRFR} which gets reflected towards Bus R with polarity '–', while G_k^{FRS} is transmitted towards Bus R with polarity '+'.

      iv. A. **Bus S**: The traveling wave G_k^{FRS} arrives at Bus S with polarity '+'.

      B. **Bus R**: The traveling wave G_k^{FRFR} arrives at Bus R with polarity '–'.

   It can be seen from above discussion that at Bus S, polarity of the traveling wave G_k^{FSFS} will be opposite to that of G_k^{FS}, while that of G_k^{FRS} is same as that of G_k^{FS}. Therefore, if the second traveling wave encountered at Bus S has opposite polarity to that of the first wave, i.e., G_k^{FS}, then the second wave is G_k^{FSFS} and the equation (6.18) should be employed for obtaining d. If, on the other hand, the polarity of the second wave at Bus S is same as that of the first wave, then the second wave is G_k^{FRS}, and equation (6.20) should be used for calculating d. Similarly, at Bus R the traveling wave G_k^{FRFR} would arrive with polarity opposite to that of G_k^{FR}, while the wave G_k^{FSR} would arrive at Bus R with same polarity as that of G_k^{FR}. Therefore, the application of [28] at Bus R would be identical to that at the Bus S. Thus, the

algorithm of [28] can be applied at both terminals of the Configuration A of the SCCTL.

2. **Configuration B**: In Configuration B, a group of transmission lines is present on each side of the SCCTL as shown in Figure 7.5 (b). Since, the equivalent characteristic impedances of the group of transmission lines will be smaller when compared to the characteristic impedance of the SCCTL, the waves reflected by each terminal will be of the opposite polarity to that of the incident waves. The trajectories and corresponding changes in polarities of the waves G_k^{FSFS}, G_k^{FRS}, G_k^{FRFR}, and G_k^{FSR}, are discussed as follows:

   (a) $\boldsymbol{G_k^{FSFS}}$ and $\boldsymbol{G_k^{FSR}}$

      i. **Fault point**: Following a fault, the traveling wave G_k^{FS} is generated with polarity '+' at the fault point which then travels towards Bus S.

      ii. **Bus S**: G_k^{FS} arrives at Bus S with polarity '+', where it is split into two parts. The polarity of the reflected part of G_k^{FS} is reversed to '–' which then travels towards fault point. The other part of the wave G_k^{FS} is transmitted onto the group of transmission lines present at Bus S with the same polarity as that of G_k^{FS}, i.e., '+'.

      iii. **Fault point**: The reflected wave from Bus S with polarity '–' arrives at fault point where it is split into two parts G_k^{FSFS} and G_k^{FSR}. The fault point changes the polarity of reflected part, G_k^{FSFS} to '+' which travels towards Bus S. The transmitted portion of the wave, G_k^{FSR} is transmitted towards Bus R with the same polarity as the incident wave on the fault point, i.e., '–'.

      iv. A. **Bus S**: The traveling wave G_k^{FSFS} arrives at Bus S with polarity '+'.

      B. **Bus R**: The traveling wave G_k^{FSR} arrives at Bus R with polarity '–'.

   (b) $\boldsymbol{G_k^{FRS}}$ and $\boldsymbol{G_k^{FRFR}}$

      i. **Fault point**: The traveling wave G_k^{FR} is generated following a fault with polarity '+' at the fault point which starts traveling towards Bus R.

      ii. **Bus R**: The traveling wave G_k^{FR} reaches Bus R with polarity '+', where the group of transmission lines reflect part of the incident wave with opposite polarity '–' towards the fault point. The other part of the incident wave G_k^{FR} is transmitted with polarity '+' onto the transmission lines present at Bus S with the same polarity as that of G_k^{FS}, i.e., '+'.

      iii. **Fault point**: At fault point, the wave reflected from Bus R is split in two parts with G_k^{FRFR} reflected back to Bus R with polarity '+' which is opposite to that

of the incident wave. The other part G_k^{FRS} is transmitted towards Bus S with the polarity '–' which is same as the incident wave at the fault point.

iv. A. **Bus S**: The traveling wave G_k^{FRS} arrives at Bus S with polarity '–'.

B. **Bus R**: The traveling wave G_k^{FRFR} arrives at Bus R with polarity '+'.

It could be observed from above discussion that for Configuration B if the polarity of the second traveling wave to arrive at Bus S is same as that of the first traveling wave then the second traveling wave to arrive at Bus S is G_k^{FSFS}, and equation (6.18) should be used for locating the fault. On the other hand, if the polarity of the second wave to arrive at Bus S is opposite to that of the first wave at Bus S then the second wave arriving at Bus S is G_k^{FRS}, and equation (6.20) should be used to estimate the location of the fault. Similarly, at Bus R the second wave to arrive will be G_k^{FRFR} if its polarity is identical to G_k^{FR}. If on the other hand the polarity of the second wave to arrive at Bus R is opposite to that of G_k^{FR} then the second wave is G_k^{FSR}. Therefore, depending upon the type of second wave arriving at Bus R, the appropriate fault location equation could be used to calculate the fault location from Bus R. Thus, the algorithm of [28] can be applied at both terminals of the Configuration B of the SCCTL.

3. **Configuration C**: In Configuration C, an inductive source is connected at Bus S while a group of transmission lines is connected at Bus R as shown in Figure 7.5 (c). The polarities of the traveling waves G_k^{FSFS}, G_k^{FRS}, G_k^{FRFR}, and G_k^{FSR} have been derived in the following section assuming that the polarity of the traveling waves generated at the fault point G_k^{FR} and G_k^{FR} is '+'.

(a) $\boldsymbol{G_k^{FSFS}}$ and $\boldsymbol{G_k^{FSR}}$

i. **Fault point**: The fault occurs and the traveling wave G_k^{FS} is generated at fault point with polarity '+' and starts traveling towards Bus S.

ii. **Bus S**: Wave G_k^{FS} arrives at Bus S where inductive source absorbs a part of it while the other part is reflected towards fault point with the same polarity which is '+'.

iii. **Fault point**: The wave reflected from Bus S arrives at fault point where part of it is reflected back towards Bus S as G_k^{FSFS} with opposite polarity, i.e., '–', while the other part is transmitted with '+' polarity towards Bus R as G_k^{FSR}.

iv. A. **Bus S**: The traveling wave G_k^{FSFS} arrives at Bus S with polarity '–'.

B. **Bus R**: The traveling wave G_k^{FSR} arrives at Bus R with polarity '+'.

(b) $\boldsymbol{G_k^{FRS}}$ and $\boldsymbol{G_k^{FRFR}}$

i. **Fault point**: The fault occurs and the traveling wave G_k^{FR} so generated starts traveling from fault point towards Bus R with polarity '+'.

ii. **Bus R**: The traveling wave G_k^{FR} arrives at Bus R with polarity '+', where the presence of multiple transmission lines split into two parts. One of the parts is transmitted into various transmission lines with same polarity as G_k^{FR} , i.e., '+'. While the other part is reflected back towards the fault point but with polarity opposite to G_k^{FR}, i.e, with polarity '–'.

iii. **Fault point**: The wave reflected from Bus R arrives at fault point with polarity '–', where the wave is split into two parts. One part of the part is transmitted through the fault point with polarity '–' which reaches Bus S as G_k^{FRS}, while the other part is reflected back with opposite polarity ('+') which arrives at Bus R as G_k^{FRFR}.

iv. A. **Bus S**: The traveling wave G_k^{FRS} arrives at Bus S with polarity '–'.

B. **Bus R**: The traveling wave G_k^{FRFR} arrives at Bus R with polarity '+'.

It is seen from above discussion that both traveling waves, G_k^{FRS}, and G_k^{FSFS} would arrive at Bus S with polarity '–'. It implies that the methodology of comparing polarities to distinguish between waves G_k^{FRS}, and G_k^{FSFS} cannot be applied at Bus S in Configuration C. Similarly, it is observed that traveling waves arriving at Bus R, i.e., G_k^{FSR}, and G_k^{FRFR} have '+' polarity. Thus, the polarity of the traveling waves G_k^{FSR}, and G_k^{FRFR} cannot be distinguished from each other at Bus R by using their polarities in Configuration C. Thus, the algorithm of [28] cannot be applied to any terminal of the Configuration C of the SCCTL.

From the above discussion, it could be seen that the methodology of [28] in its current form is applicable to only those configurations of the SCCTL in which the traveling waves reflected from each terminal have alike polarities. This condition remains true only for Configuration A and Configuration B of the SCCTL, thus implying the applicability of [28] to the Configuration A and Configuration B of the SCCTL . For Configuration C, the polarity of the traveling wave reflected from one end will always be opposite to the polarity the traveling wave reflected from the other end. Therefore, the methodology of [28] is inapplicable to Configuration C of the SCCTL.

One more challenge facing the single-ended traveling wave-based fault location algorithm needs to be addressed for those configurations of the SCCTL in which at least one transmission line has been connected to at least one of its terminals, which is true for Configurations B, and C. In order to elaborate this point consider Bus S of the Configuration B of SCCTL (Figure 7.5 (b)). It was discussed that the second traveling wave to arrive at Bus S will either be

G_k^{FSFS} or G_k^{FRS}. However, if even one of the transmission lines connected at Bus S is shorter than half of the length of the SCCTL (assuming wave speed is same in all transmission lines), there could be fault scenarios in the SCCTL for which the second traveling wave to arrive at Bus S would neither be G_k^{FSFS} nor G_k^{FRS}, it would rather be the wave reflected from the remote end of that shortest line. As an example, consider that one of the transmission lines connected at Bus S is 0.4 times the length of the SCCTL, and the fault occurs in SCCTL at 45% line length as measured from Bus S. If τ_k is the time taken by the traveling wave to traverse whole of the SCCTL, then the wave G_k^{FS} will arrive at Bus S at $0.45\tau_k$ time units after the occurrence of the fault. A part of the wave G_k^{FS} will be transmitted to the shortest transmission line which will get reflected back from its remote end and will arrive at Bus S at $1.25\tau_k$ ($= 0.45\tau_k + 2 \times 0.4\tau_k$) time units after the occurrence of the fault. It is assumed that velocity k^{th}-mode wave is same in both transmission lines. While a part of G_k^{FS} will be reflected towards the fault point from where a part of the the wave will be reflected wave which would arrive at Bus S at $1.35\tau_k$ ($= 0.45\tau_k + 2 \times 0.45\tau_k$) time units after the occurrence of the fault. Hence, we see that in above example the second wave to arrive at Bus S is neither G_k^{FSFS} nor G_k^{FRS}, rather it is the reflected wave from the remote end of the shortest transmission line connected at Bus S, which if used for fault location assuming that it is G_k^{FSFS} or G_k^{FRS} will result in erroneous fault location. There could also be the cases where multiple transmission lines out of all the lines connected at Bus S, are shorter than half of the length of the SCCTL. Thus, a procedure needs to be proposed to block the wave reflected from the remote ends of the transmission lines connected at fault locator terminal of the SCCTL from being used towards calculating the fault location in Configurations B, and C.

7.4 Test System

The proposed solution to the challenges identified in the previous section is elaborated using the simulated fault scenarios in an SCCTL. Therefore, it is imperative to describe the power system simulated in PSCAD. Since various types of electrical components could be connected at the terminals of the SCCTL for different configurations as presented in Section 7.3, the test power system will change according to the configuration. Therefore, the parameters of each component has been described separately. The test power system for each configuration then could be constructed using the described components.

The voltage level of the power system is 500 kV. The positive and zero sequence impedances for the sources used in power system are $Z_{S1} = (0.5 + j7.5)\ \Omega$ and $Z_{S0} = (1.2 + j12.5)\ \Omega$, respectively. The positive and zero sequence impedances for the transmission lines used in the test power system are $Z_{L1} = (0.0155 + j0.3719)\ \Omega$ per km and $Z_{L0} = (0.3546 + j1.0670)\ \Omega$ per km,

respectively, while the positive and zero sequence admittances are $Y_{L1} = (0 + j4.4099 \times 10^{-6})$ $\mho$ per km, and $Y_{L0} = (0 + j2.7844 \times 10^{-6})$ $\mho$ per km, respectively. The level of series compensation of SCCTL is 70% series compensation which corresponds to an equivalent capacitance of 29.11μF. The length of the SCCTL is 350 km.

7.5 The Proposed solution

As explained in Section 7.3, the traveling waves reflected from the fault point and the remote terminal of the SCCTL cannot be distinguished from each other using their polarities in Configuration C of the SCCTL. Therefore, more detailed look into the properties of the traveling waves reflected from fault point and the remote terminal of the SCCTL is warranted. First of all, the proposed method is presented for the Configuration C of the SCCTL, thereafter its application to Configuration A and B has been presented.

7.5.1 Configuration C

After the occurrence of a fault in Configuration C of an SCCTL, the second traveling wave to arrive at Bus R would either be G_k^{FRFR} or G_k^{FSR} depending upon the location of the fault in an SCCTL. First of all, let us focus our attention on the trajectory of the traveling wave G_k^{FRFR} arriving at fault locator situated at Bus R in the Configuration C. The occurrence of a fault in a transmission line acts as an application of a step voltage at the fault point. The traveling wave G_k^{FR} produced at the fault point consists of a step voltage which would reach Bus R where part of it will be reflected back as per equation (7.80). Since, the characteristic impedance of the transmission lines is almost real in nature with a very small imaginary component, the traveling wave reflected from Bus R as per (7.80) will be a step function albeit with a smaller amplitude and opposite polarity as compared to G_k^{FR}. The step function reflected wave from Bus R then reaches the fault point where part of it will be transmitted towards Bus S while other is reflected back towards Bus R as G_k^{FRFR} with polarity opposite to the incident wave. It could be noted from the equations derived in Section 7.2.2 for reflected and transmitted waves from the fault point, that all the variables occurring in equations, i.e., characteristic impedance of the transmission line (Z_{ck}) and fault resistance (R^F) are purely resistive in nature. Thus, the traveling wave reflected from fault point towards Bus R (G_k^{FRFR}) and the traveling wave transmitted towards Bus S from fault point (G_k^{FRS}) will be step functions. Consequently, the arrival of G_k^{FRFR} at Bus R would produce step change in Bus R current with same polarity as G_k^{FR}, as the group of transmission line acts as pure resistive component to the traveling waves.

The other traveling wave to arrive at Bus R fault locator is G_k^{FSR}, the trajectory of which

is discussed now. The traveling wave G_k^{FS}, which has same magnitude and polarity as G_k^{FR}, consisting of step voltage gets generated at fault point and propagates towards Bus S. After the arrival of G_k^{FS} at Bus S, part of it gets reflected back towards fault point with the same polarity as G_k^{FS} as per the equation analogous to (7.77) which is derived for Bus R. The reflected wave as could be witnessed from (7.77) is comprised of a decaying exponential component superimposed on the fundamental frequency sinusoid. The traveling wave reflected from Bus S will reach the fault point from where a part of it will be transmitted with the same polarity as the incident wave towards Bus R. The traveling wave transmitted from fault point will reach Bus R as G_k^{FSR} and will have the same properties as described by (7.77) as all variables in the equations governing the transmitted wave from the fault point are purely real in nature. The G_k^{FSR} as explained earlier, will be composed of an exponential decaying component superimposed on a sinusoidal function and a constant value. It is worth noting that the decaying exponential component of the wave G_k^{FSR} decays relatively fast while the fundamental frequency part of G_k^{FSR} does not change significantly during the time intervals encountered between the arrival of two successive traveling waves. Therefore, the fundamental frequency part of G_k^{FSR} could be seen as an application of step function. Hence, the arrival of G_k^{FSR} at Bus R will manifest itself as a step change followed by the decaying exponential component.

From the above discussion, it could be concluded that the traveling wave G_k^{FRFR} will produce a step change in the Bus R current which means that derivative of Bus R current would show an impulse function on the arrival of G_k^{FRFR} at Bus R. On the other hand, the arrival of G_k^{FSR} at Bus R would produce a step change followed by an exponentially decaying changes in the Bus R current. It means that the derivative of Bus R current following the arrival of G_k^{FSR} at Bus R will yield an impulse function followed by exponentially decaying waveform. Thus, the presence or absence of an exponential decaying component in the k^{th} mode Bus R current, or its derivative following the arrival of the second traveling wave can be used to distinguish between G_k^{FRFR} and G_k^{FSR}. In G_k^{FRFR} there will be no exponential decaying component while in the case of G_k^{FSR} an exponential decaying component will be observed.

It should be noted here that taking derivative of the current removes all the slow occurring changes in the waveform, thus, making the identification of the traveling wave type much easier. However, taking a derivative of a signal increases the noise level in the signal. Thus, denoising of the signal is necessary before taking the derivative of Bus R current. In this chapter, the current is averaged for 10 samples to decrease the noise level in its derivative. It should be noted that derivative of the current waveform is used only for the identification of the traveling waves; the time instance of the arrival of a traveling wave for the purpose of fault location should be used from the Bus R current only. In this way the accuracy limit of the algorithm does not get impacted by averaging of the current waveform.

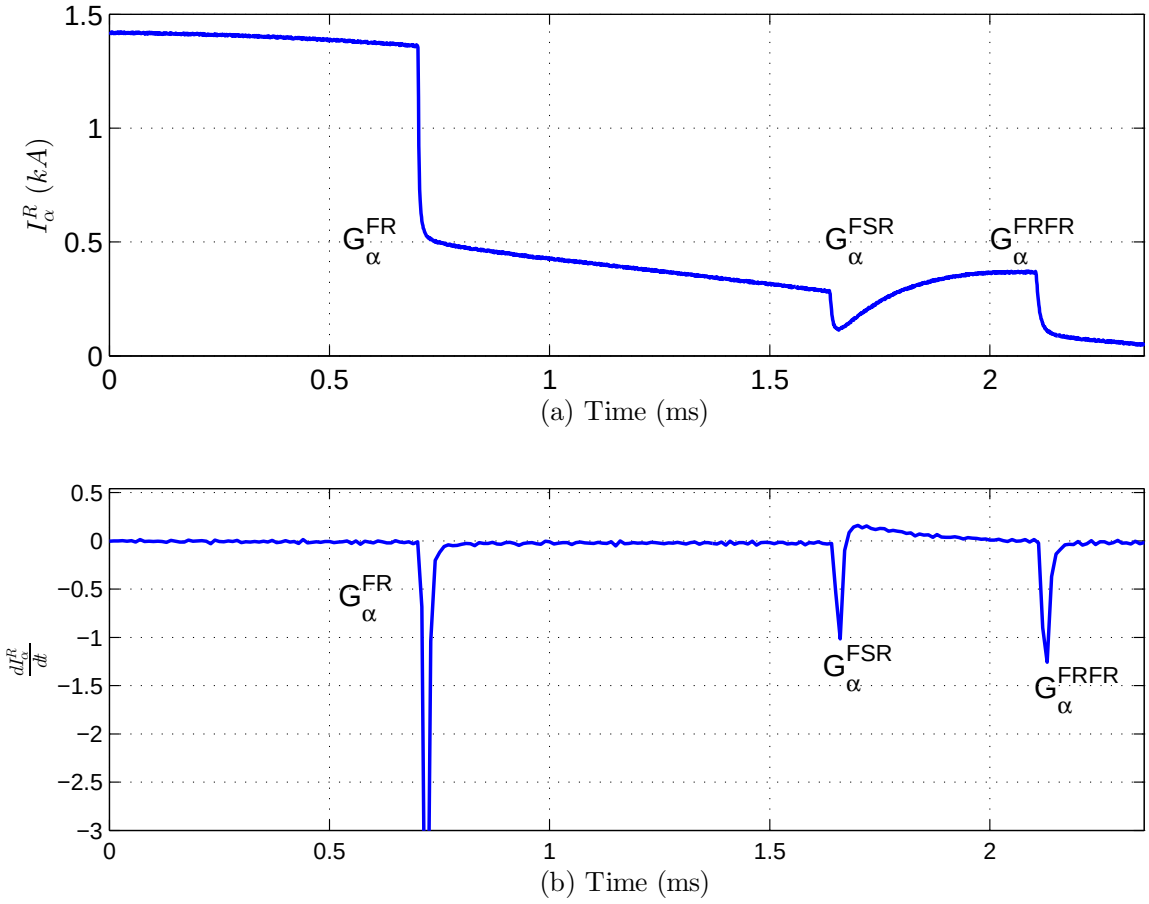

Figure 7.6: The arrival of traveling waves G_α^{FR}, G_α^{FSR}, G_α^{FRFR} at Bus R of Configuration C of the SCCTL for a 50Ω three phase fault at 40% line length measured from Bus S as observed in (a) α-mode Bus R current, (b) derivative of α-mode Bus R current.

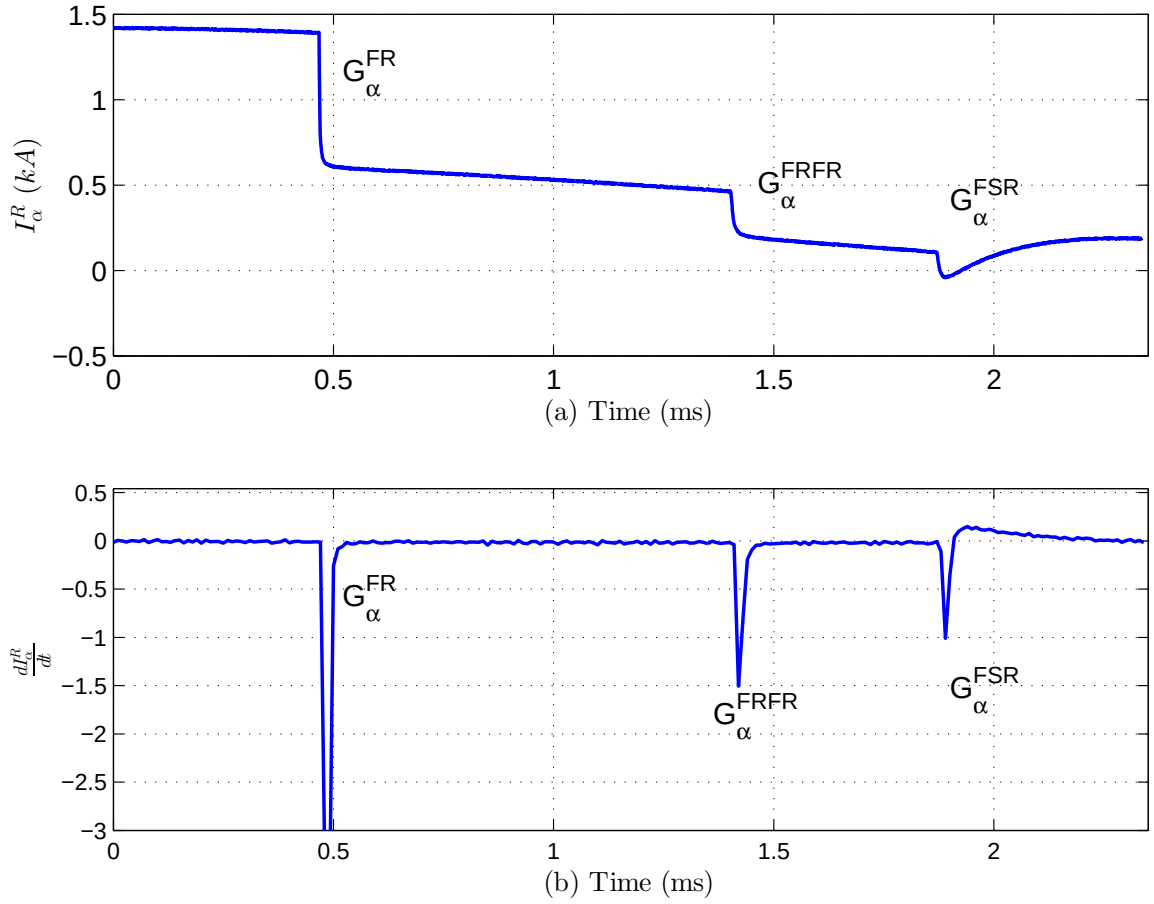

Figure 7.7: The arrival of traveling waves G_α^{FR}, G_α^{FRFR}, G_α^{FSR} at Bus R of Configuration C of the SCCTL for a three phase fault at 60% line length measured from Bus S as observed in (a) α-mode Bus R current, (b) derivative of α-mode Bus R current.

In order to verify the postulates of the above discussion, consider a three phase fault scenario with fault resistance of 50Ω lying at 40% line length as measured from Bus S. The waveforms of α-mode of the current measured at Bus R (I_α^R) and its first derivative, for the fault scenario under consideration are shown in Figure 7.6 (a) and (b), respectively. The amount of noise present in all of the signals presented in this chapter is 1%. It is a known fact that for any fault lying at 40% line length as measured from Bus S, the first three α-mode traveling waves to arrive at Bus R will be G_α^{FR}, G_α^{FSR}, and G_α^{FRFR}, respectively. The time period shown in Figure 7.6 is from the time of fault inception to the arrival of third traveling wave, i.e, G_α^{FRFR} at Bus R. The first traveling wave G_α^{FR} which is a negative step function produces a step change in the I_α^R, correspondingly, the derivative of I_α^R shows a negative impulse. The next traveling wave to arrive at Bus R is G_α^{FSR} which as explained earlier, is composed of a step function and a fast decaying exponential component. The initial change produced by G_α^{FSR} in I_α^R is like a step function marked by sudden change in I_α^R in Figure 7.6 (a), and a negative spike in derivative of I_α^R observed in Figure 7.6 (b). Thereafter, an exponential decay caused by G_α^{FSR} is observed in Figure 7.6 (a) and (b) following the initial step change. The third wave to arrive at Bus R is G_α^{FRFR} which is also a step function produces only a step change in I_α^R, and does not produce any decaying exponential component as could be observed from the Figures 7.6 (a) and (b).

Similarly, I_α^R and its first derivative are shown in Figure 7.7 (a) and (b), respectively for a 50Ω three phase fault lying at 60% line length as measured from Bus S. For this case, the first, second, and third α-mode traveling waves to arrive at Bus R will be G_α^{FR}, G_α^{FRFR}, and G_α^{FSR}, respectively. It can be observed from Figure 7.7 that the exponential decaying component is absent after the arrival of the second traveling wave, i.e., G_α^{FRFR}. On the other hand, the exponential decaying component is detected after the arrival of the third wave, i.e., G_α^{FSR} as could be observed from Figure 7.7 (a) and (b). Thus, it could be concluded that at Bus R in Configuration C of the SCCTL, the traveling waves G_α^{FSR}, and G_α^{FRFR} could be differentiated from each other by the presence or absence of the exponential decay in I_α^R or its first derivative. The exponential decaying component will be present after the arrival of G_α^{FSR}, while, it will be absent after the arrival of G_α^{FRFR}.

Similarly, the traveling waves G_k^{FRS}, and G_k^{FSFS} would arrive at Bus S after getting reflected from Bus R, and fault point, respectively. The traveling wave G_k^{FR} comprised of a step function gets generated at the fault point due to the occurrence of the fault. G_k^{FR} reaches Bus R where it gets reflected as a step function as per the equation (7.80) with a lesser magnitude and polarity opposite to that of G_k^{FR}. The reflected wave from Bus R reaches fault point where part of it gets transmitted through fault point towards Bus S with same polarity as the incident wave which then arrives at Bus S as G_k^{FRS}. Since, all the components of the equations governing the reflection and transmission of the traveling waves from the fault point as derived in Section

7.2.2 are real, the traveling wave G_k^{FRS} will maintain the profile of the incident wave and will arrive at Bus S as a step function. Now the arrival of G_k^{FRS} acts as application of step voltage at Bus S which produces the changes in k^{th} mode current at Bus S as per equation analogous to (7.75) for Bus S. It should be noted that an inductive source is located at Bus S. It could be seen from (7.75) that the change in k^{th} mode current at Bus S caused by the arrival of G_k^{FRS} comprises of a bounded exponential function superimposed on a fundamental frequency sinusoidal signals. Since, the change in the fundamental frequency signals will be relatively small during the time periods involved in traveling waves, the derivative of k^{th} mode of Bus S current after the arrival of traveling wave G_k^{FRS} will predominantly be comprised of the exponential function.

Now, let us consider the trajectory of the traveling wave G_k^{FSFS}. The traveling wave G_k^{FS} comprised of a step function gets generated at fault point, and starts traveling towards Bus S. The wave reflected from Bus S will be governed by the equation analogous to (7.77) written for Bus S. The wave reflected from Bus S will comprise of a rapidly decaying bounded exponential component superimposed on a fundamental frequency sinusoidal signal. This wave then reaches fault point from where part of it gets reflected. The wave reflected from fault point maintains its profile and arrives at Bus S as G_k^{FSFS}. It could be shown through mathematical analysis that the derivative of the k^{th} mode current at Bus S caused by the arrival of G_k^{FSFS} will have the form given by (7.82).

$$\frac{di_k^S}{dt} = p_1 e^{-\frac{Z_{ck}}{L_o}t} - \frac{Z_{ck}}{L_o} p_2 t e^{-\frac{Z_{ck}}{L_o}t} - \omega p_3 \cos(\omega t + \theta) \tag{7.82}$$

where p_1, p_2, and p_3 are real numbers of relatively comparable magnitude; θ is the phase angle of the fundamental component of the reflected wave; while t represents the time with $t = 0$ representing the instance of arrival of G_k^{FSFS} at Bus S. The term $\omega p_3 \cos(\omega t + \theta)$ would not produce any dynamic changes in the waveform plot of derivative of k^{th} mode current at Bus S as it does not change considerably within the time period between the arrival of G_k^{FSFS} and the next traveling wave. The fast occurring changes that could be observed in the waveform plot of k^{th} mode current at Bus S will only be the result of the term $p_1 e^{-\frac{Z_{ck}}{L_o}t} - \frac{Z_{ck}}{L_o} p_2 t e^{-\frac{Z_{ck}}{L_o}t}$.

As an example, consider a 50Ω three phase fault lying at 40% line length as measured from Bus S in Configuration C of the SCCTL. The first, second and third α-mode traveling waves to arrive at Bus S will be G_α^{FS}, G_α^{FSFS}, G_α^{FRS}, respectively for the fault lying at 40% of the line length. Figure 7.8 (a) and (b) shows the α-mode of Bus S current (I_α^S) and its first derivative, respectively following the arrival of the first three traveling waves at Bus S. As discussed, the derivative of I_α^S following the arrival of G_α^{FS}, and G_α^{FRS} at Bus S is comprised of a bounded exponentially decaying component as can be seen from Figure 7.8 (b). On the other hand, the

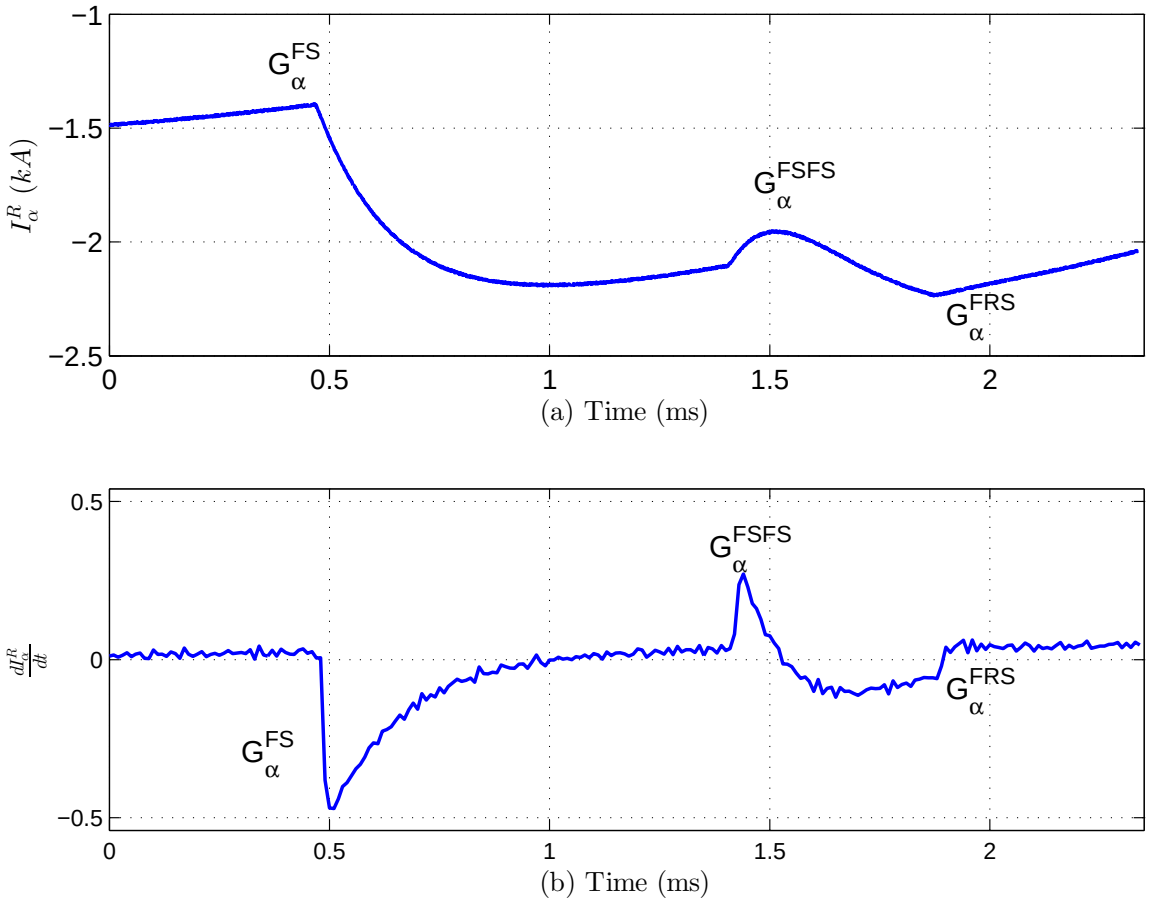

Figure 7.8: The arrival of traveling waves G_α^{FS}, G_α^{FSFS}, G_α^{FRS} at Bus S of Configuration C of the SCCTL for a 50Ω three phase fault at 40% line length measured from Bus S as observed in, (a) α-mode Bus S current, (b) derivative of α-mode Bus S current.

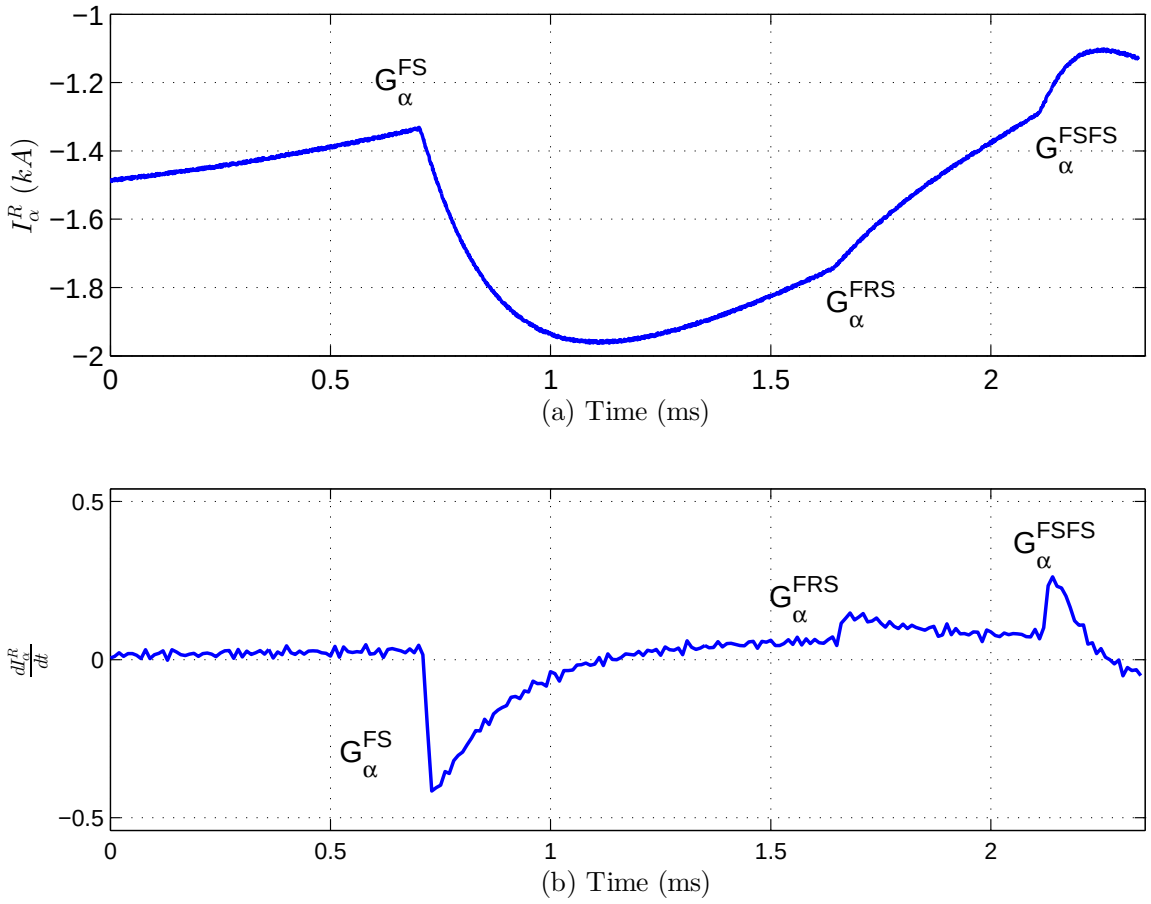

Figure 7.9: The arrival of traveling waves G_α^{FS}, G_α^{FSFS}, G_α^{FRS} at Bus S of Configuration C of the SCCTL for a 50Ω three phase fault at 60% line length measured from Bus S as observed in, (a) α-mode Bus S current, (b) derivative of α-mode Bus S current.

derivative of I_α^S following the arrival of G_α^{FSFS} is typical of the function te^{-at} characterized by the 'overshoot' of the waveform from its starting point. Though, this waveform is described more accurately by the expression $p_1 e^{-\frac{Z_{ck}}{L_o}t} - \frac{Z_{ck}}{L_o} p_2 t e^{-\frac{Z_{ck}}{L_o}t}$.

Similarly, Figure 7.9 shows I_α^S and its derivative for a 50Ω three phase fault lying at 60% line length as measured from Bus S in Configuration C of the SCCTL. For this fault scenario, the first three α-mode traveling waves to arrive at Bus S will be G_α^{FS}, G_α^{FRS}, G_α^{FSFS}, respectively. It can be seen from Figure 7.9 that the derivative of I_α^S following the arrival of the first two traveling waves is comprised of a bounded exponentially decaying component only, which is typical behavior of G_α^{FS}, and G_α^{FRS}. On the other hand, the derivative of I_α^S following the arrival of third traveling wave shows an 'overshoot' from its starting point, which is typical behavior of G_α^{FSFS}.

It can thus be concluded that at Bus S terminal of Configuration C of the SCCTL, the traveling waves G_α^{FRS}, and G_α^{FSFS} could be differentiated from each other by observing the presence or absence of the overshoot in the derivative of I_α^S from its starting point following the arrival of the second traveling wave. If the derivative of I_α^S depicts an overshoot from its starting point following the arrival of a traveling wave then this traveling wave will be G_α^{FSFS}. If on the other hand, the derivative of I_α^S following the arrival of the second traveling wave is comprised only of exponential decaying component, it would not result in overshoot of the derivative of I_α^S. In this case, the second traveling wave arriving at Bus S will be G_α^{FRS}.

As presented in this section, the origin of the second traveling wave to arrive at both terminals of an SCCTL in its Configuration C could be identified by observing the properties of the derivative of the k^{th} mode current at each terminal of the transmission line. It could be recalled here that the single-ended fault location algorithms based on polarity comparison of the first two traveling waves to arrive at each terminal are not applicable to Configuration C of the SCCTL. The waveforms of the derivative of Bus S and Bus R currents for all other fault locations and fault types in Configuration C of the SCCTL are given in Appendix D. The accuracy of the proposed algorithm for Configuration C of the SCCTL can further be validated from the Figures given in Appendix D.

7.5.2 Configuration A

In Configuration A of the SCCTL, there is only an inductive source present at each terminal of the SCCTL, i.e., at Bus S and Bus R (Figure 7.5 (a)). It has been explained in Section 7.3 through derived expressions that the traveling waves reflected from the remote terminal would arrive at the local terminal with same polarity as the first traveling wave at the local terminal, while, the traveling wave reflected from the fault point would arrive at local terminal

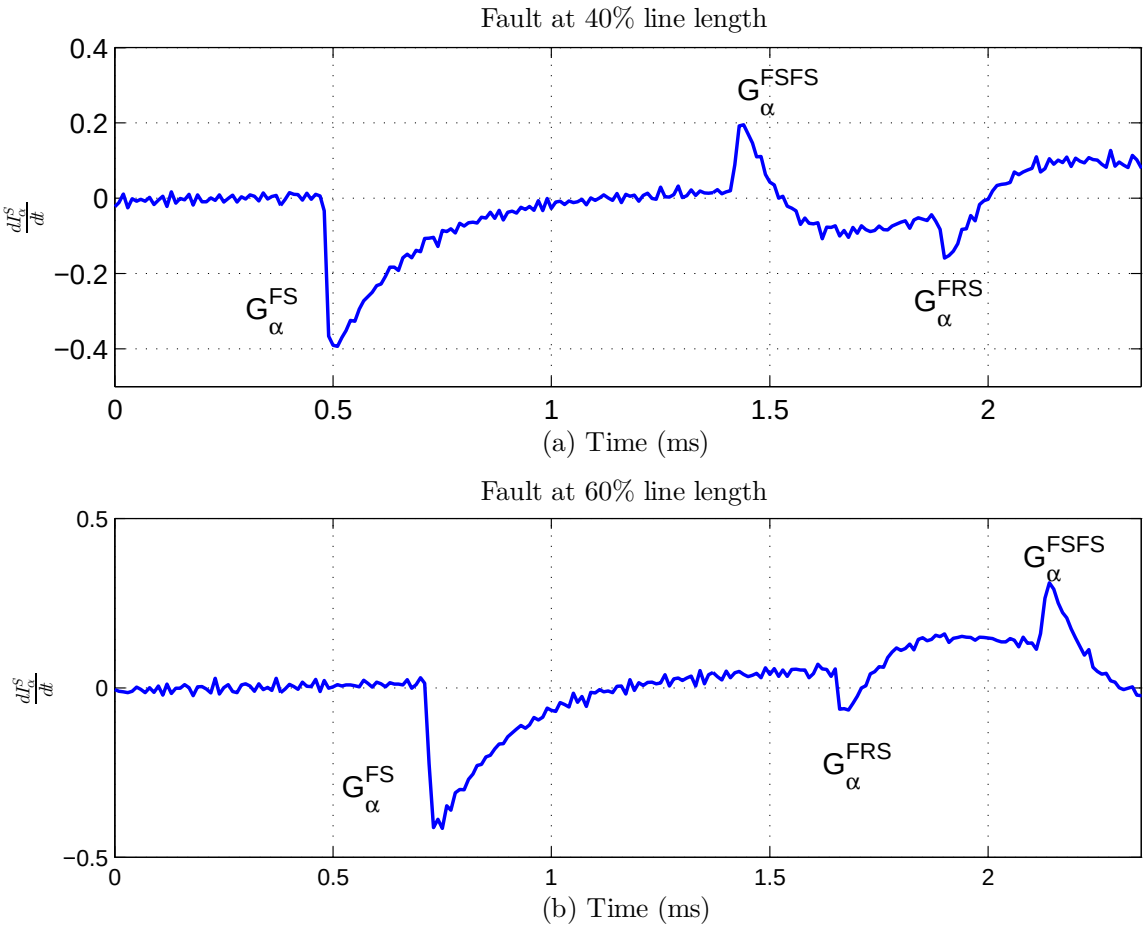

Figure 7.10: The arrival of traveling waves G_α^{FS}, G_α^{FSFS}, G_α^{FRS} at Bus S of Configuration A of the SCCTL for a 50Ω three phase fault located at: (a) 40% line length, (b) 60% line length as measured from Bus S.

with opposite polarity to that of the first traveling wave. For example, if the second traveling wave to arrive at Bus S has polarity opposite to the first one then the second traveling wave has to be G_k^{FSFS} while if it arrives with the same polarity as the first one then the second wave has to be G_k^{FRS}. The polarity of the traveling wave as defined by the [28] is the sign of the incremental change caused by the arrival of a traveling wave in the measured signal. If the incremental change is positive then the traveling wave has positive polarity and vice versa. The method proposed in this chapter to identify the traveling wave arriving at each terminal uses the derivative of the k^{th}-mode current signal at the local terminal. The derivative of the current signal would become positive for positive incremental changes and negative for negative incremental changes in the current. Therefore, the derivative of the current could be used for identifying the polarity of the traveling waves arriving at the both terminals of the SCCTL in Configuration A of the SCCTL.

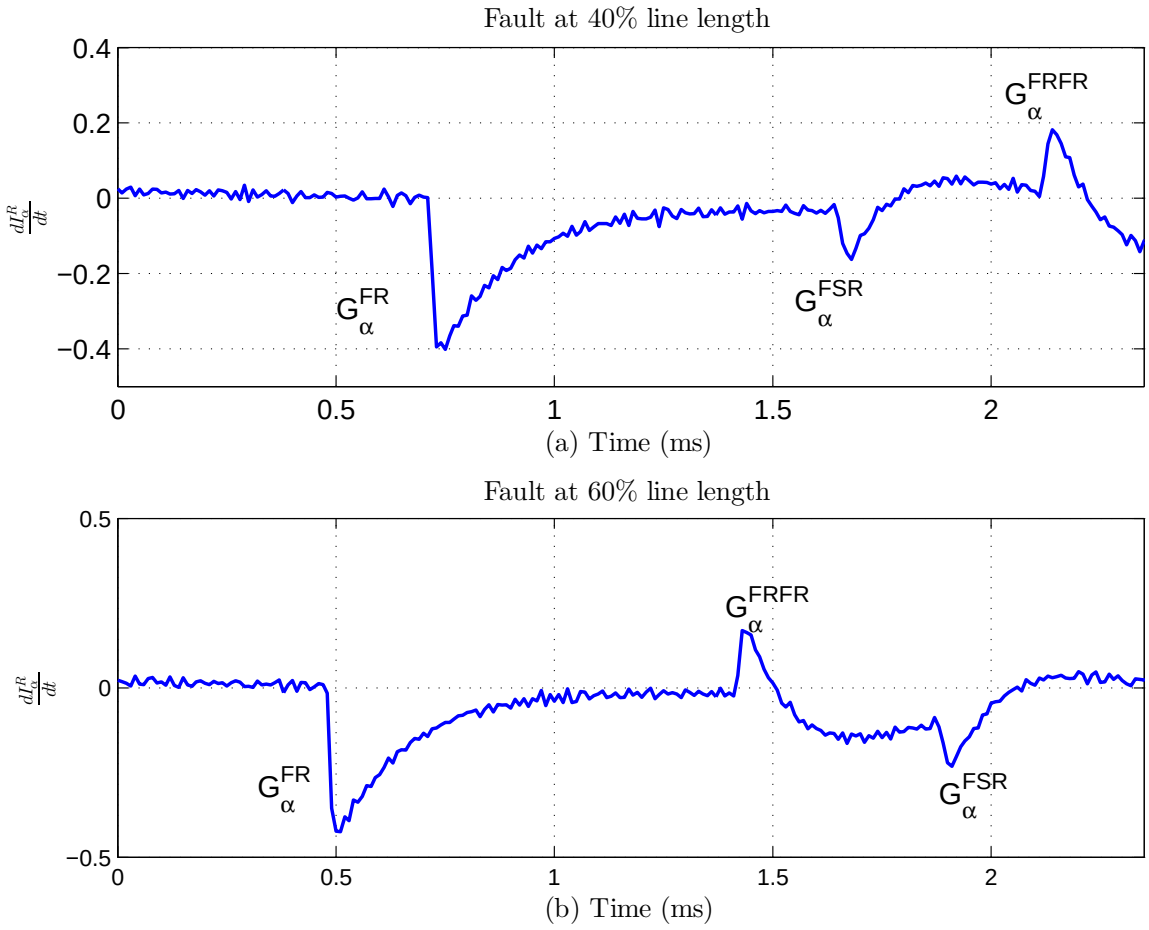

Figure 7.11: The arrival of traveling waves G_α^{FR}, G_α^{FRFR}, G_α^{FSR} at Bus R of Configuration A of the SCCTL for a 50Ω three phase fault located at: (a) 40% line length, (b) 60% line length as measured from Bus S.

The first three α-mode traveling waves to arrive at Bus S in Configuration A of SCCTL for a 50Ω three phase fault located at 40% and 60% line length as measured from Bus S are shown in Figure 7.10 (a) and (b), respectively. The first wave to arrive at Bus S in both cases is G_{α}^{FS} with derivative of α-mode Bus S current identifying its polarity as negative. The second traveling wave to arrive at Bus for a fault at 40% line length will be G_{α}^{FSFS} which could be identified from its opposite polarity as compared to that of G_{α}^{FS}. The third wave to arrive at Bus for the same fault scenario will be G_{α}^{FRS} but with same polarity as G_{α}^{FS}. It is seen from Figure 7.10 (a) that the derivative of α-mode Bus S current picks the polarity of G_{α}^{FSFS} as positive while the polarity of G_{α}^{FRS} is negative. For a fault located at 60% line length as measured from Bus S the second traveling wave to arrive at Bus S will be G_{α}^{FRS} while third one will be G_{α}^{FSFS}. It is seen from 7.10 that polarities of G_{α}^{FRS} and G_{α}^{FSFS} are identified as negative and positive by the derivative of α-mode Bus S current.

Figure 7.11 (a) and (b) show the first three α-mode traveling wave detected at Bus R through derivative of α-mode current at Bus R following a three phase fault located at 40% and 60% line length as measured from Bus S, respectively. The first traveling wave to arrive at Bus R in both cases is G_{α}^{FR} with polarity identified as negative. For the case of fault at 40% line length the second and third traveling waves to arrive at Bus R will be G_{α}^{FSR} with negative polarity and G_{α}^{FRFR} with positive polarity, respectively. For the fault located at 60%, the second, and third traveling waves arriving at Bus R will be G_{α}^{FRFR} with positive polarity, and G_{α}^{FSR} with negative polarity, respectively. It could be witnessed from Figure 7.11 (a) and (b) that the derivative of α-mode current at Bus R is able to correctly find the polarities of the traveling waves G_{α}^{FSR} and G_{α}^{FRFR} for both fault scenarios in Configuration A of the SCCTL. Thus, it could be concluded that in Configuration A of SCCTL the derivative of the current measured at a terminal could be used for identifying the second traveling wave to arrive at that terminal of the SCCTL. Consequently, the accurate fault location result could be obtained by using single ended algorithms.

7.5.3 Configuration B

In Configuration B of the SCCTL, a group of transmission lines is located at each terminal of the SCCTL as shown in Figure 7.5 (b). As detailed in Section 7.3, the traveling wave reflected from remote terminal would arrive at local terminal with opposite polarity relative to the first traveling wave while that reflected from the fault point will have same polarity as the first wave. As explained earlier the polarity of the relative polarities of the traveling waves could be obtained by observing the derivative of the k^{th}-mode current signal measured at local terminal. When the wave reflected from remote terminal would arrive at local terminal the

derivative of the k^{th}-mode current signal would attain the sign opposite to the sign it attained when the first traveling wave arrived at the local terminal. While in the case of the traveling wave being reflected from fault point the derivative of k^{th}-mode current signal will attain same sign as when the first traveling wave arrived at that terminal. Thus, the method presented in this chapter could be applied to the Configuration B of the SCCTL.

Figure 7.12 shows the first three traveling waves after the occurrence of fault arriving at Bus S of Configuration B of the SCCTL, detected through derivative of the α-mode current at Bus S. The fault is a three phase fault lying at 40% (Figure 7.12 (a)) and 60% (Figure 7.12 (b)) line length away from Bus S. The first traveling wave to arrive at Bus S in both fault scenarios is G_{α}^{FS} and its polarity is detected as negative by the derivative of α-mode current at Bus S. For the fault lying at 40% line length measured from Bus S, the second, and third traveling waves to arrive at Bus S will be G_{α}^{FSFS}, and G_{α}^{FRS}, respectively, while for the fault located at 60% line length measured from Bus S, the second, and third traveling waves to arrive at Bus S would be G_{α}^{FRS}, and G_{α}^{FSFS}, respectively. It has been explained in Section 7.3 that in Configuration B of the SCCTL the traveling wave arriving at local terminal after getting reflected from remote terminal of the transmission line will have opposite polarity to that of the first traveling wave while the traveling wave arriving at local end after getting reflected from fault point will have same polarity as the first traveling wave. Now, for the algorithm proposed in this chapter to be applicable to Configuration B of the SCCTL the derivative of α-mode current at Bus S should yield the polarity of G_{α}^{FSFS} as negative, while, for G_{α}^{FRS} the polarity should be yielded as positive. It could be witnessed from Figure 7.12 that the proposed method has been able to correctly identify the polarity of the traveling waves arriving at Bus S for both fault scenarios, thus, making the proposed method applicable to Bus S of Configuration B of the SCCTL.

Similarly, at Bus R the first traveling wave to arrive for faults lying at 40% and 60% line length away from Bus S is G_{α}^{FR} and its polarity is negative as could be seen from Figure 7.13 (a) and (b). Now for the fault lying at 40% line length away from Bus S the second and third traveling waves to arrive at Bus R will be G_{α}^{FSR} and G_{α}^{FRFR}, respectively, while for the fault lying at 60% line length as measured from Bus S the first and second traveling waves arriving at Bus R would be G_{α}^{FRFR} and G_{α}^{FSR}. For the algorithm proposed in this chapter to be applicable to Bus R of the Configuration B of the SCCTL, the derivative of α-mode current at Bus R should yield the polarity of G_{α}^{FRFR} as negative while for G_{α}^{FSR} its polarity should be yielded as positive. It could be seen from Figure 7.13 (a) and (b) that for both fault scenarios the derivative of α-mode current at Bus R is able to correctly identify the the polarities of the respective traveling waves, thus, implying the applicability of the proposed method of this chapter to the Bus R of the Configuration B of the SCCTL.

From the analysis and discussion carried out in this section it could be concluded that by

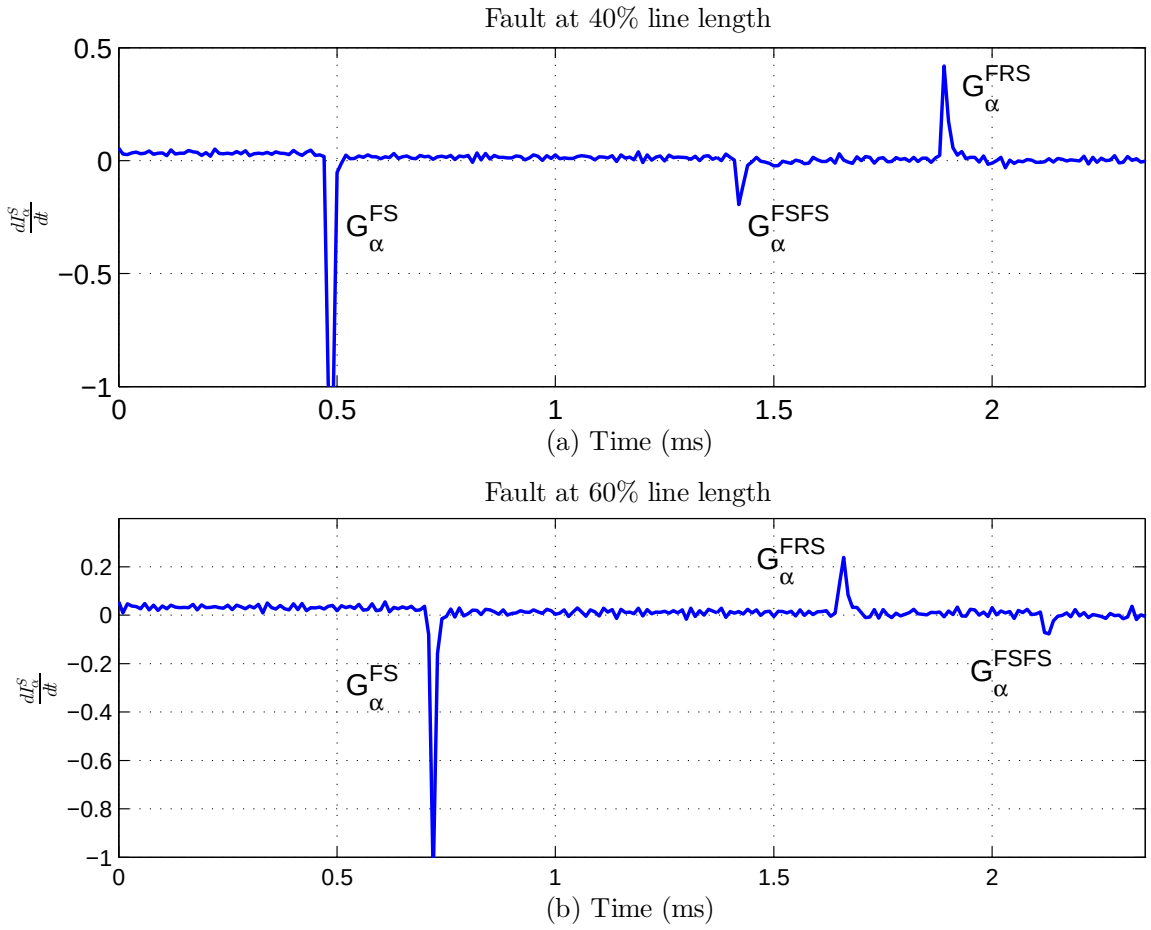

Figure 7.12: The arrival of traveling waves G_α^{FS}, G_α^{FSFS}, G_α^{FRS} at Bus S of Configuration B of the SCCTL for a 50Ω three phase fault located at: (a) 40% line length, (b) 60% line length as measured from Bus S.

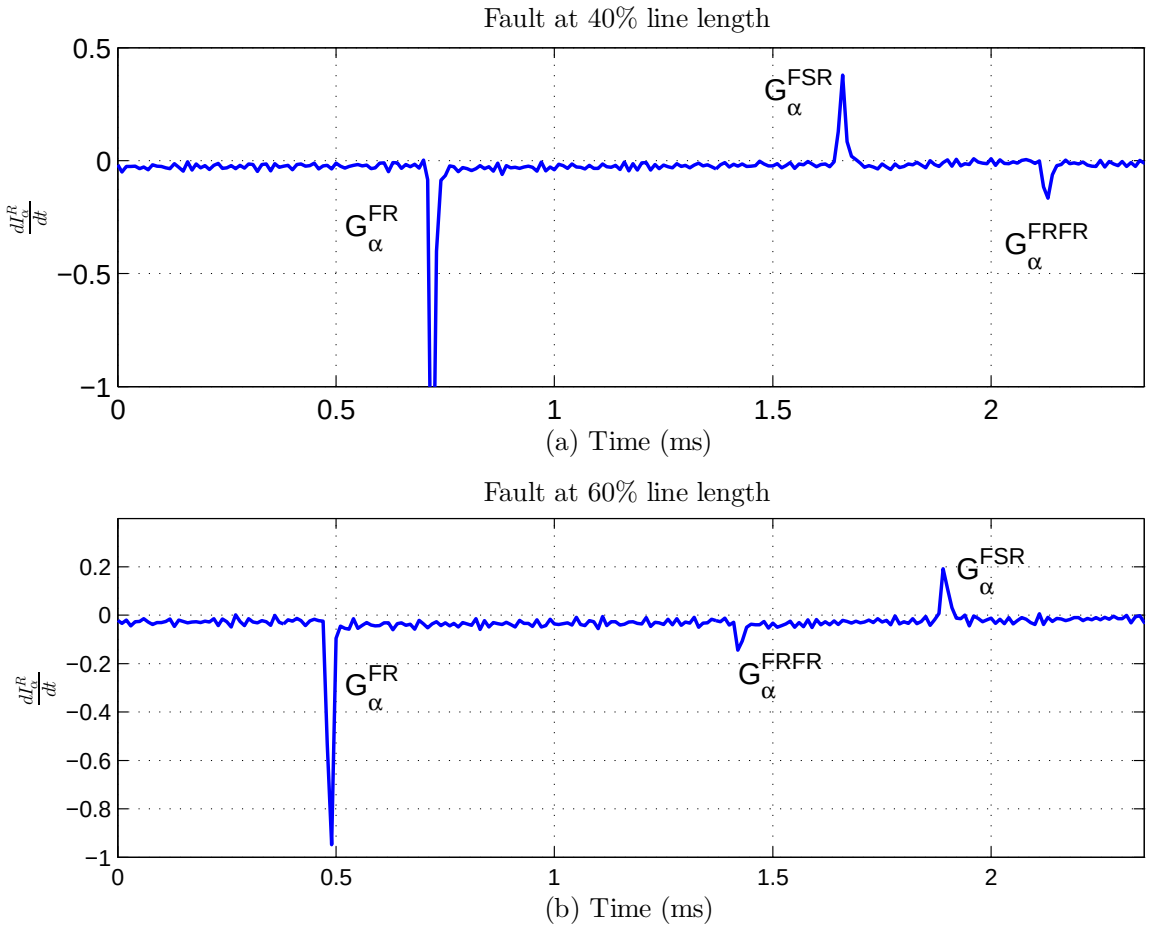

Figure 7.13: The arrival of traveling waves G_α^{FR}, G_α^{FRFR}, G_α^{FSR} at Bus R of Configuration B of the SCCTL for a 50Ω three phase fault located at: (a) 40% line length, (b) 60% line length as measured from Bus S.

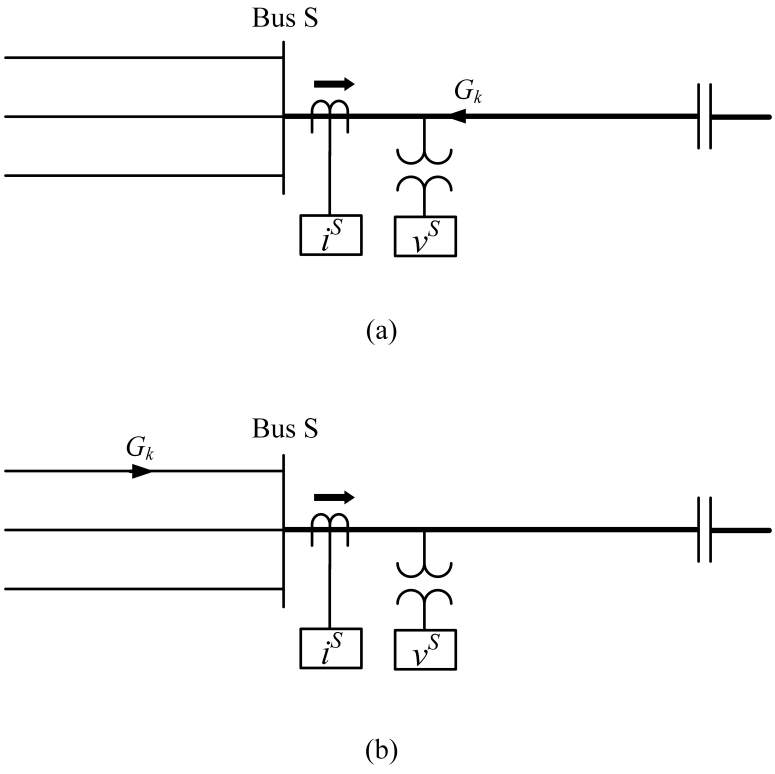

Figure 7.14: Traveling wave arriving at Bus S after traveling through (a) SCCTL, (b) a transmission line connected at Bus S.

observing the derivative of α, β, or γ-mode of the current measured at any one terminal of any configuration of SCCTL, the second traveling wave to arrive at that terminal could be identified. Consequently, the single-ended traveling wave based fault location algorithm could be applied.

Another challenge that single-ended traveling wave-based fault location algorithm will have to overcome is the blocking the traveling waves reflected from the remote terminals of the transmission lines connected at the terminals of the SCCTL in Configurations B and C. This could be achieved by comparing the polarities of the same traveling wave obtained from k^{th} mode current and voltage at that terminal. Any traveling wave reaching the terminal of the SCCTL after traveling through SCCTL will produce mutually opposite polarities in the current and voltage waveforms. This phenomenon has been explained below.

Consider a set of CT and CVT located at a terminal Bus S of the SCCTL as shown in Figure 7.14 (a) and (b). In Figure 7.14 (a), the traveling wave G_k is traveling in the SCCTL towards Bus S from the SCB. The arrival of traveling wave G_k at Bus S will produce following

incremental changes in the current and voltage measurements at Bus S:

$$\Delta i_k = -\frac{G_k}{Z_{ck}}$$
$$\Delta v_k = G_k \tag{7.83}$$

The negative sign in current equation is due to the fact that the direction of CT is opposite to the direction of the traveling wave G_k.

While if the wave G_k is traveling towards Bus S in one of the transmission lines connected at Bus S, as shown in Figure 7.14 (b), it will result in the following incremental changes in the current and voltage measurements at Bus S:

$$\Delta i_k = \frac{G_k}{Z_{ck}}$$
$$\Delta v_k = G_k \tag{7.84}$$

It can be seen from the set of equations (7.83) that incremental changes in current and voltage measurements will be of mutually opposite polarities when the traveling wave arriving at Bus S has traveled through SCCTL. On the other hand, the incremental changes produced in current and voltage measurements will be of the same polarity when the traveling wave arriving at Bus S has traveled in the other transmission lines connected at Bus S as shown in set of equations (7.84). Thus, the traveling wave which produces same polarity changes in voltage and current measurement at the terminal of the SCCTL should be blocked from being used for the purpose of the fault location.

As an example, consider a scenario in Configuration B of the SCCTL where the length of the shortest transmission lines connected at Bus S is equal to 0.3 times of the SCCTL, and the fault in the SCCTL lies at 40% line length as measured from Bus S. In this case the first traveling wave to arrive at Bus S will be G_α^{FS}, the second traveling wave to arrive at Bus S will be the one reflected from the remote end of the shortest transmission line connected at Bus S (G_α^X), while the third wave arriving at Bus S will be G_α^{FSFS}. Figure 7.15 shows the detection of the first three traveling waves from the derivative of voltage and current waveforms for the above mentioned fault scenario. It could be seen from Figure 7.15 that for the traveling wave which traveled through the transmission line connected at Bus S, i.e., G_α^X the polarities of the wave determined from current, and voltage measurements will be of similar sign. On the other hand, the polarities of the traveling waves which traveled only through SCCTL before being detected at Bus S, i.e, G_α^{FS}, and G_α^{FSFS} as determined from current and voltage will be of

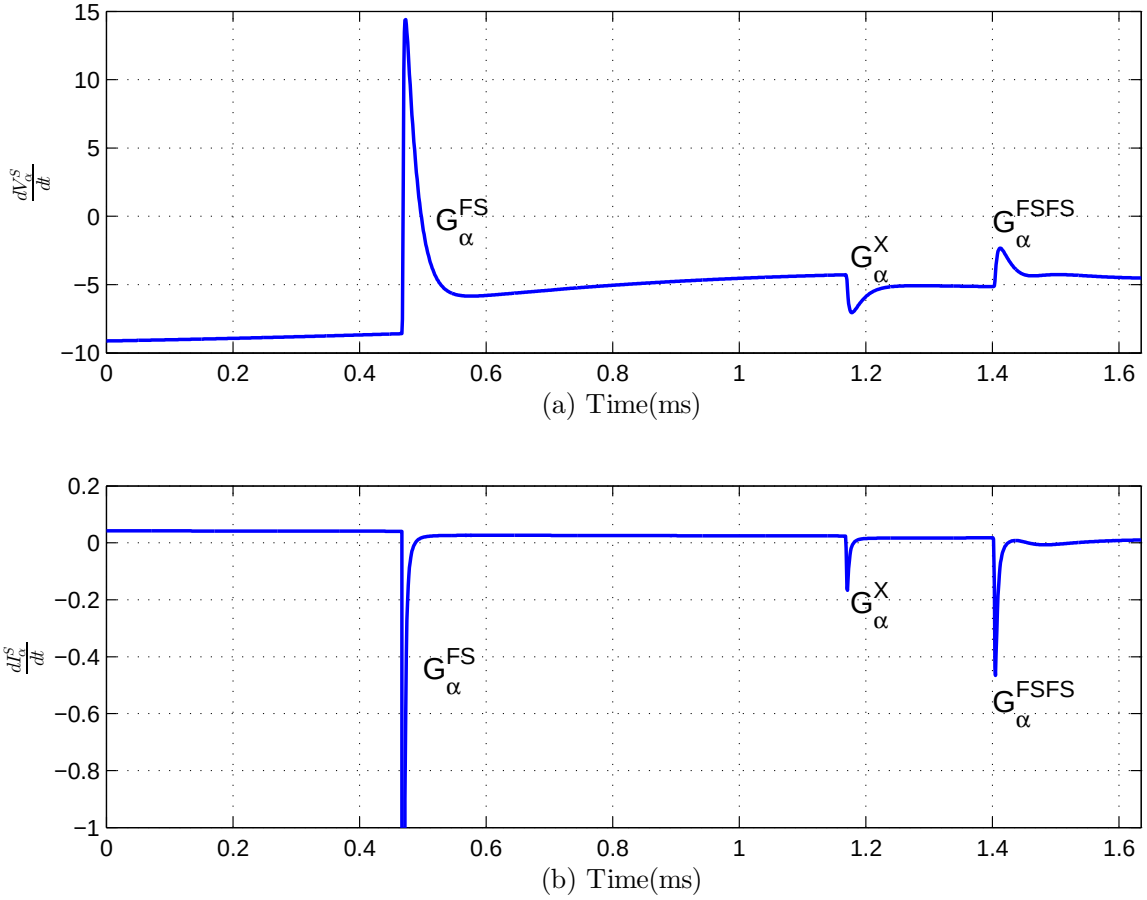

Figure 7.15: Traveling waves arriving at Bus S after traveling through SCCTL, and a transmission line connected at Bus S as observed through (a) voltage waveform (b) current waveform.

mutual opposite polarity. Thus, the traveling waves arriving at the terminal of the SCCTL after traveling through any of the transmission lines connected at that terminal of the SCCTL could be rejected by comparing the polarities of that wave determined from the current and voltage waveform.

7.6 Conclusion

In this chapter the expressions governing reflection and transmission of the traveling waves from various points of discontinuity in SCCTL have been derived. The limitations of the existing single-ended fault location algorithms which prevent their application to all the configurations of the SCCTL have been identified. A new single-ended traveling wave-based fault location algorithm which is applicable to all the configurations of the SCCTL has been presented through the analysis of derived expressions for reflection and transmission of the traveling waves for each type of discontinuity in the SCCTL. The proposed algorithm has been verified through simulations carried out in PSCAD for various configurations of the SCCTL.

Chapter 8

Summary, Conclusions, and Future Work

The impedance-based fault location algorithms for transmission lines are usually implemented as a feature of the numerical protective relays located at the terminals of the transmission line. The fault location algorithms used for conventional transmission lines are highly accurate, robust and a mature subject matter. However, the fault location in SCCTLs is relatively challenging due to the action of MOV during the fault time interval. In order to overcome the hurdles posed by the presence of MOV, the existing fault location algorithms for SCCTLs either use MOV model, or utilize the natural fault loop under the assumption that the arguments of current and voltage phasors will be identical to each other at the fault point. However, the former approach is unable to account for the varying ambient temperature, aging of MOV, different manufacturers, while, the latter is prone to losing accuracy under specific conditions. Therefore, this thesis focused on providing new impedance-based fault location algorithms which neither use MOV model nor based on the argument comparison of the fault current and voltage.

The traveling wave-based fault location algorithms for SCCTLs were not implemented in the real systems until recently, as they require higher sampling rates in the range of 1 MHz to bring the fault location error within acceptable limits. However, with the introduction of the relay SEL-T400L released by Schweitzer Engineering Laboratories in 2015 with sampling frequency of 1 MHz, the interest in traveling wave-based fault location algorithms have been rejuvenated. The single-ended traveling wave-based fault location algorithms have been proposed in the existing literature, however, they remain inapplicable to one of the most common topology of a transmission line in which an inductive source is present at one of its terminal while other transmission lines are connected at the other. Therefore, a new single-ended traveling wave-based fault location algorithm has been developed in this thesis which is applicable to all the topologies of the SCCTL.

8.1 Summary

The basic concept of series compensation of the transmission lines, the protection system of the SCBs, the process of fault location in transmission lines, the complexities and the challenges involved in the fault location in SCCTLs, and the broad classifications of the fault location algorithms were presented in Chapter 1. The opportunities for research were also identified in Chapter 1. The existing impedance-based fault location algorithms for SCCTLs were presented in Chapter 2, and the equivalence of all the existing impedance-based algorithms based on natural fault loops was shown through mathematical analysis of each algorithm. Thereafter, the conditions under which fault loop-based impedance-based fault location algorithms would lose accuracy were identified and simulated in Chapter 2.

A new impedance-based fault location algorithm was proposed in Chapter 3 for single-phase to ground, and double phase to ground faults in an SCCTL. The proposed algorithm was derived through detailed mathematical analysis, and verified through simulations carried out in PSCAD. The proposed algorithm of Chapter 3 was tested on number of metrics such as the effect of error in CT\CVT measurements, transmission line parameters, and the level of fault resistance on the performance of the proposed algorithm. In Chapter 4, the proposed algorithm of Chapter 3 was applied to the SCCTLs with multiple SCBs located at more than one location. The proposed algorithm was presented for a general case of SCBs located at N number of locations using the lumped model of the transmission line. Thereafter, a case of SCBs located at two locations was derived using more accurate model of the the transmission line, i.e., distributed model of the transmission line. The algorithm of Chapter 4 was tested for different fault locations, fault resistance, CT\CVT errors, and error in transmission line parameters using simulations in PSCAD and Matlab.

In Chapter 5, two new impedance-based fault location algorithms were proposed that utilize the MOV current phasor from the CT located in SCB. The CT is needed in MOV branch of the SCB to monitor the heat accumulated in the MOV during the faulted time period. The proposed algorithms use this current measurement, in addition to the measurements made at the terminals of the transmission line. The first proposed algorithm uses complete phasor (magnitude and angle) of the MOV current while the second proposed algorithm uses only magnitude part of the MOV current phasor. Both proposed algorithms were tested on wide range of fault scenarios simulated in PSCAD. The effect of various sources of error such as CT\CVT errors, error in transmission line parameters on the performance of both algorithms was also investigated in Chapter 5. The fault location results obtained from both proposed algorithms were compared in Chapter 5 to those obtained from the algorithm proposed in Chapter3, and the existing fault loop-based impedance-based fault location algorithm found in literature.

In Chapter 6, the phenomenon of traveling wave in an electrical transmission line was explained from which the modeling of a transmission line was derived. The principle of traveling wave-based fault location algorithms was also presented in this chapter. The detection mechanism for detecting the arrival of a traveling wave at transmission line terminal that has been used by existing traveling wave-based fault location algorithms, i.e., DWT was explained in this chapter. Thereafter, the existing traveling wave-based fault location algorithms were discussed, and their limitations were identified in Chapter 6 as well. In Chapter 7, the mathematical expressions for the traveling waves reflected and emitted from various points of discontinuity in an SCCTL such as line terminal, fault point, SCB were derived. Thereafter, a new traveling wave-based fault location algorithm employing the derived mathematical equations was proposed in Chapter 7 which overcomes the limitations of the existing traveling wave-based algorithms. The applicability of the proposed algorithm to various configurations of the SCCTL was also shown in Chapter 7.

8.2 Conclusions

The research undertaken in this thesis was focused on two areas: 1-impedance-based fault location algorithms for SCCTLs; 2-traveling wave-based fault location algorithms for SCCTLs. Thus, conclusions for each area of research is given separately.

8.2.1 Impedance-based fault location algorithms for SCCTLs

Based on the research carried out in this thesis, following conclusions could be drawn regarding the impedance-based fault location algorithms for SCCTLs:

1. It was shown in this thesis that all the fault loop-based impedance-based fault location algorithms for SCCTLs inherently involve the angle comparison of the fault voltage, and fault current phasors, and are equivalent to each other. Moreover, it was observed that all the existing studies of the fault location in SCCTL had studied that configuration of SCCTL in which SCB is located in the middle of the transmission line. However, if the SCB is located close to one of the terminals of the SCCTL, more challenging scenarios for fault location algorithms are encountered which have never been studied before. The existing fault loop-based fault location algorithms were tested on two configurations of the SCCTL simulated in PSCAD, with SCB located at one of the terminals in first case, and SCB located in the middle of the transmission line in the second case. It was observed that when the SCB was located close to one of the terminals of the SCCTL,

the fault loop-based fault location algorithms became highly erroneous for specific fault conditions.

2. Three new fault location algorithms for SCCTLs have been proposed in this thesis, and all the proposed algorithms do not require MOV model or the consideration of fault loops.

3. The first proposed algorithm is used for locating the single-phase to ground, and double phase to ground faults in an SCCTL. The proposed algorithm is based on the fact that in non-faulted phase only series capacitor is responsible for the conduction of the current, and it utilizes only the available measurements. Both subroutines of the proposed algorithm yield almost identical fault location result, and does not require special subroutines to find the faulted section of the SCCTL. The PSCAD simulations covering different fault types, fault locations, fault resistances, and different locations of SCB have shown that the proposed algorithm is able to maintain the desired level of accuracy.

4. It has also been demonstrated that the first proposed algorithm could be applied to that configuration of the SCCTL in which the series compensation is applied at more than one location. Firstly, the lumped model of the transmission line is utilized to depict the applicability of the proposed algorithm to N number of series capacitors. Thereafter, the distributed model of transmission line is used to describe the proposed algorithm with two series capacitors present in the SCCTL. The proposed algorithm is the first and the only impedance-based fault location algorithm that is applicable to SCCTLs with series compensation applied at multiple locations.

5. The second, and third impedance-based fault location algorithms, i.e., Algorithm CP, and Algorithm MP, proposed in this thesis utilize the current measurement from the MOV branch of the SCB. Algorithm CP uses the complete phasor of MOV current (magnitude as well as phase angle) for yielding fault location results. On the other hand, Algorithm MP utilizes only magnitude of the MOV current phasor for calculating the fault location. The presence of SCB in an SCCTL splits the transmission line into two parts. Both proposed algorithms will yield two fault location results assuming that the fault could in any of the two sections of the transmission lines. Thereafter, a subroutine is presented to identify the faulted section of the SCCTL, and its corresponding fault location result is treated as the correct result. Both algorithms utilize only positive sequence measurements and parameters of the transmission line, thus, making them immune to the error in zero-sequence parameters of the transmission line. The performance of Algorithm CP, and Algorithm MP has been tested rigorously through simulations carried out in PSCAD

covering all the fault types, different fault locations, fault resistances, errors in CT\CVT measurements, and zero-sequence parameters of the transmission line.

8.2.2 Traveling wave-based fault location algorithms

The following conclusions could be arrived at regarding the research carried out in the area of traveling wave-based fault location algorithms:

1. The traveling wave theory as it applies to transmission lines, along with the modeling of the transmission line with respect to the traveling wave theory has been presented in this thesis. The principle underlying the traveling wave-based fault location algorithms and signal processing technique to detect the arrival of a traveling wave at the terminal of a transmission, i.e., DWT have been presented in thesis. The research focused solely on single-ended traveling wave-based fault location algorithms as they do not require the time synchronization of the relays present at each terminal of the SCCTL.It has been observed from the literature review that the existing single-ended traveling wave-based fault location algorithms locate the fault by noting two things: 1-the time gap between the arrival of the first two traveling waves at a line terminal, 2-the point of reflection from where the second wave got reflected. It is observed that most of the algorithms have been proposed using the simplest of the topology of the SCCTL where an inductive source is present at each terminal of the SCCTL. Only one of the algorithms have studied different topologies of the SCCTL and concluded that if an inductive source is present at one terminal and group of other transmission lines is present at the other then the point of reflection of the second traveling wave cannot be determined. Thus, the single-ended traveling wave-based fault location algorithms cannot be applied to such configuration of SCCTL, necessitating the use of double-ended traveling wave-based fault location algorithms.

2. The mathematical expressions describing the reflected and transmitted traveling waves from different points of discontinuity such as fault point, line terminals, SCB has been derived. The limitations of the single-ended traveling wave-based fault location algorithms have been understood in lieu of the derived expressions. Consequently, a new single-ended traveling wave-based fault location algorithm is proposed based on the derivative of α or β modes of the current measured at the transmission line terminals. Since the expressions of reflected wave from all the types of reflection points are known, the reflection point of the second traveling wave arriving at the terminal could be determined by observing the shape of the derivative waveform. The proposed algorithm is appli-

cable to all the topologies of the SCCTL. the proposed algorithm has been tested with simulations carried out on PSCAD covering different fault types and fault locations.

The main contributions of this thesis could be summarized as follow:

1. Identified the fault scenarios where existing impedance-based fault location algorithms would become highly erroneous.
2. Proposed three impedance-based fault location algorithms:
   (a) The first algorithm Algorithm PM is proposed for single-phase to ground, and double-phase to ground faults, and uses only measurements from the transmission line terminals.
   (b) The second algorithm Algorithm CP uses phasor of the MOV current measured at SCB bus, in addition to the transmission line terminal measurements.
   (c) The third algorithm Algorithm MP uses only phasor magnitude of the MOV current measured at SCB bus, in addition to the transmission line terminal measurements.
3. Modified the proposed algorithm, i.e., Algorithm PM to obtain first and the only impedance-based fault location algorithm able to locate faults in the SCCTLs where series compensation is applied at multiple locations.
4. Derived the mathematical expressions describing the traveling waves reflected and transmitted from the various points in the SCCTL.
5. Proposed a new single-ended traveling wave-based fault location algorithm applicable to all topologies of the SCCTL.

8.3 Future Works

The following avenues have been identified for the future work in the area of this research.

1. The Algorithm PM is applicable to single-phase to ground, and double-phase to ground faults only. Thus, a research could be conducted to propose a new impedance-based fault location algorithm which yields fault location results for phase to phase and three phase faults without using SCB bus measurements.
2. The Algorithm CP and Algorithm MP utilize MOV current measurement which is used to estimate the energy stored in MOV bank. A research could be conducted to estimate the MOV current if only the value of the amount of energy stored in MOV is available from the SCB bus and then use that towards the fault location.

3. A study investigating the effect of CT and CVT error on the performance of the proposed single-ended traveling wave-based fault location algorithm could be performed.

Bibliography

[1] R.M. Mathur, R.K. Varma, "Thyristor based FACTS controllers for electrical transmission system", Wiley IEEE Press, February 2002.

[2] R. Gruenbaum, J. Samuelsson, C.Li, "Series capacitors for increased power transmission capacity of a 500 kV grid intertie," *EPEC*, pp. 164-169, 2012.

[3] R. Gruenbaum, J.Samuelsson, "Series capacitors facilitate long distance AC power transmission," *Proc. 2005 IEEE PowerTech,* St. Petersurg, Russia.

[4] "Series Capacitors for increased power transmission capacity in the Finnish 400 kV grid," ABB AB, Vasteras, Sweden, Application Note A02-0222 E, Nov. 2010.

[5] L. Bolduc, "GIC observations and studies in the Hydro-Quebec power system," *J. Atmosph. Solar-Terrestrial Phys.*, vol. 64, pp. 17931802, 2002.

[6] S. H. Horowitz, A.G. Phadke, "Power System Relaying", Wiley Press, Fourth Edition, 2014.

[7] A.G. Phadke, "Handbook of electrical engineering calculations", Marcel Dekker, 1999.

[8] G. E. Lee, D. L. Goldsworthy, "BPA'S Pacific AC Intertie series capacitors: Experience, equipment & protection," *IEEE Transactions on Power Delivery*, vol. 11, No. 1, pp. 253-259, Jan. 1996.

[9] V.Cook, "Fundamental aspects of fault location algorithms used in distance protection," *Proc.IEE*, vol. 133, no. 6, Sept. 1986.

[10] M. S. Sachdev and R. Agarwal, "A technique for estimating line fault locations from digital distance relay measurements," *IEEE Trans. Power Del.*, vol. 3, no. 1, pp. 121-129, Jan. 1988.

[11] A. A. Girgis, D. G. Hart, and W. L. Peterson, "A new fault location technique for two-and three-terminal lines," *IIEEE Trans. Power Del.*, vol. 7, no. 1, pp. 98107, Jan. 1992.

[12] J. Izykowski, E. Rosolowski, P. Balcerek, M. Fulczyk and M. M. Saha, "Accurate non iterative fault location algoriyhm utilising two-end unsynchronized measurements," emphIEEE Trans. on Power Delivery, vol. 26, no. 2, pp. 547-555, Apr. 2011.

[13] Series Capacitor Bank Protection Tutorial, 1^{st} ed., IEEE Power System Relaying Committee WG K13, Piscataway, NJ, 1997, pp. 1-35.

[14] IEEE Guide for Protective Relay Application to Transmission-Line Series Capacitor Banks, IEEE Std C37.116-2007, 2007.

[15] IEEE standard for series capacitor banks in power systems, IEEE Std. 824, 2004.

[16] J. Sadeh, N. Hadjsaid, A.M. Ranjbar, R. Feuillet, "Accurate fault location algorithm for series compensated transmission lines," *IEEE Transactions on Power Delivery,* vol.15, no.3, pp.1027-1033, Jul 2000.

[17] M. Al-Dabbagh, S. K. Kapuduwage, "Using instantaneous values for estimating fault locations on series compensated transmission lines," *Elect. Power Syst. Research*, vol. 76, pp. 2532, Sep. 2005.

[18] J. Sadeh , A. Adinehzadeh, "Accurate fault location algorithm for transmission line in the presence of series connected FACTS devices," *Int. J. Elect. Power Energy Syst.*, vol. 32, no. 4, pp. 323328, May 2010.

[19] M.G. Ahsaee, J. Sadeh, "A novel fault-location algorithm for long transmission lines compensated by series FACTS devices," *IEEE Trans. on Power Delivery*, vol. 26, no. 4, pp. 2299- 2308, Oct. 2011.

[20] M.M. Saha, J. Izykowski, E. Rosolowski, B. Kasztenny, "A new accurate fault locating algorithm for series-compensated lines," *IEEE Trans. on Power Delivery*, vol. 14, no. 3, pp. 789-797, Jul. 1999.

[21] M.M. Saha, K. Wikstrom, J. Izykowski, E. Rosolowski, "Fault location in uncompensated and series-compensated parallel lines," in *Proc. IEEE Power Eng. Soc. Winter Meeting*, Singapore, Jan. 2000, pp. 23-27.

[22] J. Izykowski, E. Rosolowski, P. Balcerek, M. Fulczyk, M.M. Saha, "Fault location on double-circuit series-compensated lines using two-end unsynchronized measurements," *IEEE Trans. on Power Delivery*, vol. 26, no. 4, pp. 2072-2080, Oct. 2011.

[23] C.S. Yu , C.W. Liu , S.L. Yu , J.A. Jiang,"A new PMU-based fault location algorithm for series compensated lines," *IEEE Trans. on Power Delivery*, vol. 17, no. 1, pp. 33-46, Jan. 2002.

[24] N. Kang, J. Chen, Y. Liao, "A fault-location algorithm for series-compensated double-circuit transmission lines using the distributed parameter line model," *IEEE Trans. on Power Delivery*, Vol. 30, No. 1, pp. 360-367, Feb. 2015.

[25] Y. Zhang, J. Liang, Z. Yun, and X. Dong, "A new fault-location algorithm for series-compensated double-circuit transmission lines based on the distributed parameter model," *IEEE Trans. on Power Delivery*, DOI: 10.1109/TPWRD.2016.2626476.

[26] R. Rubeena, M.R. D. Zadeh, T. P.S. Bains, "An accurate offline phasor estimation for fault location in series compensated lines," *IEEE Trans. on Power Delivery*, vol. 29, no. 2, pp. 876-883, Apr. 2014.

[27] T. P. S. Bains, , "Fault location in series compensated transmission lines," M.E.Sc. dissertation, Dept. of ECE, Western University, London, ON, Aug 2014.

[28] Z. Huang, Y. Chen, Q. Gong, "A protection and fault location scheme for EHV line with series capacitor based on traveling waves and wavelet analysis," *Int. Conf. on Power System Tech.*, Kunming, China , Oct. 2002, pp. 290-294.

[29] P. A. Crossely and P. G. Mclaren, "Distance protection based on traveling waves",*IEEE Trans. on Power Apparatus and Systems* Vol. 102, No. 9, pp. 2971-2983, Sep. 1983.

[30] M. Abedini, A. Hasani, A. H. Hajbabaie, and V. Khaligh, "A New Traveling Wave Fault Location Algorithm in Series Compensated Transmission Line", *21st Iranian Conf. on Elect. Eng.*, Mashhad, May 2013, pp. 16.

[31] F. H. Magnago, and A. Abur, "Fault location using wavelets," *IEEE Trans. Power Delivery*, vol. 13, no. 4, pp. 14751480, Oct. 1998.

[32] T. Gonen, "Electrical Power Transmission System Engineering: Analysis and Design", CRC Press, Third Edition.

[33] Y. Deng, Z. He, R. Mai, S. Lin, L. Fu, "Fault location estimator for series compensated transmission line under power oscillation conditions," in *IET Generation, Transmission & Distribution*, Vol. 10, Iss. 13, pp. 3135-3141, 2016

[34] T. P. S. Bains, M. R. D. Zadeh, "Supplementary Impedance-based Fault Location Algorithm for Series Compensated Lines," *IEEE Trans. on Power Delivery*, vol. 31, no. 1, pp. 334-342, Sep. 2015.

[35] D. L. Goldsworthy, "A linearized model for MOV-protected series capacitors." *IEEE Trans. Power Syst.*, vol. PWRS-2, no. 4, pp. 953-958, Nov. 1987.

[36] P. Balcerek, M. Fulczyk, E. Rosolowski, J. Izykowski, M.M. Saha, "Method for fault location on series compensated power transmission lines with two-end unsynchronized measurement," U.S. Patent 8 731 853 B2, May 20, 2014.

[37] E. Sagen and K. Workman, "Methods of time synchronization," in 63rd *Annual Georgia Tech. Protective Relaying Conf.*, Atlanta, GA, Apr. 22-24 2009, pp. 1-7.

[38] A.T. Johns, S. Jamali, "Accurate fault location technique for power transmission lines," *Proc. Inst. Elect. Eng. C*, vol. 137, no. 6, pp. 395-402, Nov. 1990.

[39] T. P. S. Bains, M.R. D. Zadeh, "Challenges and recommendations for fault location in series compensated transmission lines," in *IEEE PES General Meeting*, National Harbor, MD, Jul. 2014, pp. 1-5.

[40] *MiCOM P40 Agile: Technical Manual (Single Breaker Multi-End Current Differential IED)*, 1st ed., GE Grid Solutions, Markham, ON, 2017, pp. 518.

[41] S. Gajare, A. K. Pradhan, V. Terzija, "A method for accurate parameter estimation of series compensated transmission lines using synchronized data," *IEEE Trans. on Power Delivery*, DOI: 10.1109/TPWRS.2017.2679542

[42] L. Debnath, F. A. Shah,"Wavelet transform and their applications, in Power System Analysis and Design, 2nd ed., Springer Science+Business Media New York 2002, 2015, ch. 1, sec. 1.2 to 1.3, pp. 3-6

[43] User's Guide: EMTDC Transient Analysis for PSCAD Power System Simulation, Version 4.7, Manitoba HVDC Research Centre, Winnipeg, MB, 2010, pp. 199-209.

[44] S. Mallat, W.L. Hwang "Singularity detection and processing with wavelets"*IEEE Trans. on Information Theory*, vol.-38, no. 2, pp. 617-643, March 1992.

Appendix A

Phasor estimation techniques: Discussion

The current transformer (CT) and capacitive voltage transformer (CVT) located at a terminal of the transmission line measure the current and voltage in the transmission line. The measured current and voltage signals are then passed onto the Intelligent Electronic Device (IED), which could be a relay located at that terminal of the transmission line as shown in Figure A.1. Thereafter, the measured signals are sampled and discretized by the IED. In order to obtain the phasor of fundamental component (60 Hz) from the discrete samples of the measured signals a phasor estimation algorithm is needed. Discrete Fourier Transform (DFT) and the Cosine algorithm are the most popular phasor estimation algorithms.

Full cycle DFT (FCDFT) as the name suggests is the version of DFT which uses one complete cycle of the fundamental frequency to yield the phasor of the fundamental frequency. Mathematically, FCDFT for a fundamental component sampled with N samples per cycle could be expressed as:

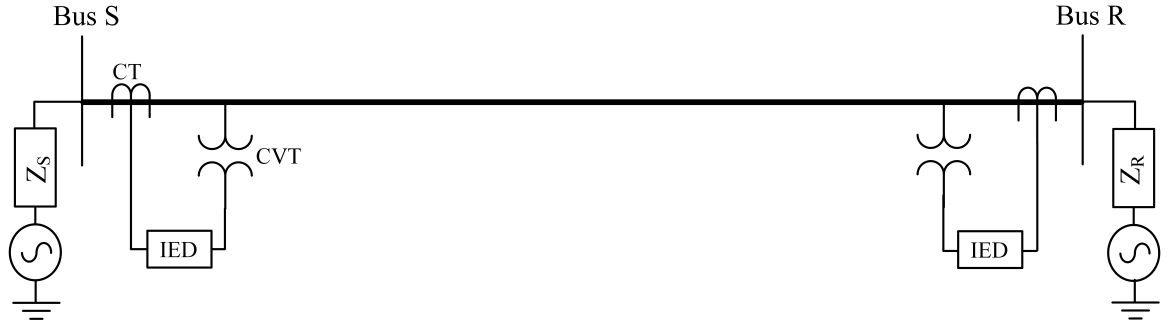

Figure A.1: Schematic showing CTs, CVTs and IEDs located at the terminals of a transmission line

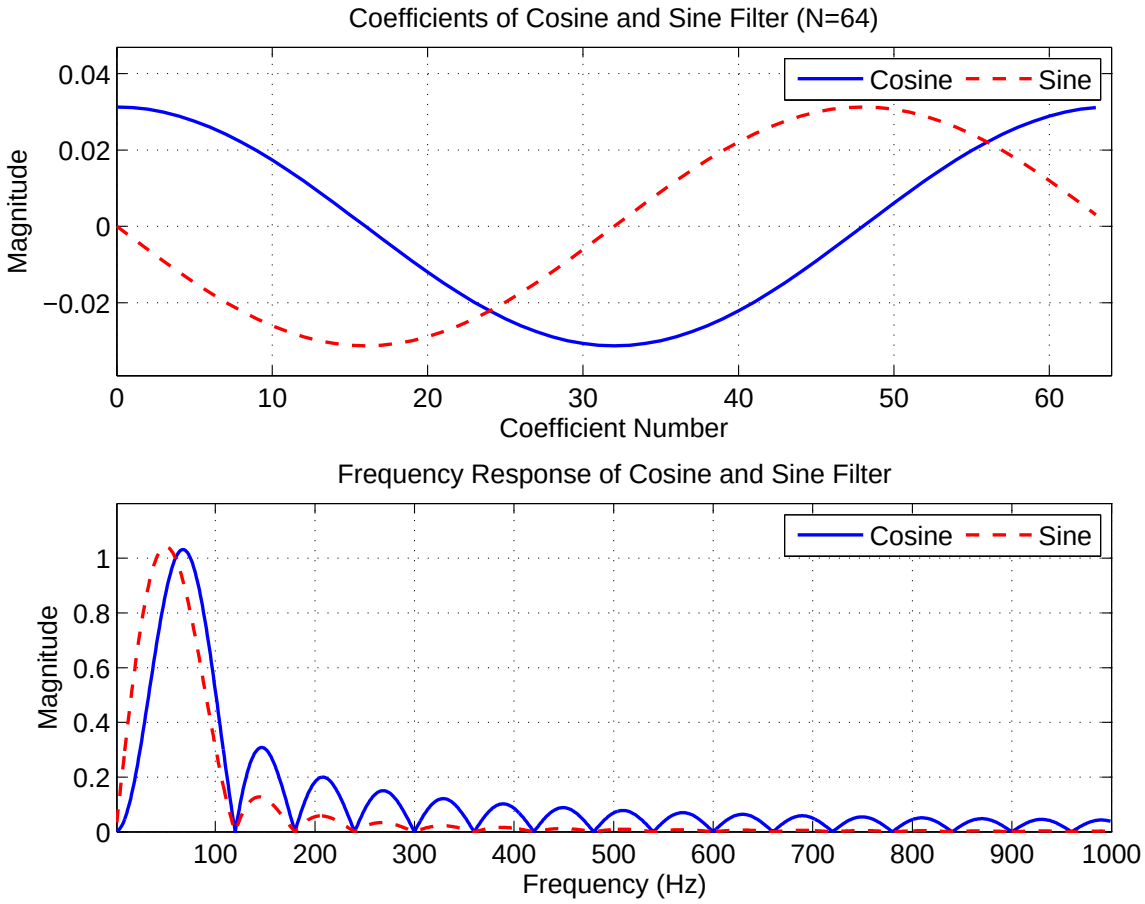

Figure A.2: Figure depicting: (a) the coefficients of Cosine and Sine filter for N=64, (b) frequency response of Cosine and Sine filter.

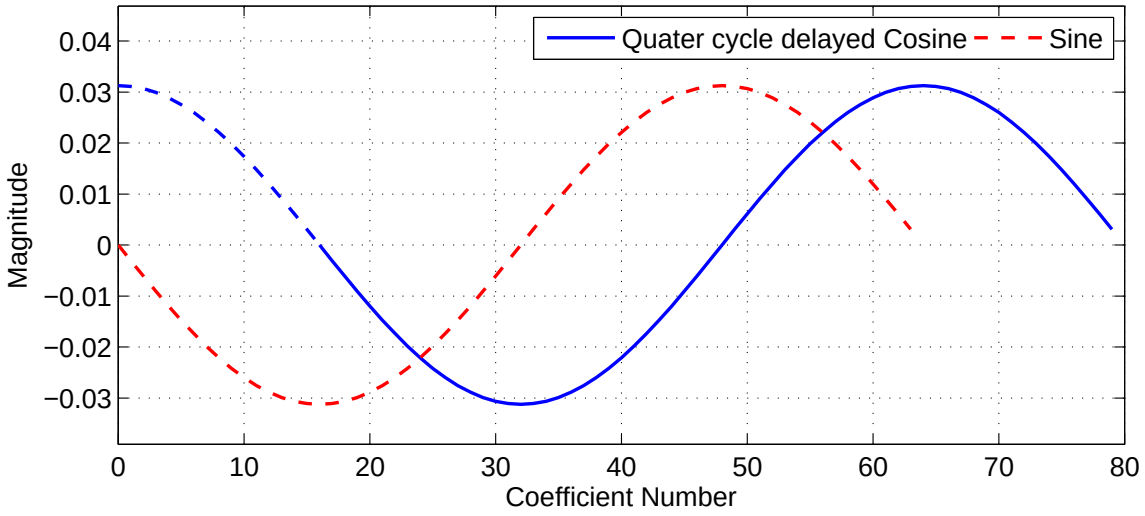

Figure A.3: Figure depicting the equivalence of Sine filter and quarter cycle delayed Cosine filter.

$$X[n] = \frac{2}{N}\sum_{k=0}^{N-1} x[n+k]e^{-j2\pi\frac{k}{N}} \tag{A.1}$$

where $j = \sqrt{-1}$; k =0, 1, 2, . . . , N-1; $x[n]$ and $X[n]$ represent n^{th} sample of the measured signal and its estimated phasor, respectively; $e^{-j2\pi\frac{k}{N}}$ is the k^{th} filter coefficient of the FCDFT. It can be seen that from (A.1) that the filter coefficient of FCDFT are complex. Therefore, the FCDFT can be split into two filters i.e., real and imaginary filters as shown in (A.2) and (A.3), respectively.

$$\Re\left(X[n]\right) = \frac{2}{N}\sum_{k=0}^{N-1} x[n+k]\cos\left(2\pi\frac{k}{N}\right) \tag{A.2}$$

$$\Im\left(X[n]\right) = -\frac{2}{N}\sum_{k=0}^{N-1} x[n+k]\sin\left(2\pi\frac{k}{N}\right) \tag{A.3}$$

Thus, the Cosine filter acts as the real filter while Sine filter acts as the imaginary filter in FCDFT. The magnitude and the phase angle of the phasor could be obtained of the phasor would be obtained using equations (A.4) and (A.5), respectively.

$$|X[n]| = \sqrt{\left(\Re\left(X[n]\right)\right)^2 + \left(\Im\left(X[n]\right)\right)^2} \tag{A.4}$$

$$\angle(X[n]) = \tan^{-1}\left(\frac{\Im\left(X[n]\right)}{\Re\left(X[n]\right)}\right) \tag{A.5}$$

The coefficients of the Cosine and Sine filters for FCDFT with 64 samples per cycle of the fundamental frequency, i.e., $N = 64$ have been plotted in the Figure A.2 (a). The frequency response of the Cosine and Sine filters of Figure A.2 (a) is given in Figure A.2 (b). From Figure A.2 (b) it could be seen that Cosine filter has better performance in the sub-synchronous region (<60 Hz), especially close to 0 Hz. On the other hand Sine filter has lower side lobes which means that Sine filter is better able to attenuate frequencies higher than 60 Hz. Another key point to be noted is that both Cosine and Sine filter completely remove the integer harmonics of the fundamental frequency. Thus, the presence of integer harmonics in the measured signal will not affect the accuracy of the estimated phasor by FCDFT.

Another one of the most popular phasor estimation technique is the Cosine algorithm. In Cosine algorithm both filters i.e., real and imaginary filters are realized using the Cosine filter only. The basis of the use of Cosine filter as imaginary filter comes from the fact that Sine filter is nothing but Cosine filter delayed by quarter cycle as shown in Figure A.3. Therefore, the output of Cosine filter could be buffered for a quarter cycle and then added orthogonally to the output of the Cosine filter, to obtain the phasor. The block diagrams showing the process

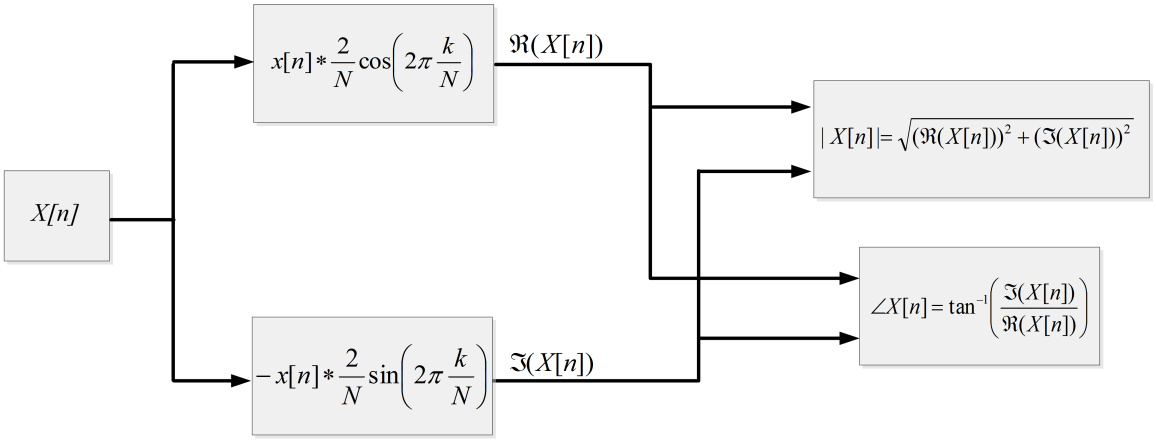

(a)

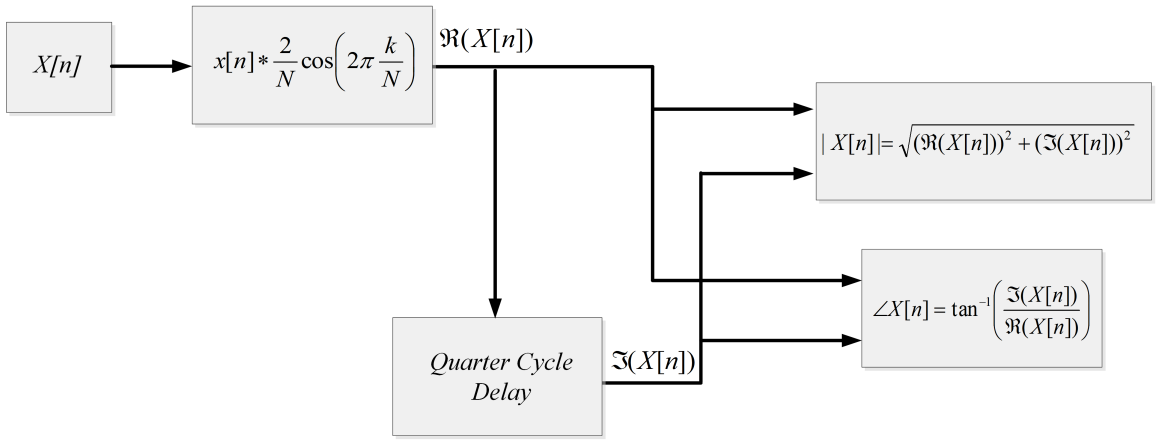

(b)

Figure A.4: Block diagrams representing (a) FCDFT, (b) Cosine algorithm.

of phasor estimation through FCDFT and Cosine algorithm are given in Figures A.4 (a) and (b), respectively. It could be observed from Figure A.4 (b) that the real and imaginary filters of Cosine algorithm are realized using Cosine filter only.

The benefit of the Cosine filter over FCDFT is that the Cosine filter would have better performance in sub-synchronous region but at the same time the Cosine algorithm would take one and a quarter cycle ($1\frac{1}{4}$ cycle) of the fundamental to yield the phasor while FCDFT would take one cycle to yield the phasor. As an example, Figure A.5 shows the estimated by FCDFT and Cosine algorithms for a signal $x = cos(\omega t + 30^o) + e^{-\frac{t}{0.25}}$ which consists of a decaying DC offset component (DDOC) superimposed on the fundamental frequency component. It could be seen Figure A.5 that the phasor estimated through the Cosine algorithm has considerably less oscillations as compared to that obtained through FCDFT. On the other hand the transient period of the FCDFT is one cycle of fundamental frequency, i.e., 16.6 ms while that of the Cosine algorithm is a quarter cycle longer i.e., 20.83 ms. However, it should be noted that the performance of FCDFT could be made almost equivalent to that of Cosine filter by using mimic filter along with FCDFT. Nonetheless, the usage of mimic filter with FCDFT would increase the time taken by FCDFT to yield the phasor. In this thesis, the Cosine algorithm is used as standard due to its superior performance in the sub-synchronous region.

Once the phasor of all the voltage and current signals is obtained, the sequence components of the current and voltage phasors are calculated which are then passed on to the impedance-based fault location algorithm.

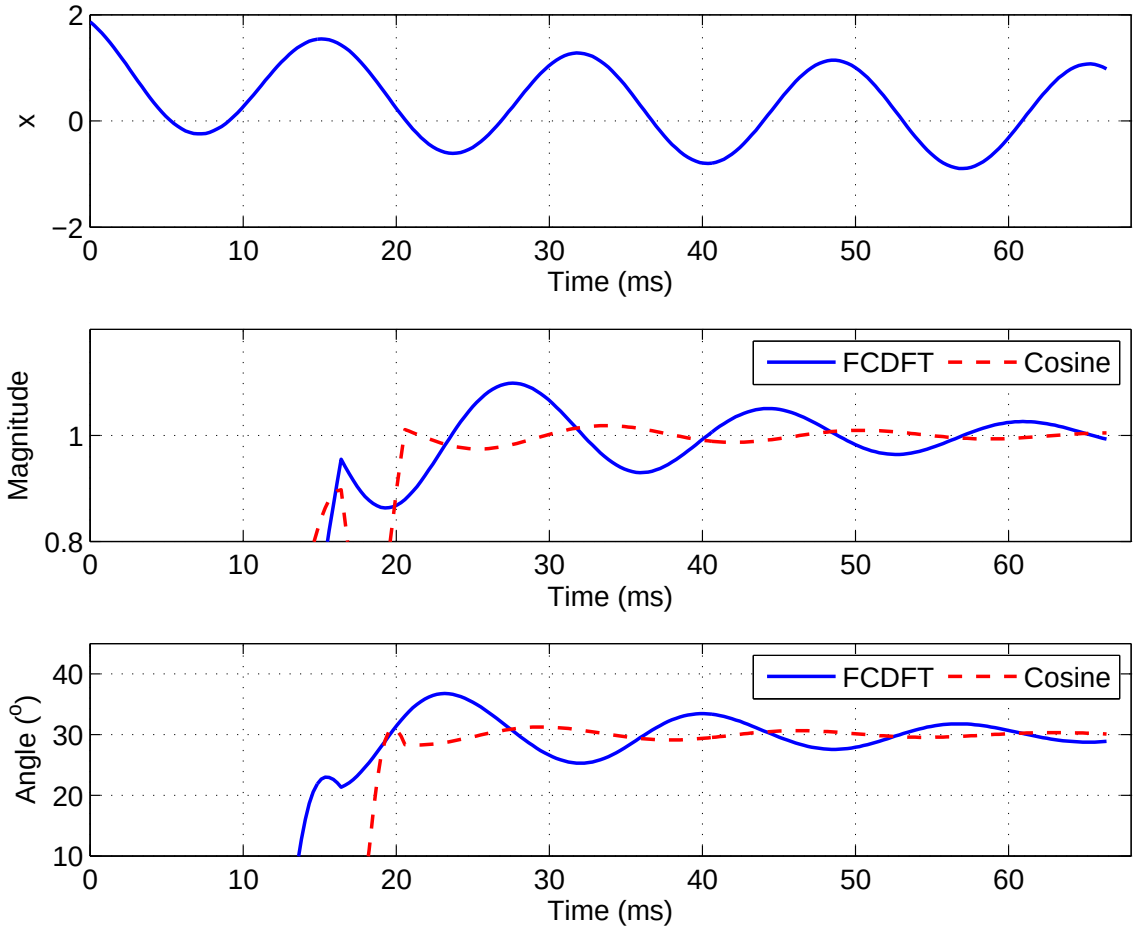

Figure A.5: Phasors estimated using FCDFT and Cosine algorithms.

Appendix B

Additional waveforms for Chapter 3

The waveforms presented in this Appendix depict the measured three phase currents and voltages, the estimated phasors of the faulted phase current and voltage, and the computed fault location result by the algorithm presented in Chapter 3. The depicted waveforms correspond to the single phase to ground faults (AG) and double phase to ground faults (BCG) located at 40% line length as measured from Bus S with different fault resistance values (0Ω, 10Ω, 50Ω, and 100Ω). Figures B.1 to B.6 correspond to AG faults while Figures B.7 to B.14 correspond to BCG faults.

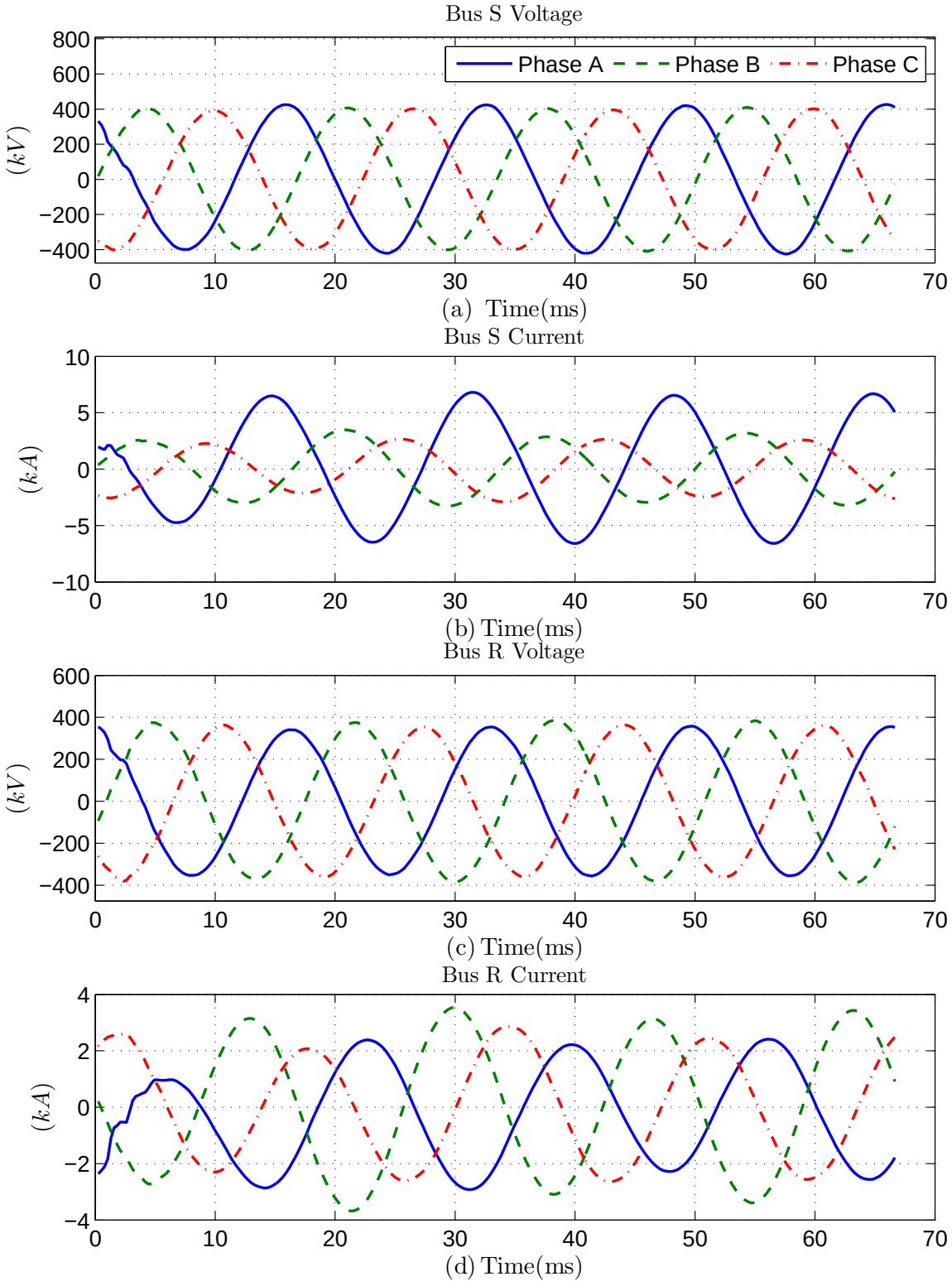

Figure B.1: Voltage and current waveforms for a 10Ω AG fault at 40% line length from Bus S: (a) Bus S voltage, (b) Bus S current (c) Bus R voltage, (d) Bus R current

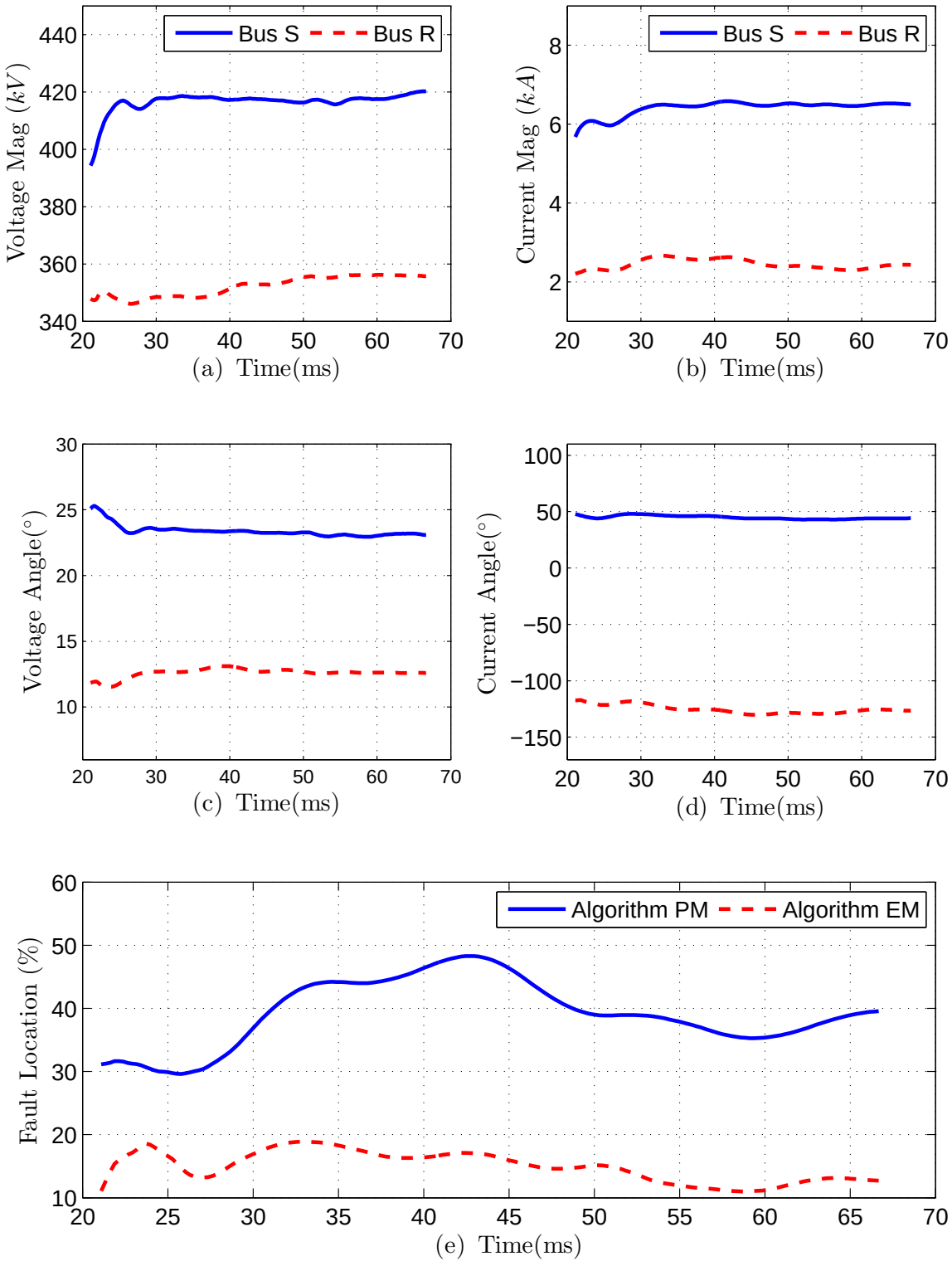

Figure B.2: (a)-(d): Estimated phasors of phase-A voltage and current signals measured at Bus S and Bus R for a 10Ω AG fault at 40% line length from Bus S; (e) fault location result obtained from Algorithm PM and Algorithm EM.

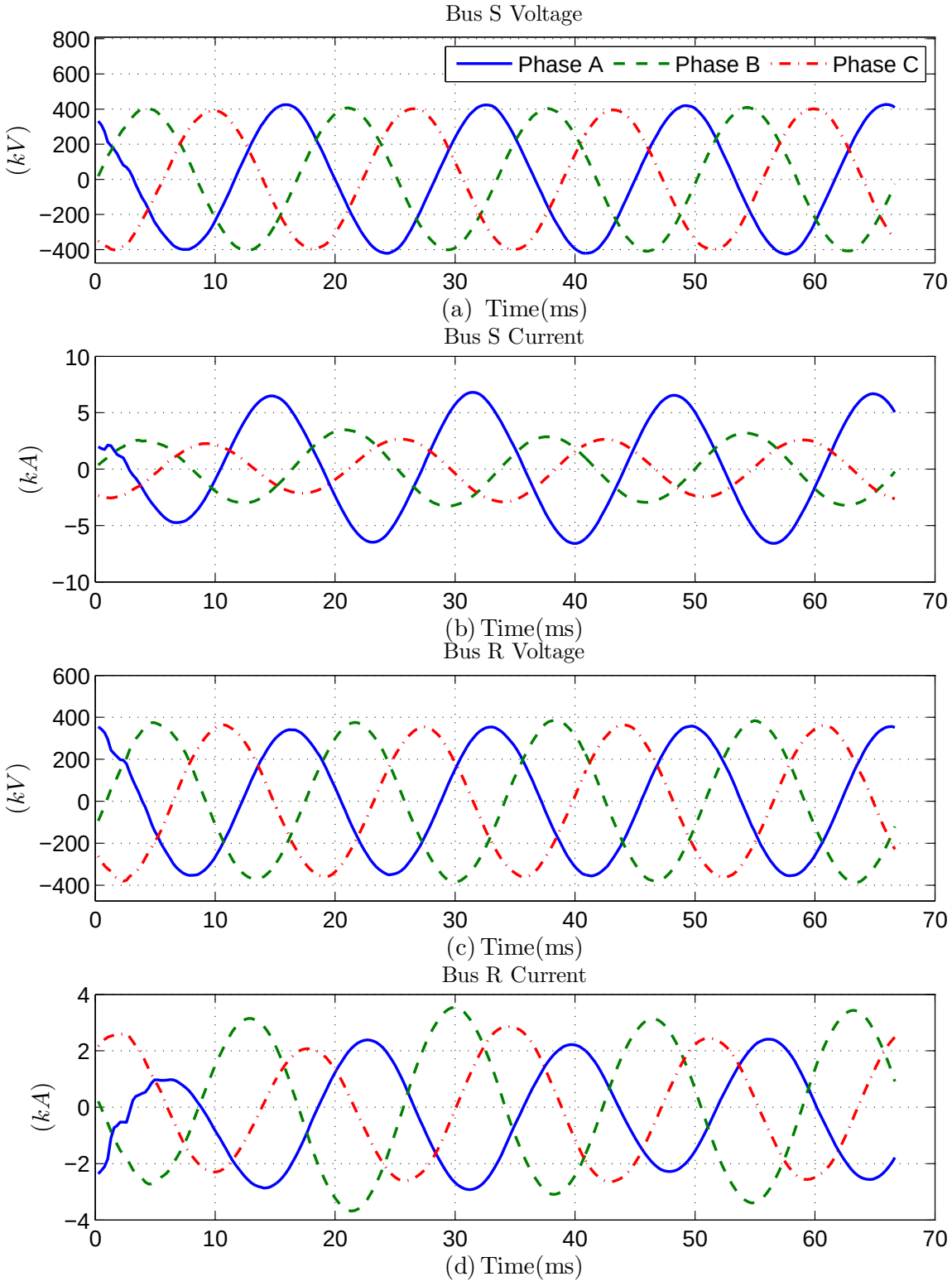

Figure B.3: Voltage and current waveforms for a 50Ω AG fault at 40% line length from Bus S: (a) Bus S voltage, (b) Bus S current (c) Bus R voltage, (d) Bus R current

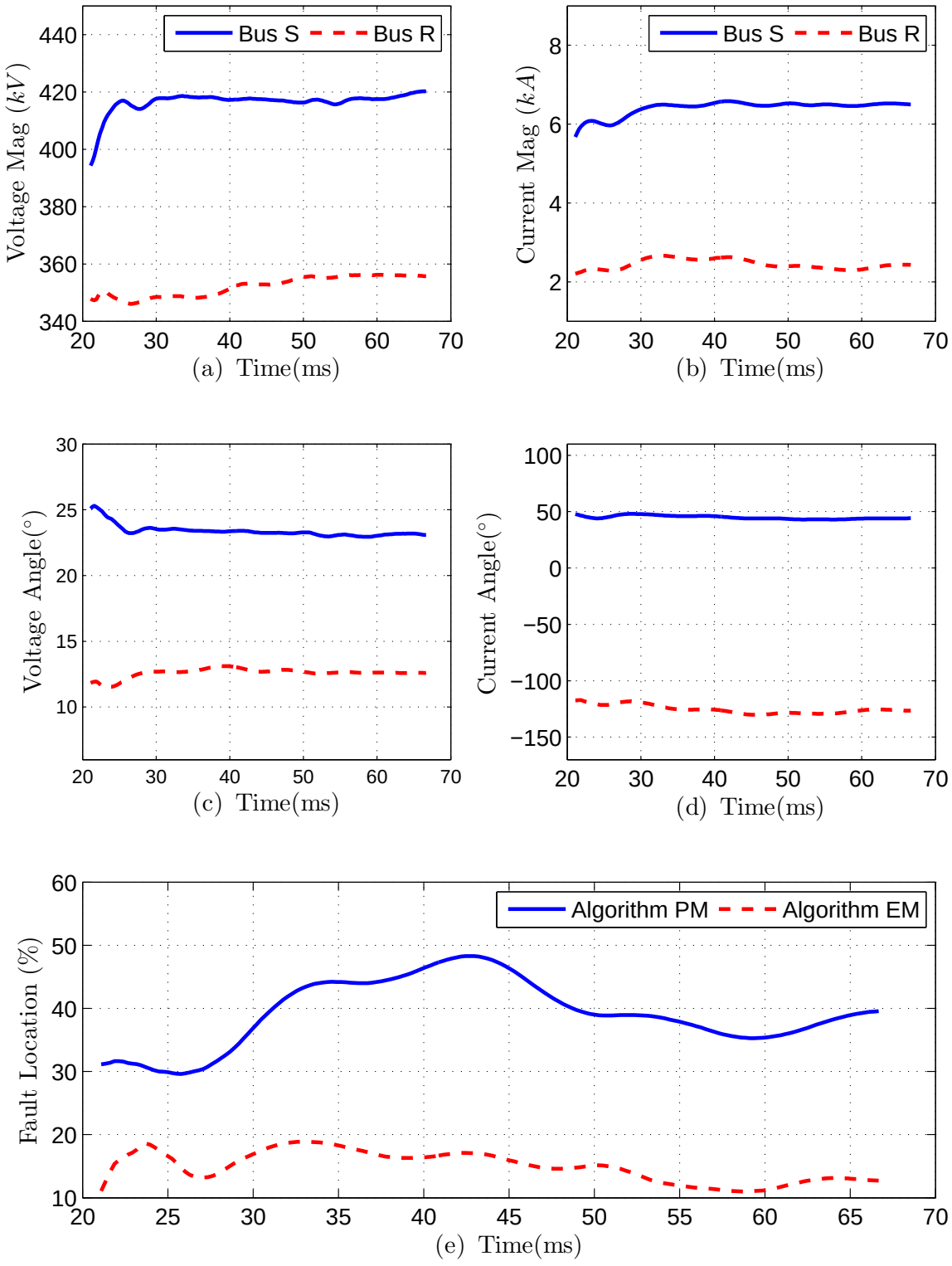

Figure B.4: (a)-(d): Estimated phasors of phase-A voltage and current signals measured at Bus S and Bus R for a 50Ω AG fault at 40% line length from Bus S; (e) fault location result obtained from Algorithm PM and Algorithm EM.

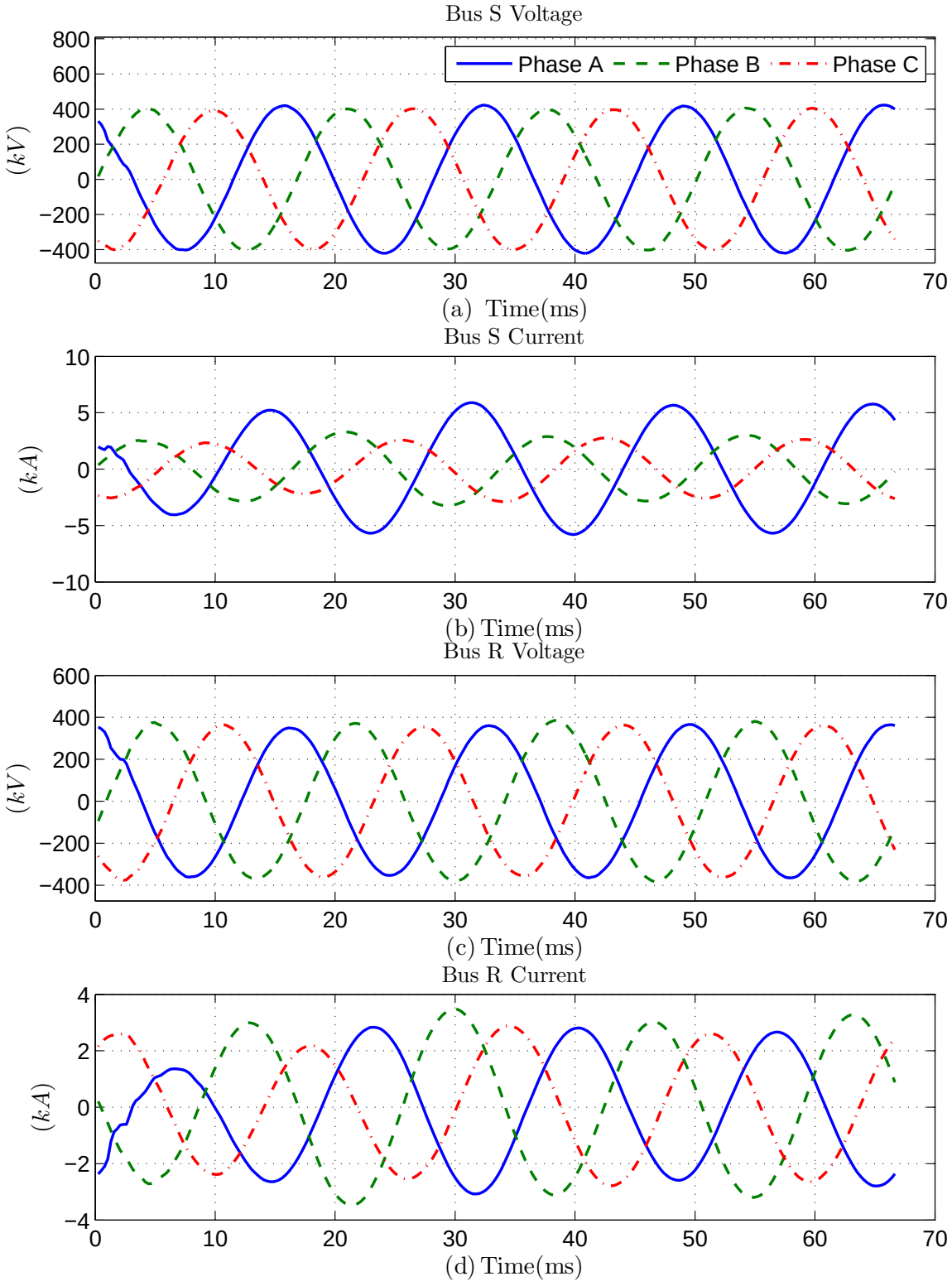

Figure B.5: Voltage and current waveforms for a 100Ω AG fault at 40% line length from Bus S: (a) Bus S voltage, (b) Bus S current (c) Bus R voltage, (d) Bus R current

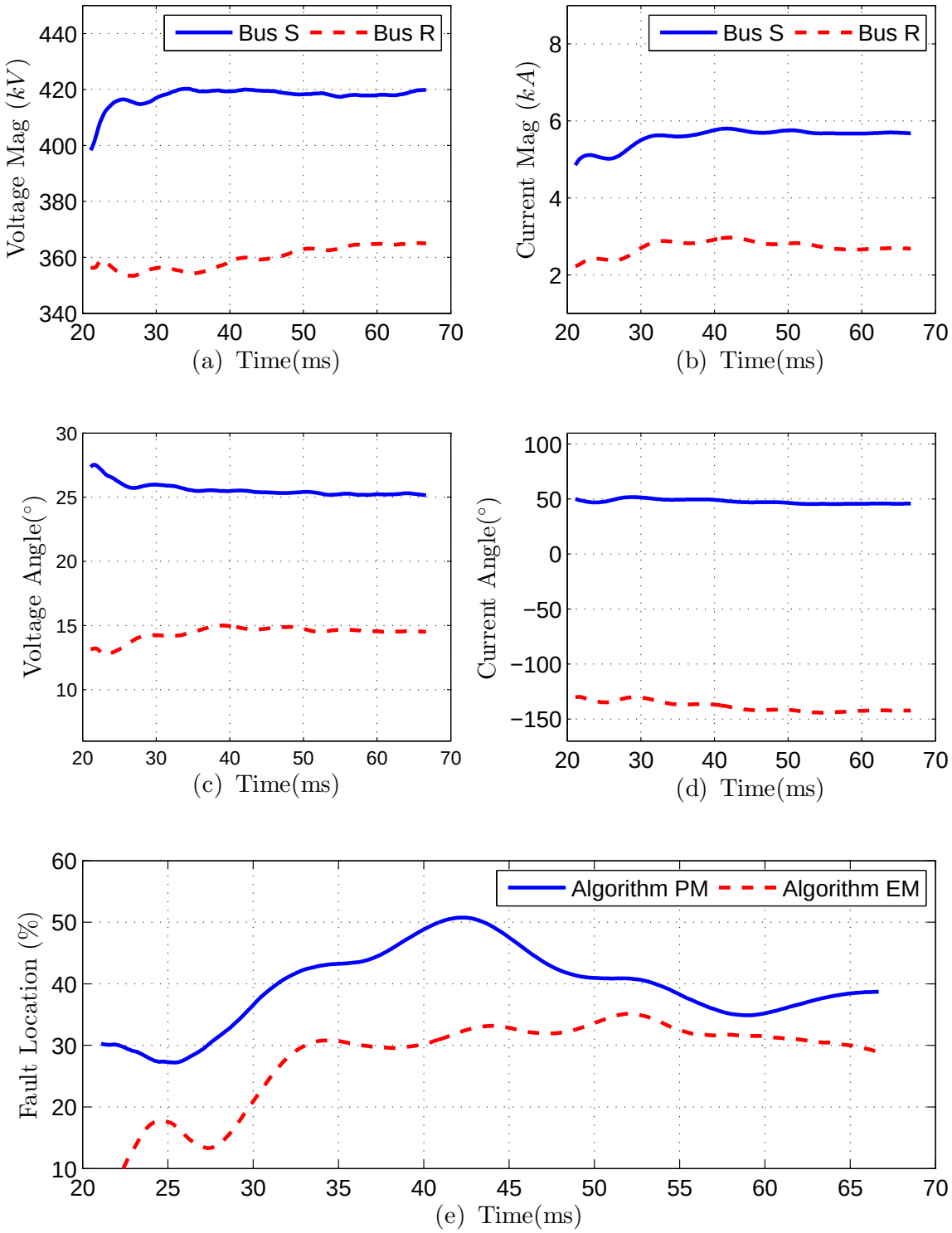

Figure B.6: (a)-(d): Estimated phasors of phase-A voltage and current signals measured at Bus S and Bus R for a 100Ω AG fault at 40% line length from Bus S; (e) fault location result obtained from Algorithm PM and Algorithm EM.

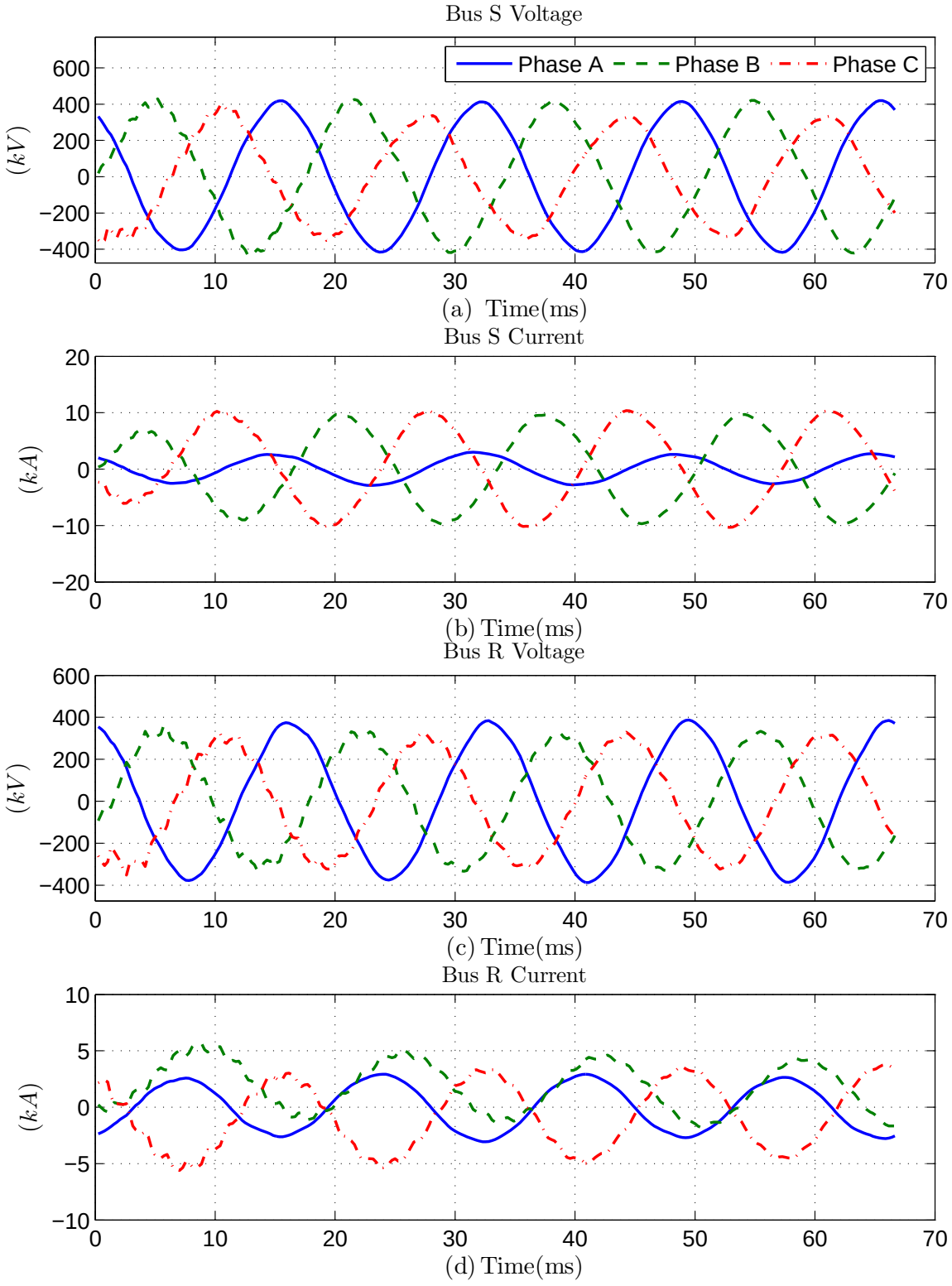

Figure B.7: Voltage and current waveforms for a 0Ω BCG fault at 40% line length from Bus S: (a) Bus S voltage, (b) Bus S current (c) Bus R voltage, (d) Bus R current

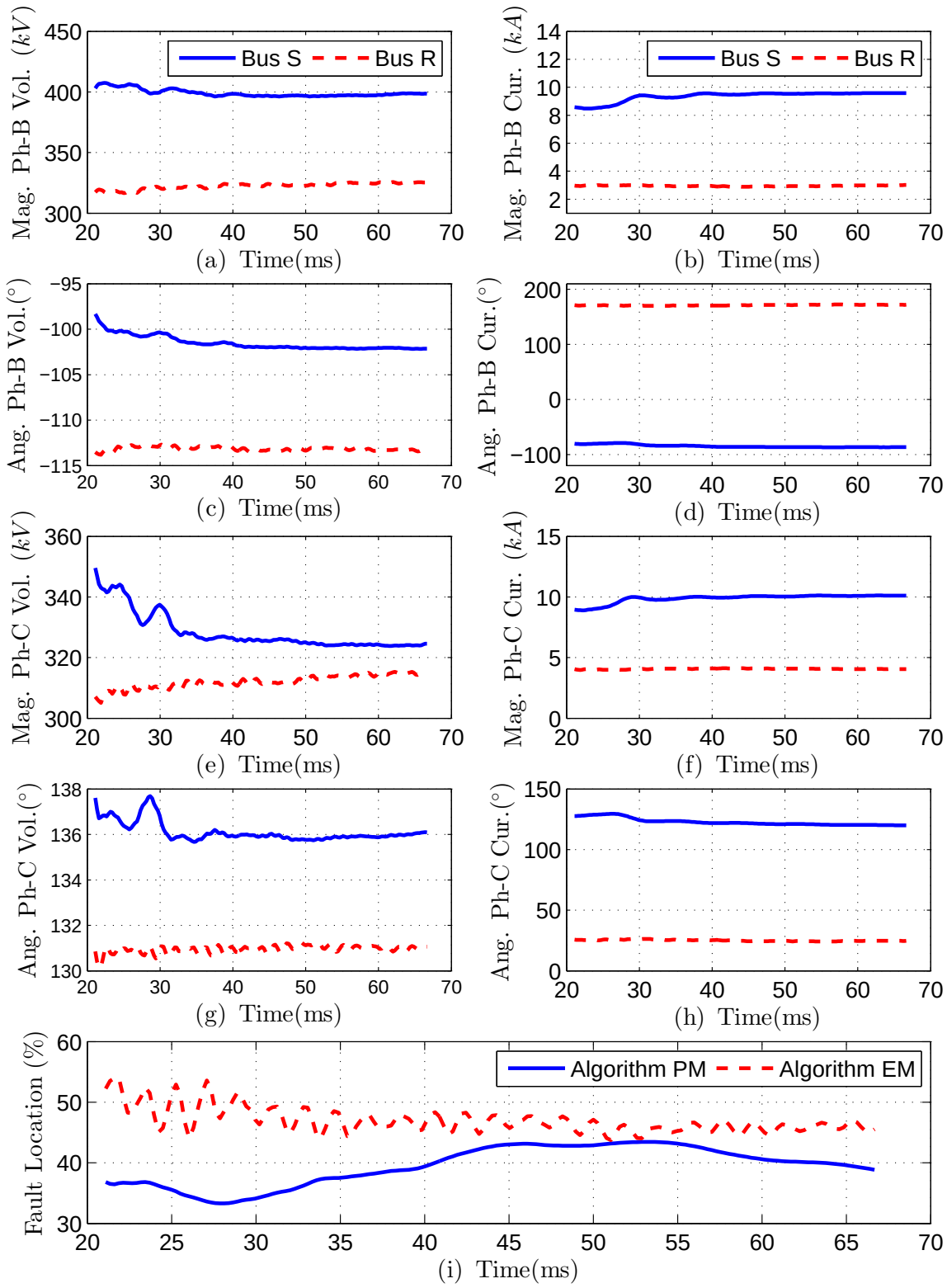

Figure B.8: (a)-(d): Estimated phasors of phase-B voltage and current signals measured at Bus S and Bus R; (e)-(h): estimated phasors of phase-C voltage and current signals measured at Bus S and Bus R for a 0Ω BCG fault at 40% line length from Bus S; (i) fault location result obtained from Algorithm PM and Algorithm EM.

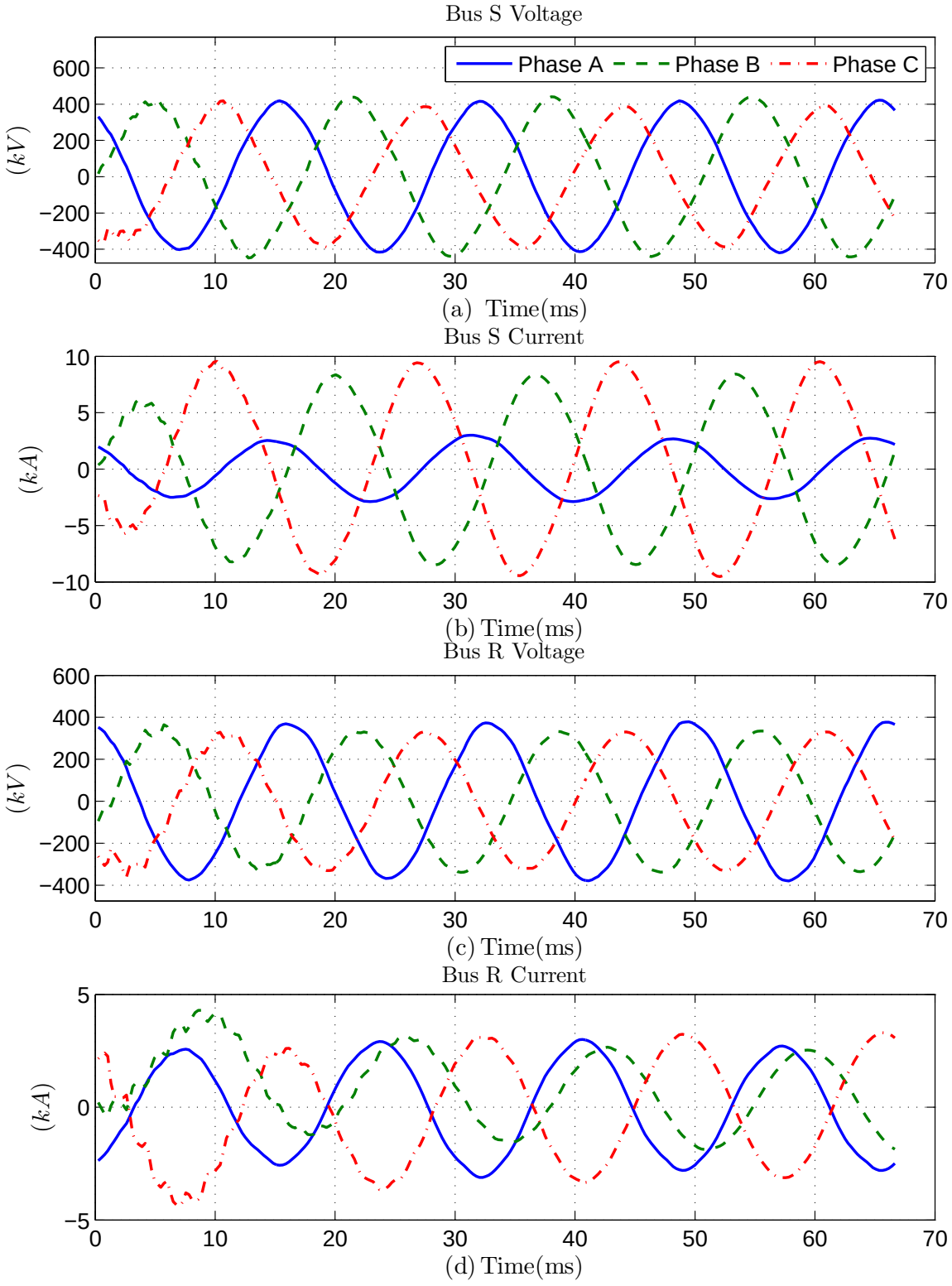

Figure B.9: Voltage and current waveforms for a 10Ω BCG fault at 40% line length from Bus S: (a) Bus S voltage, (b) Bus S current (c) Bus R voltage, (d) Bus R current

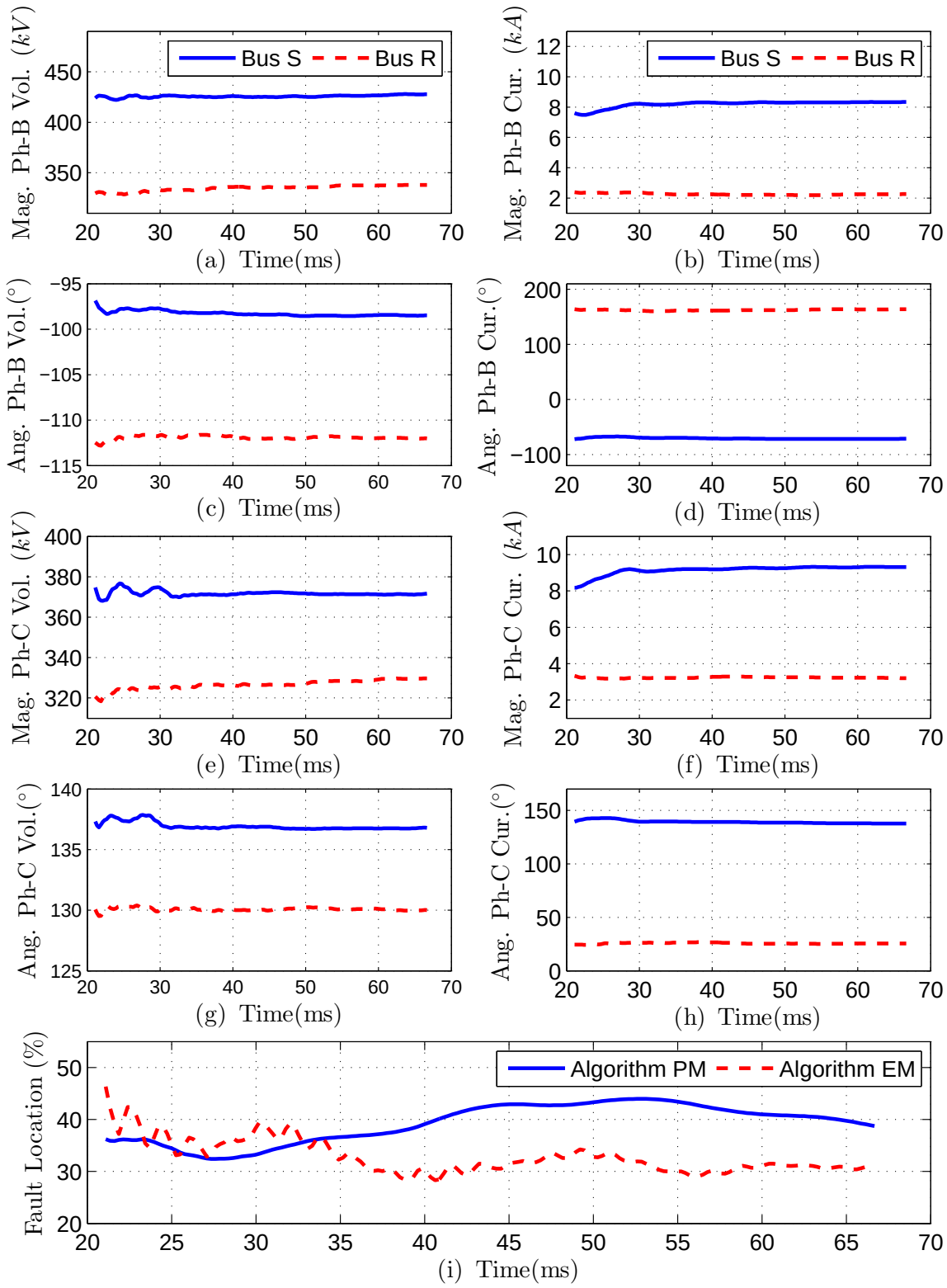

Figure B.10: (a)-(d): Estimated phasors of phase-B voltage and current signals measured at Bus S and Bus R; (e)-(h): estimated phasors of phase-C voltage and current signals measured at Bus S and Bus R for a 10Ω BCG fault at 40% line length from Bus S; (i) fault location result obtained from Algorithm PM and Algorithm EM.

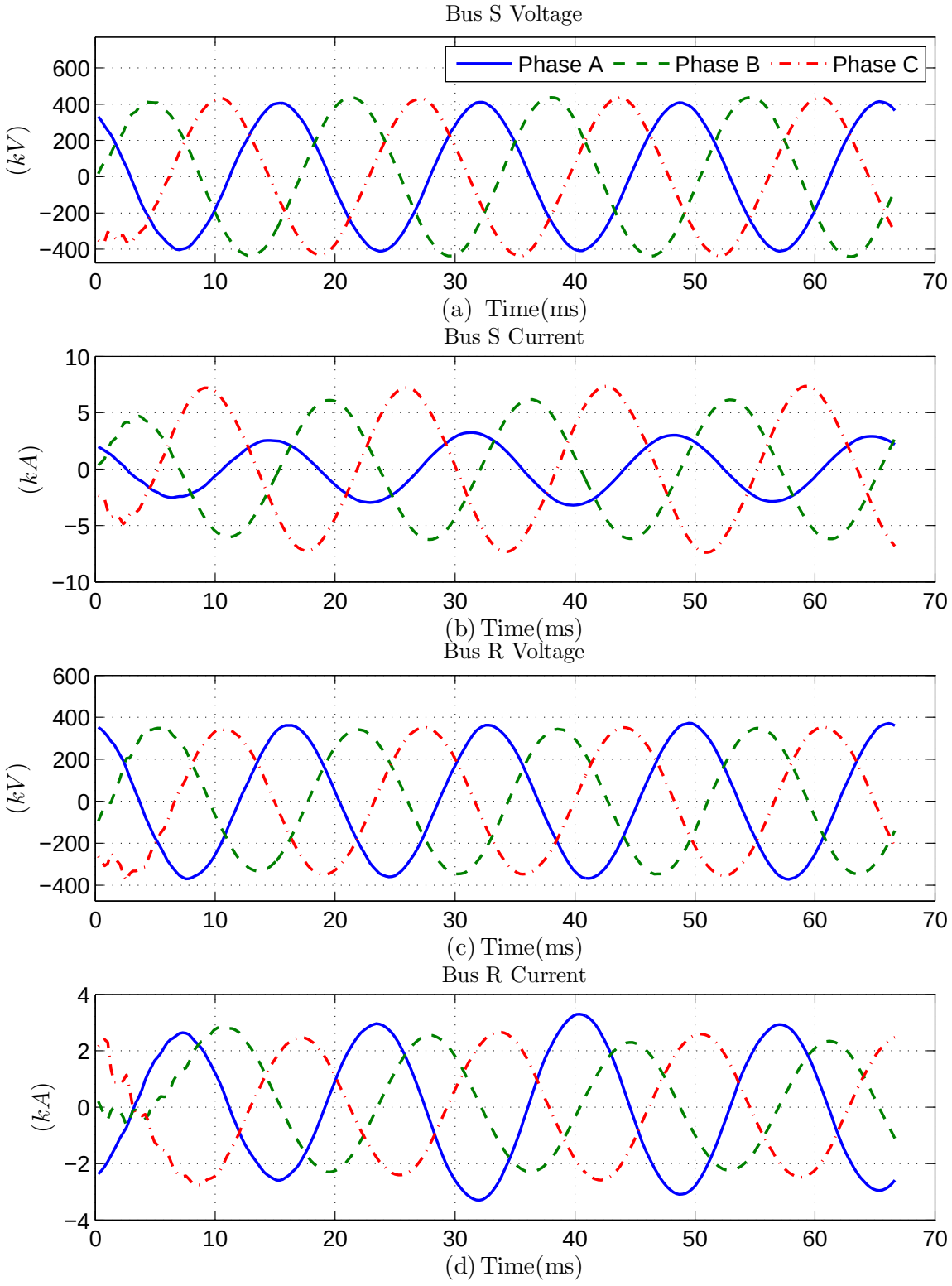

Figure B.11: Voltage and current waveforms for a 50Ω BCG fault at 40% line length from Bus S: (a) Bus S voltage, (b) Bus S current (c) Bus R voltage, (d) Bus R current

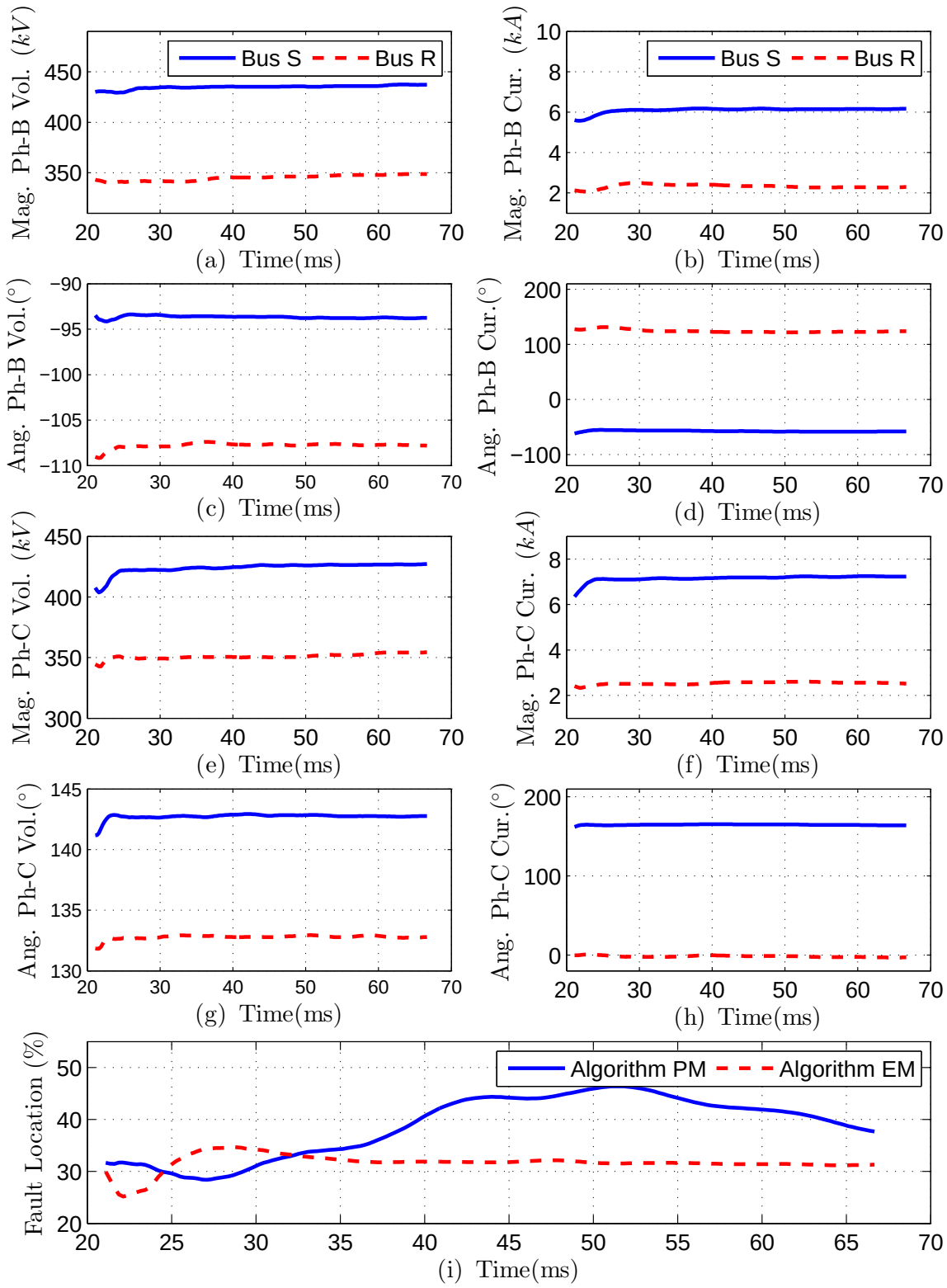

Figure B.12: (a)-(d): Estimated phasors of phase-B voltage and current signals measured at Bus S and Bus R; (e)-(h): estimated phasors of phase-C voltage and current signals measured at Bus S and Bus R for a 50Ω BCG fault at 40% line length from Bus S; (i) fault location result obtained from Algorithm PM and Algorithm EM.

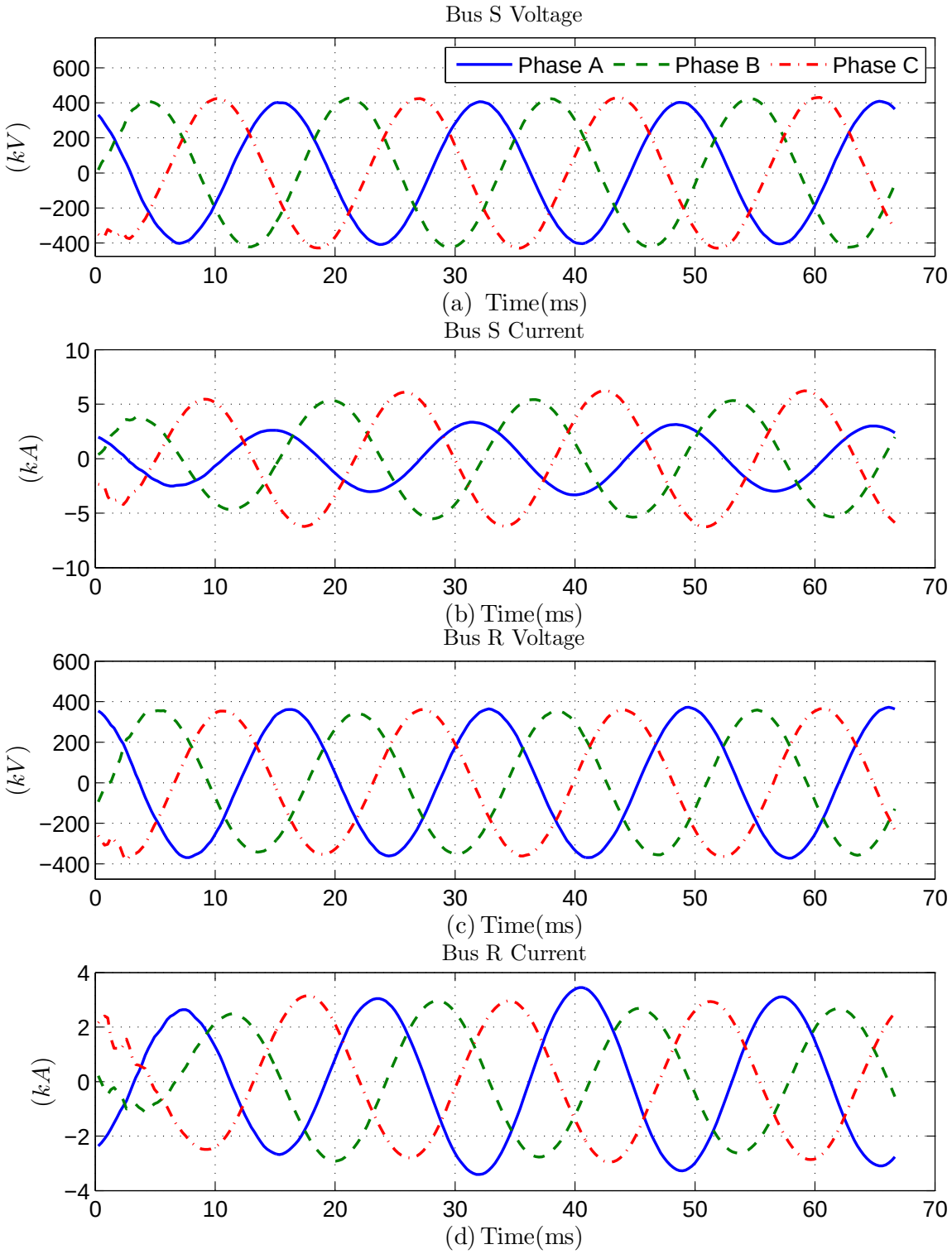

Figure B.13: Voltage and current waveforms for a 100Ω BCG fault at 40% line length from Bus S: (a) Bus S voltage, (b) Bus S current (c) Bus R voltage, (d) Bus R current

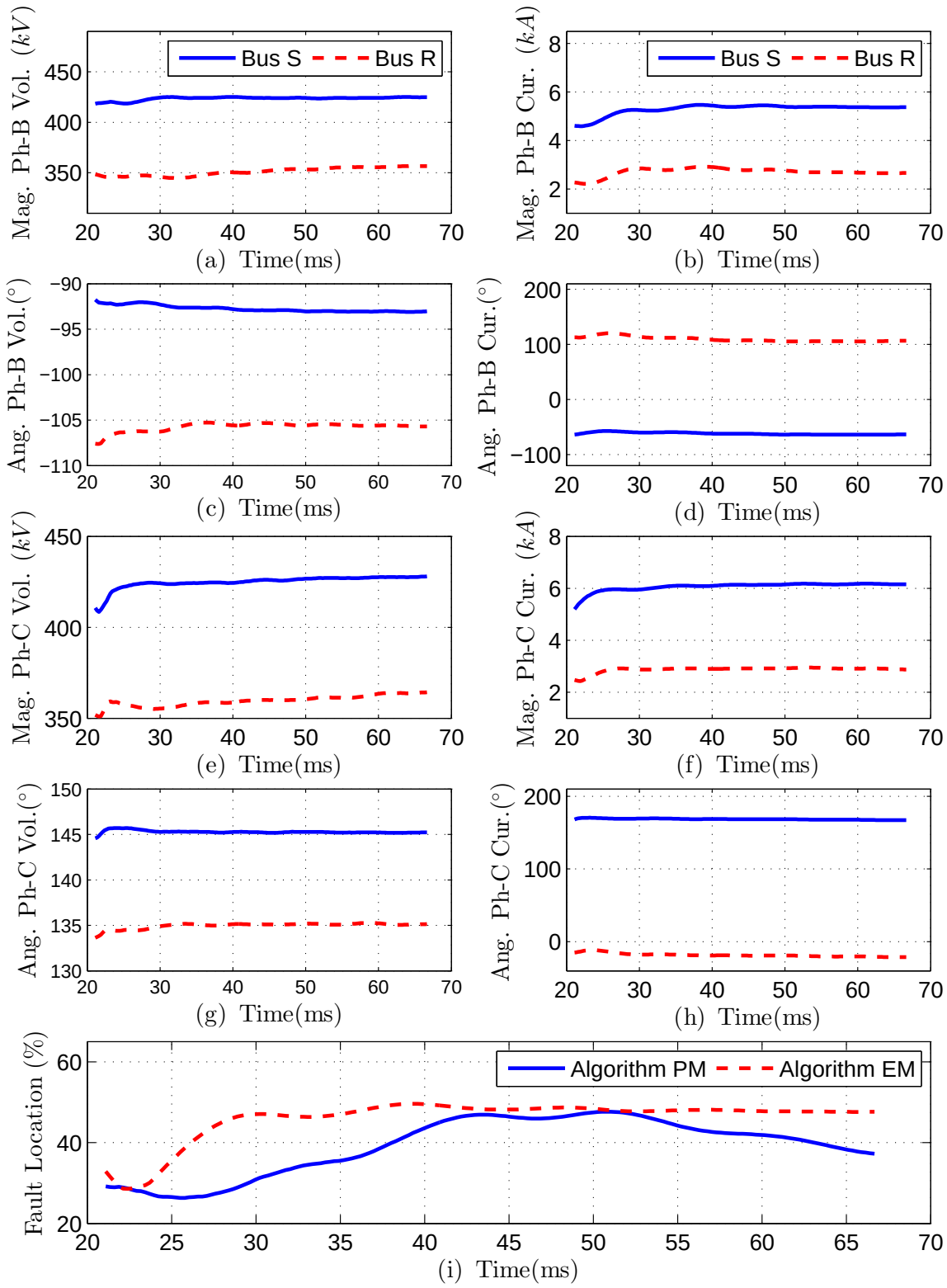

Figure B.14: (a)-(d): Estimated phasors of phase-B voltage and current signals measured at Bus S and Bus R; (e)-(h): estimated phasors of phase-C voltage and current signals measured at Bus S and Bus R for a 100Ω BCG fault at 40% line length from Bus S; (i) fault location result obtained from Algorithm PM and Algorithm EM.

Appendix C

Additional waveforms for Chapter 5

The waveforms presented in this Appendix correspond to the fault location algorithms proposed in Chapter 5. The current flowing through MOVs and SCBs in each phase for different types of faults have been depicted in Figures C.1 to C.8. The Figures C.9 to C.16 represent the estimated phasors of positive sequence of the measured quantities and the fault location results yielded by both of the proposed algorithms.

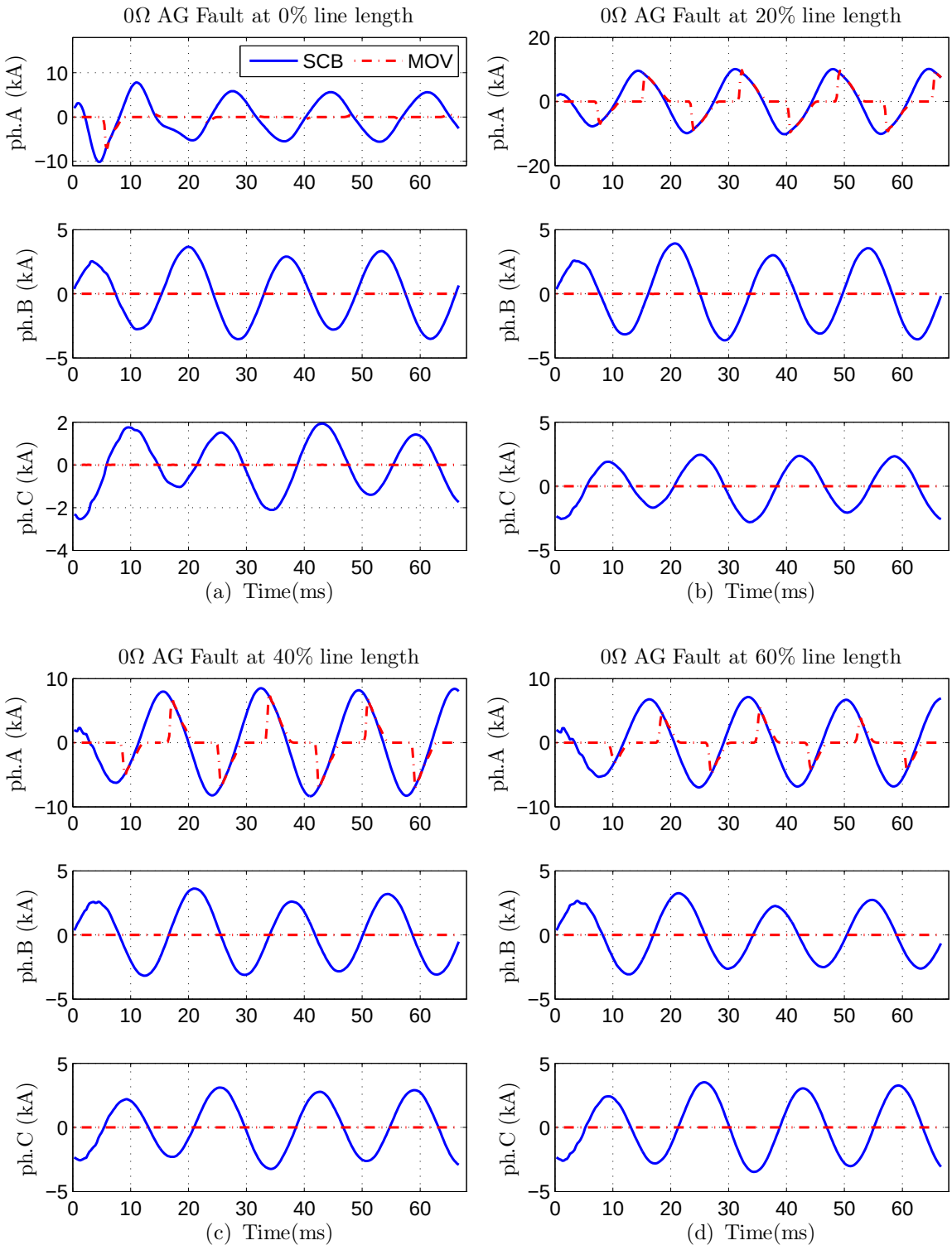

Figure C.1: The total current flowing though SCB, and the MOV current for solid AG faults at various points in an SCCTL measured as percent of the line length from Bus S: (a) 0%, (b) 20%, (c) 40%, (d) 60%.

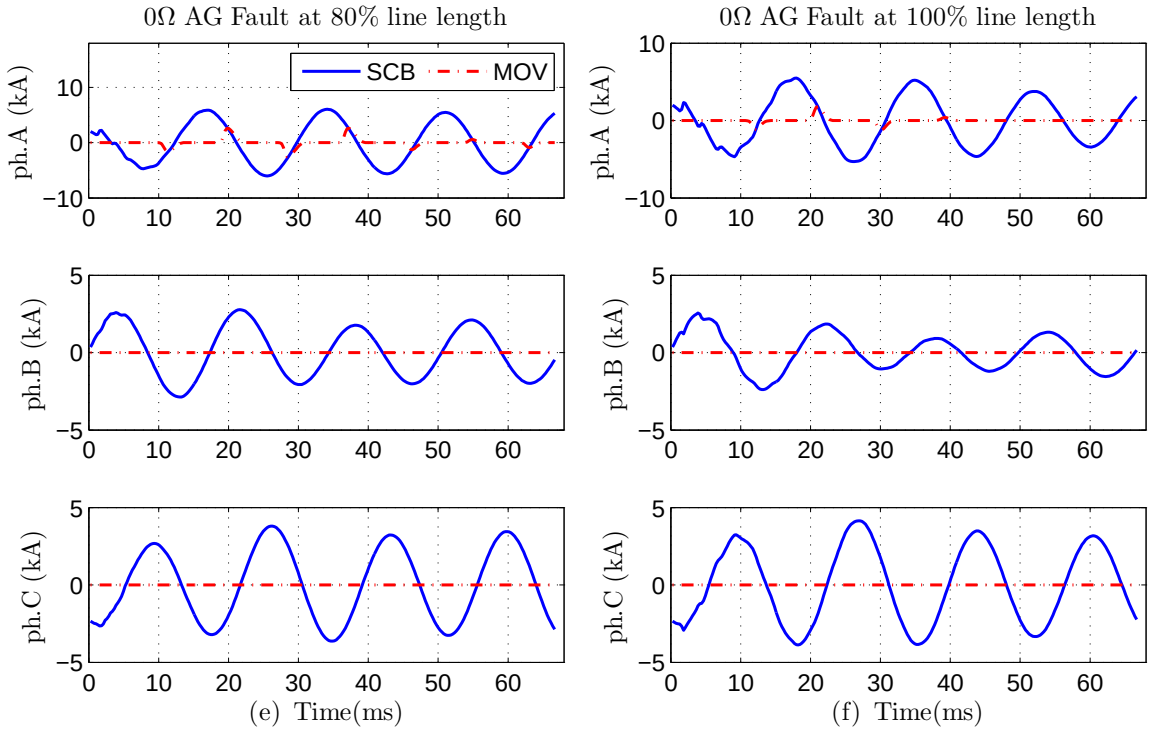

Figure C.1 (Continued): The total current flowing though SCB, and the MOV current for solid AG faults at various points in an SCCTL measured as percent of the line length from Bus S: (e) 80%, and (f) 100%.

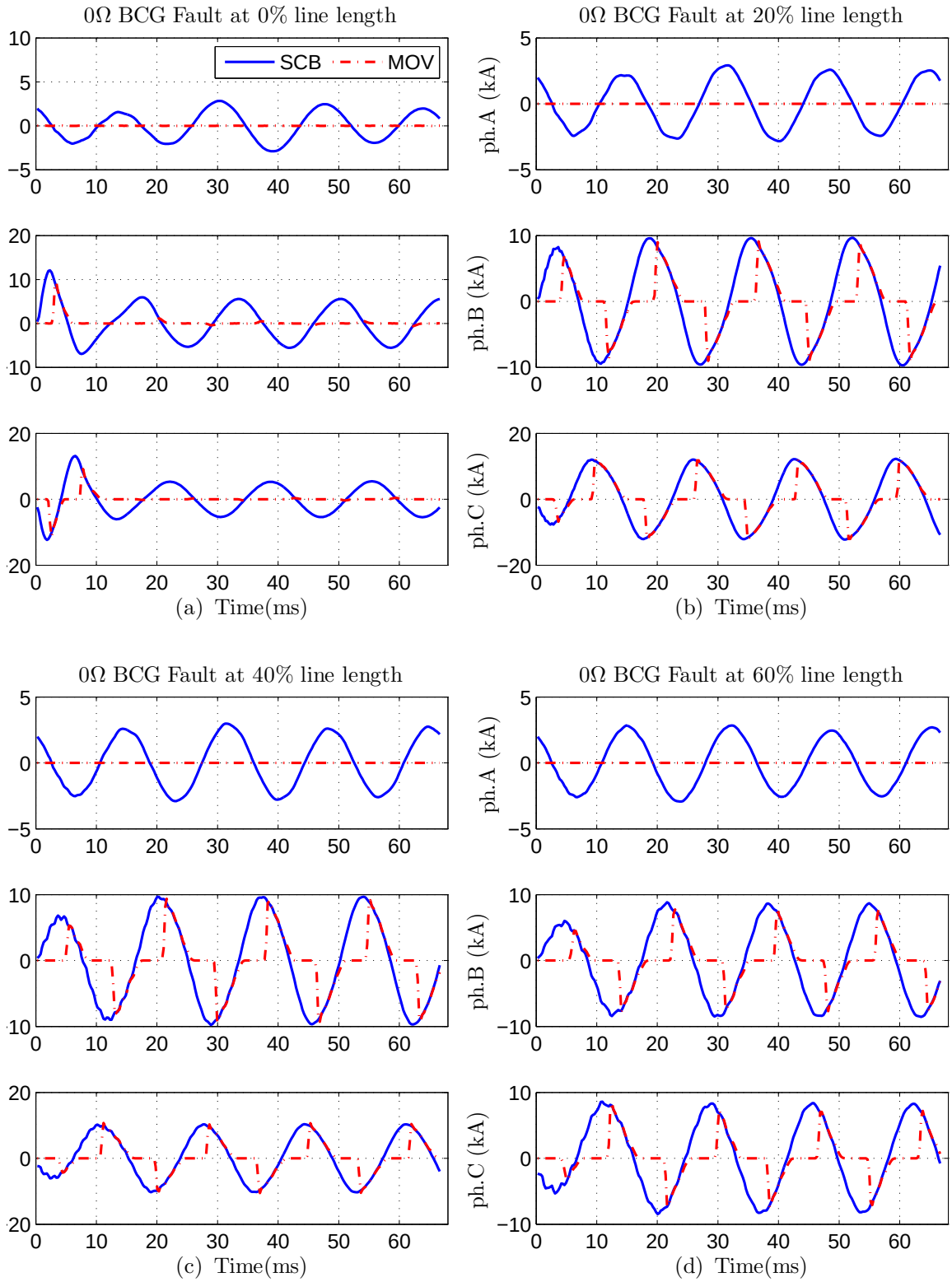

Figure C.2: The total current flowing though SCB, and the MOV current for solid BCG faults at various points in an SCCTL measured as percent of the line length from Bus S: (a) 0%, (b) 20%, (c) 40%, (d) 60%.

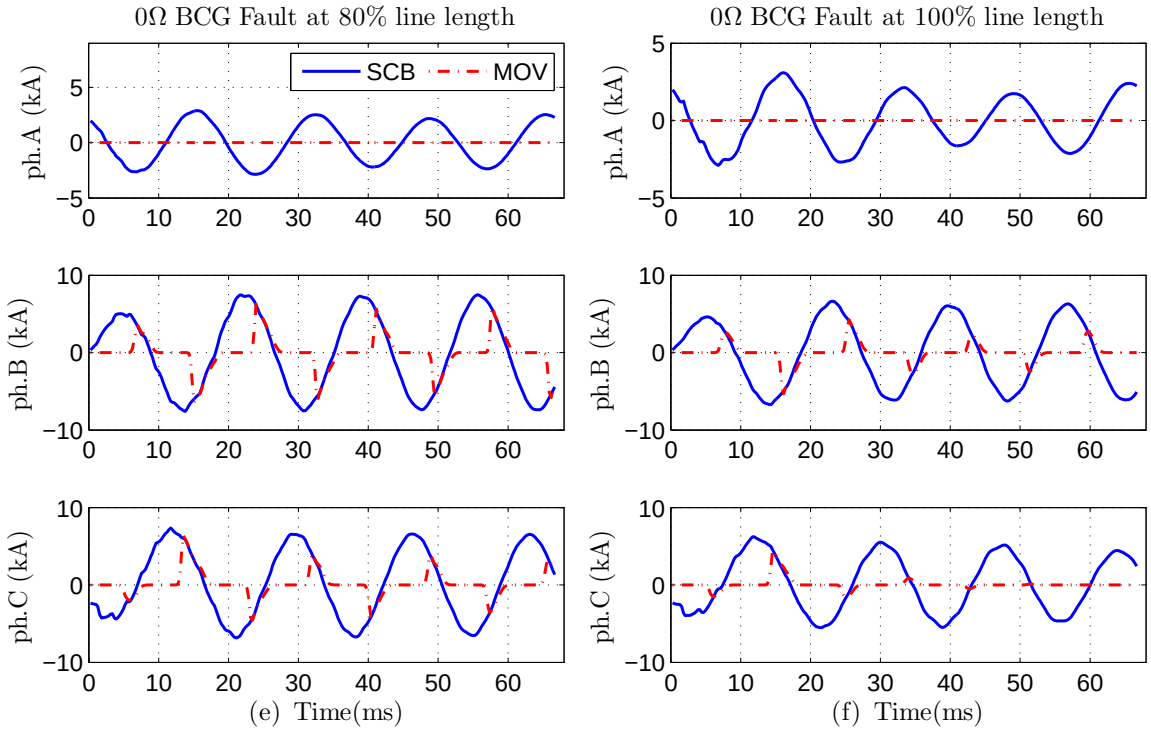

Figure C.2 (Continued): The total current flowing though SCB, and the MOV current for solid BCG faults at various points in an SCCTL measured as percent of the line length from Bus S: (e) 80%, and (f) 100%.

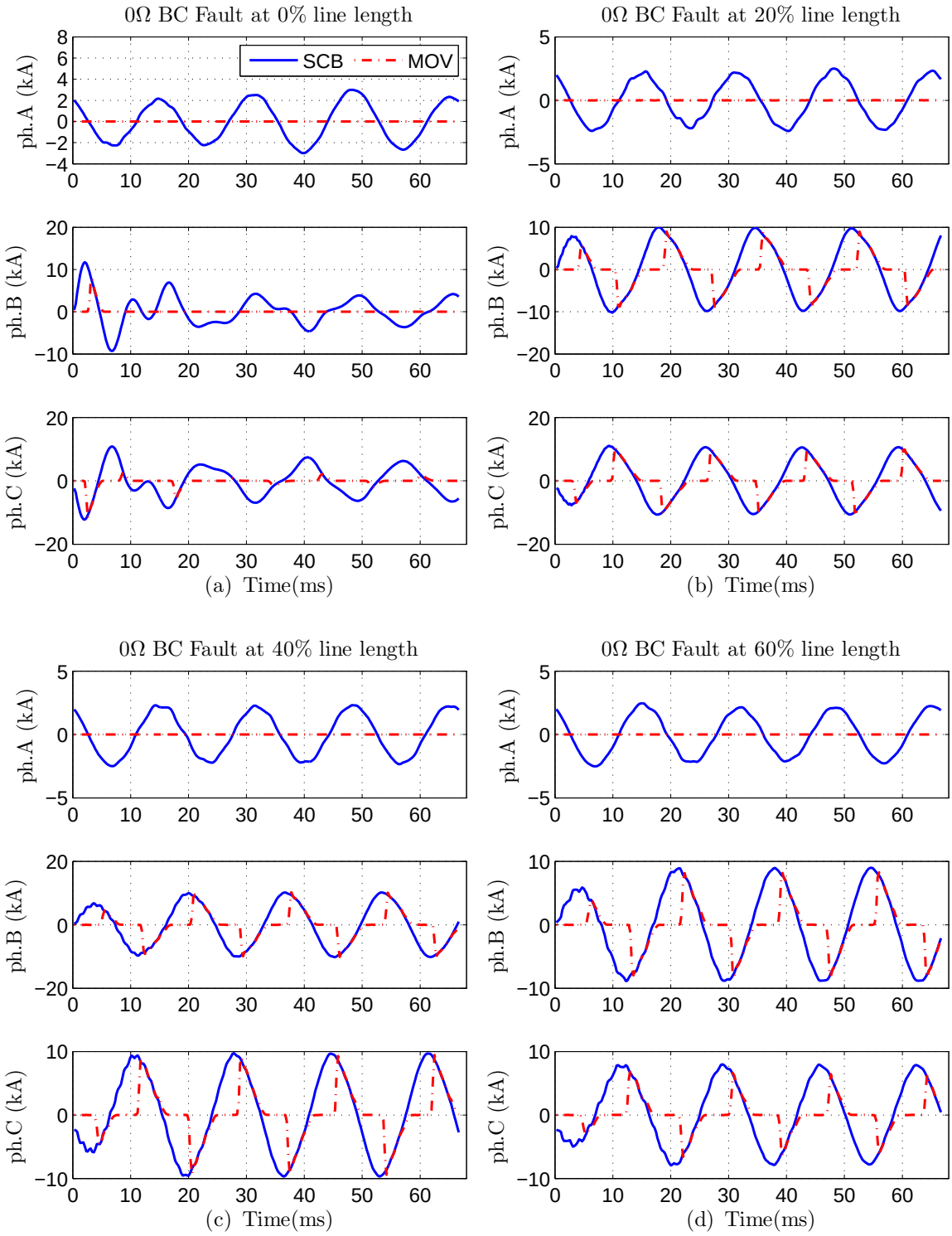

Figure C.3: The total current flowing though SCB, and the MOV current for solid BC faults at various points in an SCCTL measured as percent of the line length from Bus S: (a) 0%, (b) 20%, (c) 40%, (d) 60%.

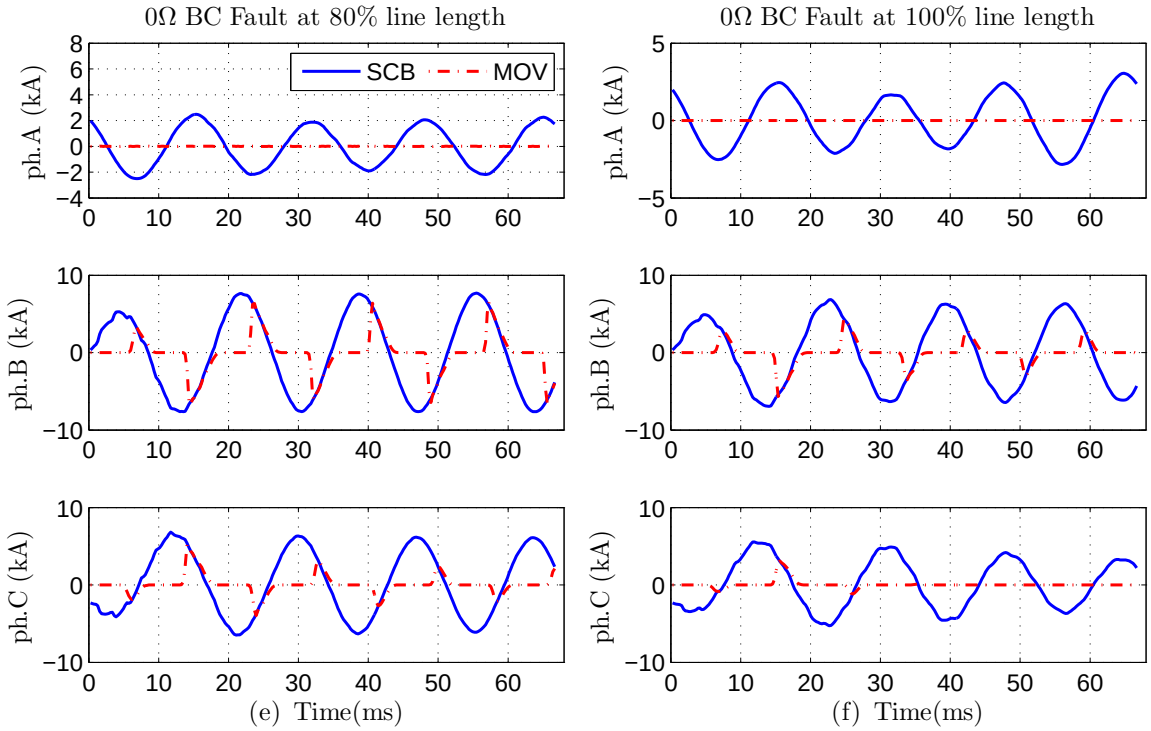

Figure C.3 (Continued): The total current flowing though SCB, and the MOV current for solid BC faults at various points in an SCCTL measured as percent of the line length from Bus S: (e) 80%, and (f) 100%.

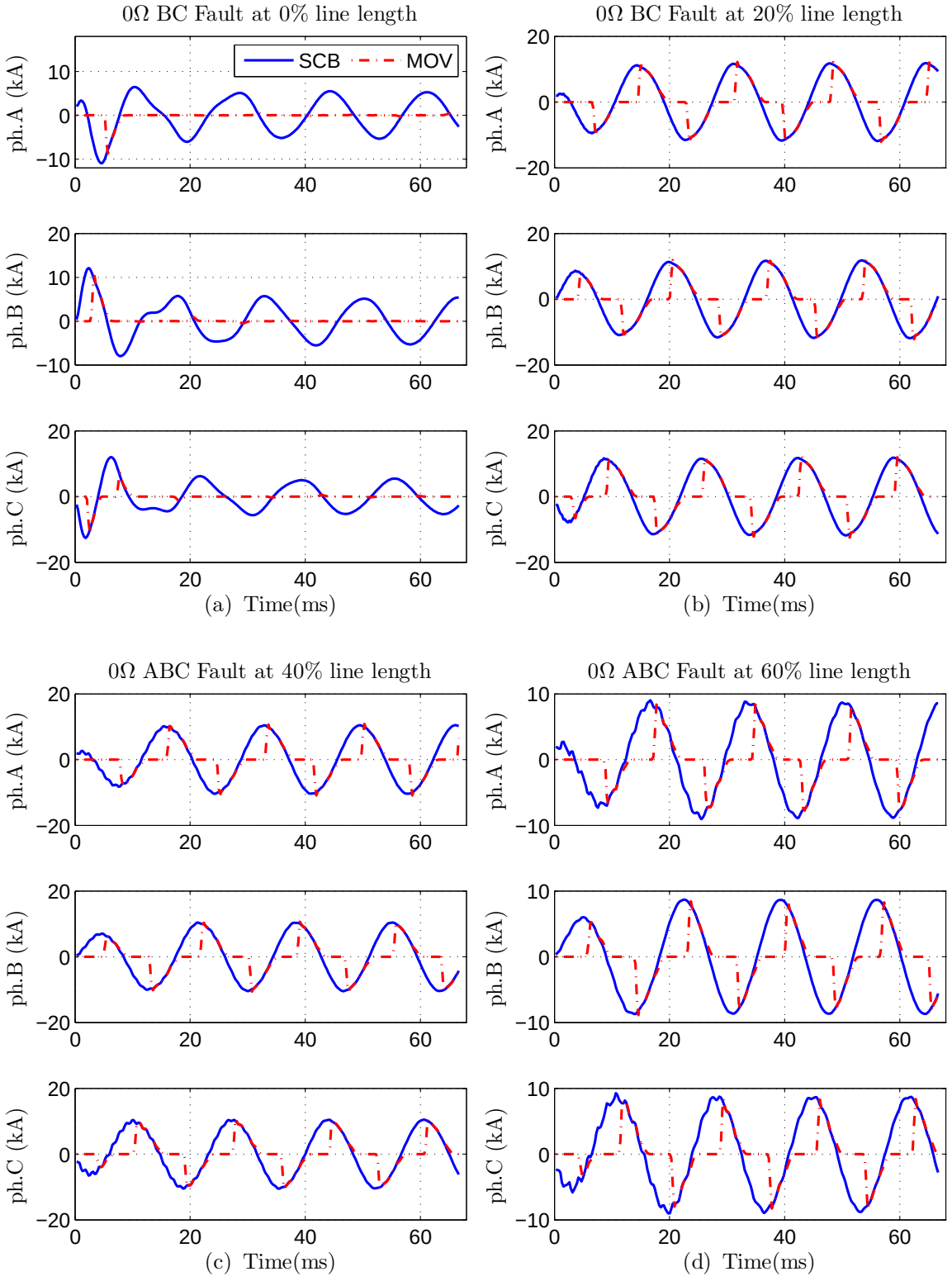

Figure C.4: The total current flowing though SCB, and the MOV current for solid ABC faults at various points in an SCCTL measured as percent of the line length from Bus S: (a) 0%, (b) 20%, (c) 40%, (d) 60%.

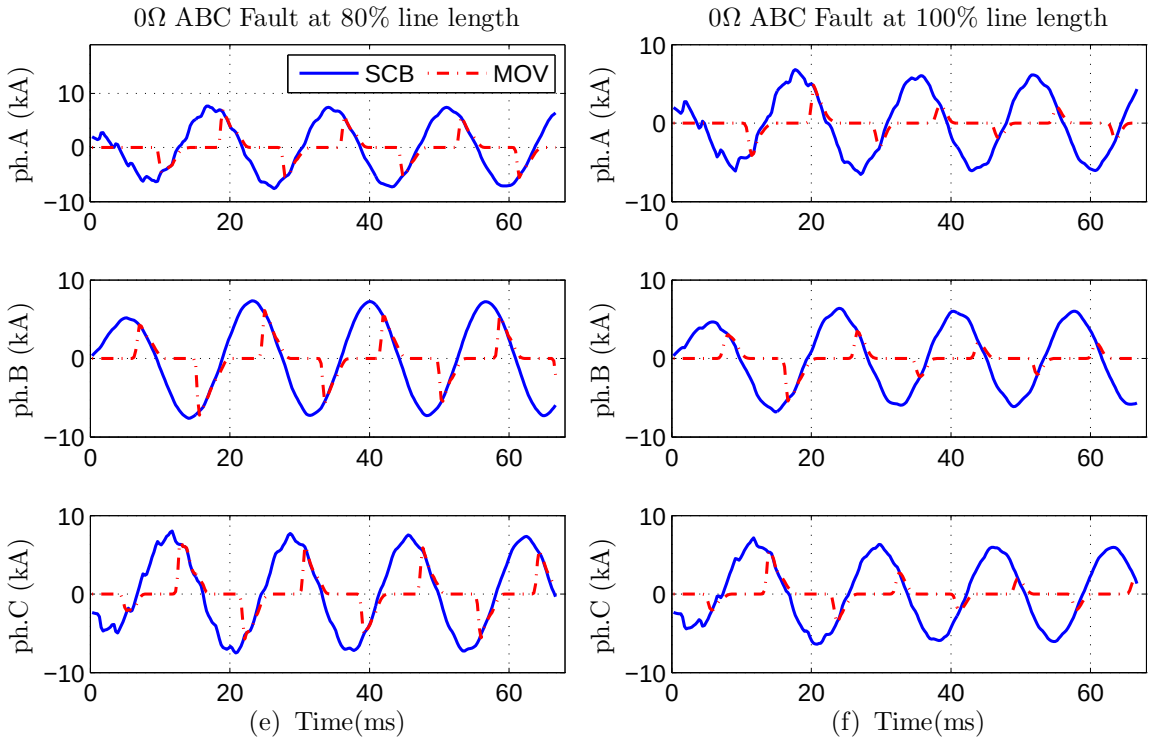

Figure C.4 (Continued): The total current flowing though SCB, and the MOV current for solid ABC faults at various points in an SCCTL measured as percent of the line length from Bus S: (e) 80%, and (f) 100%.

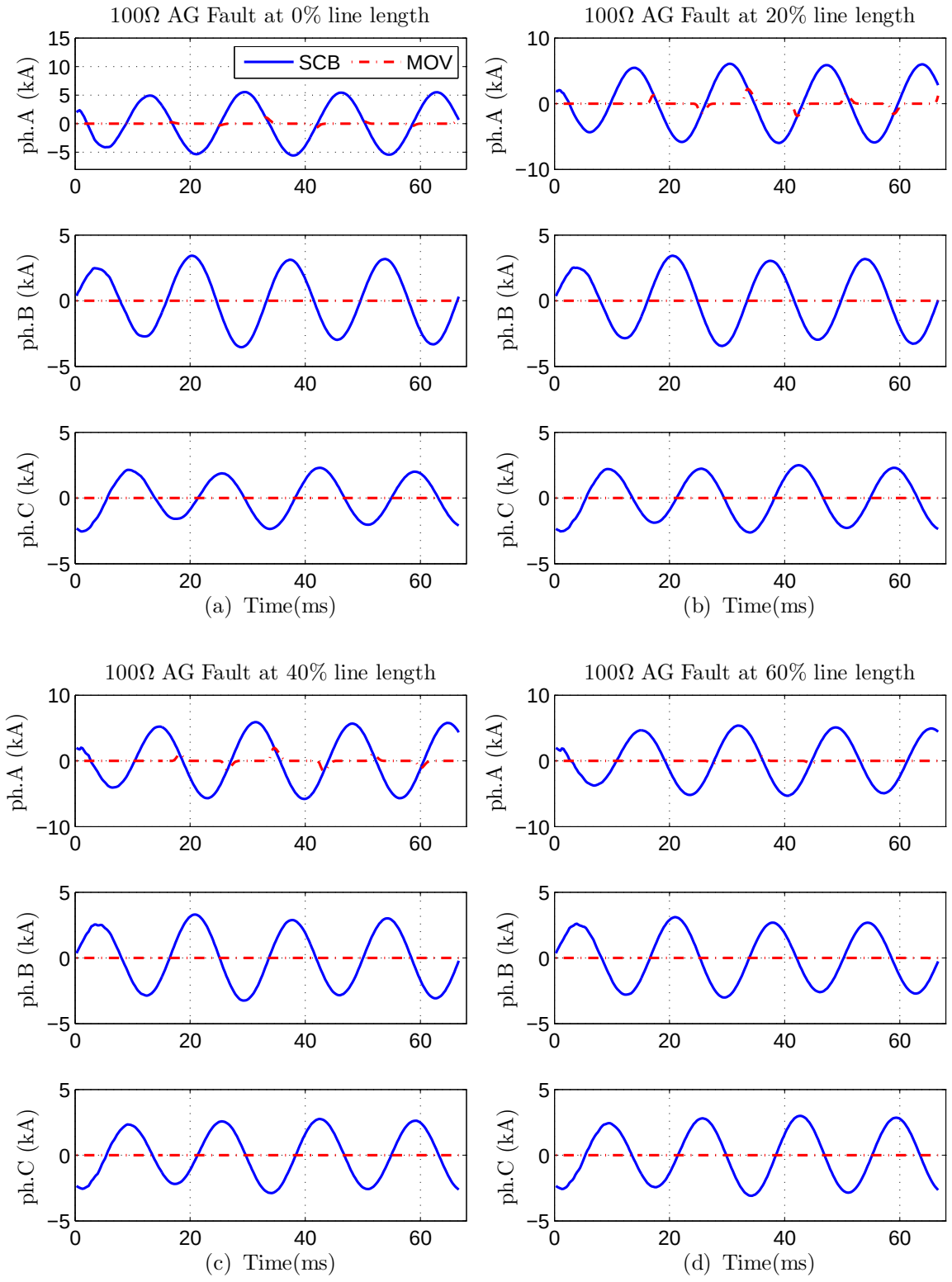

Figure C.5: The total current flowing though SCB, and the MOV current for solid AG faults at various points in an SCCTL measured as percent of the line length from Bus S: (a) 0%, (b) 20%, (c) 40%, (d) 60%.

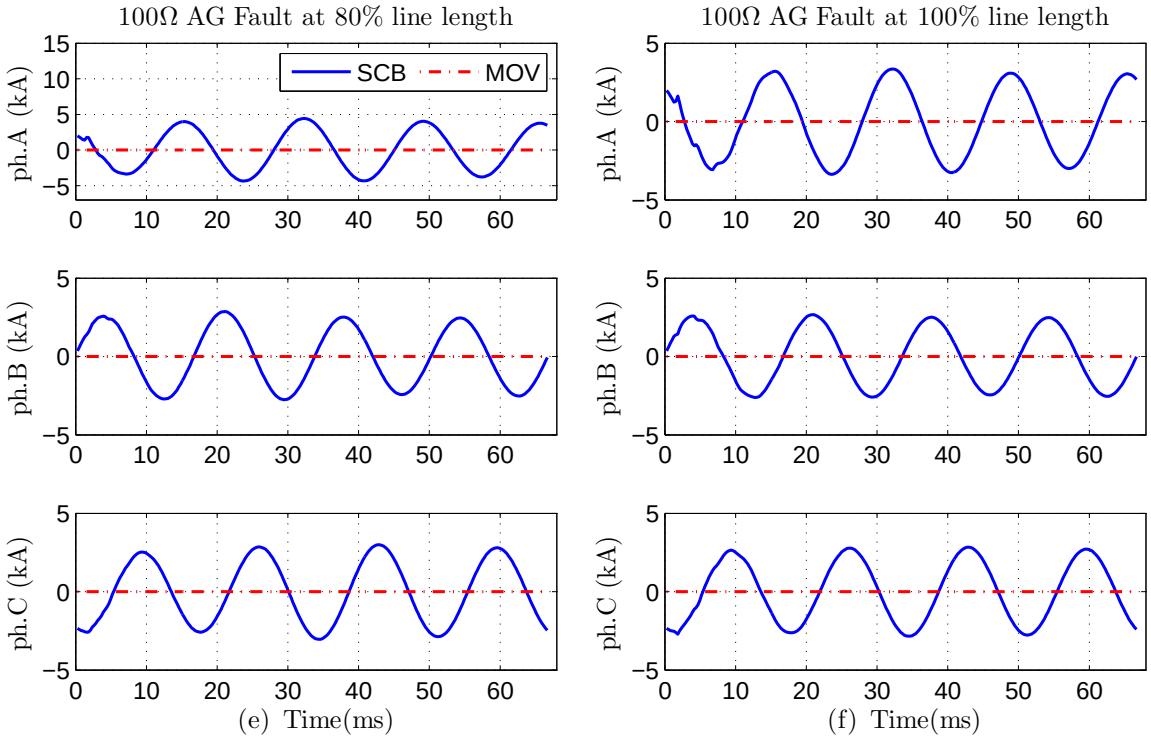

Figure C.5 (Continued): The total current flowing though SCB, and the MOV current for 100Ω AG faults at various points in an SCCTL measured as percent of the line length from Bus S: (e) 80%, and (f) 100%.

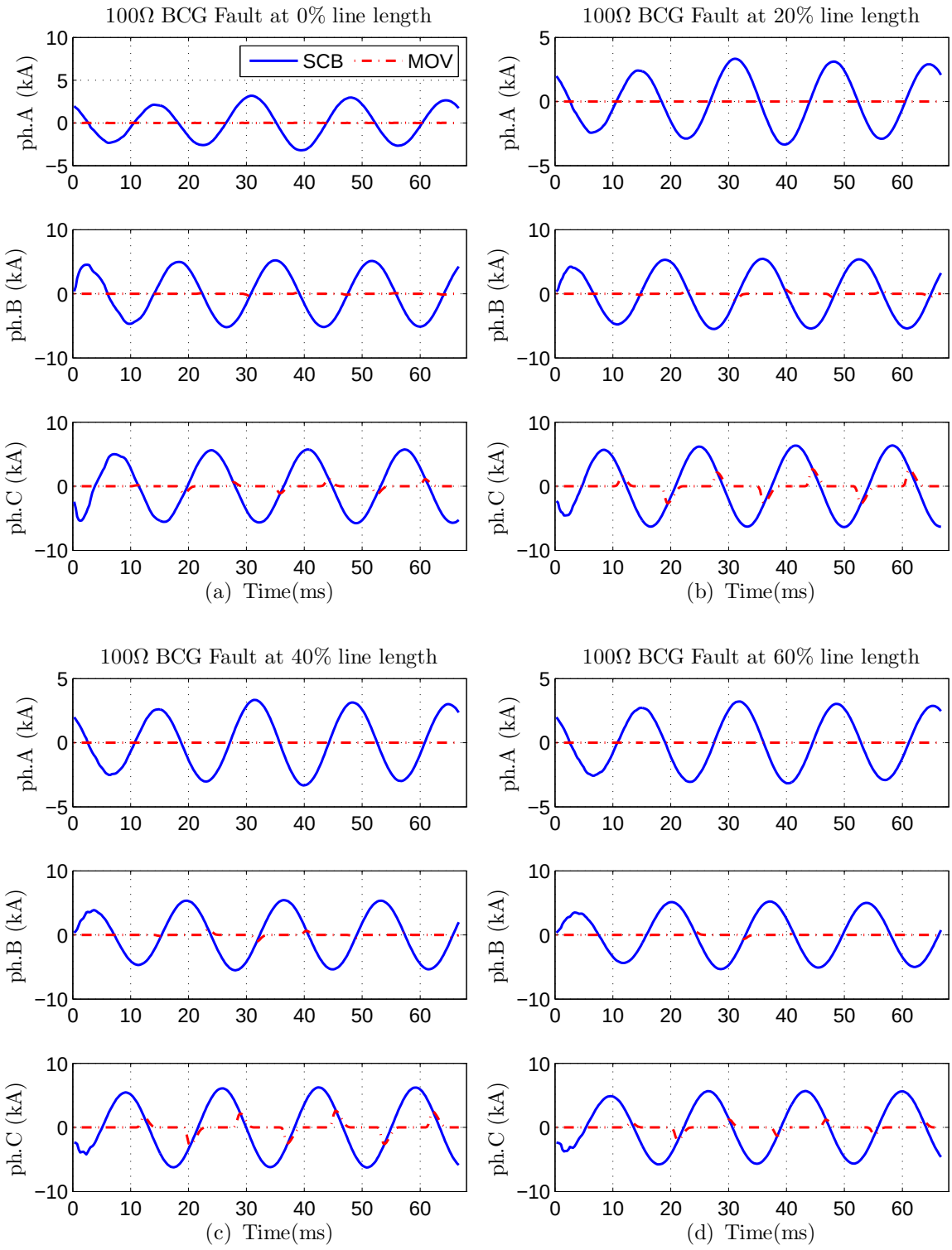

Figure C.6: The total current flowing though SCB, and the MOV current for 100Ω BCG faults at various points in an SCCTL measured as percent of the line length from Bus S: (a) 0%, (b) 20%, (c) 40%, (d) 60%.

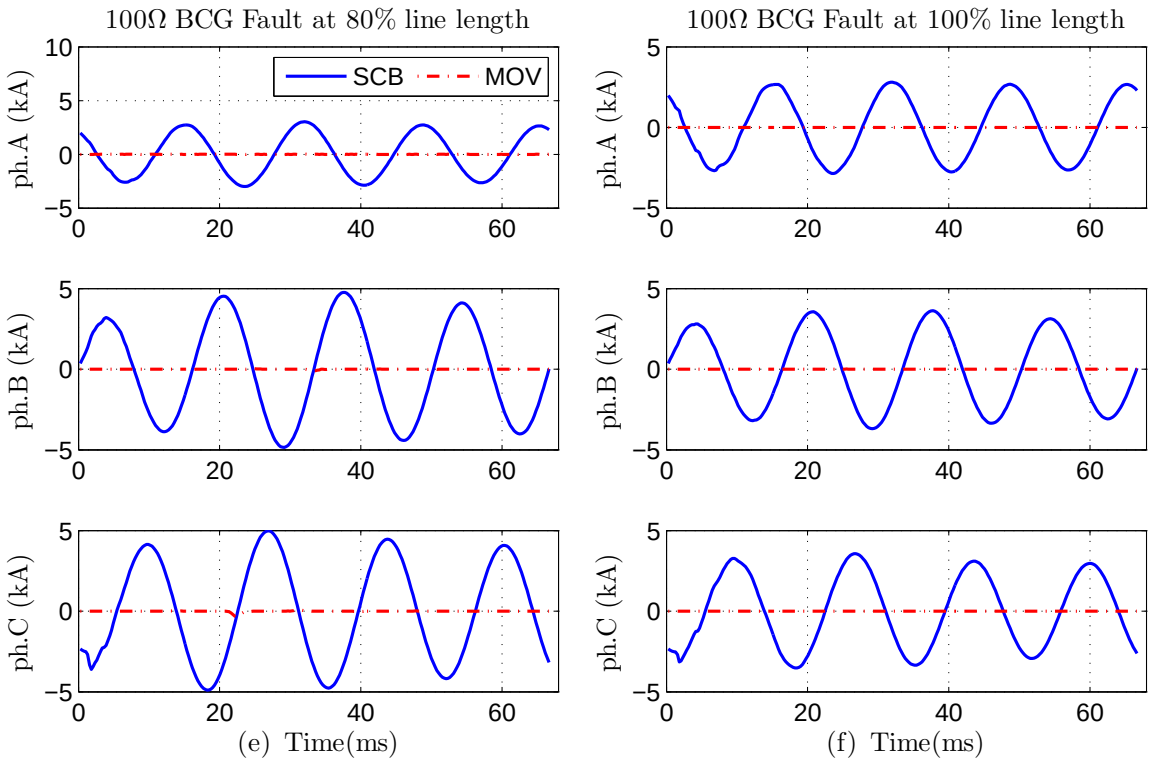

Figure C.6 (Continued): The total current flowing though SCB, and the MOV current for 100Ω BCG faults at various points in an SCCTL measured as percent of the line length from Bus S: (e) 80%, and (f) 100%.

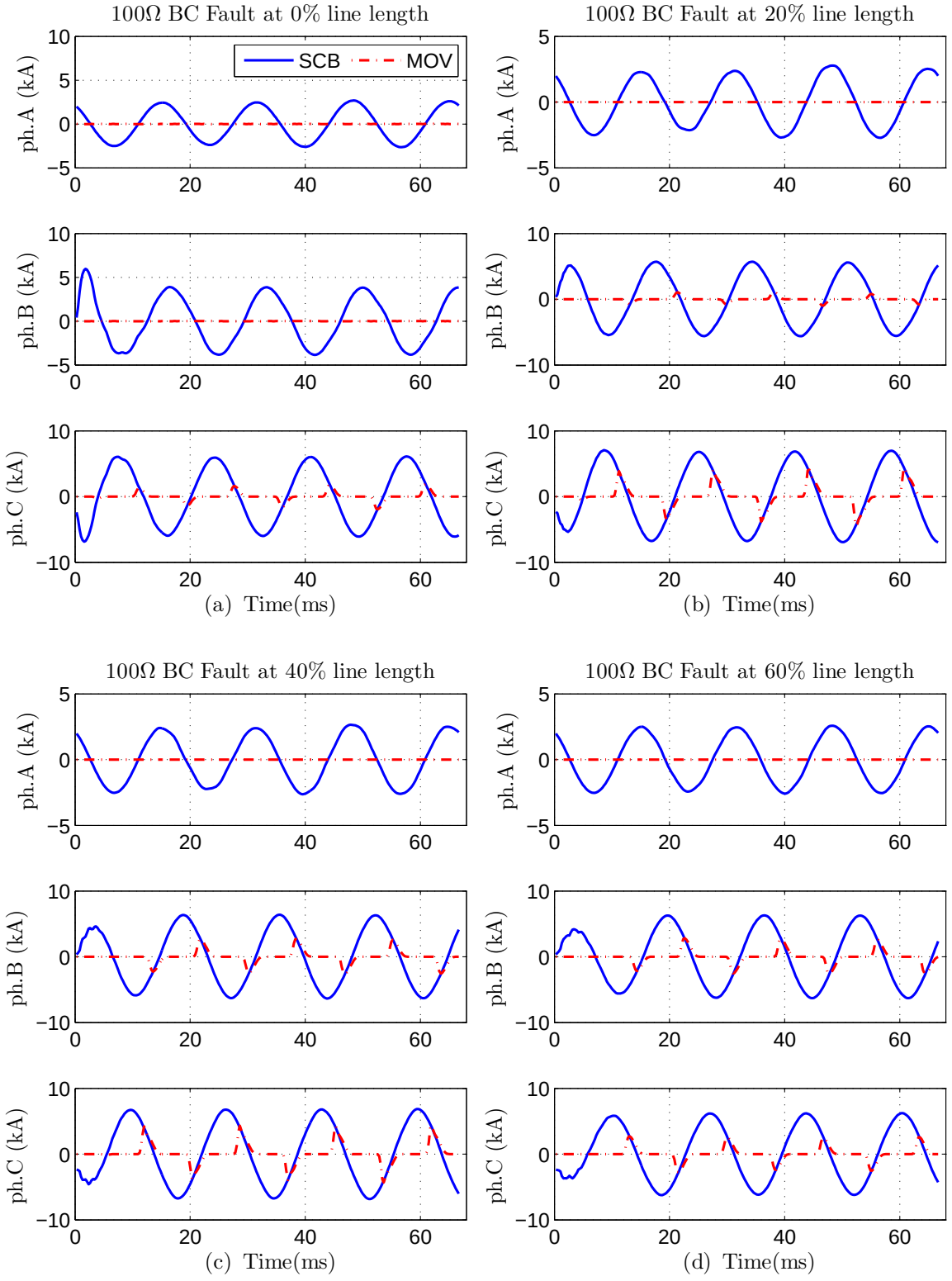

Figure C.7: The total current flowing though SCB, and the MOV current for 100Ω BC faults at various points in an SCCTL measured as percent of the line length from Bus S: (a) 0%, (b) 20%, (c) 40%, (d) 60%.

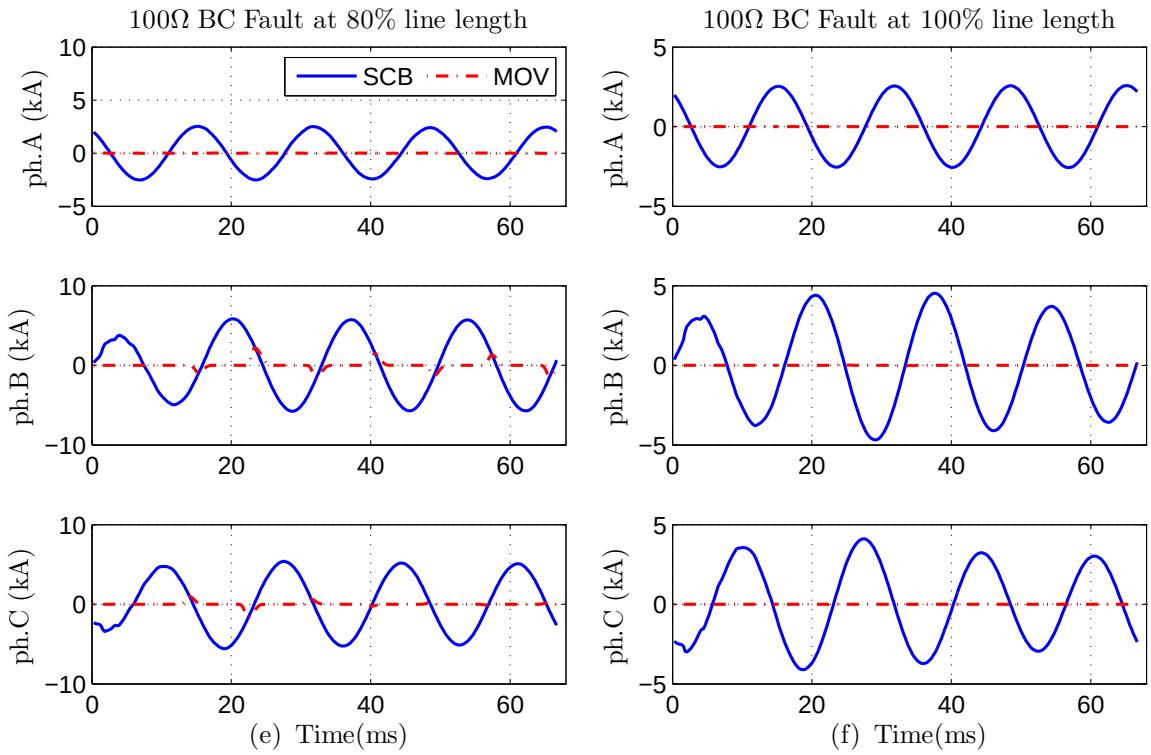

Figure C.7 (Continued): The total current flowing though SCB, and the MOV current for 100Ω BC faults at various points in an SCCTL measured as percent of the line length from Bus S: (e) 80%, and (f) 100%.

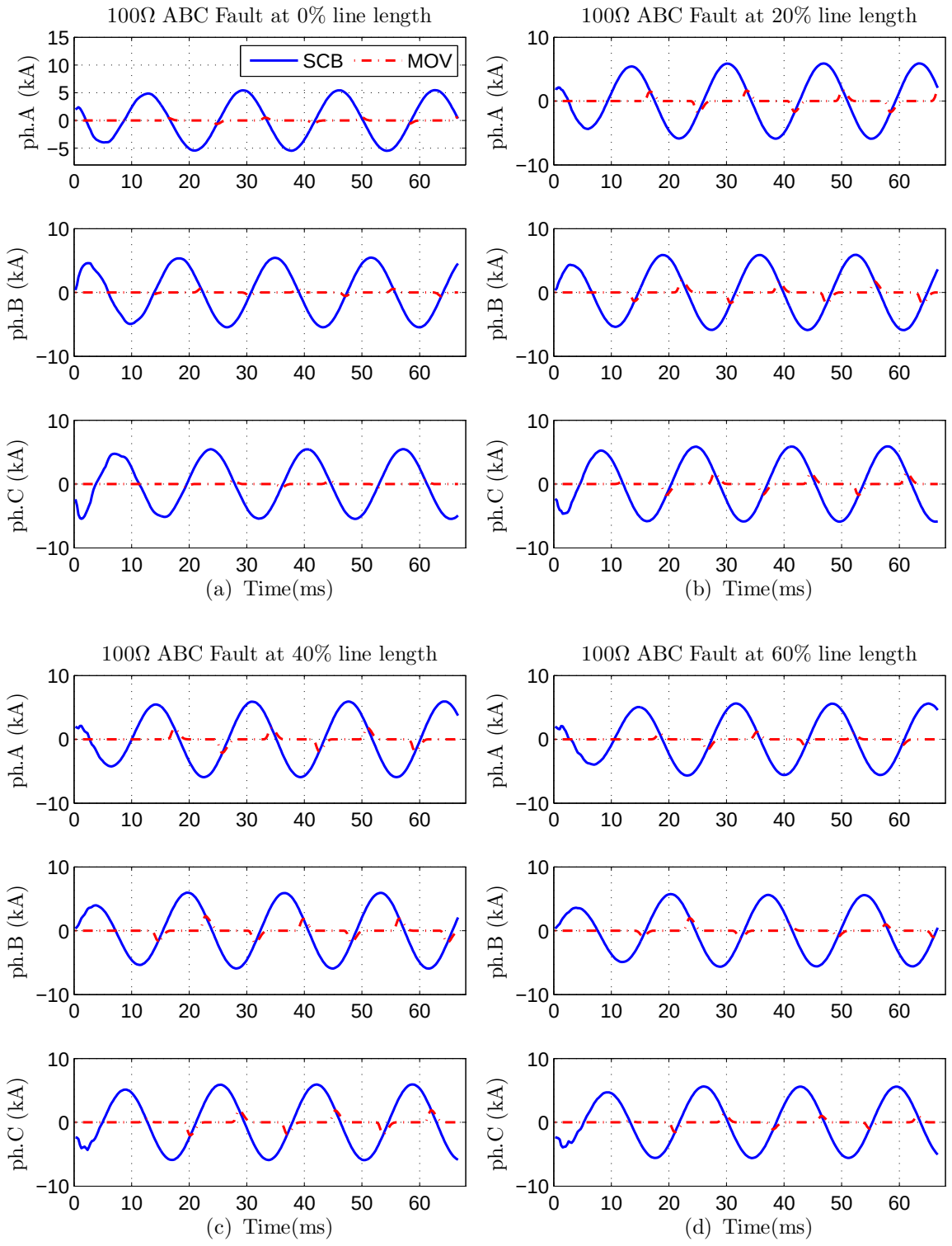

Figure C.8: The total current flowing though SCB, and the MOV current for 100Ω ABC faults at various points in an SCCTL measured as percent of the line length from Bus S: (a) 0%, (b) 20%, (c) 40%, (d) 60%.

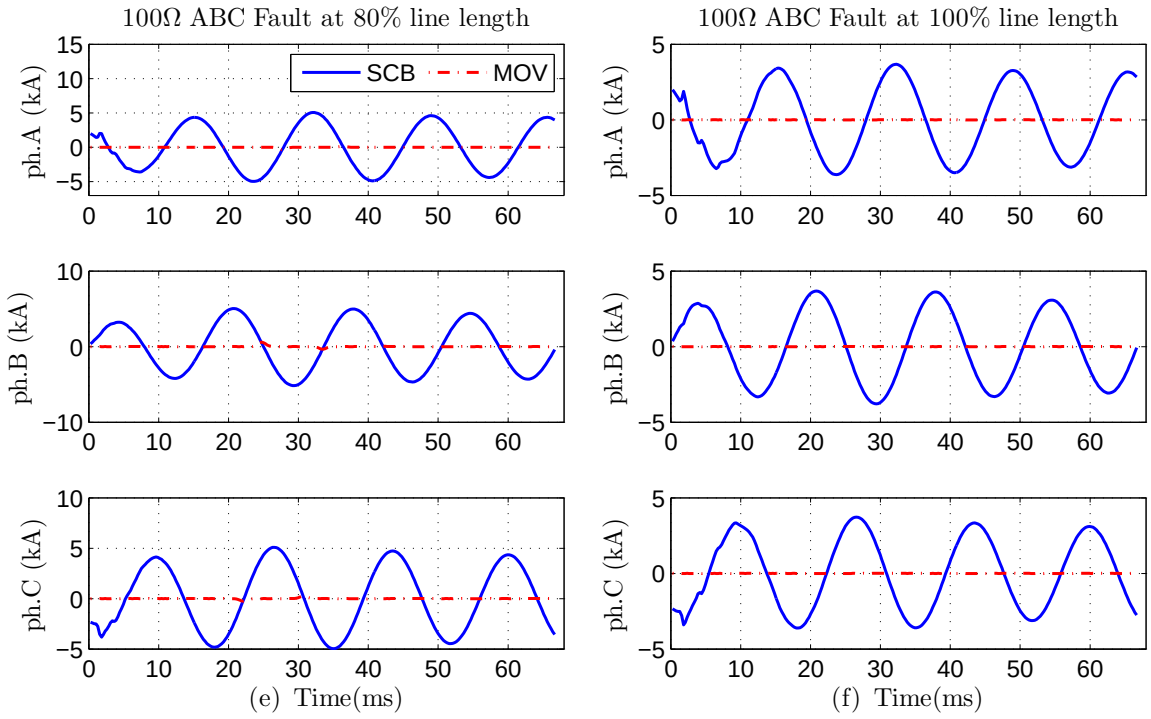

Figure C.8 (Continued): The total current flowing though SCB, and the MOV current for 100Ω ABC faults at various points in an SCCTL measured as percent of the line length from Bus S: (e) 80%, and (f) 100%.

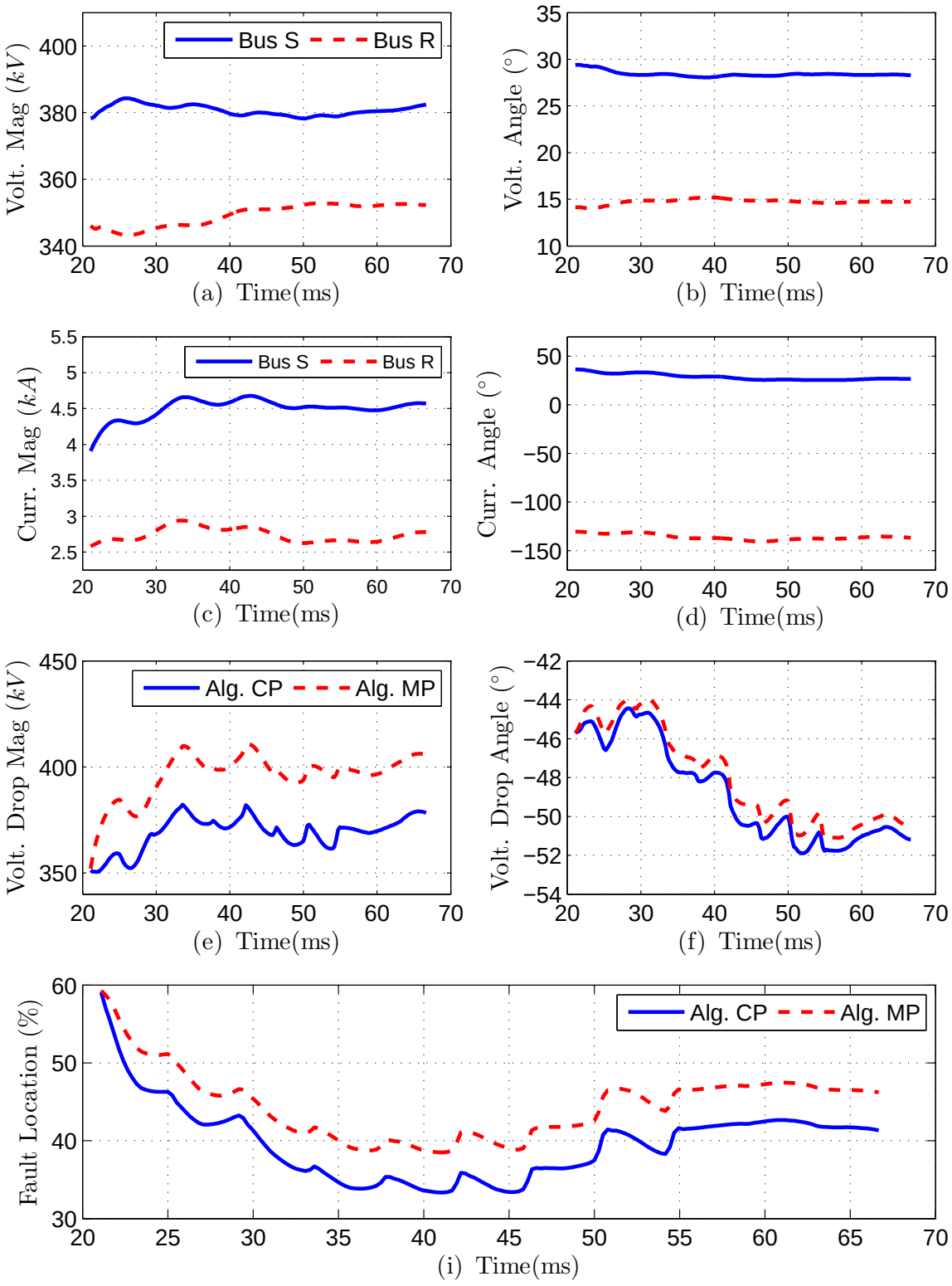

Figure C.9: Various estimated phasors for the fault scenario of a solid AG fault at 40% line length measured from Bus S: (a)-(b) positive sequence voltage magnitude and phase angle, (c)-(d) positive sequence current magnitude and phase angle, (e)-(f) magnitude and phase angle of the positive sequence of voltage drop across SCB as estimated by Algorithms CP and MP, (f) fault location results yielded by Algorithms CP and MP.

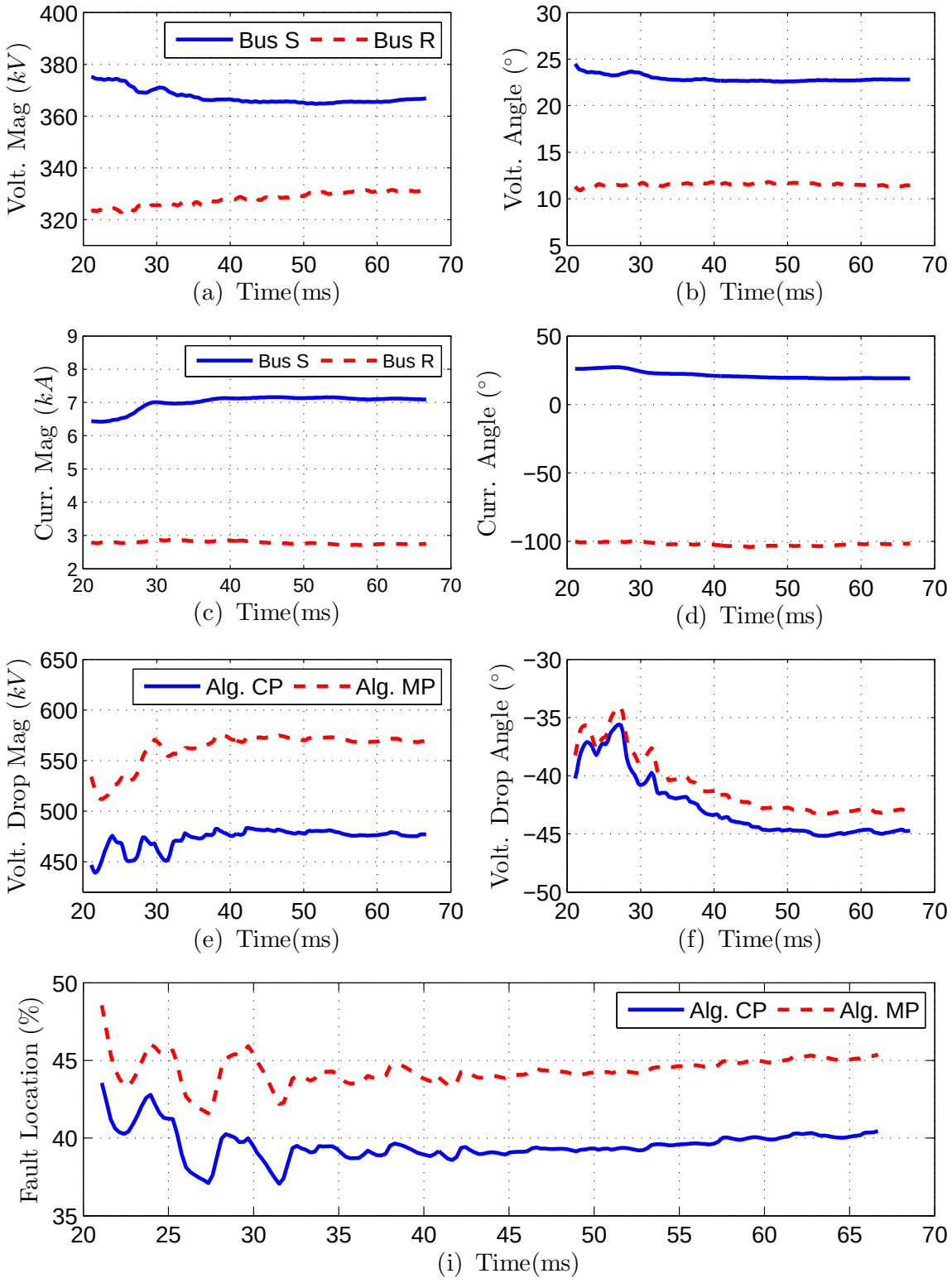

Figure C.10: Various estimated phasors for the fault scenario of a solid BCG fault at 40% line length measured from Bus S: (a)-(b) positive sequence voltage magnitude and phase angle, (c)-(d) positive sequence current magnitude and phase angle, (e)-(f) magnitude and phase angle of the positive sequence of voltage drop across SCB as estimated by Algorithms CP and MP, (f) fault location results yielded by Algorithms CP and MP.

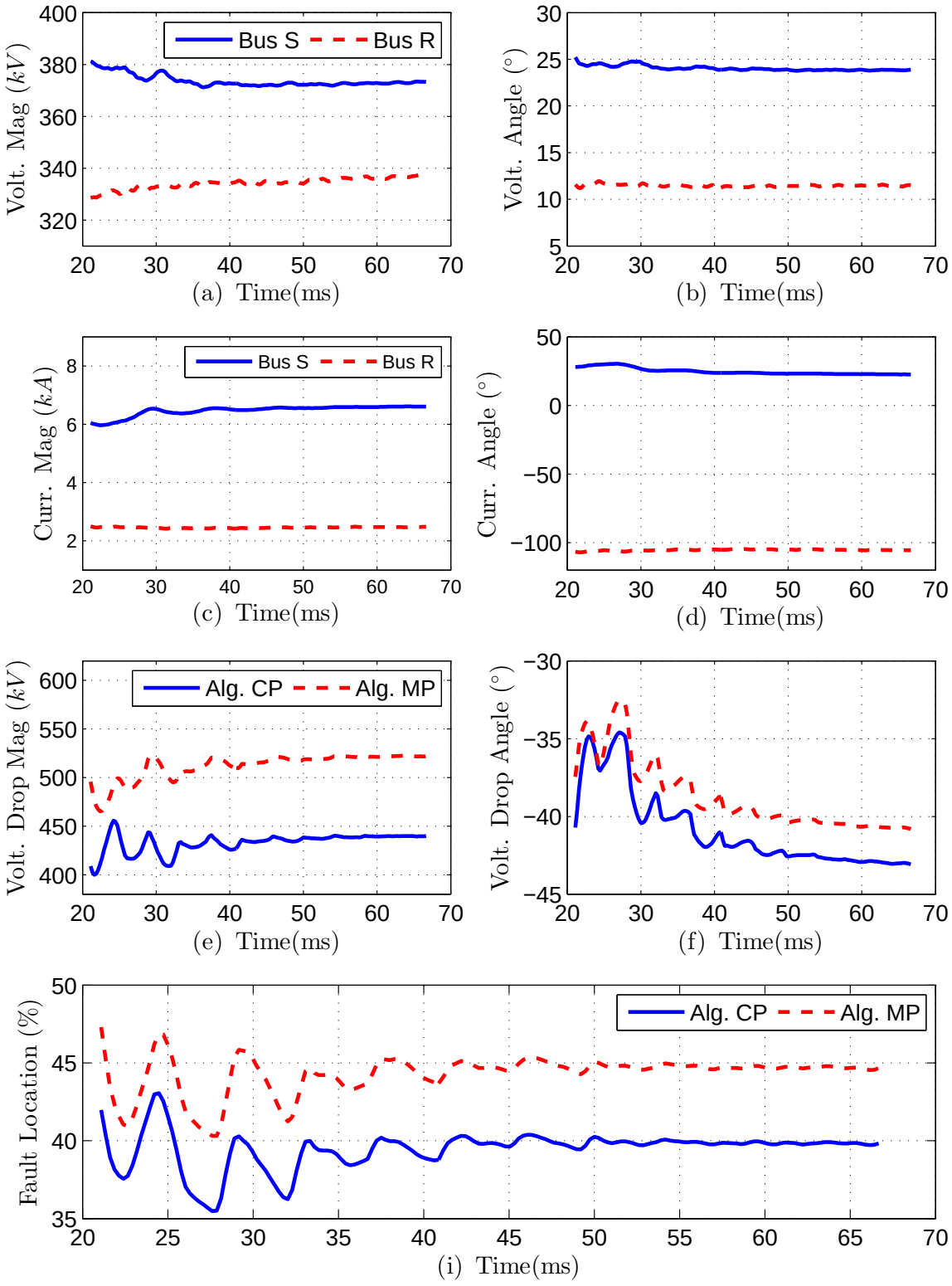

Figure C.11: Various estimated phasors for the fault scenario of a solid BC fault at 40% line length measured from Bus S: (a)-(b) positive sequence voltage magnitude and phase angle, (c)-(d) positive sequence current magnitude and phase angle, (e)-(f) magnitude and phase angle of the positive sequence of voltage drop across SCB as estimated by Algorithms CP and MP, (f) fault location results yielded by Algorithms CP and MP.

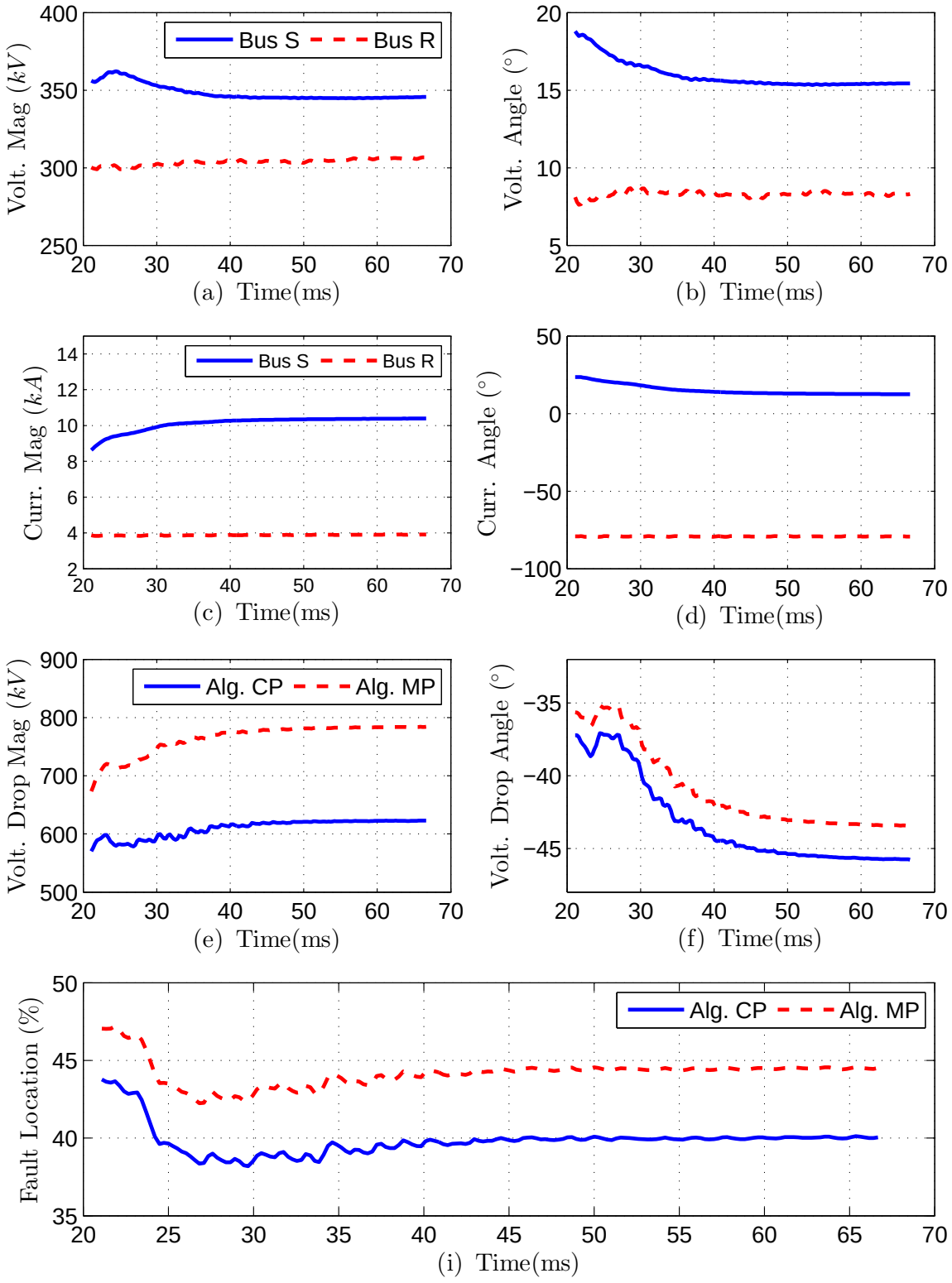

Figure C.12: Various estimated phasors for the fault scenario of a solid ABC fault at 40% line length measured from Bus S: (a)-(b) positive sequence voltage magnitude and phase angle, (c)-(d) positive sequence current magnitude and phase angle, (e)-(f) magnitude and phase angle of the positive sequence of voltage drop across SCB as estimated by Algorithms CP and MP, (f) fault location results yielded by Algorithms CP and MP.

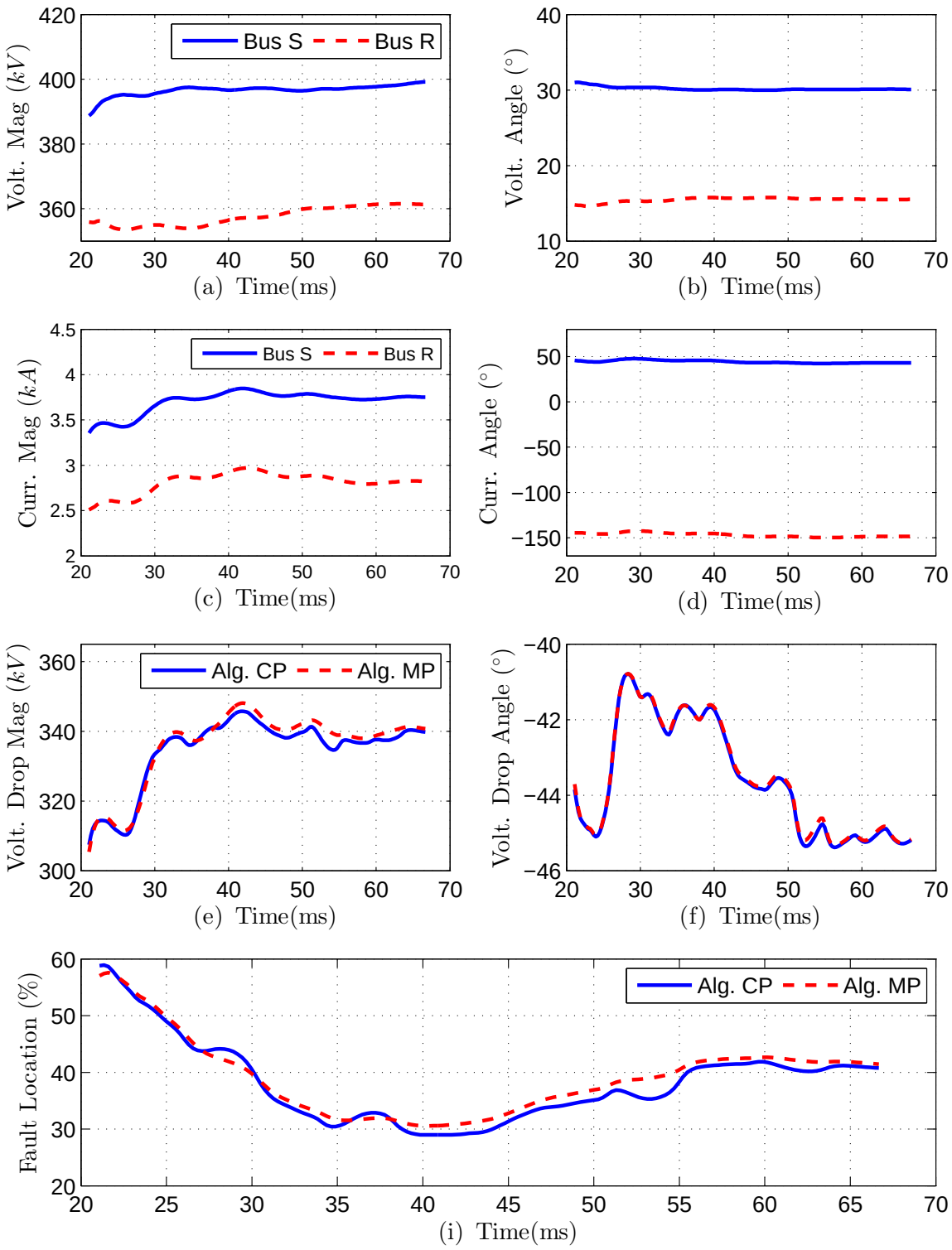

Figure C.13: Various estimated phasors for the fault scenario of a 100Ω AG fault at 40% line length measured from Bus S: (a)-(b) positive sequence voltage magnitude and phase angle, (c)-(d) positive sequence current magnitude and phase angle, (e)-(f) magnitude and phase angle of the positive sequence of voltage drop across SCB as estimated by Algorithms CP and MP, (f) fault location results yielded by Algorithms CP and MP.

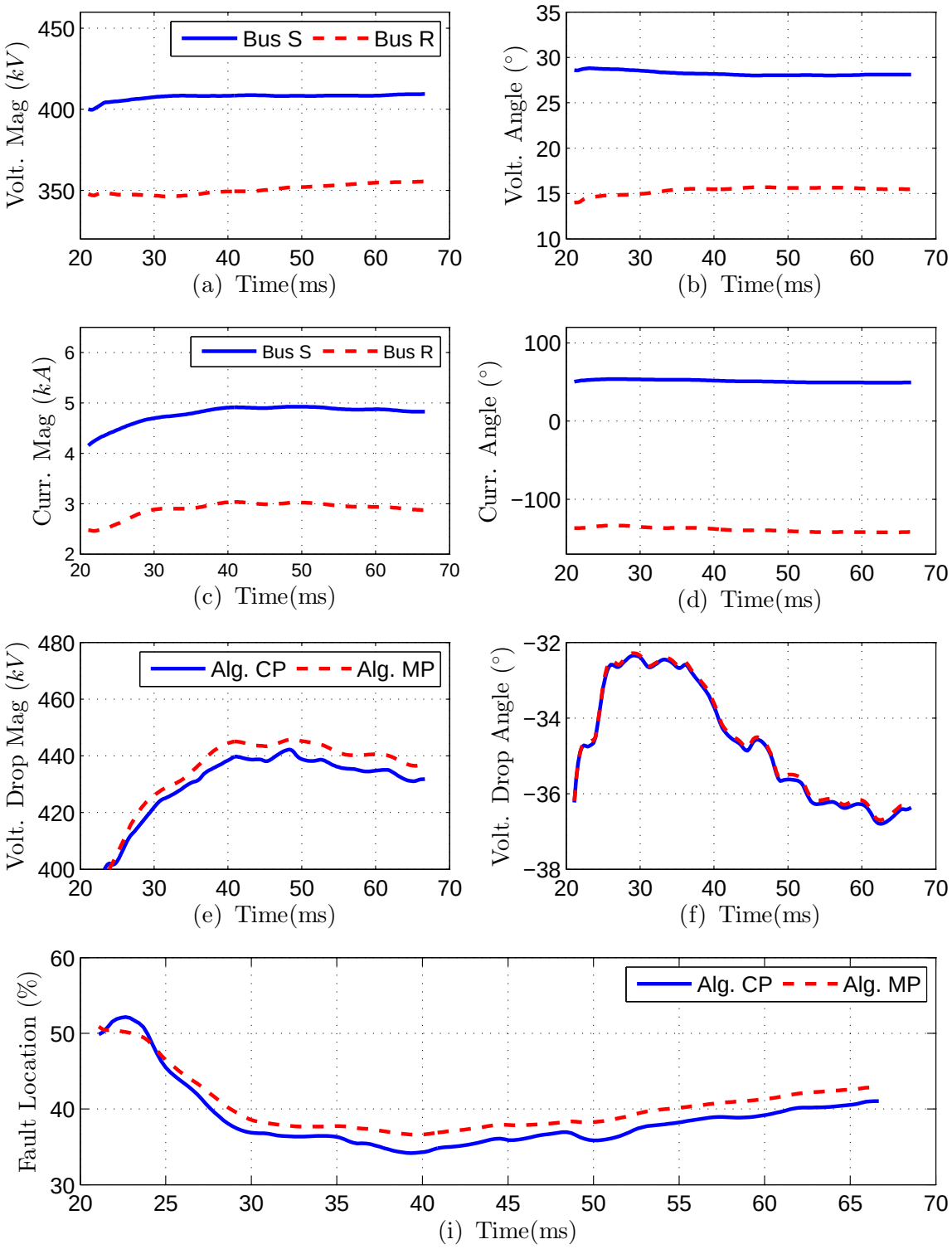

Figure C.14: Various estimated phasors for the fault scenario of a 100Ω BCG fault at 40% line length measured from Bus S: (a)-(b) positive sequence voltage magnitude and phase angle, (c)-(d) positive sequence current magnitude and phase angle, (e)-(f) magnitude and phase angle of the positive sequence of voltage drop across SCB as estimated by Algorithms CP and MP, (f) fault location results yielded by Algorithms CP and MP.

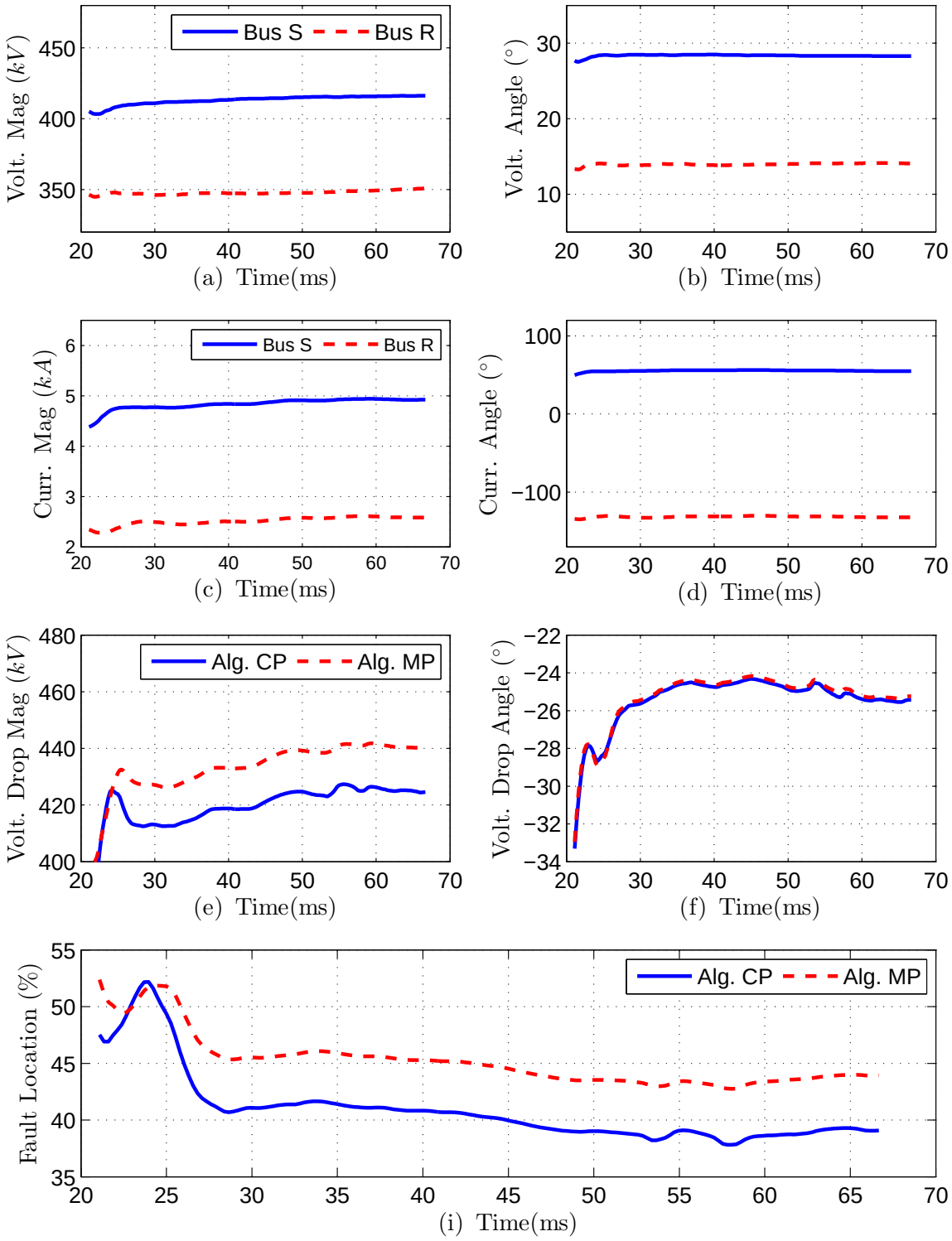

Figure C.15: Various estimated phasors for the fault scenario of a 100Ω BC fault at 40% line length measured from Bus S: (a)-(b) positive sequence voltage magnitude and phase angle, (c)-(d) positive sequence current magnitude and phase angle, (e)-(f) magnitude and phase angle of the positive sequence of voltage drop across SCB as estimated by Algorithms CP and MP, (f) fault location results yielded by Algorithms CP and MP.

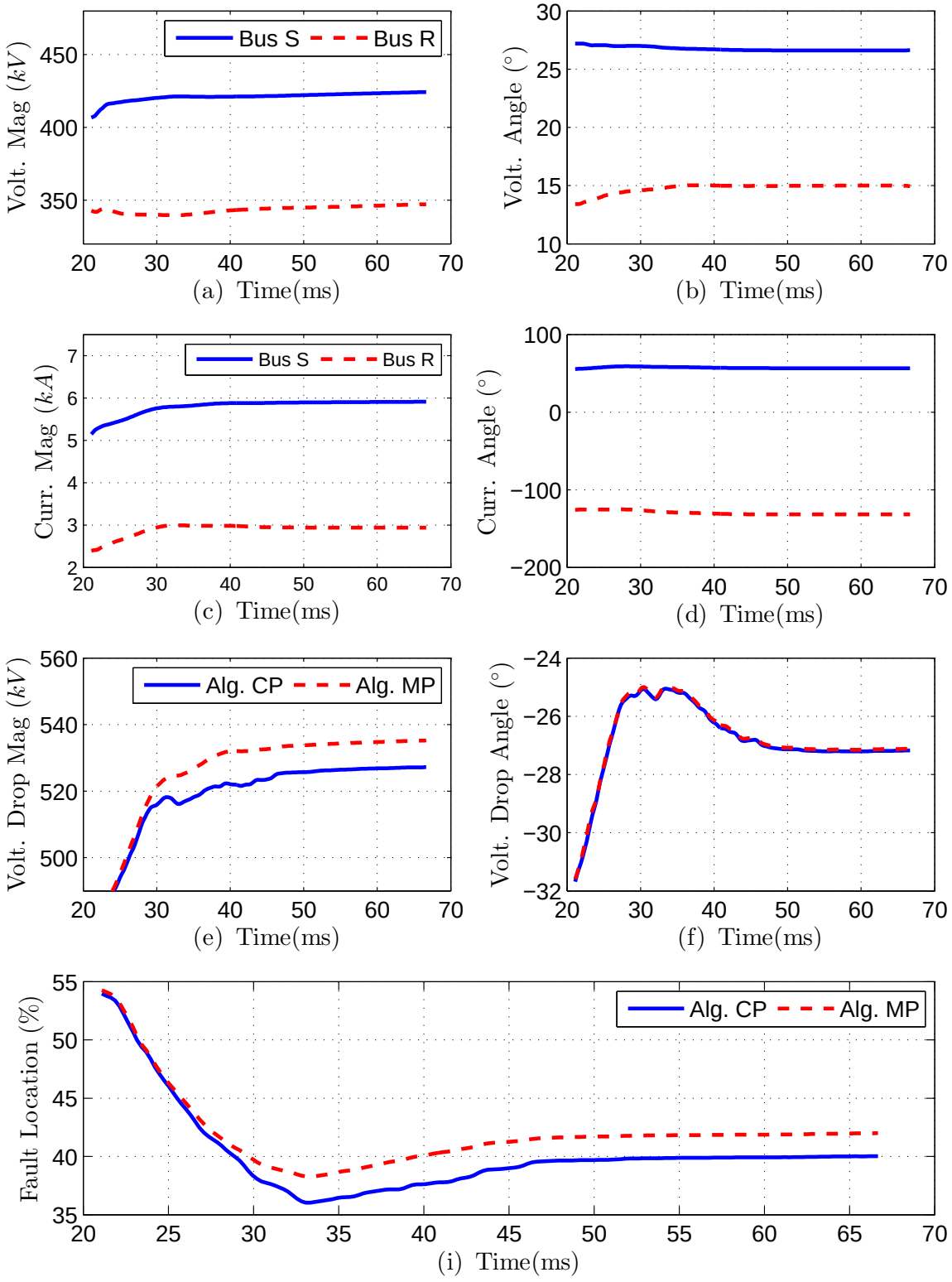

Figure C.16: Various estimated phasors for the fault scenario of a 100Ω ABC fault at 40% line length measured from Bus S: (a)-(b) positive sequence voltage magnitude and phase angle, (c)-(d) positive sequence current magnitude and phase angle, (e)-(f) magnitude and phase angle of the positive sequence of voltage drop across SCB as estimated by Algorithms CP and MP, (f) fault location results yielded by Algorithms CP and MP.

Appendix D

Additional waveforms for Chapter 7

In this appendix the first two traveling waves arriving at Bus S and Bus R in Configuration C of the SCCTL as observed in the derivative of α and β modes of the current measured at the terminals are shown. The α mode current is used for the AG and ABC faults, while β mode current is utilized for BCG and BC faults. It is due to the reason that for AG faults β mode does not see the fault. Similarly, for BCG and BC faults the α mode does not see the fault. For ABC fault all the modes see the fault, so α mode current is used for observing traveling waves for ABC faults. The time period shown in the Figures D.1 to D.12 is from the time instance of the fault occurrence to just before the arrival of third traveling wave at that terminal of the transmission line.

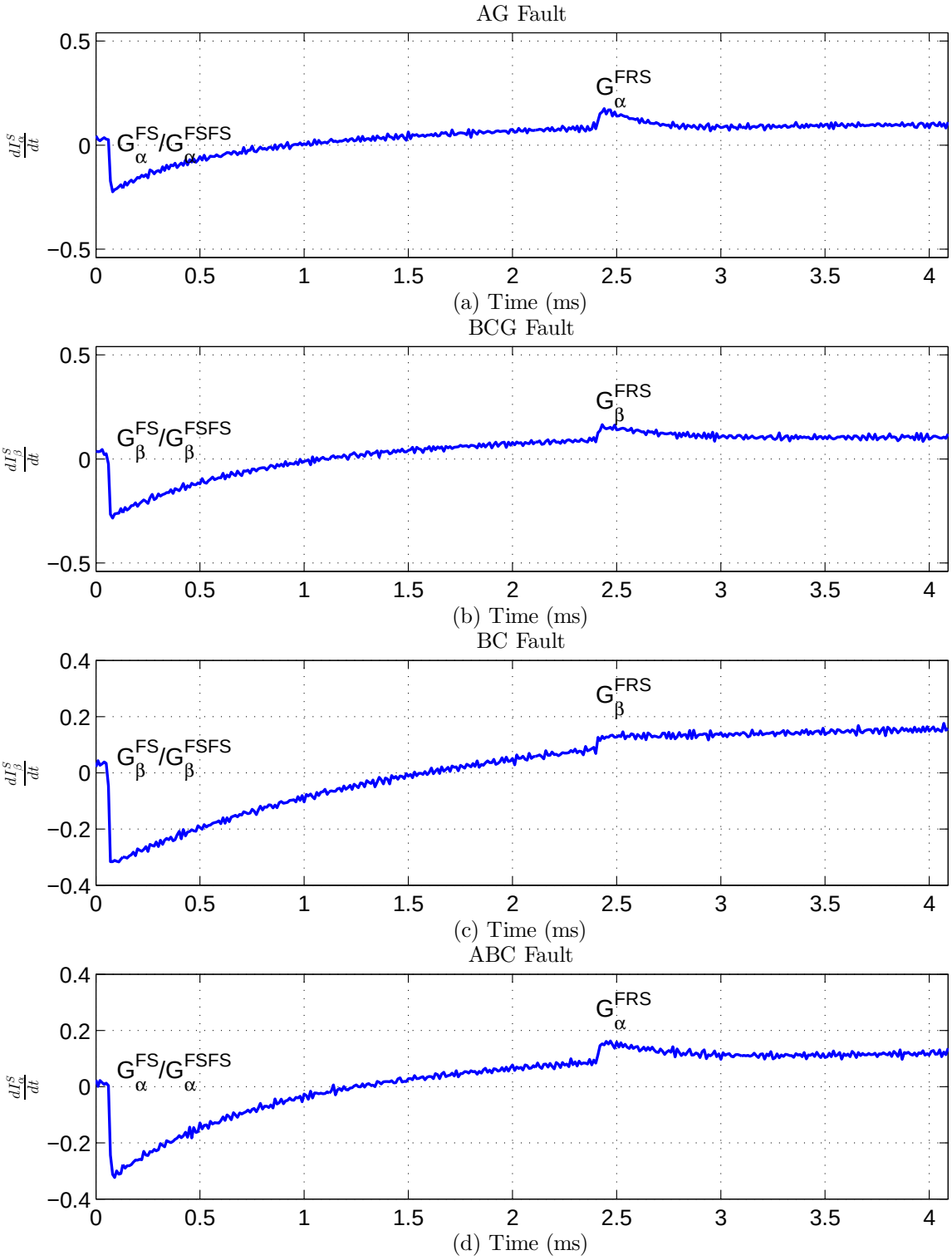

Figure D.1: The arrival of first two traveling waves at Bus S for various 50Ω faults at 0% line length measured from Bus S: (a) AG fault (α-mode), (b) BCG fault (β-mode), (c) BC fault (β-mode), (d) ABC fault (α-mode).

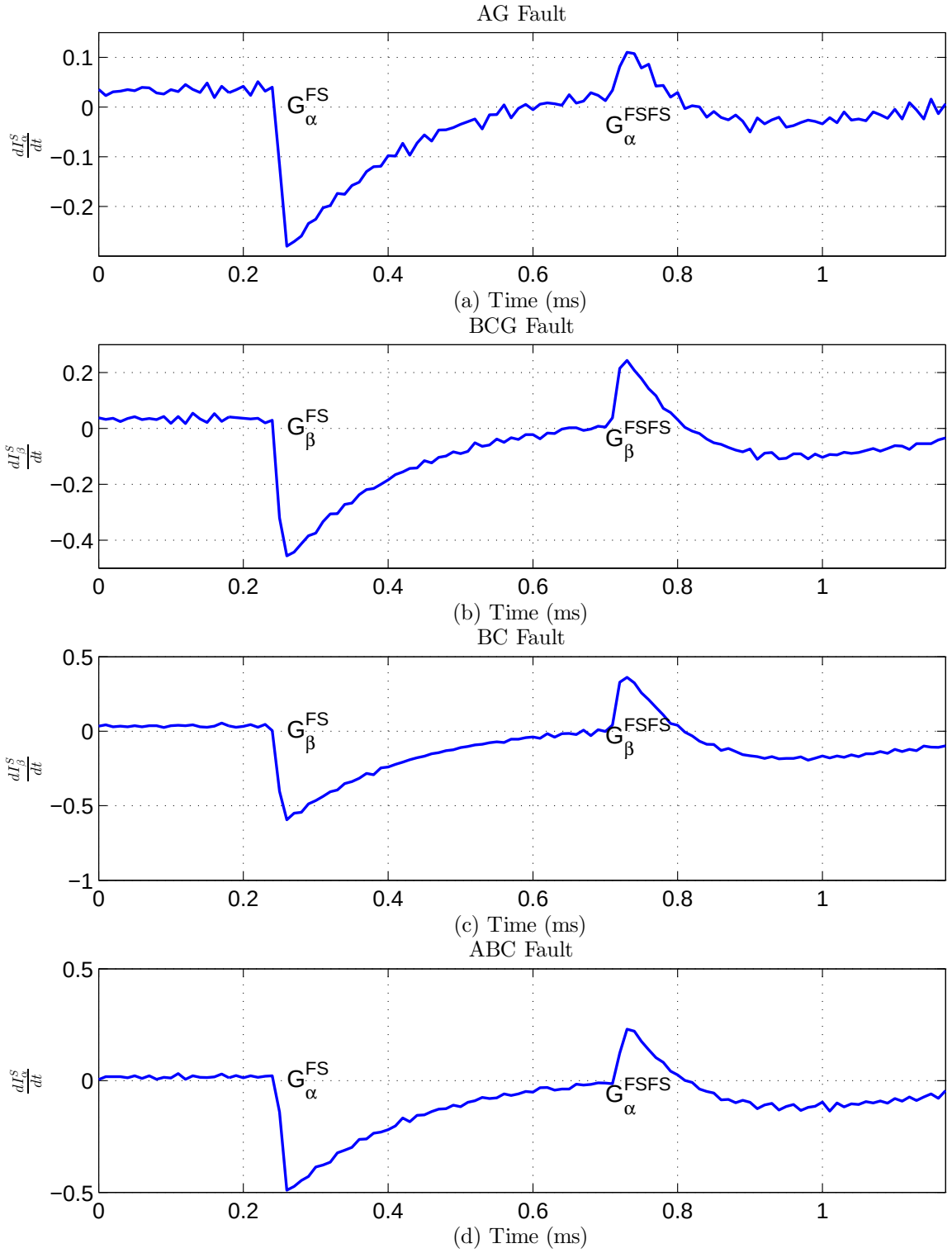

Figure D.2: The arrival of first two traveling waves at Bus S for various 50Ω faults at 20% line length measured from Bus S: (a) AG fault (α-mode), (b) BCG fault (β-mode), (c) BC fault (β-mode), (d) ABC fault (α-mode).

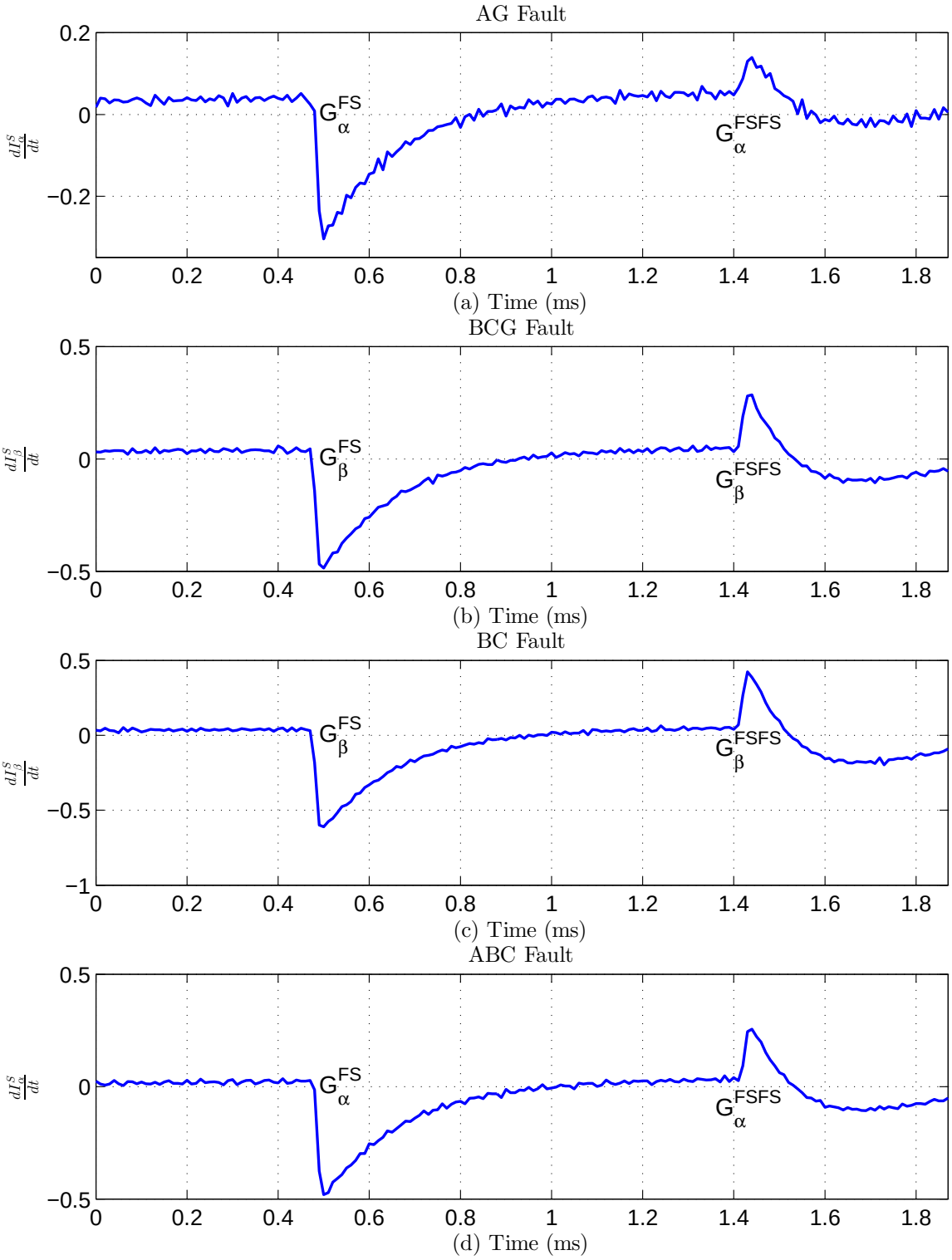

Figure D.3: The arrival of first two traveling waves at Bus S for various 50Ω faults at 40% line length measured from Bus S: (a) AG fault (α-mode), (b) BCG fault (β-mode), (c) BC fault (β-mode), (d) ABC fault (α-mode).

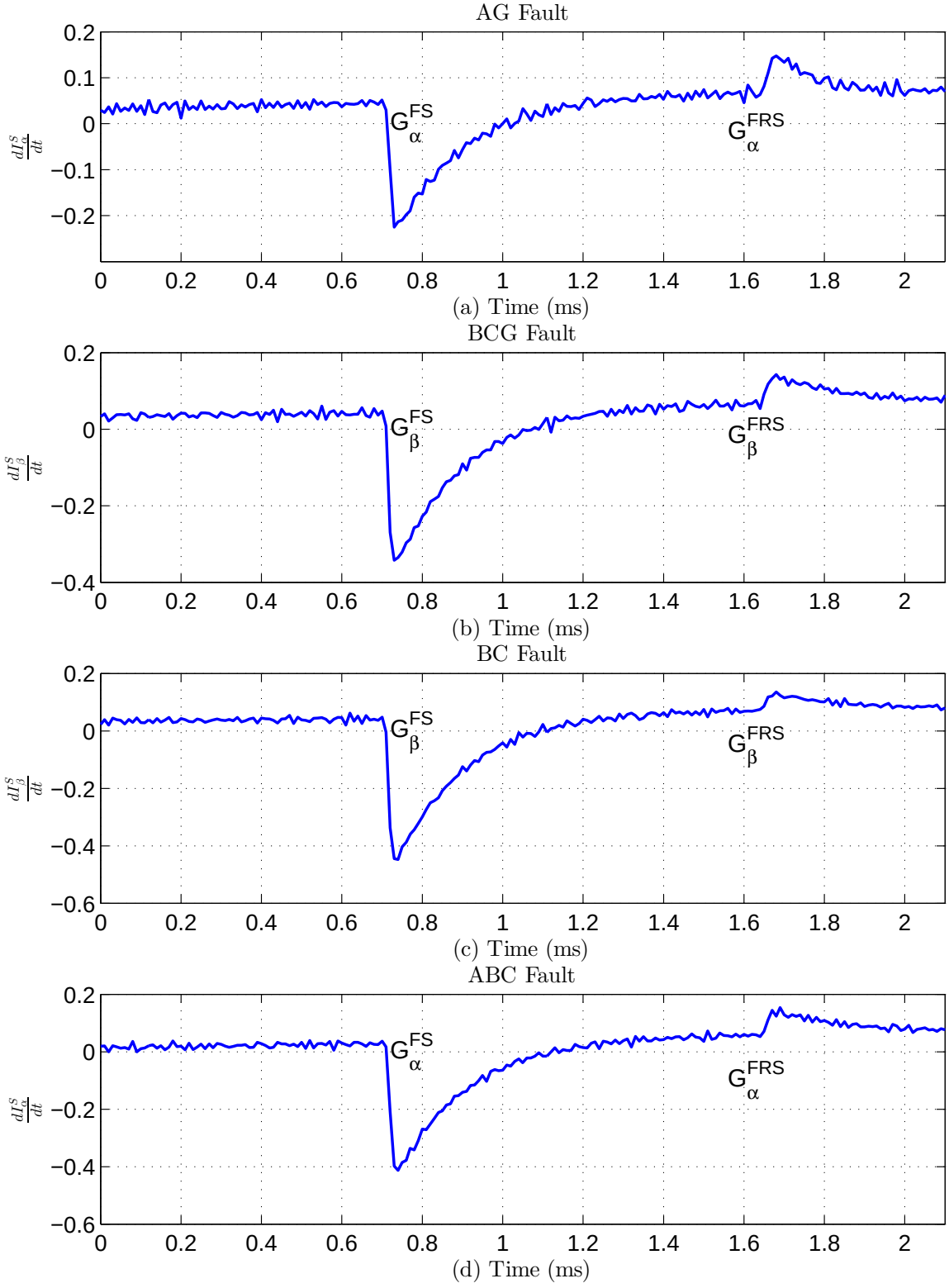

Figure D.4: The arrival of first two traveling waves at Bus S for various 50Ω faults at 60% line length measured from Bus S: (a) AG fault (α-mode), (b) BCG fault (β-mode), (c) BC fault (β-mode), (d) ABC fault (α-mode).

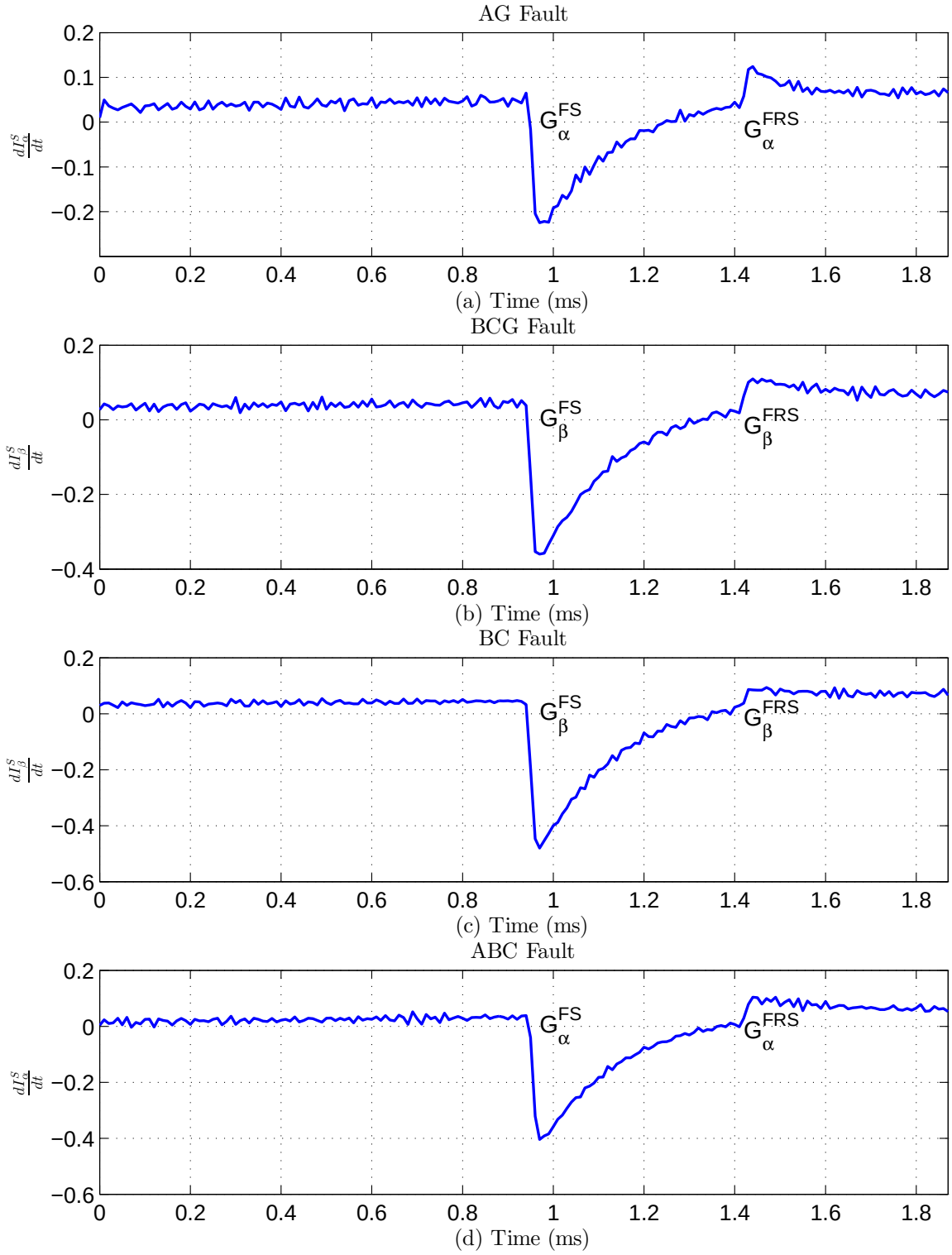

Figure D.5: The arrival of first two traveling waves at Bus S for various 50Ω faults at 80% line length measured from Bus S: (a) AG fault (α-mode), (b) BCG fault (β-mode), (c) BC fault (β-mode), (d) ABC fault (α-mode).

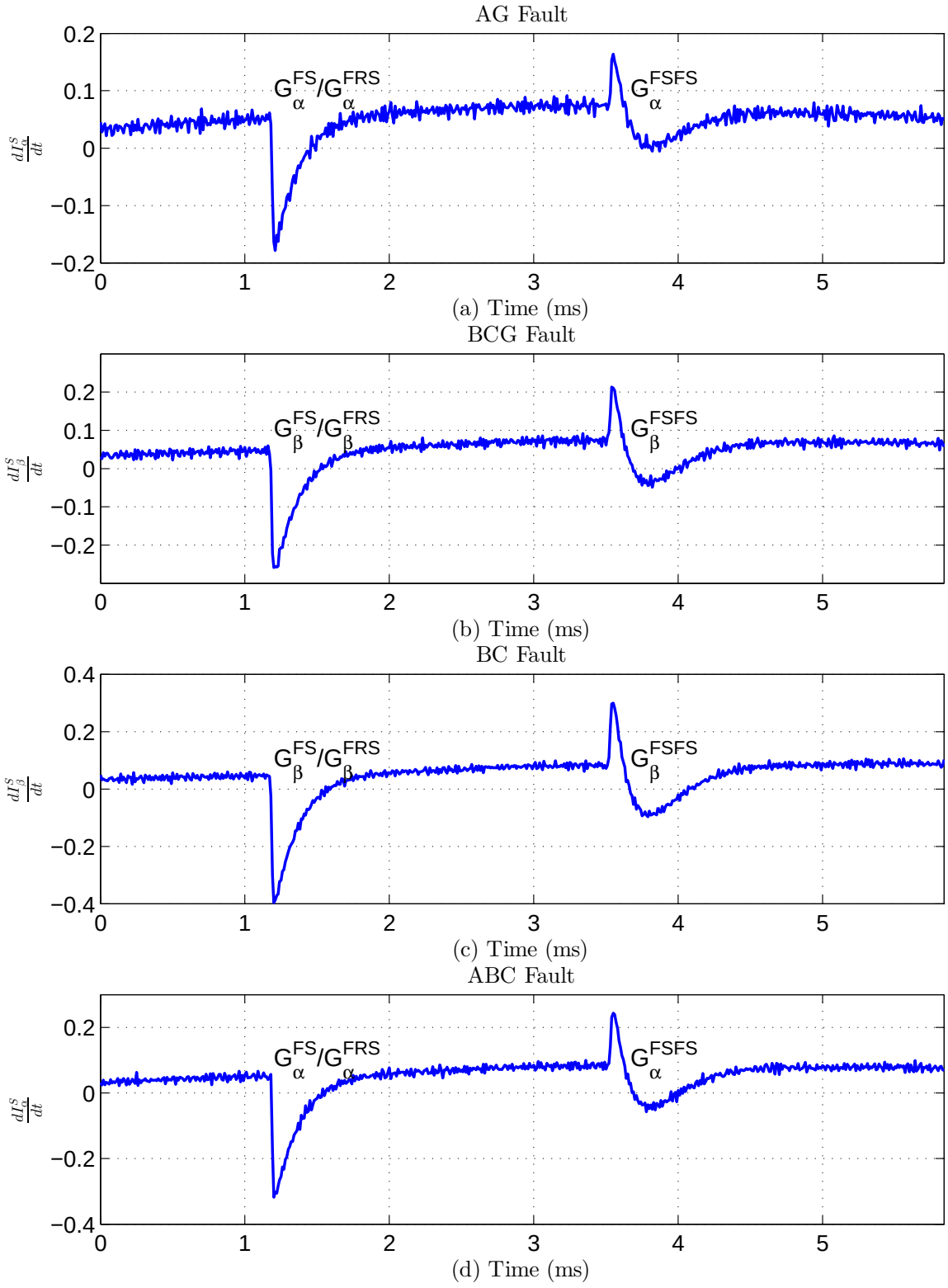

Figure D.6: The arrival of first two traveling waves at Bus S for various 50Ω faults at 100% line length measured from Bus S: (a) AG fault (α-mode), (b) BCG fault (β-mode), (c) BC fault (β-mode), (d) ABC fault (α-mode).

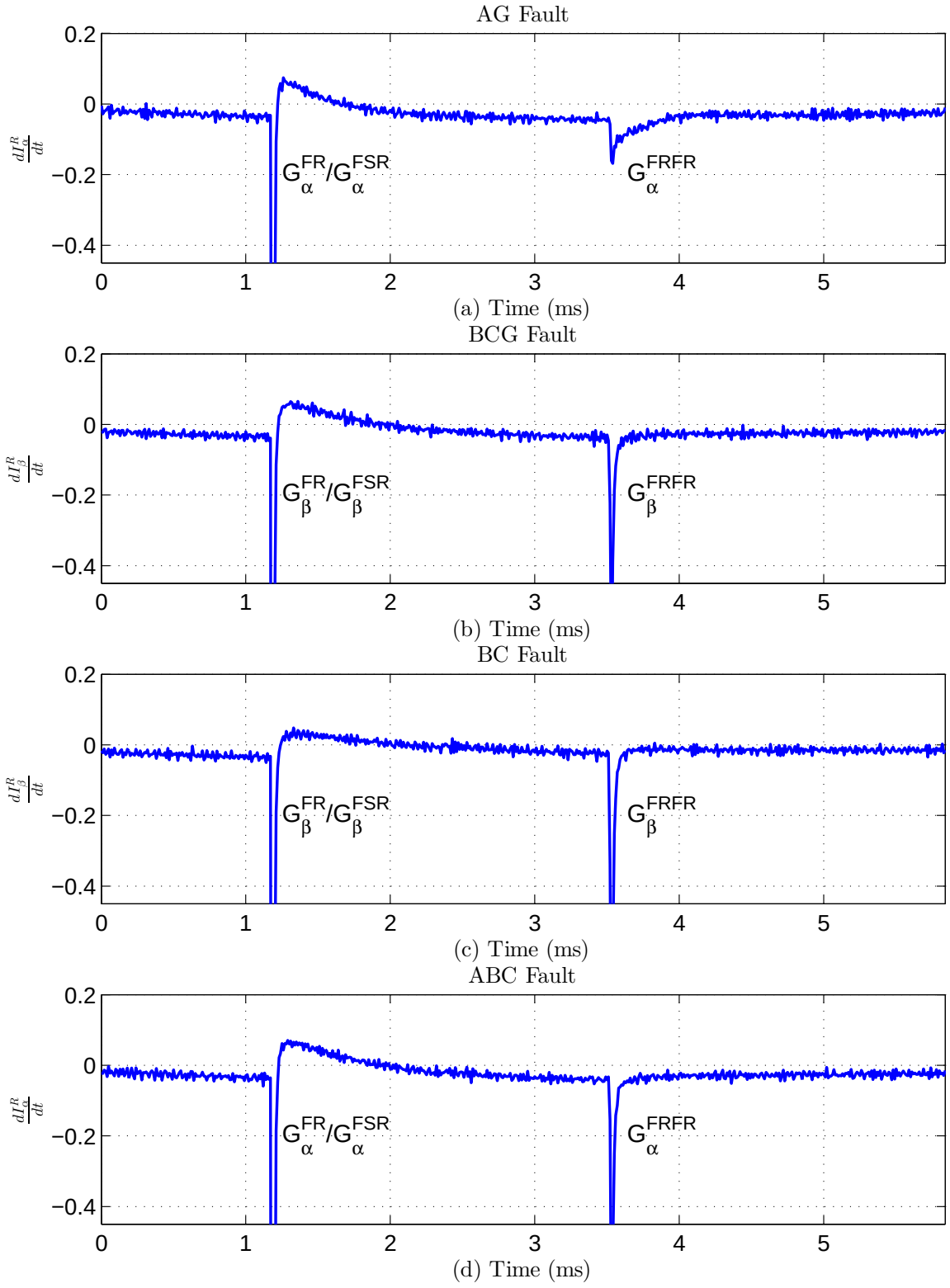

Figure D.7: The arrival of first two traveling waves at Bus R for various 50Ω faults at 0% line length measured from Bus S: (a) AG fault (α-mode), (b) BCG fault (β-mode), (c) BC fault (β-mode), (d) ABC fault (α-mode).

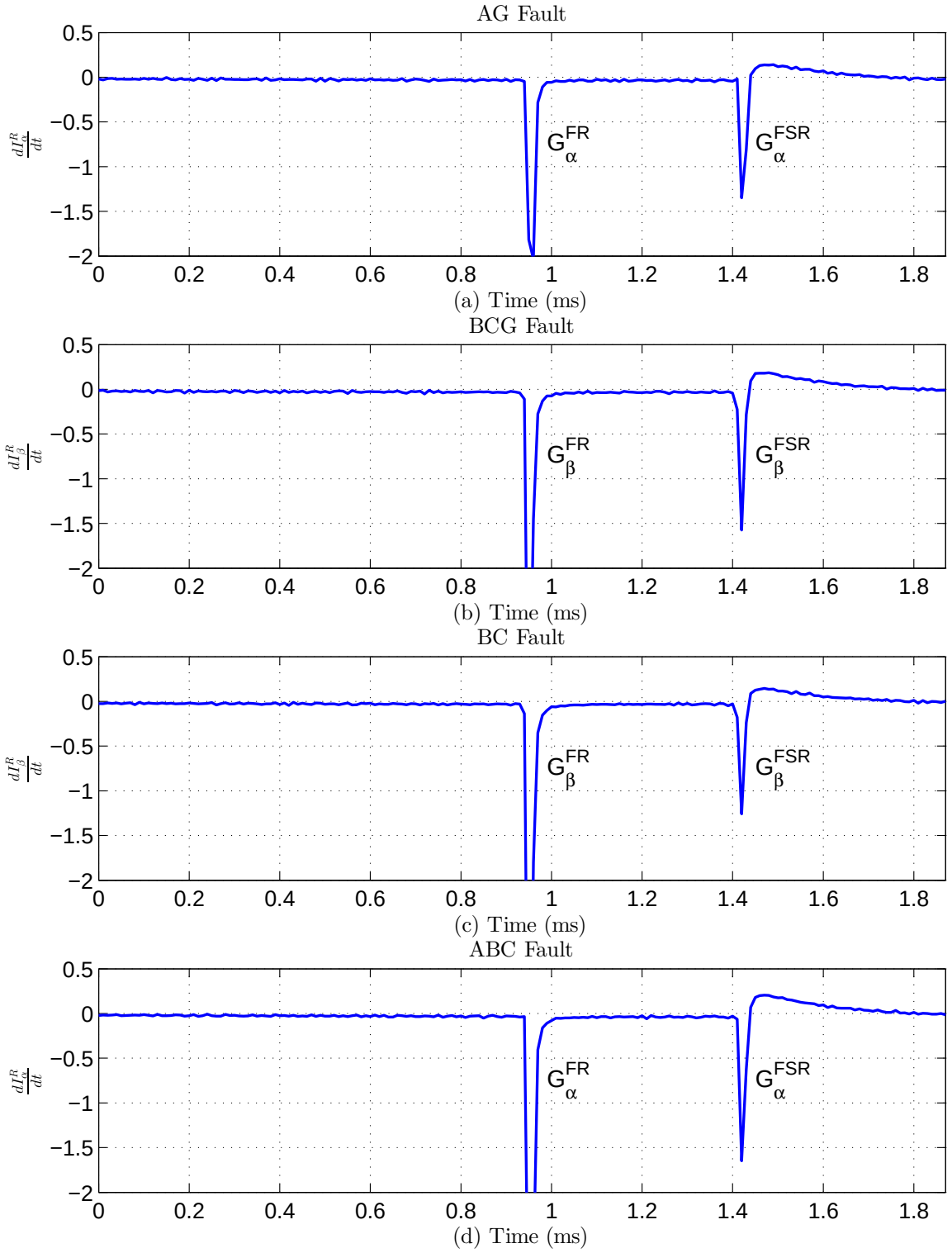

Figure D.8: The arrival of first two traveling waves at Bus R for various 50Ω faults at 20% line length measured from Bus S: (a) AG fault (α-mode), (b) BCG fault (β-mode), (c) BC fault (β-mode), (d) ABC fault (α-mode).

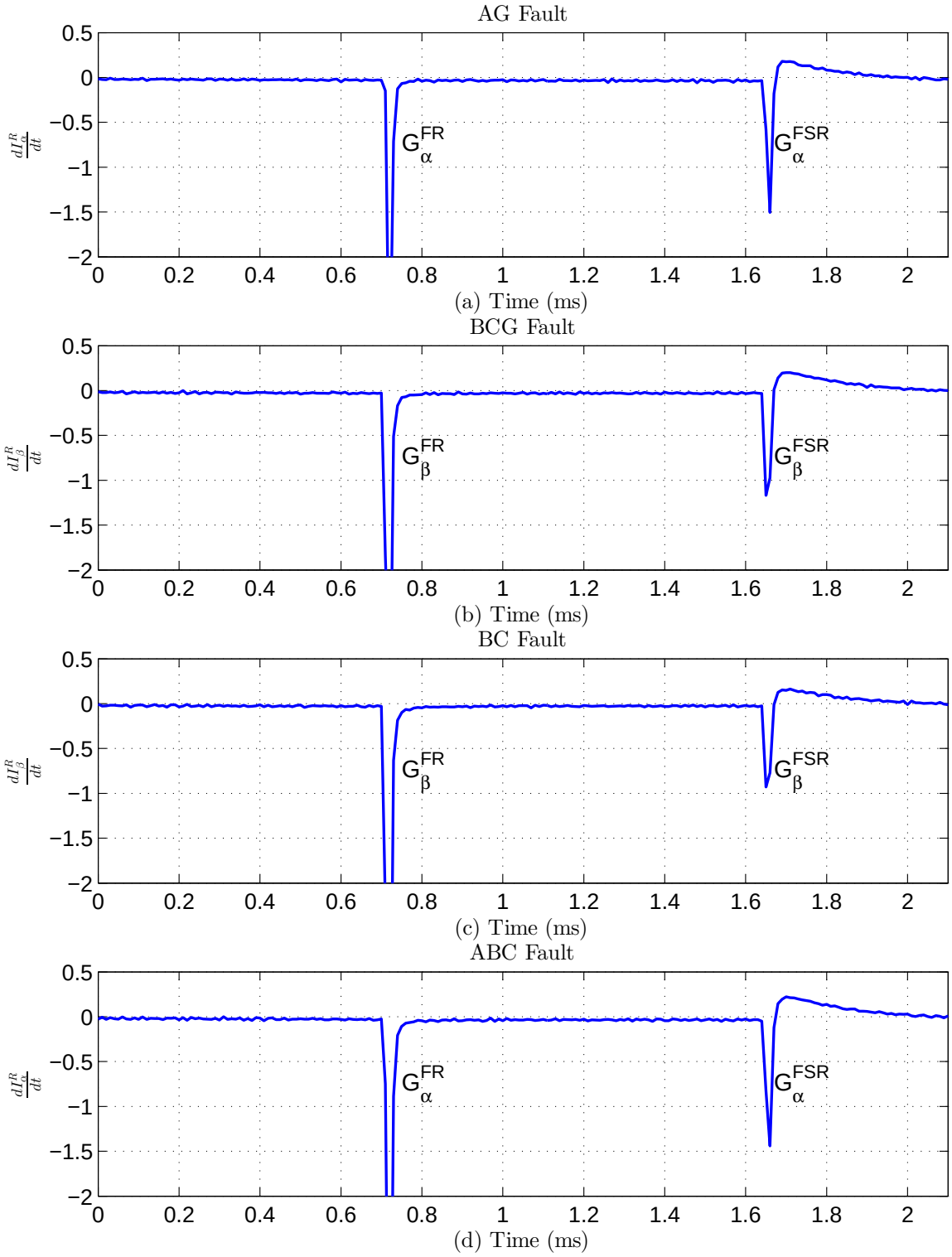

Figure D.9: The arrival of first two traveling waves at Bus R for various 50Ω faults at 40% line length measured from Bus S: (a) AG fault (α-mode), (b) BCG fault (β-mode), (c) BC fault (β-mode), (d) ABC fault (α-mode).

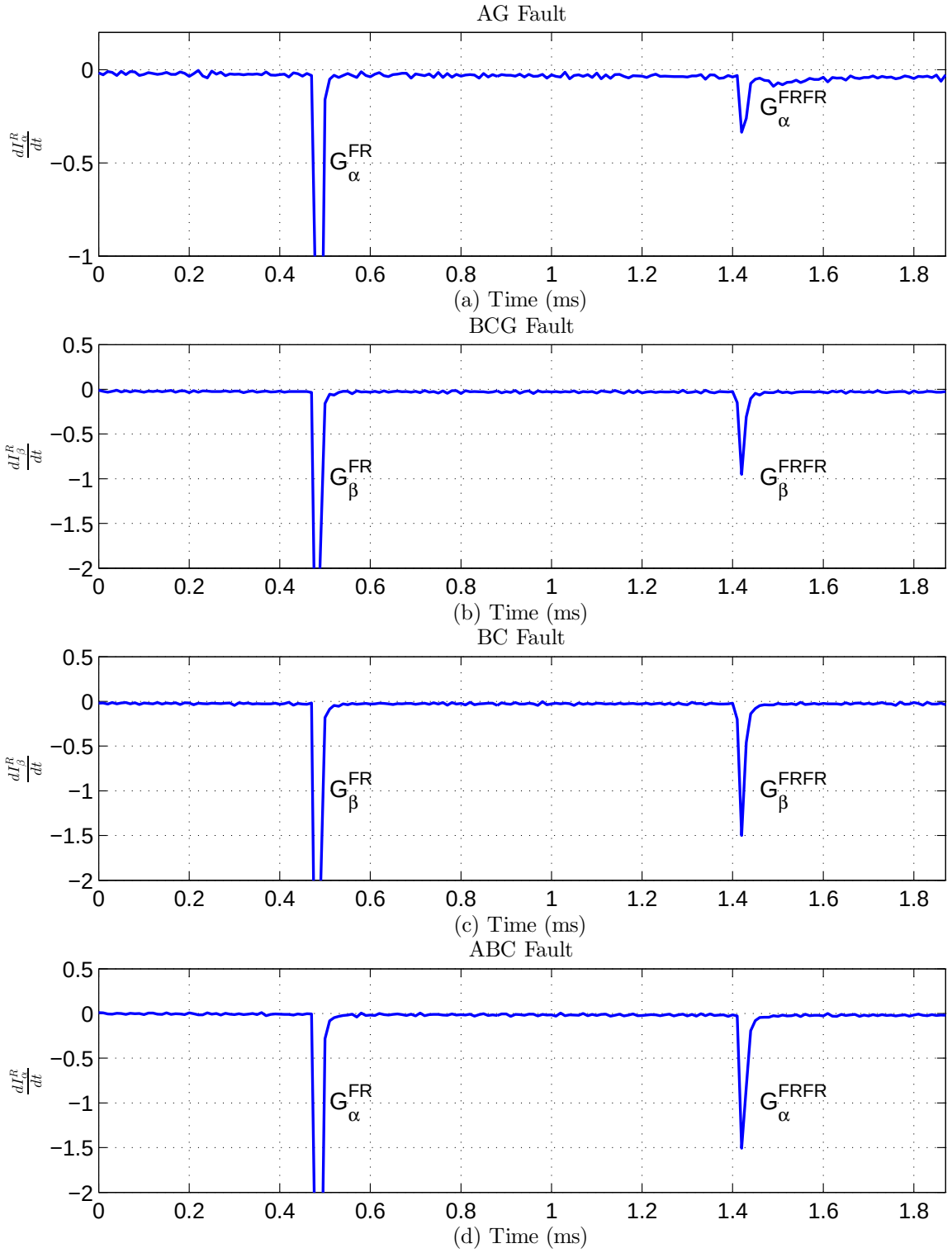

Figure D.10: The arrival of first two traveling waves at Bus R for various 50Ω faults at 60% line length measured from Bus S: (a) AG fault (α-mode), (b) BCG fault (β-mode), (c) BC fault (β-mode), (d) ABC fault (α-mode).

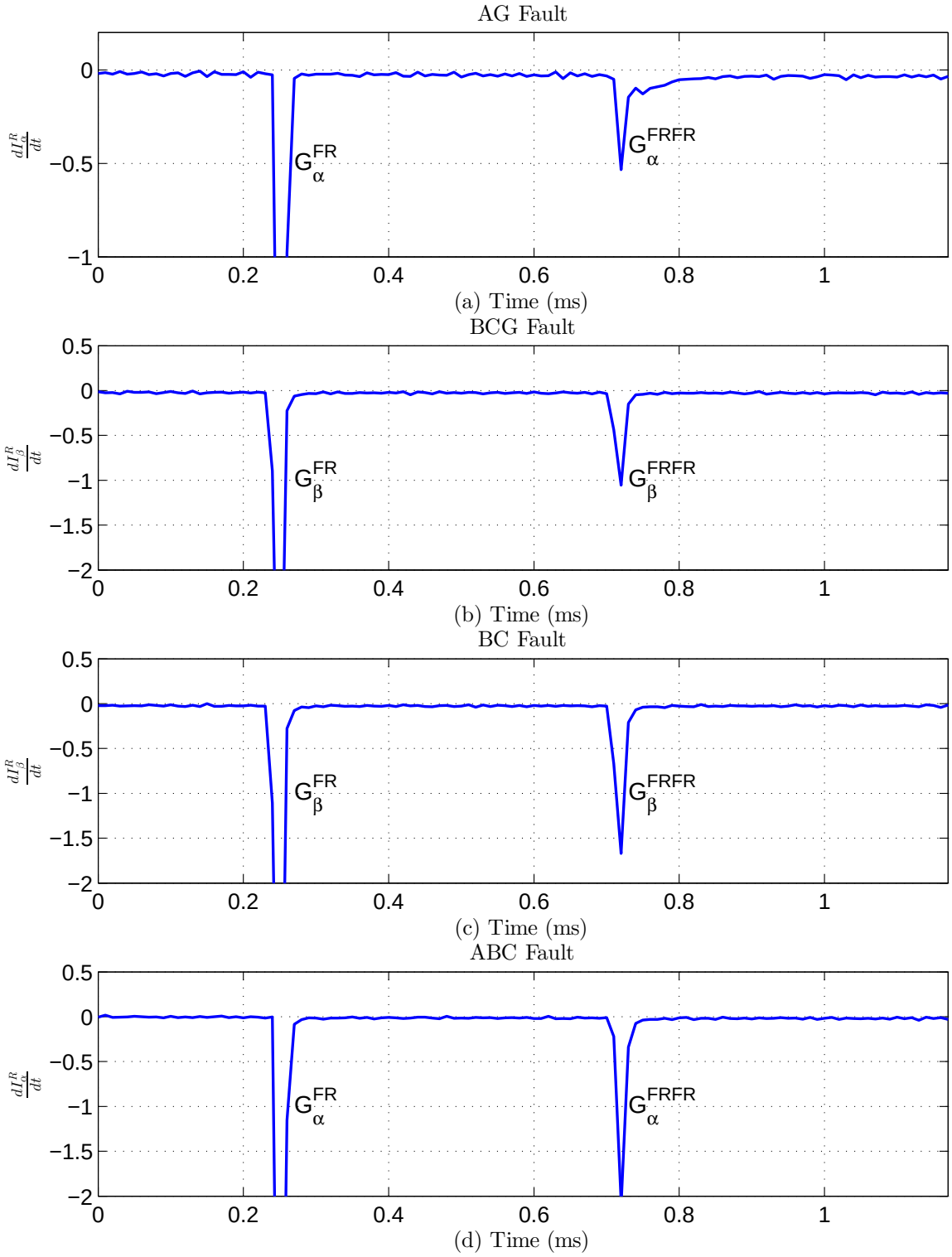

Figure D.11: The arrival of first two traveling waves at Bus R for various 50Ω faults at 80% line length measured from Bus S: (a) AG fault (α-mode), (b) BCG fault (β-mode), (c) BC fault (β-mode), (d) ABC fault (α-mode).

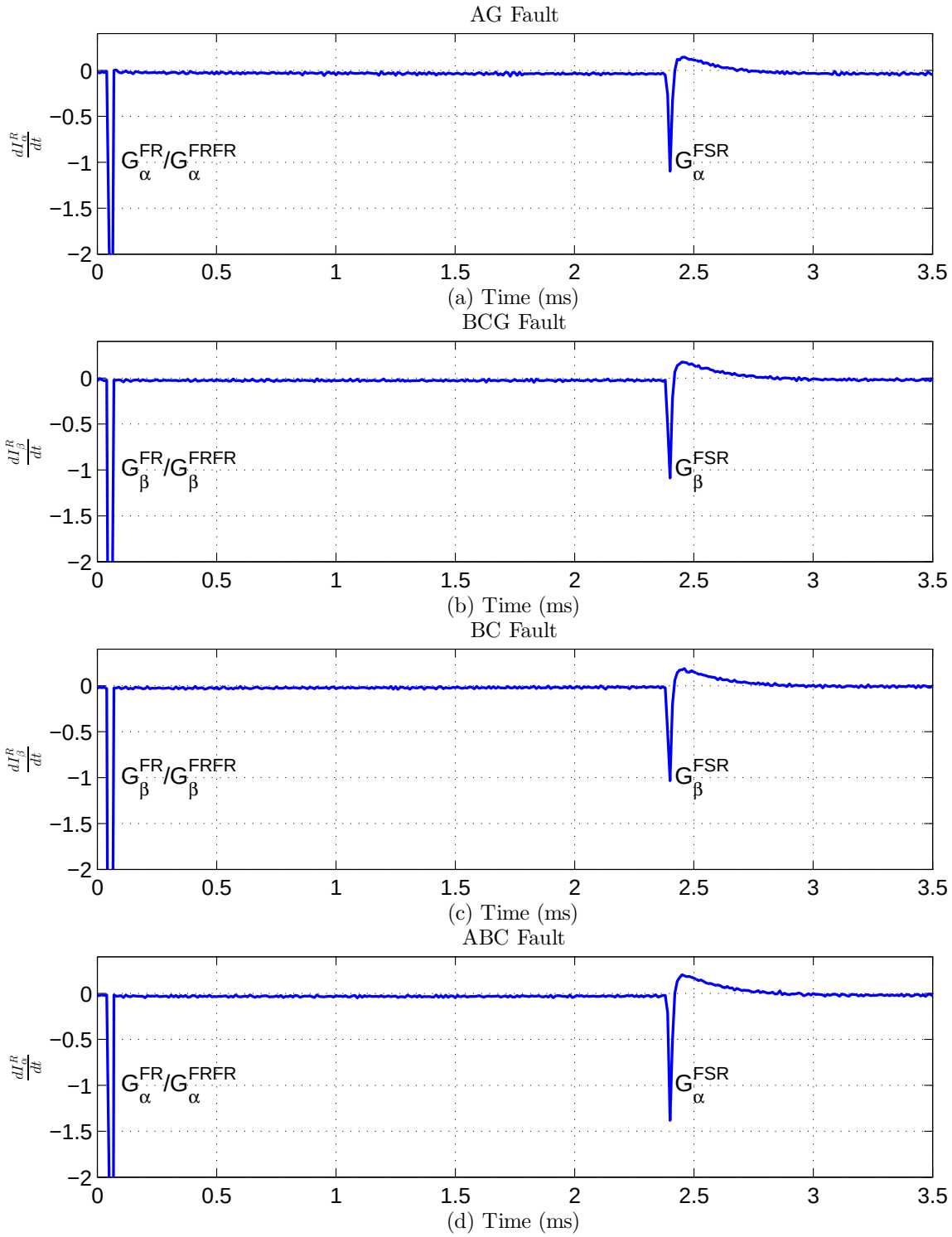

Figure D.12: The arrival of first two traveling waves at Bus R for various 50Ω faults at 100% line length measured from Bus S: (a) AG fault (α-mode), (b) BCG fault (β-mode), (c) BC fault (β-mode), (d) ABC fault (α-mode).

Curriculum Vitae

Name:	Tirath Bains
Post-Secondary Education and Degrees:	Bachelor of Engineering PEC University of Technology Chandigarh, India 2004 - 2008
	Masters in Engineering Science Western University London, ON 2012-2014
	Doctor of Philosophy Western University London, ON 2014-2018
Related Work Experience:	Alstom India Ltd. 2008 - 2009
	World Aviation Corp. 2010-2012

Publications:

1. T. P. S. Bains, T. S. Sidhu, Z. Xu, I. Voloh, M. R. D. Zadeh, " Impedance-based Fault Location Algorithm for Ground Faults in Series-Capacitor-Compensated Transmission Lines," *IEEE Trans. Power Del.*, vol. 33, no. 1, pp. 189-199, 2018.

2. T. P. S. Bains, M. R. D. Zadeh, " Supplementary Impedance-Based Fault-Location Algorithm for Series-Compensated Lines," *IEEE Trans. Power Del.*, vol. 31, no. 1, pp. 334-342, 2016.

3. T. P. S. Bains and M. R. D. Zadeh,“Enhanced Phasor Estimation Technique for Fault Location in Series Compensated Lines,” *IEEE Trans. Power Del.* , vol. 30, no. 4, pp. 2058-2060, 2015.

4. R. Rubeena, M. R. D. Zadeh and T. P. S. Bains, “An Accurate Offline Phasor Estimation for Fault Location in Series Compensated Lines,” *IEEE Trans. Power Del.*, vol. 29, no. 2, pp. 876-883, Apr. 2014.

5. T. P. S. Bains and M. R. D. Zadeh,“Challenges and Recommendations for Fault Location in Series Compensated Transmission Lines,” presented at IEEE PES General Meeting, National Harbor, MD, 2014.